Assessing the effect of reclaimed asphalt pavement on the fatigue and healing of flexible pavement materials

SATVIK PRATAP SINGH

STRUCTURAL ENGINEERING (ROAD AND RAILWAY ENGINEERING)

DELFT UNIVERSITY OF TECHNOLOGY

TU Delft | TNO innovation for life | Rijkswaterstaat Ministerie van Infrastructuur en Milieu | DURA VERMEER

Assessing the effect of reclaimed asphalt pavement on the fatigue and healing of flexible pavement materials

Master of Science, Graduation Thesis Report

Delft University of Technology

The Netherlands

Satvik Pratap Singh

Structural Engineering

(Road and Railway Engineering)

Assessing the effect of reclaimed asphalt pavement on the fatigue and healing of flexible pavement materials

By

Satvik Pratap Singh

In the partial fulfillment of the requirements for the degree of

Master of Science

in Structural Engineering

at the Delft University of Technology,

to be defended publicly on Friday, July 14th, 2023, at 3:00 PM

Student number: 5368332

Graduation Thesis Committee:	Dr. Xueyan Liu (Chair)	(TU Delft)
	Prof.dr.ir. Sandra Erkens	(TU Delft)
	Prof.dr.ir. Erik Schlangen	(TU Delft)
	Dr.ir. Panos Apostolidis	(TU Delft)
	ir. Robbert Naus	(Dura Vermeer)
	ir. G.A. Leegwater	(TNO)

Dedicated to ‘ Late Major Y. Singh & The People”

Acknowledgments

I would like to express my deepest gratitude and appreciation to Dr. Xueyan Liu, Chair of my graduation thesis committee, for his exceptional supervision and guidance throughout this journey. Dr. Liu's constructive feedback and clear scientific ideas have been instrumental in bringing out the best outputs possible in my research. His unwavering support and expertise have played a crucial role in shaping the direction and quality of my thesis. I am truly grateful for his invaluable contribution to my academic growth and success.

I would like to extend my heartfelt thanks to my daily supervisor, Dr. Panos Apostolidis, for his invaluable support and guidance throughout this research work. His continuous cooperation and unwavering availability, especially during challenging times, have been instrumental in my progress. Whenever I faced difficulties or felt stuck, Dr. Apostolidis was always there to provide assistance and motivate me to overcome obstacles. His dedication and belief in my abilities have pushed me to work harder and bring out the best in myself. I am truly grateful for his mentorship and contribution to the success of this research endeavor.

I would like to express my sincere gratitude to the members of my graduation thesis committee: Prof.dr.ir. Sandra Erkens, Prof.dr.ir. Erik Schlangen, ir. G.A. Leegwater (TNO), and ir. Robbert Naus (Dura Vermeer). Their expertise, guidance, and valuable insights have been indispensable in the successful completion of this research work. Their unwavering support, constructive feedback, and direction have greatly contributed to achieving the goals of this study.

I would like to express my heartfelt gratitude to ir. Marco Poot and ir. Michele van Angelen for their invaluable assistance throughout my research work. Their expertise, technical support, and willingness to help have played a vital role in the successful execution of experiments and data collection. I am particularly grateful to ir. Marco for sharing his wealth of knowledge and experience in the field of asphalt materials. His guidance and insights have greatly enriched my understanding of key concepts and enhanced the quality of my research.

This research work is inter-relation with an ongoing project, which aims at developing a protocol to determine the shift factors for the fatigue life of asphalt mixtures to correct healing and aging. Knowledge-based Pavement Engineering (KPE) program was initiated by Rijkswaterstaat, TNO, and TU Delft. Dura Vermeer is contributing partner to this MSc graduation research work as well. Thanks a lot to all the partnering companies in this project for providing me to be a part of such a big project.

I would like to express my sincere gratitude to Marjo J van Koppen, Senior Communication Officer at TU Delft, as well as the entire Introduction Programme team, for providing me with the valuable opportunity to work as a student assistant in the Communication Department of Education and Student Affairs for a duration of two years. The experience allowed me to gain valuable insights into the field of communication, develop essential skills, and contribute to the various projects and initiatives undertaken by the department.

To my parents, Dr. K.K.S Chauhan and Dr. Neeru Singh, thank you for being the foundation of my life. Your love, sacrifices, and constant belief in me have been the driving force behind my accomplishments. I would like to give a special mention to my brother, Er. Kautilya Pratap Singh

and Er. Vibhuti Singh (Lara), for their unwavering support and encouragement in helping me achieve my dream of studying abroad. Thank you both for believing in me and being there for me. I extend a heartfelt thank you to my my grandmother Adesh Kumari for always having my back and providing unwavering support throughout this journey. I would like to extend my gratitude to my uncles Advocate Shailendra Singh, DIG Sudhindra Singh, Pradeep Kr. Singh & Er. Manoj Kr. Singh. Also a big thanks to my aunts Dr. Nisha Singh, Preeti Singh, Archana Singh & Dr. Praggya M Singh for all the support.

I express my heartfelt gratitude to my beloved seniors, Ir. Anjali Shah, Ir. Pallavi Palla, Ir. Harisushin, Ir. Krishna, and Ir. Aishani Lotliker, for their unwavering support, motivation, and guidance throughout my journey. Their invaluable contributions have been instrumental in my pursuit of significant achievements.

I would like to express my heartfelt appreciation to all my friends who have been a constant source of support and motivation throughout my journey at TU Delft. To Saurabh Mahajan, Giulia Ricci, Emilia AA Borges, Elena Grimbacher, Romy Groeneweg, Thor Vilhjalmsson, Nóra Kovács, Shriyash Puranik, Atharva Mungale, Hrishika Rastogi, and Rianne Teeuwen, a big thank you for always being there for me, both in joyful and challenging times. Your unwavering encouragement has meant the world to me. I would like to give a special mention to U-BASE for their exceptional efforts in making the life of an international student like myself easier during the transition to a whole new culture.

I would like to extend a special heartfelt appreciation to the bonds and friendships that have transcended beyond my time at TU Delft. I am immensely grateful to Ir. Manank Shah for his constant motivation and unwavering support in every aspect of my life. I would also like to express my thanks to Er. Anjali Singh, Er. Pranjal Chaudhary, Er. Neelabh Singh, Er. Kushagra Singh, Er. Vikrant Singh, Er. Rishabh Dixit, and Er. Harshit Rathore has always been there for me, providing assistance and motivation despite being separated by distance. Your support has been invaluable to me, and I am truly grateful for our enduring friendship.

Summary

Durable yet sustainable pavements are needed to keep pace with the fast-growing world. Roads, the backbone of any economy in the globe, must be available for the rapidly increasing traffic without any impediments caused by maintenance roadworks or bad riding quality. In this light, assessing the self-healing of flexible pavements can be extremely beneficial. Under specific conditions, such as higher temperatures and longer rest periods, asphalt material can heal, a phenomenon that pavement engineers have been aware of for many years. But still, a lot of research is required to understand the underlying mechanism and quantification of self-healing in asphalt materials. An attempt to assess and quantify the self-healing capacity of base layer asphalt concrete mixtures comprised of recycled asphalt pavement materials and a recycling agent is performed in this research program. This study ranges from a literature review on the concept of self-healing in asphalt materials to extensive laboratory testing to assess fatigue and healing on the asphalt mixtures to the prediction of healing models based on the simplified viscoelastic continuum damage (S-VECD) theory to simulate pavement performance using the FlexPAVE software.

During the literature review phase, preliminary research on various fatigue and healing concepts and approaches is undertaken. Three base layer dense-graded asphalt mixtures, namely M1 (with 0% recycled asphalt material and 100% virgin aggregates), M2 (with 70% recycled asphalt material and 30% virgin aggregates), and M3 (with 70% recycled asphalt material, 30% virgin aggregates & doze of recycling agent) are taken in consideration to assess the effect of recycled asphalt pavement material and a recycling agent on fatigue and healing mechanisms. In the laboratory, first, dynamic modulus tests on cylindrical specimens as per AASHTO T-342 11 were conducted to obtain the linear visco-elastic (LVE) properties of the mixtures. To calculate the material damage using the S-VECD theory, the FlexMAT Cracking tool was used. After the prediction of stiffness modulus master curves using the time-temperature superposition principle (TTSP), uniaxial cyclic tension-compression fatigue tests were performed at three different temperatures (10, 20 and 30°C) in accordance with AASHTO TP 107-18 to assess the behavior of the different mixtures. This continuous fatigue test on the specimen was the basis for the healing quantification by implementing rest periods in asphalt mixtures.

In the third phase of the laboratory experiments, the uniaxial tension-compression cyclic fatigue-healing tests were conducted at the same three temperatures and three different rest periods (40, 80 and 160 s). The various testing combinations were used to evaluate the influence of temperature and rest periods. The healing tests were performed by implementing the group rest period at the stage of a certain damage level in the material. The representative damage characteristic curves for continuous fatigue and respective healing tests were plotted. Based on the experimental results, the quantification of healing percentages at different levels of damage was done using three different methods based on pseudo-stiffness, number of cycles and variable defining the damage in the mixture. A parameter “reduced rest period” including the effect of both the temperature and the rest period was calculated. Further, with post-processing of the results, the healing percentage master curve at different damage levels was plotted for all the mixtures. With this, it is possible to predict the amount of healing at different temperatures and damage

levels for any rest period with acceptable accuracy. Using the sigmoidal function for healing percentage, a healing model was also proposed for all three mixtures employed in this study.

To an extent, the properties of the mixtures used in this research work are used to analyze the pavement performance under the effect of vehicle load and temperature, among others, using the FlexPAVE software. A typical Dutch pavement structure cross-section is modeled using the data obtained from the experimental work performed above. This performance prediction study gives a picture of how a pavement will perform if the mixtures are used, including the properties obtained with and without healing rest periods. Further, the effect of the variation in depth and stiffness of the underlying layer on the performance of asphalt layers is also studied.

Based on the research performed, a better understanding of the occurrence and quantification of self-healing on different asphalt concrete mixtures is achieved. At the end of this research work, conclusions and future recommendations for research in this field are given. Hence, this self-healing phenomenon should be taken into consideration to obtain more durable and sustainable flexible pavements.

Samenvatting

Duurzaam asfalt is nodig om te kunnen voldoen aan de vraag van de snelgroeiende wereld. Wegen, de basis van elke economie ter wereld, moeten beschikbaar zijn voor het snel toenemende verkeer zonder hinder door onderhoudswerkzaamheden of slecht kwaliteit wegdek. In dit opzicht kan het beoordelen van het zelf herstellend vermogen van asfalt verhardingen zeer van belang zijn. Onder specifieke omstandigheden, zoals hogere temperaturen en langere rustperiodes, kan bitumen zelf herstellen. Dit fenomeen is al jaren bekend, maar nog veel onderzoek is nodig om de onderliggende mechanismes te doorgronden en te kwantificeren. Dit onderzoek richt zich op het beoordelen en kwantificeren van het zelf herstellend vermogen van asfaltbetonmengsels met gerecyclede toeslagmaterialen en gerecyclede verjongingsmiddelen. Dit onderzoek omvat een literatuurstudie naar het concept van zelfhelend asfalt, uitgebreide laboratoriumtesten om vermoeiing en heling van asfalt-betonmengsels te beoordelen, voorspelling van helingsmodellen op basis van de vereenvoudigde visco-elastische-continuïteit schade theorie en analyses op de asfalt prestatie met behulp van Flex Pave-software.

Tijdens het literatuuronderzoek is vooronderzoek gedaan naar vermoeiing en herstel concepten en aanpakken. Drie asfaltmengsels voor funderingslagen: M1 (met 0% gerecycled asfalt materiaal en 100% nieuw toeslagmateriaal), M2 (met 70% gerecycled asfalt materiaal en 30% nieuw toeslagmateriaal) en M3 (met 70% gerecycled asfalt materiaal, 30% nieuw toeslagmateriaal en gerecyclede verjongingsmiddelen) zijn beschouwd om het effect van gerecycled asfaltverhardingsmateriaal en gerecycled verjongingsmiddelen op vermoeiings- en herstelmechanismen te beoordelen. In het laboratorium zijn eerst dynamische modulustesten uitgevoerd op cilindrische proefstukken met een diameter van 100 mm en een hoogte van 150 mm. Deze testen zijn uitgevoerd volgens AASHTO T-342 11 met als doel de lineaire visco-elastische eigenschappen (LVE) van de mengsels te bepalen. Voor de wiskundige berekeningen met de S-VECD-theorie is de macro-gebaseerde tool Flex MAT cracking gebruikt. Nadat de stijfheidsmatercurves zijn voorspeld met behulp van het tijd-temperatuur superpositieprincipe (TTSP) en andere LVE-eigenschappen, is een eenassige cyclische trek-druk vermoeiingsproef uitgevoerd met een frequentie van 10 Hz bij drie verschillende temperaturen (10°C, 20°C en 30°C) in overeenstemming met AASHTO TP 107-18. Deze proef is uitgevoerd om het gedrag van de verschillende mengsels te beoordelen en vormt de basis voor de kwantificering van heling met rustperioden.

In de derde fase van de experimenten is de eenassige spanning-druk cyclische vermoeiings- en hersteltest uitgevoerd bij 10 Hz bij drie verschillende temperaturen (10°C, 20°C en 30°C) en drie verschillende rustperiodes (40 seconden, 80 seconden en 160 seconden). De verschillende testcombinaties zijn gebruikt om de invloed van temperatuur en rustperiodes te evalueren. De helingstest wordt uitgevoerd door de groepsrustperiode toe te passen bij het bereiken van een bepaald schadeniveau in het materiaal. De resultaten van zowel de continue vermoeiingstesten als de helingstesten zijn in kaart gebracht. De kwantificering van helingspercentages op verschillende schadeniveaus is gedaan met behulp van drie verschillende methoden gebaseerd op pseudostijfheid, aantal cycli of een variabele die de schade in het mengsel definieert. De parameter “gereduceerde rustperiode”, die het effect van zowel temperatuur als rustperiode omvat, wordt berekend. Bovendien is bij het verwerken van de resultaten de hoofd helingscurve bij verschillende schadeniveaus bepaald voor alle mengsels. Hiermee kan met voldoende nauwkeurigheid de mate van heling worden voorspeld bij verschillende temperaturen en

schadeniveaus. Een helingsmodel is voorgesteld voor alle drie de beschouwde mengsels door gebruik te maken van de Sigmoïdale functie voor het helingspercentage.

De prestaties van het wegdek onder invloed van voertuigbelasting, temperatuur etc. zijn geanalyseerd met behulp van Flex PAVE software en de eigenschappen van de mengsels. Een dwarsdoorsnede van een typische Nederlandse asfaltverharding is gemodelleerd met behulp van de gegevens uit de experimenten. Dit geeft een duidelijk beeld over de prestatie van een wegdek bestaande uit deze mengsels met en zonder herstellende rustperiode. Verder is ook het effect van de diepte en stijfheid van de onderliggende laag op de prestatie van het asfalt bestudeerd.

Dit onderzoek draagt bij aan een beter begrip over de werking en kwantificering van het zelfherstellende fenomeen van verschillende asfaltbetonmengsels. Aan het einde van dit onderzoek zijn conclusies getrokken en aanbevelingen gedaan. Kortom, voor duurzame flexibele wegverhardingen moet rekening gehouden worden met het zelfherstellende fenomeen.

Biography

Satvik Pratap Singh, the only child of Dr. K.K.S Chauhan and Dr. Neeru Singh, was born on September 5, 1997, in Bewar, Mainpuri, Uttar Pradesh, India. He completed his schooling with distinction at St. Thomas Sr. Sec. School in the same town. After successfully qualifying for renowned competitive exams (IIT-JEE) and obtaining an undergraduate degree in 2015, he enrolled at Pandit Deendayal Energy University (formerly known as P.D.P.U) in Gujarat, India, on a scholarship to pursue a Bachelor of Technology in Civil Engineering. In July 2019, he graduated with a gold medal in Bachelor of Technology, receiving the accolade from Shri Narendra Modi, the Honourable Prime Minister of India. Following his graduation, Satvik gained valuable experience in construction technologies involved in national highways in Arunachal Pradesh while working in the field for the next two years. During this time, he also successfully qualified for competitive exams like the Graduate Aptitude Test in Engineering (GATE). Subsequently, Satvik secured admission to the Delft University of Technology on a Holland scholarship to pursue a Master of Science in Civil Engineering, specializing in Structural Engineering. This document serves as a report for Satvik's Master of Science graduation thesis project.

Table Of Contents

List of Tables ..... **xi**

List of Figures ..... **xii - xvii**

Chapter 1 Introduction **1**

1.1 Introduction 2

1.2 Problem Statement and Objectives 2

1.3 Organization of the thesis report 3

1.4 Research Methodology 5

Chapter 2 Fatigue Damage and Healing in Asphalt Materials **7**

2.1 Introduction 8

2.2 Underlying principles of fatigue cracking 8

2.3 Fatigue – from field to laboratory 10

2.4 Biased effects in fatigue of asphalt materials 11

2.5 Failure criterion 11

2.6 Fatigue damage theories 12

2.6.1 Fracture Mechanics

2.6.2 Dissipated energy method

2.6.3 Rate of dissipated energy method

2.7 Fatigue testing methods for asphalt mixtures 17

2.7.1 Four-point bending test.

2.7.2 Cyclic indirect tensile test

2.7.3 Uniaxial tension-compression fatigue test

2.8 Healing in asphalt materials 21

2.8.1 Definition and Significance

2.8.2 Mechanism of healing

2.8.3 Factors affecting healing.

2.8.4 Methods to implement rest periods in fatigue testing.

2.9 Previous experience in healing in asphalt materials 25

Chapter 3 Visco-Elastic Continuum Damage Theory for Asphalt Materials **33**

3.1 Introduction 34

3.2 Simplified viscoelastic continuum damage theory……34
3.3 Time-temperature superposition principle……35
3.4 Mathematical interpretation of viscoelastic continuum damage theory……35
3.5 Concept of pseudo-stiffness and damage parameter……36
3.6 Computation of C-S curve……40
3.7 Previous experience……40
Chapter 4 Materials and Laboratory Test Methods……46
4.1 Introduction……47
4.2 Materials……47
4.3 Dynamic modulus test……50
4.4 Fatigue test……52
4.4.1 End Treatment
4.4.2 Fingerprint test
4.4.3 Uniaxial tension-compression fatigue test
4.5 Uniaxial tension-compression fatigue healing test……54
4.5.1 Duration and mode of application of rest periods
4.5.2 Application of rest periods
Chapter 5 Fatigue and Healing Laboratory Results and Discussion……57
5.1 Introduction……58
5.2 Dynamic modulus test results……58
5.2.1 |E| values for load variations with temperature as per AASHTO T 342-11*
5.2.2 Stiffness and phase angle master curves
5.3 Uniaxial tension-compression fatigue test results……63
5.4 Uniaxial tension-compression healing test results……69
5.4.1 Prediction of healing percentages
5.4.2 Healing master curves
5.4.3 Healing model prediction for M1, M2, M3
5.5 Summary……91
Chapter 6 FlexPAVE Analysis…… 95
6.1 Introduction……96
6.2 Percentage damage definition in FlexPAVE……96
6.3 Percentage cracking on the field from the percentage……97

6.4 Input parameters for pavement performance predictions……..98

6.5 Results and Discussion……99

6.5.1 Pavement Performance with Fatigue and Healing

6.5.2 Effect of Temperature on pavement performance

6.6 Conclusions……106

Chapter 7 Conclusion & Recommendations……109

7.1 Conclusions……110

7.1.1 Conclusion to the main research question and sub-question

7.2 Recommendations & Future work……112

Appendix A FlexMAT™ cracking……114

A.1 Processing the data using FlexMAT……115

Appendix B Laboratory Testing and Development……125

B.1 Dynamic modulus test results……126

B.2 Glue line failure……127

B.3 Prediction of phase angles in MP3 software……128

B.4 Stress-controlled fatigue testing vs strain-controlled fatigue testing……131

B.5 Some pictures from laboratory experimental work……131

Appendix C Fatigue test results……134

C.1 Variation of stiffness and phase angle values with number of cycles……135

Appendix D Fatigue healing test results……145

D.1 Variation of dynamic modulus values of materials with time……146

D.2 Calculation of healing percentages based on the number of cycles……156

Appendix E Flex PAVE Software……159

E.1 FlexPAVE Simulations……160

Appendix F Prediction of healing Master curves……164

F.1 Prediction of healing models for all the mixtures……165

List Of Tables

Table 4.1 Description of the studied asphalt mixtures..... 47

Table 4.2 Physical properties of binder and mixtures used in the test program..... 48

Table 4.3 Percentages of materials used in the studied asphalt mixtures..... 48

Table 4.4 Aggregate gradation of the studied asphalt mixture..... 48

Table 4.5 Stress ranges applied on specimens during dynamic modulus tests..... 50

Table 4.6 Number of cycles for different frequencies..... 51

Table 4.7 Load applied in dynamic stiffness test at different temperatures..... 52

Table 5.1 LVE Properties calculated by FlexMAT..... 62

Table 5.2 Shift Factors for different temperatures..... 63

Table 5.3 Damage evolution rates for different mixtures..... 63

Table 5.4 Summary of uniaxial cyclic fatigue testing for all mixtures..... 65

Table 5.5 Fitting parameters from dynamic modulus test..... 85

Table 5.6 Calculated shift factors for different temperatures..... 85

Table 5.7 Calculated shift factors and reduced rest periods..... 86

Table F.1 Fitting parameters for all mixtures..... 165

List Of Figures

Figure 1.1 Organization of the thesis report……4

Figure 1.2 Research Methodology……5

Figure 2.1 Stress formation under a wheel load……9

Figure 2.2 Stress formation in asphalt layers due to wheel loading……9

Figure 2.3 Typical fatigue curve for asphalt mixture……10

Figure 2.4 The energy ratio method……12

Figure 2.5 Elastic and viscoelastic behavior……14

Figure 2.6 Hysteresis loop variation with each cycle for a different mode of loading……14

Figure 2.7 Dissipated energy for an elastic material (left) and two different viscoelastic materials……16

Figure 2.8 RDEC Approach……17

Figure 2.9 Four-point bending test setup in TU Delft laboratory…… 18

Figure 2.10 Cyclic indirect tensile test setup……19

Figure 2.11 TU Delft laboratory set-up of the indirect tensile modulus test……19

Figure 2.12 Test setup for uniaxial fatigue and healing testing……20

Figure 2.13 Three-step Mechanism of Healing……22

Figure 2.14 The mechanism involved in self-healing through inter-diffusion……23

Figure 2.15 Tests method with and without a rest period……25

Figure 2.16 Example schematic for group-rest healing test……26

Figure 2.17 Normalized dynamic modulus vs. the number of loading cycles……27

Figure 3.1 C-S curve representing the effect of rest period in cyclic fatigue testing……41

Figure 4.1 Aggregate gradation curves of the studied asphalt mixtures……49

Figure 4.2 Specimen: (a) as received from Dura Vermeer (b) mounted in core cutter at TU Delft lab (c) after cored out (d) mounted in the polishing machine (e) after coring and polishing (f) mounted in the hydraulic testing machine ready for stiffness testing……49

Figure 4.3 Characteristic plot of (a) compressive load vs. time during the dynamic modulus test (b) average LVDTs displacement vs. time during the dynamic modulus test per AASHTO T 342-11 (M1 at 25 Hz and 10°C)……50

Figure 4.4 (a) White Vaseline and plastic sheet for end treatments (b) Ball and plate arrangement for uniform load distribution in stiffness testing……51

Figure 4.5 (a) Sandblasted loading plates and (b) different equipment required for end treatment (Powdered glue, 3M mask, specimen, hardener, rubber gloves, PVC rings, Mixing cup & Acetone)……52

Figure 4.6 Gluing (a) the lower end of the specimen and (b) the upper end under compression loading……53

Figure 5.1 Variation in values of dynamic modulus among two specimens of three different mixtures……59

Figure 5.2 Dynamic modulus master curve……61

Figure 5.3 Phase angle master curve……61

Figure 5.4 Shift factors calculated for different mixtures at different temperatures……62

Figure 5.5 The slope of the relaxation curve (E(t)) vs. time (t) in the log-log scale……62

Figure 5.6 Variation of fingerprint values of different mixtures with temperatures……63

Figure 5.7 Representative plots for (a) stiffness and phase angle variation with the number of cycles in fatigue test for M3 at 20°C…… 64

Figure 5.8 Number of cycles to failure for all mixtures vs. the temperature……65

Figure 5.9 Damage characteristics curve for all mixtures at 30°C……66

Figure 5.10 Damage characteristics curve for all mixtures at 20°C……67

Figure 5.11 Damage characteristics curve for all mixtures at 10°C……67

Figure 5.12 Damage Characteristics curves for all the mixtures at all test temperatures……68

Figure 5.13 Damage characteristics curve at two different strain rates……69

Figure 5.14 Comparison of the stiffness modulus variation during fatigue-healing tests: (a) 160 (b) 80 (c) 40 s rest periods……70

Figure 5.15 Visual comparison of the increase in time to failure with an increase in rest periods (a)160 s (b) 80 s (c). 40 s……71

Figure 5.16 Comparison of recovery of stiffness in three mixtures (a)M1 (b)M2 (C)M3……72

Figure 5.17 C-S curves for three mixtures at 30°C (a) M1 (b) M2 (c) M3……73

Figure 5.18 C-S curves for three mixtures at 20°C……74

Figure 5.19 C-S curves for three mixtures at 10°C……75

Figure 5.20 Parameters to calculate the damage level and the healing percentages……76

Figure 5.21 Percentage healing calculation as a function of damage level based on Method 1 at 20°C for (a) M1, (b) M2, and (c) M3……78

Figure 5.22 Percentage healing calculation as a function of the shift in load cycle based on Method 2 for M3 at (a) 10, (b) 20, and (c) 30˚C……80

Figure 5.23 Percentage healing calculations for M1 based on Method 3 at (a) 10, (b) 20, and (c) 30°C……82

Figure 5.24 Percentage healing calculations for M2 based on Method 3 at (a) 10, (b) 20, and (c) 30°C……83

Figure 5.25 Percentage healing calculations for M3 based on Method 3 at (a) 10, (b) 20, and (c) 30°C……84

Figure 5.26 Steps involved in the prediction of the healing master curve……85

Figure 5.27 Percent healing master curves at various damage levels in (a)arithmetic space, (b)semi-log space, & (c) log-log space for M1……88

Figure 5.28 Percent healing master curves at various damage levels in (a)arithmetic space, (b)semi-log space, & (c) log-log space for M2……89

Figure 5.29 Percent healing master curves at various damage levels in (a)arithmetic space, (b)semi-log space, & (c) log-log space for M3……90

Figure 6.1 Reference area for “percentage damage" definition in FlexPAVE……96

Figure 6.2 Reference pavement structure and properties used for FlexPAVE predictions……98

Figure 6.3 Damage for all mixtures in fatigue without considering the healing effect……99

Figure 6.4 Damage growth for all mixtures in fatigue with considering the healing effect……100

Figure 6.5 Damage growth of (a) M1 (b) M2 (c) M3 in fatigue and fatigue-healing……101

Figure 6.6 Damage propagation with fatigue mechanism over 30 years in (a) M1 (b) M2 (c) M3……103

Figure 6.7 Damage propagation with fatigue mechanism over 30 years in (a) M1 (b) M2 (c) M3……104

Figure 6.8 Comparison of damage growth in fatigue of M3 at 20 and 30°C……105

Figure 6.9 Comparison of damage growth in fatigue-healing of M3 at 20, 30, and 50°C……105

Figure 6.10 Comparison of damage growth in fatigue-healing of M3 at 20 and 30°C……106

Figure 7.1 Possible Correlation in fatigue life of 4-point bending and Uniaxial fatigue testing……113

Figure A.1 Flex MAT™ flow overview……115

Figure A.2 Raw data as collected from the laboratory……116

Figure A.3 Formatted .csv file as per Flex MAT guidelines……117

Figure A.4 .txt file of the final output format file……117

Figure A.5 Representation of the 2S2P1D model……118

Figure A.6 Start window in FlexMAT……119

Figure A.7 Flex MAT dynamic modulus input screen……119

Figure A.8 Output window in FlexMAT……120

Figure A.9 Format .csv file as per Flex MAT fatigue requirements……120

Figure A.10 .txt files as per format required by FlexMAT……121

Figure A.11 Flex MAT Cyclic fatigue input screen……121

Figure A.12 Flex MAT cyclic fatigue model overview screen……122

Figure A.13 (a) C vs S curve before representative fitting filtering. (b) C vs S curve after representative filtering……122

Figure A.14 Failure cycle determination……123

Figure A.15 Data Quality Indicator Screen……123

Figure B.1 |E*| vs Frequency for M1, M2, M3 (Loads as per AASHTO T 342-11) ……127

Figure B.2 (a) Glue line failure in the specimen during fatigue testing and (b) intact specimen along with glue……127

Figure B.3 Failure in asphalt material while removing the glue……127

Figure B.4 Double PVC ring instead of one to give extra confinement……128

Figure B.5 (a) Cylindrical Teflon specimen (b) Specimen mounted in MTS for the check of phase angles……128

Figure B.6 Failure pattern in tension-tension mode of loading……129

Figure B.7 Strain-Controlled Haversine Loading……129

Figure B.8 Strain-Controlled Sine Loading……130

Figure B.9 Failure pattern in the tension-compression mode of loading……130

Figure B.10 Cores and shell for gyratory compacted specimen……131

Figure B.11 Demarcation of locations to mount LVDTs……131

Figure B.12 Polishing machine and polished specimen……132

Figure B.13 Sandblasting process and sandblasted loading platens……132

Figure B.14 Fatigue & fatigue- healing specimen failure in the material……132

Figure B.15 Failed specimens after fatigue & healing testing……133

Figure C.1 M1 -Dynamic modulus and phase angle variation with N at 10°C……136

Figure C.2 M1 -Dynamic modulus and phase angle variation with N at 20°C……137

Figure C.3 M1 -Dynamic modulus and phase angle variation with N at 30°C……138

Figure C.4 M2 -Dynamic modulus and phase angle variation with N at 10°C……139

Figure C.5 M2 -Dynamic modulus and phase angle variation with N at 20°C……140

Figure C.6 M2 -Dynamic modulus and phase angle variation with N at 30°C……141

Figure C.7 M3 -Dynamic modulus and phase angle variation with N at 10°C……..…..142

Figure C.8 M3 -Dynamic modulus and phase angle variation with N at 20°C……..…..143

Figure C.9 M3 -Dynamic modulus and phase angle variation with N at 30°C……144

Figure D.1 Dynamic modulus values with time at 30°C temperatures for M1 at different rest periods……147

Figure D.2 Dynamic modulus values with time at 30°C temperatures for M2 at different rest periods……148

Figure D.3 Dynamic modulus values with time at 30°C temperatures for M3 at different rest periods……149

Figure D.4 Dynamic modulus values with time at 20°C temperatures for M1 at different rest periods……150

Figure D.5 Dynamic modulus values with time at 20°C temperatures for M2 at different rest periods……151

Figure D.6 Dynamic modulus values with time at 20°C temperatures for M1 at different rest periods……152

Figure D.7 Dynamic modulus values with time at 10°C temperatures for M1 at different rest periods……153

Figure D.8 Dynamic modulus values with time at 10°C temperatures for M2 at different rest periods……154

Figure D.9 Dynamic modulus values with time at 10°C temperatures for M3 at different rest periods……155

Figure D.10 Healing percentages for M1 at (a)10°C (b) 20°C (c) 30°C……156

Figure D.11 Healing percentages for M2 at (a)10°C (b) 20°C (c) 30°C……157

Figure D.12 Healing percentages for M3 at (a)10°C (b) 20°C (c) 30°C……158

Figure E.1 Development of the cracks over the course of 30 years in M1 with (a)Fatigue (b) Healing mechanism……160

Figure E.2 Development of the cracks over the course of 30 years in M2 with (a)Fatigue (b) Healing mechanism……161

Figure E.3 Development of the cracks over the course of 20 years in M1 for 150 MPa subbase……162

Figure E.4 Development of the cracks over the course of 20 years in M1 for 300 MPa subbase……162

Figure E.5 Development of the cracks over the course of 20 years in M1 for 700 MPa subbase……162

Figure E.6 Development of the cracks over the course of 20 years in M1 for 1000 MPa subbase……163

Figure E.7 Development of the cracks over the course of 20 years in M1 for 1200 MPa subbase……163

Figure E.8 Development of the cracks over the course of 20 years in M1 for 4300 MPa subbase……163

Figure F.1 Fitting parameters for percent healing master curves vs. damage level in M1……165

Figure F.2 Fitting parameters for percent healing master curves vs. damage level in M2……166

Figure F.3 Fitting parameters for percent healing master curves vs. damage level in for M3…..166

Chapter 1

Introduction

1.1 Introduction

Asphalt binder is one of the most used materials for road construction. Since the turn of the century, mixtures of fine and coarse aggregates held together with asphalt binder have been the materials most frequently utilized in pavement construction due to their high cost-effectiveness, noise reduction, safety, and comfort. Note that the asphalt mixtures are 100% recyclable. The Netherlands has approximately 139,000 kilometers of public roads comprised of asphalt. The Netherlands also has one of the densest motorway networks in the world, with a motorway density of 64 kilometers per 1000 square kilometers.

Asphalt concrete mixtures are prone to damage due to heavy traffic loading and weather conditions. Distresses like raveling, potholes, cracking, and so on can deteriorate the pavement's service conditions. One of the most important distress phenomena in flexible pavements made of asphalt materials is fatigue cracking. The main cause of fatigue cracking is the repeated load with moving traffic (NASEM 2022). With repetitive load cycles, small micro-cracks originate due to moving loads. These microcracks densify over time and form larger cracks called macro-cracks, with the most dominant cracking mechanism originating at the bottom of the asphalt layer. At the bottom of the layer, tensile stresses are the highest, initiating the crack, which moves in the above directions forming longitudinal cracks on the surface. This is named "bottom-up" or "classical" fatigue cracking. This phenomenon is relevant in the case of thick pavements. For thin pavements (i.e., thickness <160 mm), the cracks generate due to highly localized tensile stresses due to tire-pavement interaction and asphalt aging. Generally, these cracks propagate to 500 mm, known as top-down cracking (Molenaar 1983).

To model and assess the fatigue characteristics, the constitutive relationship should represent the viscoelasticity of the matrix, fatigue damage growth, and healing that happens due to the rest periods between the application of loading cycles. Healing during the rest period in asphalt materials is a well-known and accepted phenomenon. Due to this healing process, the microcracks formed due to damage cycles can be cured, and the mixture regains its strength partially or completely (Ashouri 2014).

Healing is affected by many phenomena, such as damage level prior to the rest period, temperature, duration of the rest period, physical properties and chemical composition of the binder, properties of the mixture itself, aging, etc. Healing is also defined in several ways as the reversal of microcracks, the increase in the stiffness and integrity of the material, and an increase in fatigue life (Qiu 2012).

One of the most pressing issues is the effect of reclaimed asphalt pavement (RAP) in base layers on their aging, healing, and fatigue resistance. Usage of RAP is not decided in layers by any rule of thumb but rather depends on the agency, contractors, or country user guidelines. The Netherlands already uses a higher proportion of RAP than many parts of the world and has already employed mixtures containing almost 100% RAP in the base layers. This research is focused on assessing the effect of RAP, or recycled asphalt materials, on the fatigue and healing behavior of the dense-graded asphalt mixtures designed for the base pavement layer.

1.2 Problem statement and objectives

Based on the information mentioned in the above section, to achieve those goals, the main research question drawn for this research can be given as follows:

"How to assess the effect of reclaimed pavement materials and recycling agents on the fatigue and healing characterization of the asphalt mixtures?"

In the process of answering the main research question, mentioned tasks are also required to be addressed:

- *How to perform laboratory testing and develop a method to quantify fatigue and healing characterization of the asphalt mixtures using VECD theory.*
- *Which would be the reliable healing model for asphalt mixtures containing recycled asphalt materials and recycling agents involving temperature, damage state, and rest periods?*
- *How to validate the flexible pavement performance using the mixtures tested in the laboratory, which combines the time-scale differences and layered viscoelastic analysis.*

This study uses a hypothesis proposed by Dr. Kim and colleagues at North Carolina State University (NCSU) to characterize fatigue damage progression in asphalt mixtures generally independent of the mode of loading (FHWA 2022). This theory is based on the work potential theory (Schapery, 1990), which defines two internal state variables: pseudo-stiffness (C) and internal state parameter (S). The pseudo-stiffness C represents the overall integrity of the mixture, whereas S represents the overall damage within the specimen. The relationship between these internal state variables by means of the curve is called Damage Characteristics Curve. This curve represents the accumulation of damage in the mixture and is unique for a given mixture regardless of loading rate, stress-strain amplitude, and temperature. This model characterizes the damage. Healing is also defined as the reversal of damage in the material; hence this laid the basis for characterizing asphalt healing with VECD theory.

For the purposes of this research, a procedure to develop the healing model for the mixtures consisting of a high percentage of RAP was motivated by Ashouri, 2014. This model will consider the effect of temperature, rest period, and mixture damage condition on the healing potential of the asphalt mixtures. A procedure to perform the group rest healing test using a test setup other than an asphalt mixture pavement tester (AMPT) is also discussed in this thesis. The characterization parameters are then used in the FlexPAVE software to predict damage in a hypothetic multi-layer pavement structure.

1.3 Organization of the thesis report

This thesis report consists of 7 chapters and appendices.

Chapter 1 introduces the general need, approach, and research questions that should be answered for assessing fatigue and healing on asphalt mixtures.

Chapter 2 gives an insight into the mechanism involved in the fatigue and healing characterization of the asphalt mixtures. It also depicts the various laboratory testing methods available to characterize the fatigue and healing behavior of the asphalt mixtures. This chapter also includes all the literature review done for the healing mechanism in asphalt materials.

Chapter 3 details the background of viscoelastic continuum damage theory. This chapter discusses all the mathematics and formulations for damage prediction.

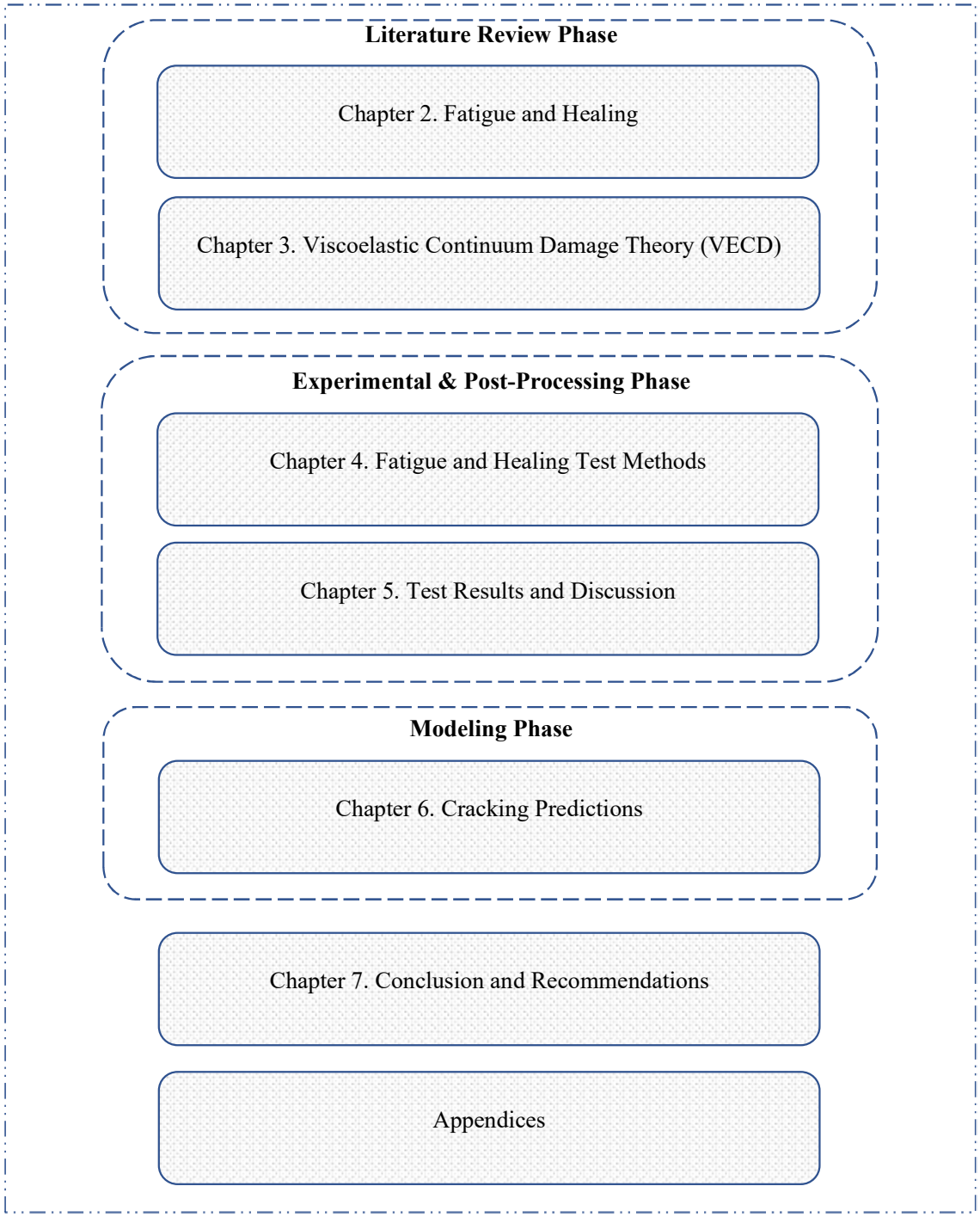

Figure 1.1. Organization of the thesis report.

Chapter 4 describes the approach and procedure for the laboratory experiments performed in this research. It entails all the details about the testing methods involved.

Chapter 5 discusses the main results and findings. Fatigue and healing characterization results are included in this chapter of the thesis.

Chapter 6 includes the results obtained from a damage prediction software named FlexPAVE. It gives the actual pavement performance results based on the post-processed results.

Chapter 7 provides the main conclusion and recommendations for future research.

Appendix A gives the procedure for formatting raw laboratory data to the required FlexMAT format for dynamic modulus and fatigue testing. **Appendix B** discusses the developments during the laboratory testing in this study. **Appendix C** elaborates on the fatigue testing results. **Appendix D** contains full results from the fatigue healing tests conducted during the study. **Appendix E** contains a thorough explanation of the FlexPAVE analysis results. **Appendix F** includes the details of the prediction of healing master curves.

1.4 Research Methodology

The research methodology for assessing asphalt mixtures regarding fatigue and healing characterizations involves a series of steps and tests, as in **Figure 1.2**. The first step is specimen preparation, where asphalt specimens are carefully prepared for experimental testing. Following this, the specimens undergo a dynamic modulus test to determine their linear viscoelastic properties, providing insights into their stiffness under varying load conditions. Subsequently, a cyclic fatigue test is performed on the specimens to evaluate their fatigue behavior, simulating the stresses experienced by pavements over time. The results obtained from the fatigue test serve as a basis for the subsequent healing test, which assesses the self-healing capability of the asphalt mixtures. This healing test examines the material's ability to repair and recover from damage caused during the fatigue test, including the closure of cracks and restoration of mechanical properties. The findings from the dynamic modulus, fatigue, and healing tests are then incorporated into FlexPAVE software, allowing for a pavement performance analysis. Finite element modeling analysis is conducted using a typical Dutch pavement structure to simulate and evaluate the behavior of the asphalt mixtures under various loading and environmental conditions. This comprehensive methodology combines experimental testing and computational analysis to provide valuable insights into the durability and performance of asphalt mixtures for pavement applications.

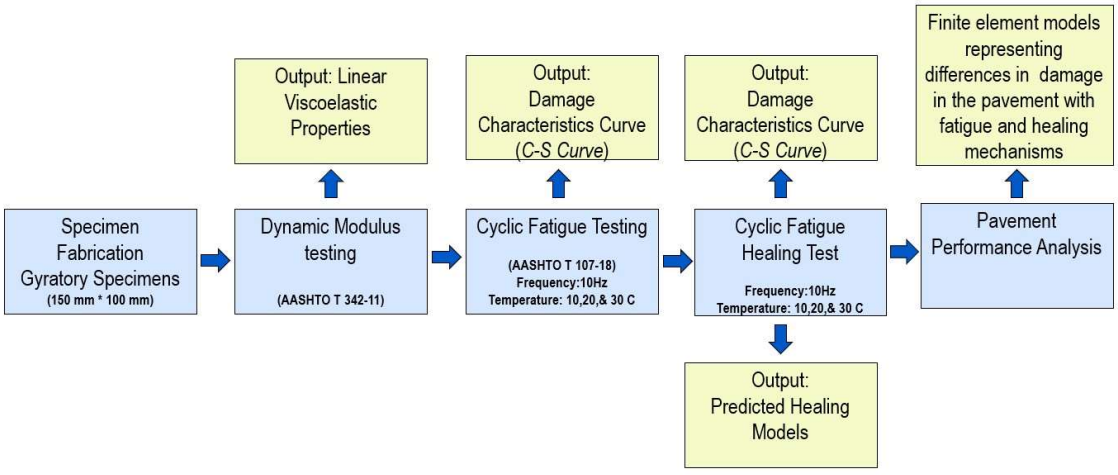

Figure 1.2. Research methodology.

References

Ashouri, M. (2014). *Modeling Microdamage Healing in Asphalt Pavements Using Continuum Damage Theory*. Ph.D. Thesis, North Carolina State University.

Federal Highway Administration. (2022). *Hot-Mix Asphalt Performance Related Specification based on Viscoelastoplastic Continuum Damage (VEPCD) Models*. Washington, DC.

Molenaar, A.A.A. (1983). *Structural Performance and Design of Flexible Road Construction and Asphalt Concrete Overlays*. Ph.D. Thesis, Delft University of Technology.

National Academies of Sciences, Engineering, and Medicine. (2022). *Relationships between the Fatigue Properties of Asphalt Binders and the Fatigue Performance of Asphalt Mixtures*. Washington, DC: The National Academies Press.

Qiu, J. (2012). *Self Healing of Asphalt Mixtures: Towards a Better Understanding of the Mechanism*. Ph.D. Thesis, Delft University of Technology.

Schapery, R.A. (1990). A Theory of Mechanical Behavior of Elastic Media with Growing Damage and Other Changes in Structure. *Journal of the Mechanics and Physics of Solids 38(2)*, pp. 215-253.

Chapter 2

Fatigue Damage and Healing in Asphalt Materials

2.1 Introduction

Due to its superior road performance, convenient restoration techniques, and comfortable driving conditions, asphalt pavement is a crucial type of pavement and has been extensively employed worldwide. With the rapid development of national economies and the further growth of modern road transportation demand, a considerable amount of asphalt pavement has been built. Fatigue is a phenomenon that causes a decrease in stiffness and strength, which eventually leads to the material failing under repeated loads. Fatigue resistance of the material is the propensity of materials to withstand such recurrent loads. Asphalt mixtures deteriorate under repetitive loading. The lack of maintenance, exceptional loads, absence of technological control of the materials, the deficiency in inspecting the quality parameters in the construction and operation stages, and the inexistence of drainage devices comprise the casual damage factors. Extreme weather conditions, combined with repetitive loading, cause significant pavement damage. Inadequate fatigue resistance leads to cracking, which is considered the major distress in pavement engineering.

Fatigue cracking in pavements has become a significant issue due to increased traffic loading on flexible pavements. Many researchers developed numerous test methods and prediction models over the past four decades to comprehend the idea behind pavement cracking (Hajj and Bhasin 2018; Ahmed, et al., 2019; Cheng et al., 2022; Sudarsanan & Kim 2022). With the initiation of cracks, pavements' structural capacity decreases, ultimately increasing the maintenance cost. These pavement fatigue fissures allow water and other substances to penetrate between pavement layers and damage components underneath. As a result, fatigue performance is an important factor to consider when designing flexible pavements.

2.2 Underlying Principles of Fatigue Cracking

Vehicle movement causes a variety of stresses on pavements. For a critical point under a wheel, they are given tensile and compressive stresses. The bottom of pavement layers experiences tensile stresses, whereas compressive stresses influence the top portion. The maximum tensile stresses are commonly developed at the bottom of the asphalt pavement layer under repetitive loadings. It is believed that the cracking initiates from the bottom part of the asphalt pavement and moves in an upward direction under the action of repetitive loading. These cracks appear on the surface as one or more longitudinal cracks. The phenomenon of the formation of cracks in the upward direction is termed “bottom-up cracking” (ARA, 2004) and is more evident in the case of thick pavements (thickness > 160 mm) (Molenaar 1983). Bottom-up cracking, or alligator cracking, is primarily attributed to the fatigue phenomenon. It occurs when the tensile stresses at the bottom of the base layer exceed a critical stress limit due to repeated traffic loading. This excessive tensile stress initiates cracks at the bottom of the layers, and these cracks gradually propagate toward the pavement surface, leading to pattern resembling alligator skin. Thus, bottom-up cracking is a result of crack formation and propagation from the bottom layers upwards, primarily caused by the fatigue-induced stress conditions at the base layer's bottom part. Top-down cracking is majorly due to wheel-pavement interaction and is more localized. The moisture in the base and subgrade layers increases the chances of bottom-up cracking in pavement structures. (Sudarsanan & Kim 2022).

As discussed above for pavements, the moving wheel induces horizontal, vertical, and shear stresses in pavement layers beneath. Understanding how the wheel load is transferred to a

pavement structure becomes important. **Figure 2.1** shows that alternate tensile and compressive stresses originate in the horizontal direction. The viscoelasticity of asphalt materials will affect the magnitude of the tensile strains developed in the pavements (Collop & Cebon 1995).

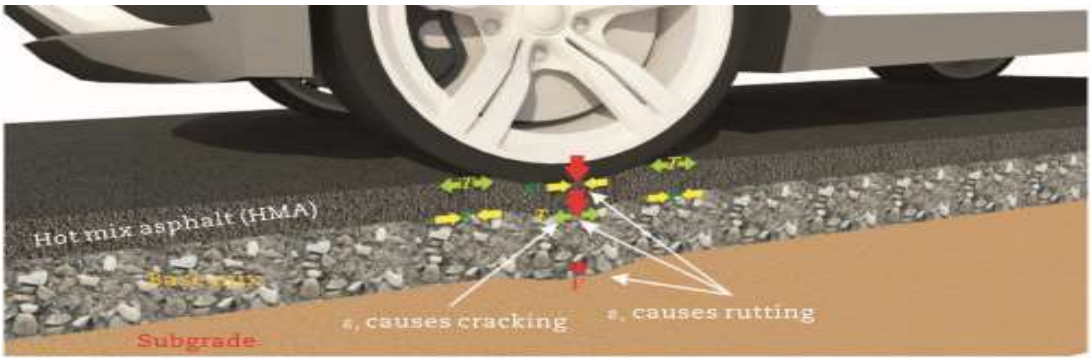

Figure 2.1 Stress formation under wheel load (Sudarsanan & Kim 2022).

According to **Figure 2.2**, the structural element is subjected to alternate tensile and compressive stresses in the horizontal direction while the vertical compressive stress changes with the wheel's movement in a half-sine wave. In general, for a well-designed material, the intensity of tensile stresses at the bottom layer is way less than the asphalt mixture's tensile strength, but over time due to the accumulation of these stresses with time exceeding the local tensile strength of the mixture leads to the formation of micro-cracks. Micro-cracks are a series of distributed parallel thin cracks in the top layer of pavements. Under fatigue due to wheel load, this micro-crack gets connected with transverse cracks forming macro-cracks. These cracks adopt a shape like an alligator's back hence termed "alligator cracking".

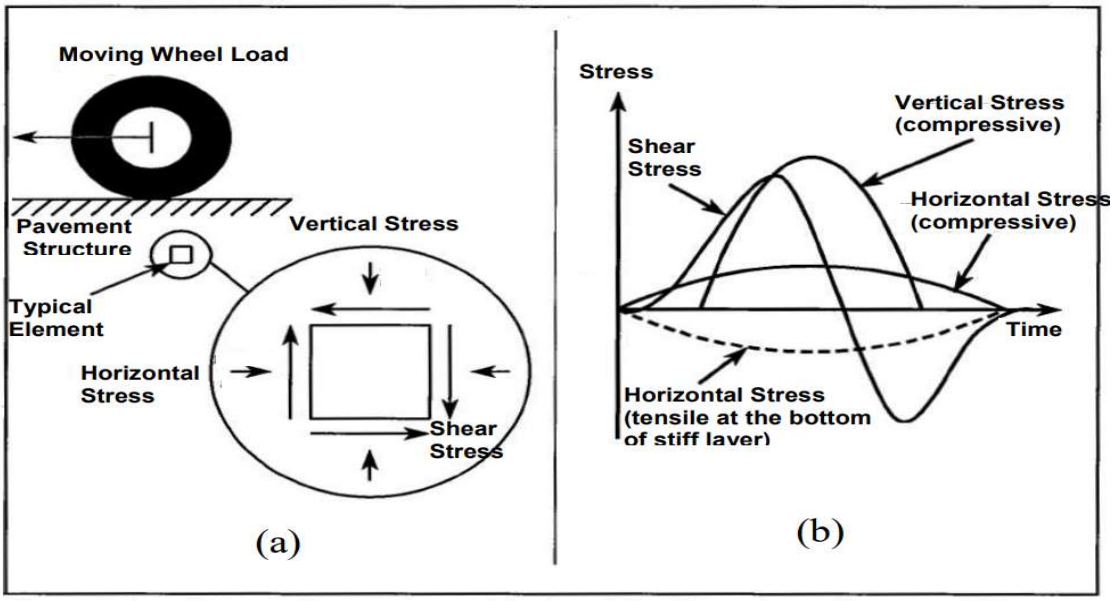

Figure 2.2. Stress formation in asphalt layers due to wheel loading.

2.3 Fatigue – From Field to Laboratory

Fatigue cracking occurs due to repetitive traffic loading. To simulate this effect in the laboratory, specimens of different shapes and sizes are tested at different temperatures, moisture conditions, and frequencies for various loading modes, rest periods, and other parameters. In the laboratory, cyclic loading on a specimen corresponds to the loading encountered by pavements. The specimen is subjected to cyclic loading, and the results of fatigue tests are expressed in the relationship of stress or strain with a few cycles to failure (Pell 1962). Pell represented this relationship with a straight line in a double logarithmic coordinate system as

$$N_f = k \cdot \delta^{-b} \tag{2.1}$$

where N_f is the number of cycles to failure, δ is applied stress or strain level [MPa], and k and b are material coefficients.

The specimen is put under high-frequency repetitive loads to assess the fatigue life in the laboratory. Then, a curve known as the E-N curve is plotted for fatigue analysis, where E stands for stiffness modulus, and N stands for the number of load cycles. A typical curve is shown in **Figure 2.3**. Three distinct phases for a material undergoing fatigue testing can be seen.

Phase I - adaptation phase: It is a crack initiation phase in which the stiffness modulus of the test specimen decreases rapidly due to repetitive loading; this decrease is because of non-linearity, self-heating, and thixotropy. These effects are also called biased effects. Micro-cracks are formed in the binder film present between the aggregates.

Phase II - quasi-stationary phase: It is the longest phase in the fatigue analysis of test specimens. The rate of stiffness modulus decrease due to fatigue slows down in this phase. The biased effects are present but are in a constant state (Pronk 1996). Their effect in the decrease of stiffness is small compared with damage due to fatigue.

Phase III - failure phase: The micro-cracks connect, and the creation of macro cracks begins. The stiffness modulus progressively declines, and the specimen is declared failed based on various failure criteria (Jacobs 1995).

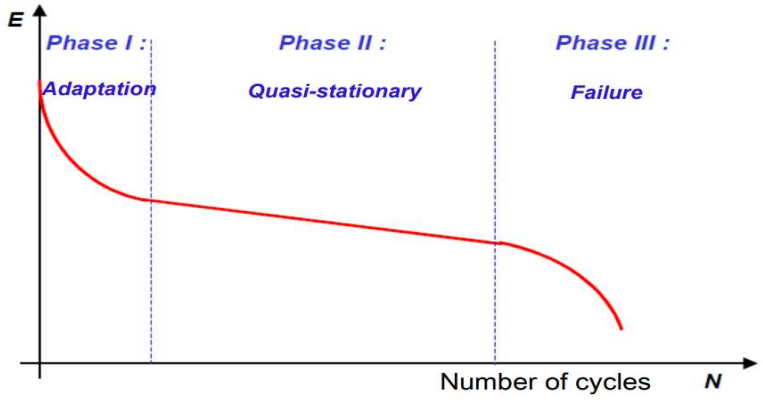

Figure 2.3. Typical fatigue curve for asphalt mixture (Li 2013).

2.4 Biased Effects in Fatigue of Asphalt Materials

The biased effects in fatigue of asphalt materials are as follows:

- **Materials non-linearity:** Nonlinearity in transmitting stresses can occur in asphalt materials due to the heterogeneity of the materials included in the mixtures. Due to the inter-aggregate spaces, the binder might undergo higher strain levels than the other material (Di Benedetto et al., 2004).
- **Thixotropy:** This is a characteristic phenomenon in non-Newtonian fluid (i.e., bitumen that causes its viscosity to decrease because of shear stress). The viscosity of the substance within the asphalt mixture fluctuates, causing the material to thin or thicken (Perraton et al., 2015).
- **Self-heating:** In fatigue testing, the specimen is subjected to cyclic loading, which induces energy in the sample. This energy is dissipated in the form of heat. The sample in the air-cooling chamber radiates this heat out. Pronk worked on this and showed that normal bitumen increased by 1°C (Pronk 1996).

These effects are considered to occur at a constant rate in Phase II of the *E*-*N* diagram. The assessment of these effects is beyond the scope of this study.

The time lag between the load input and displacement output cycles is defined as the phase angle (φ). It represents the viscosity and elastic properties of the asphalt binder. A viscous material has a phase angle of 90^{o}, whereas a 0^{o} phase angle is completely elastic. Whereas φ can be calculated using **Equation 2.2**

$$\varphi = 360 \cdot f \cdot \Delta t \tag{2.2}$$

where Δt is the time lag in maximum load and deflection [s] and f is loading frequency [Hz].

2.5 Failure Criterion

A consistent failure criterion must be specified to evaluate fatigue in asphalt material. Several studies have defined failure criteria regarding stiffness, phase angle, or dissipated energy. With the increase in the viscosity in the mixture due to the formation of micro-cracks, the phase angle also increases. There is more lag in the response of load to displacement. However, once the macro-cracks are formed, there is no accumulation of damage anymore; hence phase angle decreases rapidly (Kim et al., 2006).

To evaluate fatigue life, an endpoint to laboratory tests must be defined. However, the definition of failure is still a discussion among researchers. The fatigue failure criteria differ due to the type of loading on the sample, sample size, test setup, and even the different standardization norms of different countries. There is still a need for single fatigue failure criteria, which will apply to the whole field of asphalt fatigue testing.

Fatigue life is also defined by the Wohler curve, which is described as

$$\log N = n \cdot \log \lambda + k_1 \tag{2.3}$$

where k_1 and n are the fatigue coefficients determined experimentally, λ is the loading amplitude which can be load or displacement amplitude, and N is the number of cycles defining the fatigue life.

The most used failure criteria for fatigue analysis are the reduction of stiffness to 50% of its initial stiffness (Van Dijk & Visser 1977). The initial stiffness is defined as the stiffness of the material during the first 50 to 100 cycles. Under the stress-controlled test, the crack is observed in less time than in the strain-controlled fatigue test, for which the fatigue failure point in the stress-controlled test is near the fracture point of the specimen. Whereas in strain-controlled tests, the fracture is observed over a long period.

With the increase in the number of cycles, the phase angle increases to maximum value and drops. Researchers also consider this peak in phase angle a failure point (Reese 1997). There is another way to define the failure point based on the slope of stiffness vs. load on the specimen. It is observed to have two slopes in the curve of stiffness modulus vs. load. The first slope is during micro-cracks formation, and the other indicates macro-cracks formation. There is a visible transition point between both slopes, the failure point (Kim et al., 2002).

For the strain-controlled test, the energy ratio method defined by Hopman has also been used by many researchers in defining the failure point in fatigue testing. A curve for energy ratio to the number of cycles is shown in **Figure 2.4,** and a transition point is marked with a change of slopes in a curve, transitioning from micro-cracks to macro-cracks (Hopman et al., 1989).

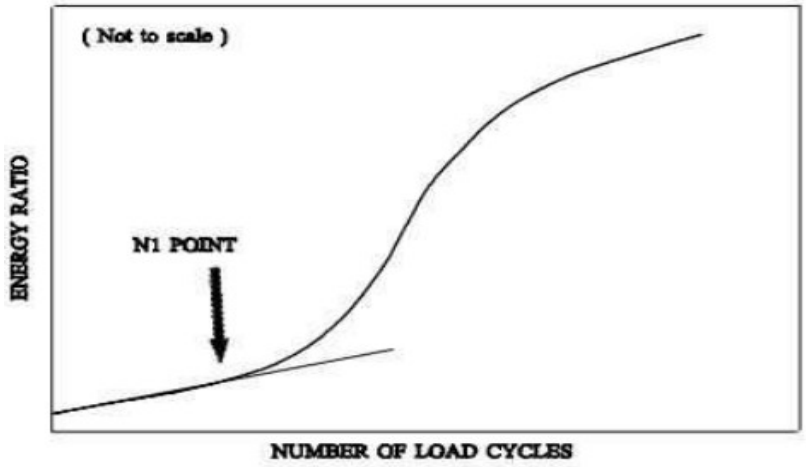

Figure 2.4. The energy ratio method (Hopman et al., 1989).

These are some major failure criteria opted by researchers to define the failure point in fatigue testing. In this study, before applying the viscoelastic continuum damage model, the fatigue failure point is defined with most conventional methods, which is the reduction in stiffness to 50%, and the corresponding number of cycles will give the fatigue life of the specimen.

2.6 Fatigue Damage Theories

The fatigue behavior of asphalt mixtures can be characterized using fracture mechanics, classical fatigue analysis (50% of the initial stiffness), phase angle transition point, dissipated energy methods, and S-VECD.

2.6.1 Fracture mechanics

For flexible pavements under cyclic loading, fatigue assessment can also be done based on fracture mechanics. The empirical-based mechanism to assess the fatigue life of materials such as Palmgren-Milner had some limitations. For rigid pavements, practical fracture mechanics-based models for fatigue prediction are emerging. The basic concepts of fracture mechanics are introduced, giving an alternative way to define fatigue properties (Griffith, 1921). The improved understanding of crack formation and propagation in pavement materials is reflected in fracture simulations. This mechanistic approach is a more feasible method for replacing the conventional flexural strength parameter used in the design.

The major benefits of using fracture mechanics for the assessment of the fatigue life of materials are:

- stresses are incorporated in the design approaches, considering the energy dissipation to display the growth of a crack. To describe the development of the crack in asphalt materials, the stress level at which the fracture starts and the fracture energy required to grow the crack must be known.
- structures with the same materials will not have the same flexural strengths due to size effects. The stiffness modulus of rupture will depend on the geometry of the structure. The accuracy of predicting fatigue life in flexible pavements due to size effect and boundary conditions by beam fatigue test is questionable. Fracture mechanics accounts for the size effects and the difference in the energy released at the fracture point. The more energy is released, the earlier the damage will be. For this, fracture mechanics predict the size effect using size-independent material properties (Wu et al., 2009).

The fracture mechanics concept assumes that fatigue failure occurs in a material in three phases. These three phases are (1) crack initiation, (2) stable crack growth, and (3) unstable crack propagation. The duration of the second phase (i.e., propagation of cracks) is the longest.

Paris and Erdogan coined this crack propagation phase (Paris & Erdogan 1963). To quantify this phase, models based on fracture mechanics are proposed. The rate of propagation of the crack with the number of cycles is given by

$$\frac{dc}{dN} = A \cdot K^n \tag{2.4}$$

where c is the crack length [inches], N is the number of cycles [1], K is the stress intensity factor [ksi*in^0.5] which defines the stress condition at the crack tip, and A, and n are the parameters that depend on the material and experimental conditions.

2.6.2 Dissipated energy method

The dissipated energy method is an approach opted for by many researchers in characterizing fatigue failure in asphalt mixtures. It is believed that there is always a loss of energy with every cycle of constant load implemented to any material. Dissipated energy (DE) is termed as the damping energy or the energy loss per load cycle in any repeated, cyclic, or dynamic test (Carpenter and Ghulzan, 2000). Different materials try to recover the energy in different ways upon removing the load. A comparison to which is depicted in **Figure 2.5.**

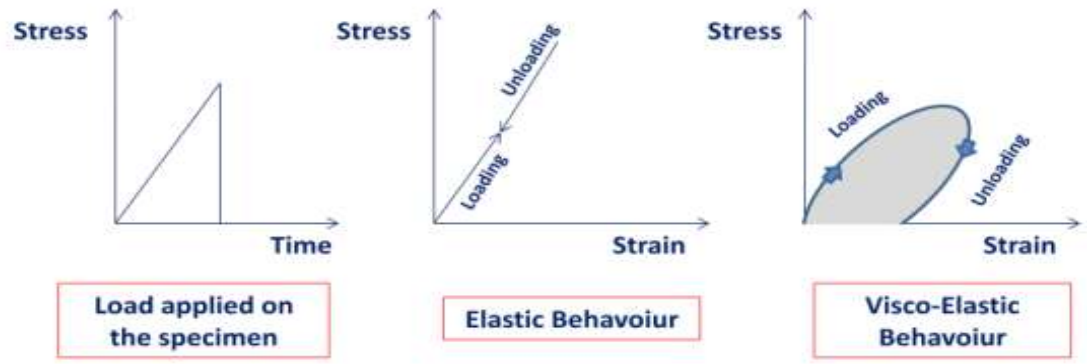

Figure 2.5. Elastic and viscoelastic behavior (Maggiore et al., 2012).

For an elastic material, the loading and unloading follow the same path. The stress vs. strain curve for an elastic material varies linearly. The loading and unloading follow the same path due to the full recovery of energy lost due to the application of load. The dissipated energy for elastic material can be calculated as the area under the stress-strain curve. In visco-elastic materials such as bitumen, this trend is a bit different. When a viscoelastic material is loaded sinusoidal, a phase lag is observed in the stress applied to the strain. Due to this phase lag, the stress-strain curve cannot trace the same path upon unloading. A loop is created in loading and unloading such materials, known as "hysteresis". The area of this hysteresis loop gives the dissipated energy. The dissipated energy per cycle can be calculated as

$$W = \pi \cdot \sigma \cdot \varepsilon \cdot sin\varphi \tag{2.5}$$

where W_i is the dissipated energy in cycle i, σ_i is the stress level for cycle i, ε_i is the strain level in cycle i, and the phase angle for that cycle is defined by Φ_i.

This energy loss in the case of visco-elastic material is in the form of mechanical work, heat generation, or damage as the formation of micro-cracks. During cyclic testing, it is already mentioned that the stiffness of the mixture keeps changing during different cycles. Hence stresses, strains, and phase angle changes per cycle as well. Ultimately, it led to variable dissipated energy per loading cycle. The factors on which the dissipated energy per cycle depends change with each cycle based on the loading mode. For stress-controlled loading, the stress is kept constant, and strain increases. The strain is constant for strain-controlled testing, and stress decreases with load cycles. Hence, the dissipated energy increases for every load cycle in stress-controlled testing and decreases for strain-controlled testing (**Figure 2.6.**).

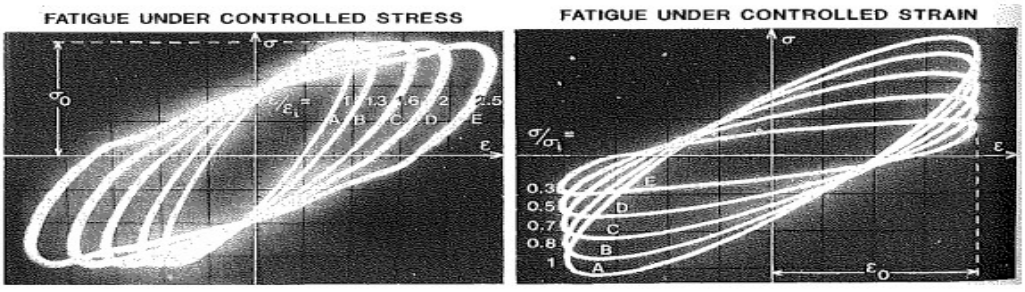

Figure 2.6. Hysteresis loop variation with each cycle for a different mode of loading (Francken, 1987).

Using this mechanism, the failure criteria for fatigue characterization can be given using the 'Energy Ratio'. This energy ratio is given as

$$Energy\ Ratio = \frac{n \cdot w_0}{w_i} \tag{2.6}$$

where n is the number of cycles, w_o is the dissipated energy at the start of the test, and w_i is the dissipated energy for the i cycle.

This "Energy Ratio" is plotted against the number of cycles that gives a change in slope at the N_1 cycle. The behavior of material changes at N_1 gives information about the formation of the macro-cracks, the failure point. Further simplification can be done by substituting **Eq. 2.5** in **Eq. 2.6**.

$$Energy\ Ratio = \frac{n \cdot (\pi \cdot \sigma_0 \cdot \varepsilon_0 \cdot sin\varphi_0)}{\pi \cdot \sigma_i \cdot \varepsilon_i \cdot sin\varphi_i} \tag{2.7}$$

Further, the stresses σ can be substituted with $E{\cdot}\varepsilon$. The equations will be reduced to

$$Energy\ Ratio = \frac{n \cdot (\pi \cdot E_0^* \cdot \varepsilon_0^2 \cdot sin\varphi_0)}{\pi \cdot E_i^* \cdot \varepsilon_i^2 \cdot sin\varphi_i} = \frac{n \cdot E_0^* \cdot sin\varphi_0}{E_i^* \cdot sin\varphi_i} \tag{2.8}$$

$E_0^* \cdot sin\varphi_0$ can further be removed as it will be a constant and will not affect the shape of the curve. The final equation for energy ratio in a strain-controlled test can be given as follows

$$Energy\ Ratio = \frac{n}{E_i^* \cdot sin\varphi_i} \tag{2.9}$$

Studies showed that the change in sinφ is very small compared to the change in E^*, which will be ineffective in changing the curve shape. Hence finally, the equation for energy ratio be written as after all simplifications.

$$Energy\ Ratio \simeq \frac{n}{E_i^*} \tag{2.10}$$

2.6.3 Rate of dissipated energy change method

The Rate of Dissipated Energy Change (RDEC) is another parameter some researchers use to characterize the fatigue performance of asphalt mixtures (Ghuzlan and Carpenter, 2000; Shen, 2007). This parameter does not include energy dissipation due to mechanical work or heat generation. Therefore, it is a more accurate factor to assess fatigue characteristics and be used as a failure criterion. *RDEC* for cycle n can be given as follows

$$RDEC = \frac{DE_{n+1} - DE_n}{DE_n} \tag{2.11}$$

where *RDEC* is the ratio of dissipated energy change per load cycle, DE_n is the dissipated energy in load cycle n [kPa], and DE_{n+1} is the dissipated energy produced in load cycle n+1 [kPa].

For the measurements over time, the equation can be further modified based on non-standard intervals as (Shen and Carpenter, 2007)

$$RDEC_n = \frac{DE_{n+1} - DE_n}{DE_n \cdot (N_{n+1} - N_n)} \tag{2.12}$$

where N_n is the number of load cycles at n, DE_n is the dissipated energy in load cycle n [kPa], DE_{n+1} is the dissipated energy produced in load cycle n+1 [kPa], N_{n+1} is the number of load cycles at n+1.

$RDEC_n$ gives the dissipated energy change over two cycles over time. It also accounts for the percentage of dissipated energy that damages the material. The hysteresis curve plotted for dissipated energies of two cycles will partially overlap each other. The area which is left out in the overlapping part will give the dissipated energy change between the two cycles. The area in red in the given diagram will give the change between the two cycles, as mentioned in **Figure 2.7**.

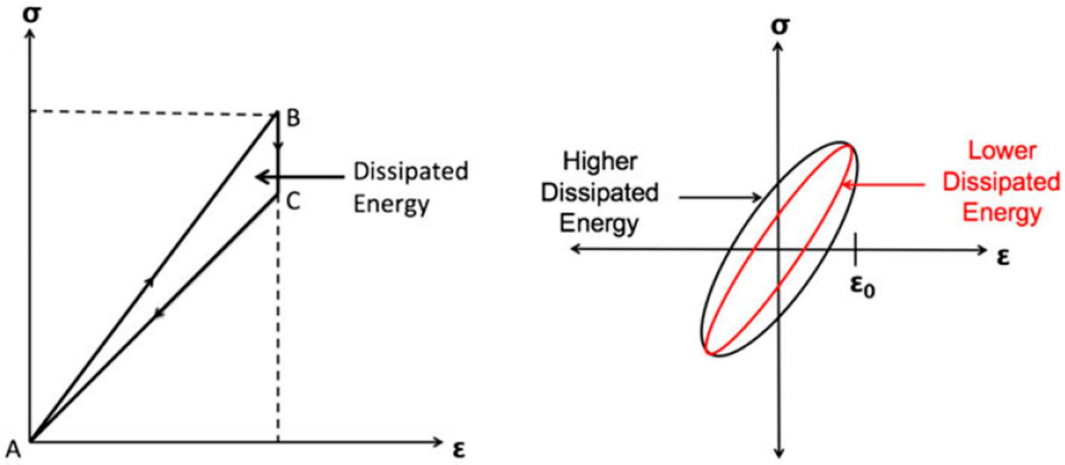

Figure 2.7. Dissipated energy for an elastic material (left) and two different viscoelastic materials (right) (Hajj & Bhasin 2018).

For strain-controlled testing, which is adopted in this study, the plot for the *RDEC* vs. the number of loading cycles for asphalt binders is shown in **Figure 2.8.** Especially, there are three phases obtained from *RDEC* vs. a number of cycles curve. Firstly, the *RDEC* value decreases rapidly and reaches an almost constant value known as Plateau Value (*PV*). This plateau value represents the state at which the constant rate of energy input is converted into damage. Lastly, the *RDEC* increases rapidly, causing fatigue failure with initiation in forming macro-cracks. The point of initiation of macro-cracks or the point of increase of *RDEC* is the failure point; hence the number of cycles corresponding to that point is the fatigue life of the sample.

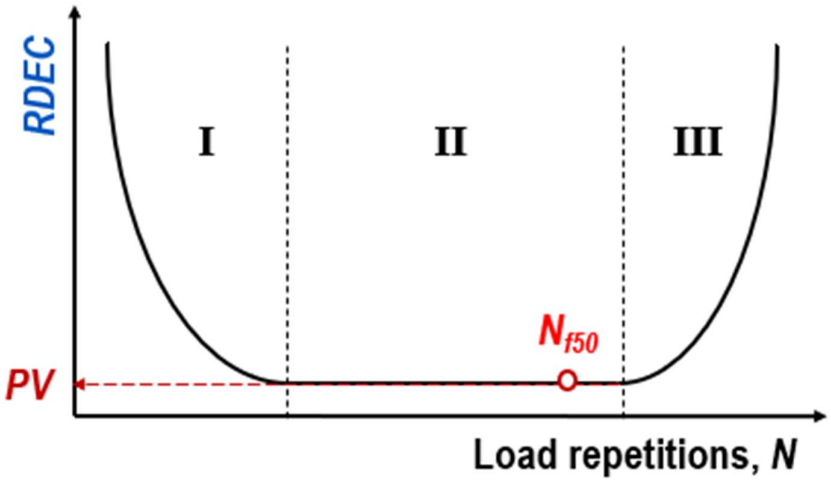

Figure 2.8. RDEC Approach.

2.7 Fatigue Testing Methods for Asphalt Mixtures

Fatigue cracking occurs on the field due to the repetitive movement of vehicles on the pavement. The failure criteria based on stiffness, energy, stress degradation, etc., are used to define the fatigue life of the asphalt mixtures. This section of the thesis discusses recommended laboratory test methods for simulating such loads as pavement experiences to assess the performance of various asphalt mixtures. Fatigue performance evaluation on asphalt materials gives an essential reference for the asphalt mixture and pavement structure design (Cheng et al., 2022).

The ability to anticipate the structural performance of pavement near field applications is aided by the combination of fatigue tests and models generated based on laboratory testing. Researchers and engineers have widely used a variety of laboratory fatigue tests to assess the fatigue performance of the asphalt mixture due to the low cost, high efficiency, and strong operability (Cheng et al., 2022). Test methods differ in loading mode, frequency, waveforms, temperature, and controlled mode. Uniaxial tension-compression fatigue loading, indirect tensile fatigue, four-point beam bending, three-point beam bending, two-point beam bending, and supported flexure tests are the major test methods used in analyzing the fatigue of asphalt mixtures (Sudarsanan & Kim 2022).

2.7.1 Four-point bending test

The fatigue life and the failure energy determined by this standard can be used to estimate the fatigue life of the asphalt pavement layers under repeated traffic loading. The performance of asphalt mixtures can be more accurately predicted when these properties are known (AASHTO T 321-147). This test gives information about the fatigue characteristics of different temperatures and loading frequencies. The major advantage of the constant bending moment is almost zero shear force. According to NEN-EN12697-24, the four-point bending (4PB) fatigue test is carried out, and NEN-EN 12697-26 is used to compute stiffness. Other norms available to perform a 4PB test are AASHTO T 321-147.

For the 4PB cyclic test, a standard prismatic beam of 380 mm in length, 63 mm in width, and 50 mm in height is required (see **Figure 2.9**). Two inner clamps are generally separated by 120 mm. The 4PB test is a displacement-controlled test that evaluates standards. Loads are applied at two third points to keep the bending moment constant throughout the mid-span of the beam. The load magnitude applied by the actuator and the deflection measured at the center of the beam are recorded and used to calculate the stiffness. The displacement and hence the strain are maintained constant over time. The beam is in-homogenous and perfectly inelastic.

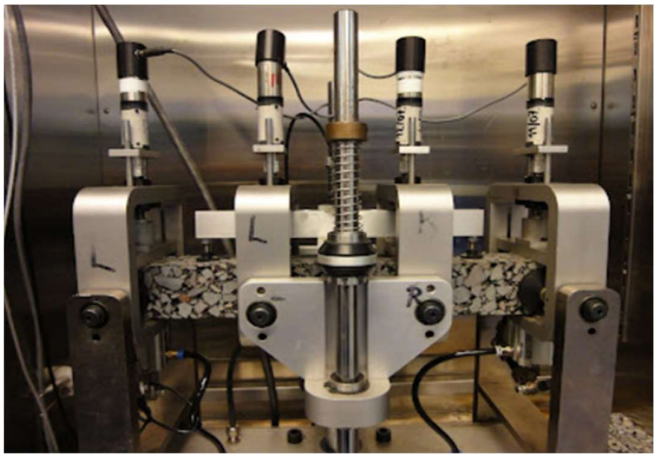

Figure 2.9. Four-point bending test setup in TU Delft laboratory.

At a specific strain level, the top and bottom of the beam experience the highest strain, with the top in tension and the bottom in compression. Generally, the desired initial strain ranges from 250 to 750 μstrain, and the loading frequency ranges from 5 to 10 Hz. It is preferred to choose a strain level such that the specimen will experience at least 10,000 load cycles before failing. In 4PB tests, a reduction to 50% of the initial stiffness is typically used as the failure criterion (Molenaar 1983). In the 4PB test, the stiffness at the 50^{th} load cycle is used as the initial stiffness. With the 4PB test, the stiffness moduli as a function of time and frequencies and the fatigue behavior of the asphalt mixture in displacement-controlled mode are calculated. The load cycle at which the peak occurs in the plot of stiffness multiplied by load cycles versus the load cycles indicates the formation of a crack in the mixture (AASHTO T 321-147).

2.7.2 Cyclic indirect tensile test

The cyclic indirect tensile test (CY-ITT) is an advanced development for the monotonic indirect tensile test or ITT. This test is developed in the early 1970s to characterize asphalt materials for their strength and stiffness (Kennedy 1968). In CY-ITT, the force is applied at a constant rate. The displacement will be measured from which the stiffness or resilient modulus of the specimen is calculated. The linear slope of this constant force with measured displacement gives the stiffness. The test in the TU Delft laboratory is performed in accordance with EN 12697-26 or ASTM Designation: D4123-82, which includes rest periods as well. A pulse loading force is generally applied to the specimen, and the total diametrical stain is measured from axes 90^{o} to applied forces. In this test, only the horizontal displacement is measured. There is a visible displacement in the vertical direction, but it is not measured. Instead, the horizontal displacement is measured, and the vertical displacement can be computed using the Poisson number. Poisson's ratio is generally taken as 0.4 by default.

Figure 2.10. Cyclic indirect tensile test setup.

The sample preparation for this test is generally 100-150 mm in diameter and 40-50 mm in height. In the test setup, two LVDTs are used to measure the displacement in the horizontal direction. Load is generally transferred via a small steel beam with a width of 12.7 mm (**Figure 2.10**). All test specifications are performed with specifications mentioned in NEN-EN12697-24:2018. The frame used to clamp and transfer the load can influence the sample. The heavier and stiffer frame will have a stiffer response from the sample. This test differs from other tests because it requires a sample always in compression. The sample in compression will ensure that only deformation will be in the horizontal direction. The test setup available in the TU Delft laboratory is shown in **Figure 2.11.**

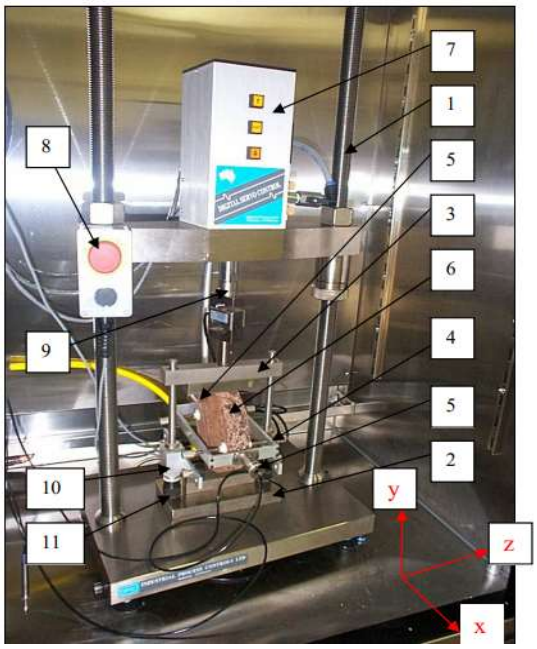

1 = loading frame with cross head and nuts
2 = indirect tensile jig
3 = top platen
4 = transducer yoke
5 = radial LVDTs
6 = seated specimen
7 = controlpanel of the actuator
8 = emergency stop
9 = loading shaft
10= cross-arms
11= threaded support spacers

Figure 2.11. TU Delft laboratory set-up of the indirect tensile modulus test.

Mainly for each five loading pulses, from the data Resilient Modulus E_r, total and individual recoverable deformations and peak loading force are calculated. Along with calculated data from five loading pulses, mean, standard deviation and coefficient of variance are calculated. A master curve is generally developed by performing tests at several temperatures for a series of different

pulse widths. With this master curve, the stiffness is expressed as a function of temperature and frequency. The principle behind this approach is the equivalence of temperature and frequency for linear viscoelastic materials. Haversine load is specified as full sine below zero. In other words, the pulse width is defined by the reciprocal value. The sample will probably crack. Generally, the pulse width for CY-ITT is kept to 3 s. By performing this test, the stiffness modulus, horizontal deformations, and peak load will be calculated. Performing CY-ITT is beyond the scope of this research. Fatigue fracture under indirect tensile loading ideally should occur by splitting the sample into two halves with minimum permanent deformation. The loading time should be 120 ms, and the temperature should be less than 30°C (Read & Collop 1997).

2.7.3 Uniaxial tension-compression fatigue test

The uniaxial tension-compression fatigue test method covers the procedure for preparation and testing asphalt concrete mixtures to determine the damage characteristics curve and the failure criterion. This research is based on the Visco-Elastic Continuum Damage (VECD) theory (FHWA 2022). According to this hypothesis, crosshead-controlled testing with zero-minimum crosshead displacement should be used to subject samples to tensile and compressive stresses. The applied stress will be measured on the specimen along with the axial strain response to calculate the necessary quantities. The damage characteristic curve and failure criterion for the specimen can be determined using the Asphalt Mixture Performance tester (AMPT) cyclic fatigue test (AASHTO TP 107-18). The standard test is applicable for the nominal maximum size aggregate less than 25 mm, which is 22 mm in sample preparation for the mixtures involved in this research.

Figure 2.12. Test setup for uniaxial fatigue and healing testing.

The main outputs required are damage (S) and pseudo-secant modulus (C), which will be plotted against to give damage characteristics curve. These variables are independent of temperature, rate of loading, and frequency. This eradicates the viscoelastic behavior of asphalt material,

further easing the analysis of the fatigue characteristics of asphalt concrete mixtures. Cylindrical specimens are prepared in a Superpave Gyratory Compactor (SGC). 150 mm by 100 mm cores from 160 mm by 120 mm cylindrical samples are removed and polished from both ends to provide perpendicular surfaces for testing (see **Figure 2.12**). **Chapter 4** provides additional information regarding test setup, specimen fabrication, and testing protocols. Even the testing process for measuring healing will be comparable.

The main reasons to use this test method instead of going for conventional tests by road contractors are as follows (adapted by Tian 2010)

- The stress state is non-uniform and varies over depth.
- Beam element fabrication equipment is not easily accessible.
- Some fatigue tests are empirical, which can result in significant errors in the prediction of material performance (due to several assumptions). In contrast, industry and researchers are moving towards mechanistic approaches with rigorous theoretical considerations. Axial uniaxial compression tension testing is one of them, and it is used for VECD.
- Future testing will be simpler if the core is taken from existing pavements rather than testing the beam in a lab.
- Load and deformation are in similar directions, keeping deformation and load in the phase.

2.8 Healing in Asphalt Materials

2.8.1 Definition and significance

Asphalt materials can heal. With governments and contractors moving toward constructing more sustainable pavements, self-healing pavements are of great interest to researchers (Tabakovic & Schlangen 2016). The main challenge in modeling the fatigue performance of asphalt mixtures is predicting the performance of asphalt pavements in laboratories for complex traffic loading in the field. The laboratory studies can be correlated with field fatigue performance using certain shift factors. NCHRP Project 9-38 reported the shift factors determined from four test sections in the 2003 NCAT test track study range from 4.2 to 75.8 (NASEM 2010). The shift factor relating laboratory tests to pavement fatigue life in service ranges from 10 to 100 (Deacon et al., 1997).

The fatigue performance of asphalt pavements under traffic loading differs in the laboratory and the field. The main reason is the occurrence of rest periods on pavements in the field. This rest period induces healing in pavements, differentiating the laboratory and field performance. The rest period has a significant role in the performance of asphalt pavements, and there is a need to investigate healing.

According to the literature on asphalt materials, healing is defined as partial or complete damage recovery, further defined as the increase in material stiffness and strength. To analyze the fatigue life of asphalt mixtures in field conditions, the process for fatigue damage propagation and healing during rest periods must be known. Considering this, self-healing of asphalt has the potential to reduce carbon dioxide (CO_2) production, the usage of natural resources, the demand for new aggregates, and enhance road safety. In this research, the loss in stiffness is damage, whereas, with the implication of rest periods, the increase in material stiffness will be due to healing.

Self-healing of a material can be defined as:

"The ability to substantially return to an initial, proper operating state or condition prior exposure to a dynamic environment by making the necessary adjustments to restore normality and/or ability to resist the formation of irregularities and/or defects" (Fisher 2010).

A schematic representation of the steps involved in the healing mechanism with means of different processes is depicted in **Figure 2.13.** Any response resisting the damage is in the direction of healing materials. Fisher 2010 explained two categories of healing: attribute repair (complete repair to the original state) and functional repair (restoration till functionality of the system). Some researchers believe that healing in asphalt materials momentarily increases the material stiffness, while others argue that it improves the fatigue life of the material. Most of the research on asphalt mixture healing has been conducted on the factors affecting the amount of healing, such as temperature, rest period, loading mode, specimen damage prior to the healing period, the effect of polymer-modified asphalt binder on material healing, aging, properties of binder used in the mixture, and so on. Healing is a concurrent phenomenon that occurs with the development of damage in the specimen during the fatigue test, not merely during rest periods applied between loading cycles (Ashouri 2014). However, most researchers believe that healing occurs in asphalt mixtures and substantially impacts the fatigue life of asphalt mixtures.

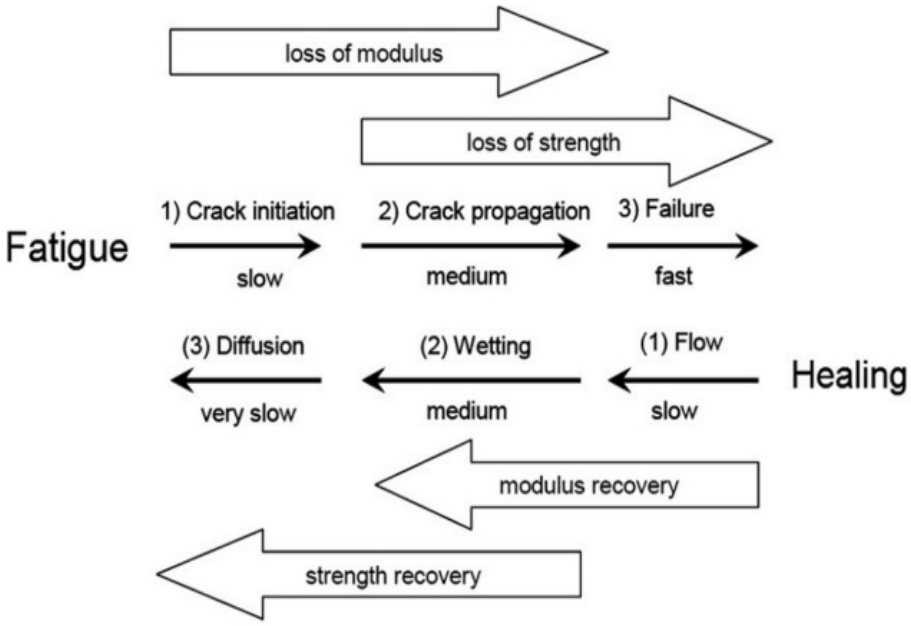

Figure 2.13. Three-step mechanism of healing (Qiu 2012).

To model such a problem in laboratories, what kind of stresses and strains the pavement experiences under field conditions should be thoroughly understood. Cyclic loading in laboratories can take two forms: strain-controlled and stress-controlled loading. However, the load combination generated in pavements by tire pressure and vehicle weight is neither. It is a combination of these, but achieving this in a laboratory is impossible. To do this, the test is carried out to be as close to the field condition as possible.

2.8.2 Mechanism of healing

With the movement of vehicles on the pavement, micro-cracks are generated along the pavement structure, which are restorable with the implementation of rest periods. Asphalt pavements can

restore stiffness and strength by closing these micro-cracks. The asphalt binder type and content, aggregate type and gradation, aging, material, pavement thickness, temperature, loading history, rest period, and other environmental factors are some factors that affect the healing potential of asphalt mixtures. Although it is believed that environmental factors could influence the performance and, subsequently, the healing potential of asphalt materials in base layers, they are assumed negligible. The effect of environmental factors on the healing potential of asphalt materials in the base layer is beyond the scope of this study.

Under recurrent loads, external loading produces pavement deformation. When this stress is removed, flexible pavement is subjected to two key processes: viscoelastic recovery and micro-crack healing. The mechanism of viscoelastic recovery is the rearranging of molecules in the substance. The primary idea behind micro-crack healing is the wetting and inter-diffusion of binders in the crack faces, which leads to increased stiffness and strength. When a liquid encounters a solid, the capacity of the liquid to retain that contact, which is dependent on intermolecular interactions, is referred to as wetting. This intermolecular property of the binder defines its surface energy. The higher the surface energy of the binder, the greater its wetting power and the greater the healing capacity of the mixture with this binder (Bhasin et al., 2008).

The healing mechanism described in prior studies is a three-step process(**Figure 2.14.**). In the process given by Wool & O'Connor in 1981, the healing process begins with wetting, which is the gap closure caused by adhesion, mostly due to the free surface energy of binders. It is then followed by a flow of binder molecules in the crack faces, known as molecule diffusion. Third, the randomization of these molecules results in stiffness and strength recovery. In this study, it is also believed that wetting is the most responsible for stiffness recovery (**Figure 2.14**.).

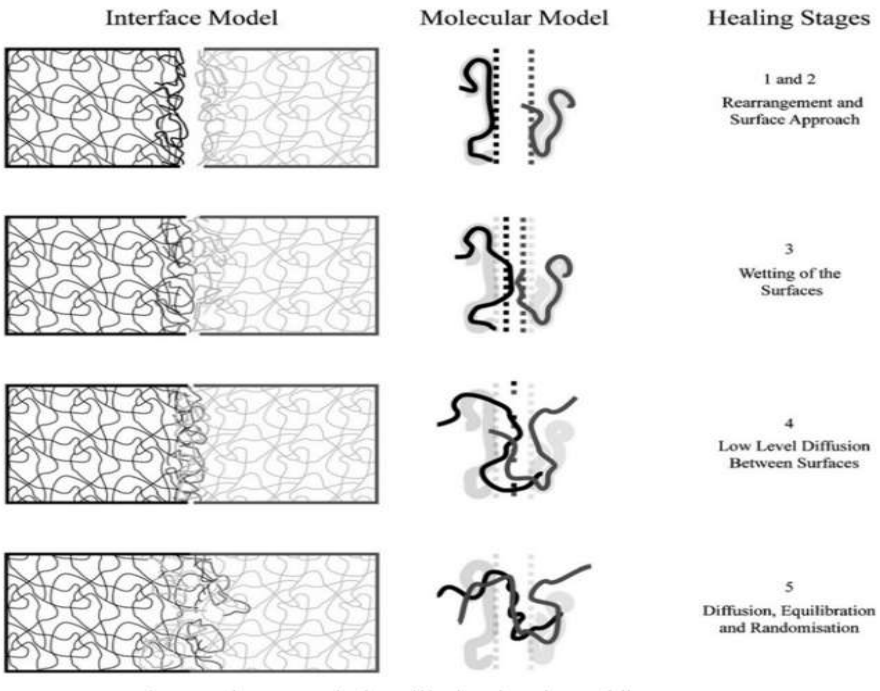

Figure 2.14. The mechanism involved in self-healing through inter-diffusion (Wool & O'Connor 1981).

2.8.3 Factors affecting healing

Several factors affect the healing of asphalt mixtures. An overview of such factors is given in this sub-section. The major factors that affect healing potential are:

- Temperature: It is one of the most important factors in healing asphalt mixtures. As the temperature rises, the binder becomes less viscous and begins to flow. This temperature increase causes the binder to flow into micro-cracks, resulting in crack healing. As a result, as the temperature rises, so does the healing potential of the mixture.
- Rest Period: It is defined as the time between cyclic loads to allow the mixture to heal and regain lost stiffness and other mechanical properties. It is another crucial aspect in assessing the mixture's healing capability. The longer the rest period, the better the mechanical property recovery in the mixtures.
- Damage Level Prior to Rest Period: As the number of cycles increases, the damage also increases. After a certain level of damage, the rest period is applied to heal the asphalt mixture in this study. The mixture tends to heal, but the amount of damage prior to applying the rest period increases. The healing capacity in the mixture decreases, and higher damage growth is visible in the mixtures.
- Binder: It is the major component that defines the performance of the mixture. The chemical composition and physical properties of the binder affect the mixture's performance. The aging of the binder will have an inverse effect on healing in the mixture. As already mentioned, a binder with higher free surface energy will positively affect the healing of the mixture.
- Aging: It makes the material brittle. The aged binder ceases to flow as compared to the virgin binder. It is believed that the more aged binder in the mixture is, the less flowability is. Hence lower will be the healing capacity of the mixture. This factor in healing has more significance in the mixtures of this study with 70% of reclaimed asphalt pavement (RAP).
- Water: The presence of water has an immense significance in asphalt healing. Water might have a higher affinity toward aggregates than that binders, causing negative effects on the healing of the binder-aggregate adhesive bonds. It promotes fracture rather than healing.
- Mixture Gradation: The ultrasonic wave velocity is used to assess fatigue damage and healing in asphalt mixtures. This test is carried out on samples before and after the fatigue test and the rest periods. Higher size aggregate samples will have a smaller transition zone and a thicker binder film between aggregates, increasing the sample's healing capacity.

2.8.4 Methods to implement rest periods in fatigue testing

It has already been discussed that the rest periods in laboratory fatigue testing are analogous to healing time on pavements when there is no movement of vehicles. If sufficient time for healing is provided for a mixture, it will tend to recover mechanical properties. In the field, this rest period exists between the load pulses of vehicle axles. Generally, two major ways of simulating this rest period in laboratories exist.

- **Group-rest healing test:** In group-rest healing or rest interval testing, firstly, the point at which the rest period must provide will be fixed. It can be based on the number of cycles. After reaching that point, the decided rest period will be provided, and the fatigue test will be performed for another number of cycles. The testing of samples with this method is faster as compared to intermittent testing. It becomes easier to simulate such testing in the laboratory. This research will select this methodology to analyze the healing providing rest periods in uniaxial tension-compression fatigue testing.

- **Pulse-rest healing test:** In the pulse-rest healing test or intermittent testing, each loading cycle is followed by a rest period. The rest period in this testing is generally a multiple of loading time. This type of loading resembles the real application of loading on the pavements. But the disadvantage of simulating such tests in the laboratory is time consumption.

The above-mentioned methods to apply rest periods in the fatigue testing to assess the healing along with the fatigue tests are depicted by means of a schematic diagram in **Figure 2.15.**

Figure 2.15. Tests method with and without rest period (Castro & Sanchez 2006).

The fatigue-healing tests are also classified based on the application of rest periods as storage healing tests and intermittent healing tests. In the storage healing test, the rest periods are provided after the specimen reaches a pre-decided level of damage. The loading pattern in intermittent healing tests is the same as the pulse rest healing test mentioned above.

2.9 Previous Experience in Healing in Asphalt Materials

Healing in flexible pavements has been a research topic since the early 60s. The major studies assessing the healing potential at the asphalt mixture level are discussed in this sub-section.

The effect of the rest periods in cyclic fatigue testing was investigated on asphalt mixtures. The loading time was 1 s, and three different rest period of 1, 3, and 19 s was used at 3, 15, and 30 cycles per minute of frequency. The temperature during the test was kept at 77^{o}F. This study predicted that the increase in the rest period did not increase life (Secor & Monismith 1961).

In another study, longer rest periods were implemented on samples to assess the influence of rest periods. The two-point bending fatigue test was performed at 50 Hz and 10^{o}C up to failure. Then, a test with a rest period of hours extending up to 100 days was performed, yielding twice the fatigue life of materials tested without the rest periods (Bazin & Saunier 1967).

The beam with dimensions of 75 mm* 75 mm * 225 mm was subjected to an axial load test. At 10 and 25^{o}C, tension-compression load-controlled mode was used. The loading frequency was kept between 2.5 and 25 Hz. The intermittent application of rest times ranging from 40 ms to 800 ms increased fatigue life by a factor of 5 compared to the specimen examined without rest periods. After achieving an optimum rest period, the fatigue life of asphalt mixtures no longer improved (Raithby & Sterling 1970).

The fatigue testing was carried out in a three-point bending apparatus at 20^{o}C and 40 Hz. As expected, the introduction of rest periods in tests improved fatigue life (Van Dijk & Visser 1977).

The fatigue testing was performed on the beam 230 mm * 30 mm * 20 mm dimension in three-point bending apparatus. For the test, the frequency of loading is taken as 40 Hz. Three temperatures 5, 20 and 25^{o}C were chosen for testing. The rest period was given in pulse-rest form

as 0, 3, 5, 10 and 25 times the length of the loading cycle. The outcome concluded an increase in the fatigue life of the asphalt mixture (Bonnaure et al., 1982).

The controlled-strain uniaxial tensile test under cyclic loading was performed at different strain amplitudes to derive VECD model parameters. In the VECD model, the induced damage was generally represented in terms of the internal state variable. This model can be used in modeling micro-damage healing and damage growth. This model is based on the study performed by Schapery in 1990, where he delivered a continuum damage model for elastic materials. With the help of the elastic-viscoelastic corresponding principle, a new viscoelastic continuum damage model has been produced. The advantage of this model is that the effect of loading rate (i.e., the viscoelastic effect) is eradicated (Lee & Kim 1998).

The combination of group-rest and pulse-rate rest healing tests was also performed using Indirect Tensile Test to assess the healing in asphalt concrete. The frequency of haversine loading was kept at 10 Hz. The rest period of 0.9 s was applied after every load cycle. The temperature for pulse loading rest period testing was kept at 10°C. Then, a 12-hour rest period was given to the specimen, enhancing the testing temperature to 30°C. Healing was observed during the rest period, and healing was assessed in terms of dissipated creep strain energy (Zhang et al., 2001).

A schematic of the interruption for the loading sequence also termed the group-rest healing test, is given in **Figure 2.16**. The stress-controlled tension-compression cyclic test was interrupted by rest periods at the different percentage reductions in the specimen's initial stiffness. With this type of testing, healing potential change could be monitored with respect to the damage level before applying the rest period. The test was also conducted at different temperatures. Hence, the effect of two factors on the material's healing potential could be captured. Combining the results of these tests at different temperatures and rest periods applied at the various damage levels of tested specimens, a functional form for the healing potential of the material was obtained (Ashouri 2014).

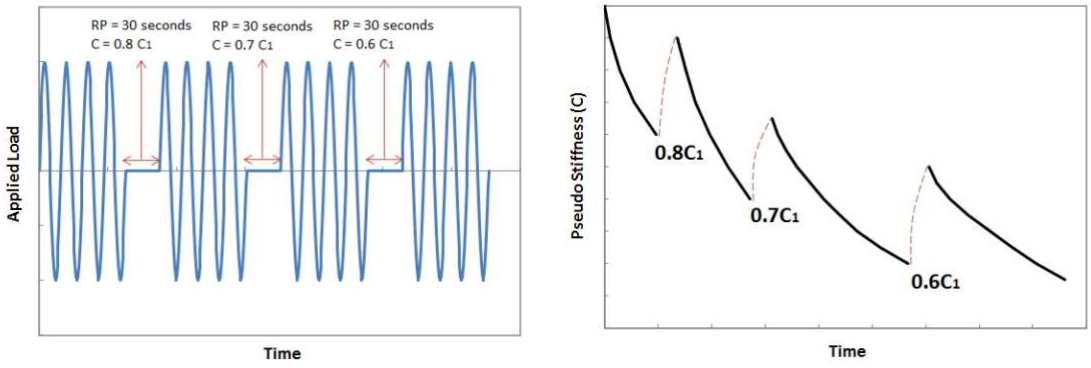

Figure 2.16. Example schematic for group-rest healing test (Ashouri 2014).

The controlled strain repeated cyclic uniaxial tensile fatigue test was performed on a Superpave gyrator compacted specimens of 150 mm height and 100 mm diameter. Three LVDTs were attached to the specimen at 120° with the help of epoxy glue. Different rest periods of 2, 5, 10 and 30 minutes were applied at 1000-cycle intervals. Pseudo-stiffness was opted as a parameter to define healing in a mixture. This study predicted the extension in the fatigue life of specimens. The longer the rest period, the higher the healing potential of the mixture (Si et al., 2002).

The controlled-strain torsional test was performed on two asphalt mixtures. Three different strain rates opted for testing at 25°C with a loading of 10 Hz. Healing and damage were assessed with stiffness, dynamic modulus, and dissipated strain energy changes. The fatigue life of the specimen with the rest period was more than without the rest period. **Figure 2.17** depicts the enhancement in the fatigue life due to the rest period (Kim 2003).

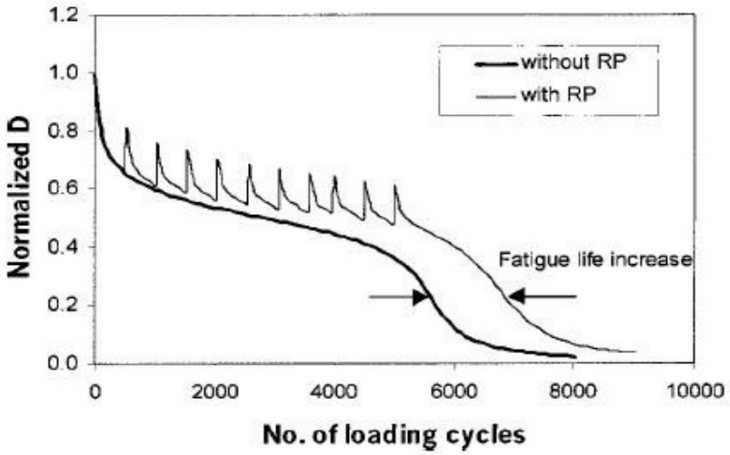

Figure 2.17. Normalized dynamic modulus vs. the number of loading cycles (Kim 2003).

Binders primarily fuel the healing mechanism in asphalt materials. The interfaces that the fine and coarse aggregates produce make it more difficult to determine how well a mixture is healing. From the literature, two types of healing in the asphalt mixtures have been discussed, i.e., adhesive healing (focuses more on the binder-stone interface) and cohesive healing (on the binder level) (Williams et al., 2001; Lytton et al., 2003; Song et al., 2005).

The three-point bending test was performed on a beam of asphalt mixture with 300 mm * 50 mm * 50 mm made with an air void of 3.7%. The test was performed at 20°C temperature and 10 Hz frequency, and the failure criterion was adopted when the initial force reaches 50% of the initial force. Both pulse rest and group rest healing tests were performed. For the pulse-rest healing test, the cyclic test was performed with a sinusoidal loading wave with 0.1 s followed by a rest period of 1 s until the failure. It is observed that the fatigue life got extended by five to ten times. An attempt to find an optimum rest period for the specimen during fatigue testing was performed. The rest period of more than 10 times the length of the loading cycle was of no significance in enhancing the fatigue life of the sample (Castro & Sanchez 2006).

When micro-cracks are generated, diffusion and wetting due to materials (e.g., binder) flowing between the two faces of a crack contribute to healing. In asphalt materials, firstly, the binder diffusing in cracks will cause the wetting of surfaces, and then molecules will start diffusing from one face to another. This randomization of molecules will tend the materials to restore their original strength by healing the cracks formed.

Viscosity is the major contributing factor in the self-healing process of asphalt binders which depends highly on rest periods and temperature (Qiu 2012). The longer healing time and higher temperature will enhance the extent to which asphalt materials can be healed. In a shorter time, the links formed across the faces of micro-cracks are less, resulting in weaker bonds (Cordier 2008). On a molecular level, this healing is due to the formation of hydrogen bonds across the cracks to the broken molecules ready to form bonds with other molecules. This is named

"reversible hydrogen bonding" (Qiu 2009). At higher temperatures, asphalt pavements heal due to the "thixotropic effect," where the binder moves from solid to gel state, healing the damage.

The main aim of all the research is to enhance the performance of the asphalt mixture. The performance is defined as the durability and load-carrying capability of the asphalt mixture. Adding additives and modifiers can improve the self-healing properties of the asphalt mixture. For healing in materials, certain requirements that the mix should comply with can be given as

i. High-temperature stability
ii. Good compatibility with bitumen
iii. Ability to survive mixing and construction conditions
iv. Healing temperature between -30°C and 40°C
v. Capable of continuous healing

Techniques like nanoparticle application, induction heating, or rejuvenation are used to speed up healing. For example, the assessment of self-healing in asphalt mixtures using steel fibers and induction heating showed positive results in the recovery of stiffness and healing of asphalt mixtures (Liu 2012), while others attempted healing in asphalt with encapsulation of rejuvenator in asphalt mixtures (Xu 2020). With time, due to the exposure of materials to fatigue and various environmental factors, volatile components from the asphalt binder in mixtures oxidize, resulting in the aging of the binder, making the mixture brittle (Elwardany 2017). In the mechanisms mentioned as induction heating and rejuvenator encapsulation, recovery almost takes four hours of rest time. There is always a demand to develop a healing model in asphalt mixtures to quantify the applicability of self-healing techniques in asphalt mixtures. It is assessed in terms of recovery in the mechanical strength of these mixtures. With such models, it will be easy to construct asphalt pavements that can consider both the internal state and external environment and act accordingly. To evaluate this in real field production up to industry standards, it should justify advantages based on functional, economic, and environmental aspects (Kim & Roque 2006).

Most studies assessing healing rely on how a material reacts before and after rest periods. The main question, however, is the factors considered when defining and evaluating healing. This study will also concentrate on adhesive healing, and it will be assumed that failure brought on by fatigue will spread along the binder line rather than within the aggregates, with various studies investigating adhesive healing (Bhasin 2006). Atomic force microscopy has also been used in studies of micro-scale healing (Pauli 2014; Nahar 2016). Mesoscale healing analysis might employ fluorescence microscopy and X-ray tomography (Sun et al., 2018; Sun & Deng, 2020). Overall, The microscale, mesoscale, and macroscale are the three scales where the study has found healing to occur (Sun et al., 2018).

From all the studies performed in the past, it can be concluded that the quantification of healing is of huge significance and must be incorporated into asphalt modeling. With proper consideration of healing potential in asphalt mix design, the design life of the mixture can be extended under a repetitive load cycle. Investigating various factors mentioned in the literature that affect healing potential becomes necessary. A proper method to predict the fatigue life of asphalt mixture is to be produced considering the pulse-rest healing methodology without consuming much time. This research will try to answer these problems with extensive testing and comparison performed on three different properties of mixtures.

References

Ahmed, T.M., Al-Khalid, H., Ahmed, T.Y. (2019). Review of Techniques, Approaches and Criteria of Hot-Mix Asphalt Fatigue. *Journal of Materials in Civil Engineering 31(12).*

ARA, Inc. (2004). *Guide for Mechanistic-Empirical Design of New and Rehabilitated Pavement Structures, NCHRP 1-37A Final Report.* ERES Consultants Division, Transportation Research Board, National Research Council, Washington, D.C.

Ashouri, M. (2014). *Modeling Microdamage Healing in Asphalt Pavements using Continuum Damage Theory*. Ph.D. Thesis, North Carolina State University.

Bazin, P., Saunier, J. (1967). Deformability, Fatigue and Healing Properties of Asphalt Mixes. In *International Conference of Structural Design of Asphalt Pavements*.

Bhasin, A. (2006). *Development of Methods to Quantify Bitumen-Aggregate Adhesion and Loss of Adhesion Due to Water*. Ph.D. Thesis, Texas A&M University.

Bhasin, A., Little, D.N., Bommavaram, R., Vasconcelos, K. (2008). A Framework to Quantify the Effect of Healing in Bituminous Materials using Material Properties. *Road Materials and Pavement Design 9(1)*, pp. 219-242.

Bonnaure, F., Huibers, A., Boonders, A. (1982). A Laboratory Investigation of the Influence of Rest Periods on the Fatigue Characteristics of Bituminous Mixes. *Journal of the Association of Asphalt Paving Technologists 51*, pp. 104-128.

Carpenter, S.H., Shen, S. (2006). A Dissipated Energy Approach to Study HMA Healing in Fatigue. *Transportation Research Record 1970*, pp. 178-185.

Castro, M., Sanchez, J.A. (2006). Fatigue and Healing of Asphalt Mixtures: Discriminate Analysis of Fatigue Curves. *Journal of Transportation Engineering 132(2).*

Cheng, H., Sun, L., Wang, Y., Liu, L., Chen, X. (2022). Fatigue Test Setups and Analysis Methods for Asphalt Mixture: A State-of-the-Art Review. *Journal of Road Engineering 2(4),* pp. 279-308.

Collop, A.C, Cebon, D. (1995). A Theoretical Analysis of Fatigue Cracking in Flexible Pavements. *Proceedings of the Institution of Mechanical Engineers, Part C: Journal of Mechanical Engineering Science 209(5),* pp. 345-361.

Cordier, P., Tournilhac, F., Soulie-Ziakovic, C., Leibler, L. (2008). Self-Healing and Thermoreversible Rubber from Supramolecular Assembly. *Nature 451*, pp. 977-980.

Deacon, J.A., Harvey, J.T., Tayebali, A., Monismith, C.L. (1997). Influence of Binder Loss Modulus on the Fatigue Performance of Asphalt Concrete Pavements. *Journal of the Association of Asphalt Paving Technologists 66*, pp. 633-668.

Di Benedetto H., de la Roche C., Baaj H., Pronk A. Lundstrom R. (2004), Fatigue of Bituminous Mixtures. *Materials and Structures 37(3),* pp. 202–216.

Elwardany, M.D. (2017). *Phenomenological Modeling and Laboratory Simulation of Long-Term Aging of Asphalt Mixtures*. Ph.D. Thesis, North Carolina State University.

Federal Highway Administration. (2022). *Hot-Mix Asphalt Performance Related Specification based on Viscoelastoplastic Continuum Damage (VEPCD) Models*. Washington, DC.

Fischer, H. (2010). Self-Repairing Material Systems - A Dream or a Reality? *Natural Science 2(8)*, pp. 873-901.

Ghuzlan, K., Carpenter, S.H. (2000). Energy-Derived/Damage-Based Failure Criteria for Fatigue Testing. Transportation Research Record 1723, pp. 141-149.

Griffith, A.A. (1921). The Phenomena of Rupture and Flow in Solids. *Philosophical Transactions of the Royal Society,* London, Series A, Vol. 221.

Hajj, R., Bhasin, A. (2018). The Search for a Measure of Fatigue Cracking in Asphalt Binders – A Review of Different Approaches. *International Journal of Pavement Engineering 19(3),* pp. 205-219.

Hopman P.C., Kunst P.A. Pronk A.C. (1989). A Renewed Interpretation Method for Fatigue Measurements-Verification of Miner's Rule. In *Proceeding of the 4th Eurobitumen Symposium*, Madrid, Spain.

Jacobs, M.M.J. (1995). *Crack Growth in Asphaltic Mixes*. Ph.D. Thesis, Delft University of Technology.

Kennedy, T.W., Hudson, W.R. (1968). Application of the Indirect Tensile Test to Stabilized Materials. *Highway Research Record 235*, Highway Research Board, Washington, D.C.

Kim Y., Lee H.J., Little D.N., Kim Y.R. (2006). A Simple Testing Method to Evaluate Fatigue Fracture and Damage Performance of Asphalt Mixtures (with discussion). *Journal of the Association of Asphalt Paving Technologists 75*, pp. 755-788.

Kim, B., Roque, R. (2006). Evaluation of Healing Property of Asphalt Mixtures. *Transportation Research Record 1970*, pp. 84-91.

Kim, Y.R., Little, D.N., Lytton, R.L. (2002). Use of Dynamic Mechanical Analysis (DMA) To Evaluate The Fatigue And Healing Potential Of Asphalt Binders In Sand Asphalt Mixtures (with discussion and closure). *Journal of the Association of Asphalt Paving Technologists 71*, pp. 176-206.

Kim, Y.R., Little, D.N., Lytton, R.L. (2003). Fatigue and Healing Characterization of Asphalt Mixtures. *Journal of Materials in Civil Engineering 15(1),* pp. 75- 83.

Liu, Q. (2012). *Induction Healing of Porous Asphalt Concrete*. Ph.D. Thesis, Delft University of Technology.

Maggiore, C., Airey, G., Marsac, P. (2012). A Dissipated Energy Comparison to Evaluate Fatigue Resistance using 2-Point Bending. *Journal of Traffic and Transportation Engineering (English Edition) 1(1),* pp. 49-54.

Molenaar, A.A.A. (1983). *Structural Performance and Design of Flexible Road Construction and Asphalt Concrete Overlays*. Ph.D. Thesis, Delft University of Technology.

Nahar, S.N. (2016). *Phase-Separation Characteristics of Bitumen and their Relation to Damage-Healing*. Ph.D. Thesis, Delft University of Technology.

National Academies of Sciences, Engineering, and Medicine. (2010). *Validating the Fatigue Endurance Limit for Hot Mix Asphalt*. Washington, D.C.: The National Academies Press.

Paris, P.C., Erdogan, K. (1963). A Critical Analysis of Crack Propagation Laws. *Transactions of the ASME, Journal of Basic Engineering*, Series D, 85(3).

Pauli, A.T. (2014). *Chemomechanics of Damage Accumulation and Damage-Recovery Healing in Bituminous Asphalt Binders*. Ph.D. Thesis, Delft University of Technology.

Pell, P.S. (1962). Fatigue Characteristics of Bitumen and Bituminous Mixes. In *Proceedings of the International Conference on the Structural Design of Asphalt Pavements*.

Perraton, D., Touhara, R., Di Benedetto, H., Carter, A. (2015). Ability of the Classical Fatigue Criterion to be Associated with Macro-Crack Growth. Materials and Structures 48, pp. 2383-95.

Pronk, A.C. (1996.). *Theory of the Four Point Dynamic Bending Test*. Ministerie van Verkeer en Waterstaat Dienst Weg en Waterbouwkunde, The Netherlands.

Qiu, J. (2012). *Self Healing of Asphalt Mixtures: Towards a Better Understanding of the Mechanism*. Ph.D. Thesis, Delft University of Technology.

Raithby, K.D., Sterling, A.B. (1970). The Effect of Rest Periods on the Fatigue Performance of a Hot-Rolled Asphalt under Reversed Axial Loading and Discussion. *Journal of the Association of Asphalt Paving Technologists 39*, pp. 134-152.

Read, J.M., Collop, A.C. (1997). Practical Fatigue Characterization of Bituminous Paving Mixture. *Journal of the Association of Asphalt Paving Technologists 66*, pp. 74-108.

Reese, R.A. (1997). Properties of Aged Asphalt Binder Related to Asphalt Concrete Fatigue Life. *Journal of the Association of Asphalt Paving Technologists 66*, pp. 604-632.

Rowe, G.M (1996). *Application of the Dissipated Energy Concepts to Fatigue Cracking in Asphalt Pavements*. Ph.D. Thesis, University of Nottingham.

Secor, KE., Monismith, C.L. (1961). Analysis of Triaxial Test Data on Asphalt Concrete using Viscoelastic Principles. In *Proceedings of the Fortieth Annual Meeting of the Highway Research Board*, Washington, D.C.

Shen, S., Carpenter, S. (2007). Development of an Asphalt Fatigue Model based on Energy Principles. *Journal of the Association of Asphalt Paving Technologists 71*, pp. 525-573.

Si, Z., Little, D.N., Lytton, R.L. (2002). Characterization of Microdamage and Healing of Asphalt Concrete Mixtures. *Journal of Materials in Civil Engineering 14(6)*.

Song, I., Little, D.N., Masad, E.A., Lytton, R. (2005). Comprehensive Evaluation of Damage in Asphalt Mastics using X-Ray CT, Continuum Mechanics, and Micromechanics (with discussion). *Journal of the Association of Asphalt Paving Technologists*, *74*, pp. 885-920.

Sudarsanan, N., Kim, Y.R. (2022). A Critical Review of the Fatigue Life Prediction of Asphalt Mixtures and Pavements. *Journal of Traffic and Transportation Engineering (English Edition) 9(5),* pp. 808-835.

Sun, D., Sun, G., Zhu, X., Guarin, A., Li, B., Dai, Z., Ling, J. (2018). A Comprehensive Review on Self-Healing of Asphalt Materials: Mechanism, Model, Characterization and Enhancement. *Advances in Colloid and Interface Science 256*, pp. 65-93.

Tabakovic, A., Schlangen, E. (2016). Self-Healing Technology for Asphalt Pavements. In: *Hager, M., van der Zwaag, S., Schubert, U. (eds.) Self-Healing Materials: Advances in Polymer Science 273*.

Tian, H. (2010). *Fatigue Performance Prediction of North Carolina Mixtures Using the Simplified Viscoelastic Continuum Damage Model*. M.Sc. Thesis, North Carolina State University.

Van Dijk, W., Visser, W. (1977). Energy Approach to Fatigue for Pavement Design. *Journal of the Association of Asphalt Paving Technologists 46*, pp. 1-40.

Williams, D., Little, D.N., Lytton, R.L., Kim, Y.R., Kim, Y. (2001). *Microdamage Healing in Asphalt and Asphalt Concrete, Volume II: Laboratory and Field Testing to Assess and Evaluate Microdamage and Microdamage Healing.* No. FHWA-RD-98-142.

Wool, R.P., O'Connor, K.M. (1981). A Theory of Crack Healing in Polymers. *Journal of Applied Physics 52(10)*, pp. 5953-63.

Wu, R., Denneman, E., Harvey, J. (2009). Evaluation of Embedded Discontinuity Method for Finite Element Analysis of Cracking of Hot-Mix Asphalt Concrete. *Transportation Research Record 2127(1)*, pp. 82-89.

Xu, S. (2020). *Self-Healing Porous Asphalt: A Combination of Encapsulated Rejuvenator and Induction Heating*. Ph.D. Thesis, Delft University of Technology.

Zhang, Z., Roque, R., Birgisson, B., Sangpetngam, B. (2001). Identification and Verification of a Suitable Crack Growth Law (with discussion). *Journal of the Association of Asphalt Paving Technologists 70*, pp. 206-241.

Chapter 3

Visco-Elastic Continuum Damage Theory for Asphalt Materials

3.1 Introduction

Fatigue cracking concerning repeated traffic loading is a major distress in flexible pavements. Demand for an accurate method to assess the damage caused by the fatigue phenomenon is high, enhancing the accuracy in pavement design with different techniques. Damage assessment is complex because of loading rate, rest periods, temperatures, and aging. The inclusion of healing in the assessment makes it more complex. As the fatigue response data of the asphalt mixture is measured by means of fatigue tests, an analysis method is also required to process the data and identify the fatigue behavior of the material. The most used fatigue data analysis methods include the fatigue life mode, stiffness-modulus-based model, energy-based methods, and viscoelastic continuum damage (VECD) method (Cheng et al., 2022). This method is developed to quantify the damage accumulation process of a continuum material. Many mechanistic models have been proposed in this direction, and the viscoelastic continuum damage (VECD) method is one of those. For viscoelastic materials, the VECD method removes the viscous effect and monitors the change in pseudo-stiffness. In the case of asphalt materials, the change in the rheology of the binder part (e.g., creep and relaxation) can be considered in assessing the material damage (Kim et al., 1997). It is obvious from this that the stress-strain relationship derived from the displacement-controlled tension-compression test contains two effects: damage development and relaxation owing to viscoelasticity. As a result of the time/temperature reliance and loading method dependency, this phenomenon can be eliminated from the analysis. Continuum damage theory ignores the micro-scale behavior of material and characterizes material using the macro-scale level on a broader scale.

The VECD theory is used to model the material's loading condition. It is a branch of continuum mechanics, which deals with the deformation and failure of materials at the macroscopic scale. The VECD theory is effective for asphalt mixtures with uniaxial cyclic tests in assessing fatigue performance, which has been incorporated in this study. This theory is even valid for different loading conditions for analyzing the fatigue and healing behavior of conventional and polymer-modified asphalt mixtures for stress-controlled and strain-controlled cyclic loading tests. Modeling micro-cracks brings non-linearity in the context of fatigue and healing assessment which is never easy to tackle. Several studies have assumed conditions for developing cracks in tension and compressions separately to ease this. Traditional fatigue tests, such as beam fatigue tests, are empirical and can generate large errors when used for predictions. With the VECD approach, it becomes helpful to use the properties of the material and helps develop a -simplified laboratory program.

3.2 Simplified Viscoelastic Continuum Damage Theory

The simplified viscoelastic continuum damage (S-VECD) model is a simplified form of the full VECD model (Underwood et al., 2009). In the case of cyclic loads, the VECD model, with simplifications, reduces analysis time and effort, usually referred to as the S-VECD model (Underwood et al., 2009). It removes millions of calculations required for applying the VECD model to the vast loading history of loads. The VECD model is a mechanistic model that accounts for material damage and resulting stiffness reduction under monotonic and cyclic loading. Three major principles involved with this theory are as follows:

i. **Correspondence principle:** Studying the effects in terms of pseudo-strain removes the viscoelastic effect. It eliminates the concern for loading rate and temperature effect on the

asphalt mixture. It helps understand asphalt mixture behavior from stress-strain data and allows the accurate modeling of fatigue damage and healing mechanisms.

ii. **Continuum damage mechanics:** It is a mechanistic foundation based on work potential to model micro-crack generation and further occurring macro-crack. Non-linearity formed due to the formation of cracks be transformed in linearly elastic analysis with pseudo-strain concept and with the formation of damage characteristics curve.

iii. **Time-Temperature Superposition Principle** with growing damage, implying this principle, the tests can be performed at a single combination of loading rate or frequency and temperature to measure asphalt mixture performance to various combinations of loading rates and temperatures. It eases data at various datasets based on single test combinations performed with frequency and temperature by means of master curves.

3.3 Time-Temperature Superposition Principle

It is necessary to prove that the time-temperature superposition (TTS) principle is valid for predicting the asphalt mixtures' stresses and strains at different temperatures and frequencies. The TTS principle helps assess this at larger strains in tension-compression loading mode (Chehab & Kim, 2005). This theory helps replace the time and frequency used in the equations with reduced time and frequency, respectively. Reduced time and reduced frequencies are both functions of temperature, as expressed by **Eq. 3.1** and **Eq. 3.2**

$$t_r = \frac{t}{a_t(T)} \tag{3.1}$$

and

$$f_R = f \cdot a_T(T) \tag{3.2}$$

where $a_t(T)$ is the temperature shift factor and T is the test temperature. To predict this shift factor, a second-order polynomial is given in **Eq. 3.3**

$$\log a_T = a_1 T_{ref}^2 + a_2 T + a_3 \tag{3.3}$$

where T_{ref} is the reference temperature chosen independently, a_1 and a_2 are the shift parameters. This factor can be used in the damaged state as well as in the viscoplastic state. The validity of the TTS principle makes it easier to assess the fatigue and healing of asphalt mixtures.

3.4 Mathematical Interpretation of Viscoelastic Continuum Damage Theory

The VECD model uses Schapery's work potential theory and the elastic-viscoelastic principle to simulate the mechanical behavior of asphalt mixtures. Schapery 1984 introduced a concept for linear and non-linear viscoelastic continuum material called 'elastic-viscoelastic correspondence (E-VC) material (Schapery 1984). With this principle implemented, the equations turning out are equivalent to elastic materials constitutive equations with pseudo-strain instead of physical strain. The pseudo-strain can be given as

$$\varepsilon^R = \frac{1}{E_R}\int_0^t E(T-\tau)\frac{\partial \varepsilon(\tau)}{\partial \tau}d\tau \tag{3.4}$$

where ε^R is the pseudo-strain, E_R is a reference modulus (usually equal to unity), $E(t)$ is the linear viscoelastic (LVE) relaxation modulus, t is time and τ is the variable of time integration.

The stress-strain relationship with the correspondence principle can be expressed as

$$\sigma = E_R \cdot \varepsilon^R \tag{3.5}$$

where σ is the uniaxial stress.

In the cyclic tension test conducted in this study to analyze fatigue and healing, the pseudo-strain amplitude (ε^R) can be calculated as the product of strain amplitude and dynamic modulus $|E^*|$, which can be given as follows

$$\varepsilon^R = |E^*| \cdot \varepsilon_0 \tag{3.6}$$

The limit of integration in **Eq. 3.4** is from 0 to *t*. This calculation of pseudo-strains is a bit memory intensive and time-consuming. Certain models are opted for by researchers where $E(t)$ follows the generalized Maxwell model as given below

$$\varepsilon^R = E_\infty \varepsilon(t) + \sum_{i=1}^{n} \sigma_i^{el}(t) \tag{3.7}$$

where E_∞ is the long-term elastic modulus, n is the number of elements in the Prony series, $\sigma_i^{el}(t)$ is the stress in each Maxwell element at time *t*. This stress can be calculated as the incremental formulation given in **Eq. 3.8** below

$$\sigma_i^{el}(t) = e^{-\frac{\Delta t}{\rho_i}} \sigma_i^{el}(t - \Delta t) + \frac{\Delta \varepsilon}{\Delta t} \eta_i [1 - e^{-\frac{\Delta t}{\rho_i}}] \tag{3.8}$$

where ρ_i is the retardation time of each generalized Maxwell model, η_i is the viscous damping of the element of the generalized Maxwell model, and E_i is the elastic coefficients of each element in the generalized Maxwell model.

3.5 Concept of Pseudo-Stiffness and Damage Parameter

The deviation from the LVE stress to the applied stress is observed with the asphalt mixture specimen undergoing damage in the fatigue testing. This LVE stress is the pseudo-strain (ε^R) for the unity reference modulus of elasticity (Kutay & Lanotte 2018). This deviation is quantified in the parameters called pseudo-stiffness (C) and the damage parameter (S). Pseudo-stiffness is defined as the ratio of the modulus of material elasticity at a certain loading time to the initial undamaged modulus of the material. The value of C ranges from 0 to 1, where 1 represents the undamaged material. For cyclic tests, C can be calculated using **Eq. 3.9**,

$$C_N = \frac{|E^*|_N}{|E^*|_{LVE}} \tag{3.9}$$

where C_N is the pseudo-stiffness for the cycle, $|E^*|_N$ is the stiffness modulus of elasticity of the cycle, and $|E^*|_{LVE}$ is the initial stiffness modulus.

The pseudo-stiffness at a certain loading time can be computed as in **Eq. 3.10.**

$$C(t) = \frac{\sigma(t)}{\varepsilon^R(t)} \tag{3.10}$$

where $\sigma(t)$ is the stress & $\varepsilon^R(t)$ is the pseudo strain calcualted from **Eq. 3.4.**

Damage factor (*S*) is a fictitious parameter representing the amount or the volume of total microcracks/microdamage. The internal heating due to the fatigue in the material causes an increase in *S* and a decrease in *C* (Kim et al., 1997). The curve obtained is termed as *C*-*S* curve and defines the damage characteristics of the material, which is independent of temperature, magnitude, rate, and mode of loading. Hence, once a *C*-*S* curve of an asphalt mixture is obtained, it helps predict the stress-strain response of the same material at different temperatures, loading magnitudes, rates, and modes of loading from it. But it is to be noted that these *C*-*S* curves are not universal. Changes in the microstructure of the material change the characteristics of the curve; such one factor is air-void content in the asphalt mixture (Kutay & Lanotte 2018). It also changes with the type of load induced on the material. The *C*-*S* curve for the tension-tension mode of loading will differ from that of tension-compression loading for the same type of material. In a cyclic test, if it is a tension-only or compression-only test, the damage parameter for each direction of loading will be different. Under the compression-only loading mode, the material cracks when it exceeds the limit of viscoplastic deformation and the material is fully strain-hardened (Zhang et al., 2014).

Following the correspondence principle, Schapery applied irreversible thermodynamics processes to develop work potential theory (WPT) (Schapery 1990). Internal state variables (ISV) are used to quantify the damage due to microstructural changes in the material. The viscoelastic continuum theory can be explained using three basic equations:

Pseudo-strain energy density function

$$W^R = f(\varepsilon^R, S) \tag{3.11}$$

Stress-pseudo strain relationship

$$\sigma = \frac{\partial W^R}{\partial \varepsilon^R} = I\, C(S)\, \varepsilon^R \tag{3.12}$$

Damage evolution law

$$\frac{dS}{dt} = \left(-\frac{\partial W^R}{\partial S_m}\right)^{\alpha_m} \tag{3.13}$$

where W^R is the pseudo-strain energy density, ε^R is the pseudo-strain, S_m is the damage parameter (ISV), and α_m is the material constant. It is suggested to use $\alpha_m = (1+1/m)$ for the controlled strain mode and $\alpha_m = 1/m$ for the controlled stress mode. m is the maximum slope of the relaxation modulus vs. time curve plotted in the log-log scale, $\dot{S}$ is the damage evolution rate. α_m is a measurement of the material's tendency to release energy during micro-crack formation. This factor is analogous to a factor used in fracture mechanics to determine the crack propagation speed with the formula mentioned in **Eq. 3.14**,

$$\frac{da}{dt} = A(J_v)^k \tag{3.14}$$

where da/dt is the crack propagation rate, J_v is the generalized *J*-integral and A and k are the constants.

In the work potential theory, a key formulation between W^R, σ and ε^R is given in **Eq. 3.15**.

$$W^R = \frac{1}{2} I\, C(S)\, \varepsilon^{R^2} \tag{3.15}$$

where $C(S)$ is the pseudo stiffness, defined as the function of the damage parameter S, I represents the initial stiffness parameter used to account for the sample-to-sample variability. It can be calculated using **Eq. 3.16.**

$$I = \frac{E^*_{N=1}}{E^*_{LVE}} \tag{3.16}$$

where $E^*_{N=1}$ is the dynamic modulus at the 1st cycle of the fatigue testing while E^*_{LVE} is the linear viscoelastic dynamic modulus of the mixture.

This factor k relates to the materials creep or the relaxation curve (Schapery 1975). Uniaxial stress loading at a constant temperature follows a constitutive relationship that depends on pseudo-strain and the damage state of the material at that point of testing.

$$\sigma = IC_1(S_1)\varepsilon^R \tag{3.17}$$

where C_1 is the function of damage parameter S_1, this function represents the change in the material's stiffness with the change in the material's microstructure represented by healing or damage of material.

Using **Eq. 3.13** and **3.15** and applying the chain rule (**Eq. 3.18**), a relationship can be derived as in **Eq 3.20**.

$$\frac{dC}{dS} = \frac{dC}{dt}.\frac{dt}{dS} \tag{3.18}$$

$$\frac{dS}{dt} = \left[-I\frac{\varepsilon^{R^2}}{2}\frac{dC}{dt}\right]^{\frac{\alpha}{1+\alpha}} \tag{3.19}$$

$$S = \int_0^t \left[-I\frac{\varepsilon^{R^2}}{2}\frac{dC}{dt}\right]^{\frac{\alpha}{1+\alpha}} dt \tag{3.20}$$

Under the action of cyclic loading, this damage parameter S can be given as in **Eq. 3.21**.

$$S = \sum_{i=1}^{N} \left[\frac{1}{2}(\varepsilon^R)^2(C_{i-1} - C_i)\right]^{\frac{\alpha}{1+\alpha}} (t_i - t_{i-1})^{\frac{1}{1+\alpha}} \tag{3.21}$$

For the cyclic tests at constant loading frequency, the term involved in the **Eq. 3.21** can be calculated as given in **Eq. 3.22.**

$$(t_i - t_{i-1}) = \frac{N_i - N_{i-1}}{f} \tag{3.22}$$

where N is the number of loading cycles and f is the loading frequency.

Substituting **Eq. 3.22** in **3.21**, the equation to compute S in the cyclic fatigue tests (Kutay & Lanotte, 2018) is given in **Eq. 3.23.**

$$S = \sum_{i=1}^{N} \left[\frac{1}{2}(\varepsilon^R)^2(C_{i-1} - C_i)\right]^{\frac{\alpha}{1+\alpha}} \left[\frac{N_i - N_{i-1}}{f}\right]^{\frac{1}{1+\alpha}} \quad (3.23)$$

The stiffness during the fatigue testing will decrease with increased damage to the material. Hence the slope of the stress - pseudo-strain curve will decrease. This slope is termed pseudo-stiffness, represented by S^R.

$$S^R = \frac{\sigma_{max}}{\varepsilon^R_{max}} \quad (3.24)$$

where σ_{max} is the peak stress for each cycle, ε^R_{max} is the peak pseudo-strain in each cycle.

Using **Eq. 3.23,** *S* values for a number of cycles and increments of *S* between the different loading times can be calculated. Many researchers also believe that only the tensile part of the pseudo-strain pulse contributes to the increase in *S* (Daniel & Kim, 2002; Underwood et al., 2010). Hence, a modifier *K* is introduced to only consider the effect of the tensile pseudo-strain in **Eq. 3.25**.

$$S = \sum_{i=1}^{N} \left[\frac{1}{2}(\varepsilon^R)^2(C_{i-1} - C_i)\right]^{\frac{\alpha}{1+\alpha}} [K(t_i - t_{i-1})]^{\frac{1}{1+\alpha}} \quad (3.25)$$

where *K* can be calculated by using **Eq. 3.26.**

$$K = \frac{1}{t_p}\int_{ti}^{tf} g(t)^{2a} dt \quad (3.26)$$

where t_p is the loading pulse time, i.e., $t_p=1/f$, $g(t)$ is the function of normalized pulse, t_i and t_f are the start and end times of the tensile loading portion.

Using all equations mentioned above, *S* of the asphalt mixture is computed. Afterward, *S* is plotted with *C* to form a *C*-*S* curve, which is used for the damage characterization of the asphalt mixtures. It is noted that *C* decreases with the accumulation of damage in the material in terms of *S*.

The equation to develop such a relationship is given as follows (Kutay et al., 2008)

$$C(S) = C_{10} - C_{11}S^{C_{12}} \quad (3.27)$$

where, C_{11}, and C_{12} are the fitting parameters.

Another model has been developed to fit the *C*-*S* curve based on the power function in **Eq. 3.18**.

$$C(S) = e^{aS^b} \quad (3.28)$$

where *a* and *b* are the fitting parameters for the model.

Out of both the models, the model given in **Eq. 3.27** based on the exponential function is incorporated to predict the damage characteristics curve in FlexMAT software which is used to perform all the mathematical calculations involving VECD theory. The author would like to point out that he did not perform any mathematical calculations in this study concerning VECD theory. All mathematics involved is studied for a better understanding of concepts.

3.6 Computation of *C-S* Curve

The computation of the damage characteristics curve is a multi-step process. In tension-compression testing, as performed in this study, several steps are required to assess the fatigue and healing of asphalt mixtures using the VECD principle. The damage characteristics curve describes the growth pattern of damage in the material, and hence a failure criterion is opted to define the failure of the material. The physical loads and displacements are reported in the TU Delft test. Fatigue tests are performed at 10 Hz for 3 different temperatures (10, 20 and 30°C).

Similarly, a test for healing is also performed at these temperatures and frequencies, incorporating 3 different rest periods (40, 80 and 160 s). With the help of geometries and gauge length, the data is converted into stress-strain time data. The steps mentioned below are opted to predict the damage characteristics curve (Kutay & Lanotte 2018):

Step 1: Dynamic modulus test is performed in accordance with AASHTO T 342-11 in compression mode of loading. $|E^*|$ master curves are developed with the data reported for all 3 mixtures at 3 different temperatures.

Step 2: Relaxation modulus ($E(t)$) master curve is produced through the viscoelastic interconversion. With this, the damage exponent α is calculated, which is the maximum slope of the log $E(t)$ – log(t) curve. In this research work, the FlexMAT cracking software is used. This curve is produced with the help of this software in this study.

Step 3: Using the value of α, the pseudo-strain – time curve is plotted.

Step 4: Pseudo-stiffness – time curve will be plotted.

Step 5: Similarly, damage parameter ($S(t)$) – time will be calculated.

Step 6: The final *C-S* curve will be plotted, and a best-fit line is developed to showcase this *C-S* curve, known as the damage characteristics curve.

3.7 Previous Experience

The *C-S* curve represents the fatigue mechanism in the asphalt mixtures but stays unaffected by the loading conditions, including loading amplitude, temperature, frequency and loading mode (monotonic or cyclic) (Underwood et al., 2010; Kutay & Lanotte, 2018; Wang & Kim, 2019). Assessing the fatigue characteristics of asphalt mixtures for wider conditions becomes easier using these *C-S* curve properties. And a unique fatigue model can be predicted for a particular asphalt mixture which is also beneficial in generating the unified fatigue assessment results on the mixture independent of loading conditions (Cheng et al., 2022). But the *C-S* curve is not universal. For example, the *C-S* curve of a tension-only loading will be different than the tension-compression mode of loading. It applies the same to the compression-only mode of loading as well. An attempt to calculate the *C-S* curve also makes it independent of loading mode by only using the tension portion of cyclic load while calculating the damage parameter *S* (Underwood et

al., 2010). Furthermore, the changes in the microstructure of the asphalt mixtures as the moisture and air void content give the different *C-S* curves.

The effect of the rest period is assessed on the *C-S* curves of the mixture, predicting different *C-S* curves. Including the rest periods, the *C-S* curve shifted above the continuous loading case as in **Figure 3.1**. These discrepancies in the *C-S* curves could be attributed to the healing impact of the unloading rest times on the asphalt mixture (Zeiada et al., 2018). Because the present VECD model does not account for healing mechanisms during rest periods, generating individual *C-S* curves for the various rest period situations becomes difficult. (Zeiada et al., 2018).

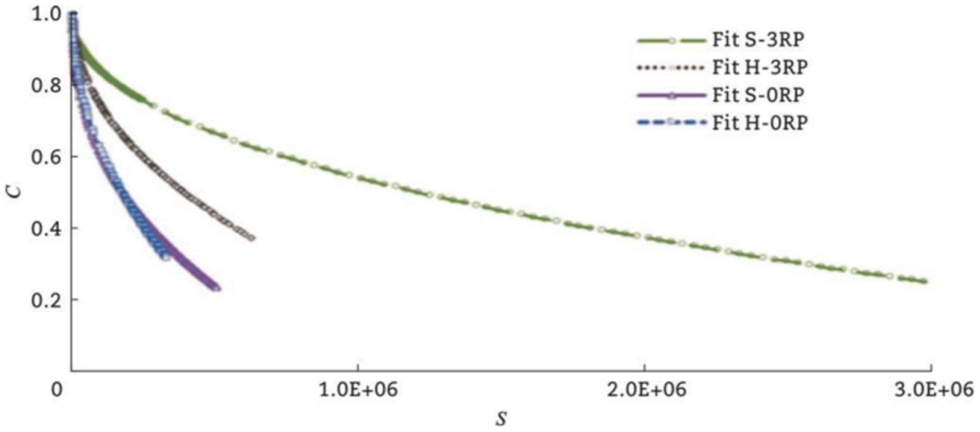

Figure 3.1. C-S curve representing the effect of rest period in cyclic fatigue testing (Zeiada et al., 2018).

The comparison of *C-S* curves of asphalt mixtures under the different loading forms is also performed, resulting in dissimilar *C-S* curves. The *C-S* curves for the single-axle wave are positioned above the haversine and tandem-axle loading mode (Cheng et al., 2022). It is because the damage accumulation only utilizes the tensile part of the loading wave. In the current VECD calculations, the potential healing of the materials that occurs during the compression portion (due to the closure of the micro-cracks) is neglected. The proportion of tensile to compression areas in the haversine, single axle, and tandem axle waves are different, leading to discrepancies in the corresponding *C-S* curves. "The VECD formulations will not produce a single *C-S* curve that can be used to predict the response of a truly random loading that includes tension, compression, as well as the rest periods" (Kutay & Lanotte 2018). There is still a large gap in research to incorporate the harm and healing impacts of loading waves in the existing VECD approach.

It is also worth noting that the loading rate does not affect the *C-S* curve of an asphalt mixture. This study tested a mixture with 70% RAP under tension-compression cycle fatigue testing without a rest interval at 20°C. The uniqueness of the *C-S* curve for different loading rates (200 strain and 300 strain) is tested for two different strain rates. The resulting *C-S* curve follows the same trajectory and remains independent of the loading rate. It is worth noting that including RAP does not affect this property of *C-S* curves.

This damage characteristics curve yields two important VECD indicators, D^R and S_{app}, used to evaluate materials fatigue properties (Wang, et al., 2019 & 2020). The D^R accounts for the average reduction in the pseudo stiffness till the failure and is calculated using **Eq. 3.29.**

$$D^R = \frac{\int_0^{N_f}(1-C)dN}{N_f} \tag{3.29}$$

S_{app} is the total damage capacity of the asphalt mixture, which can be calculated using **Eq. 3.30.**

$$S_{app} = 1000^{\frac{\alpha}{2}-1}\frac{\left[\frac{D^R}{C_{11}}\right]^{\frac{1}{C_{120}}}}{|E^*|^{\frac{\alpha}{4}}} \tag{3.30}$$

where C_{11} and C_{12} are the fitting parameters for the C-S curve, E^* is the materials' dynamic modulus, and α is the damage parameter.

D^R is thought of to be a material constant that is independent of the loading mode, temperature, and stress-strain amplitude. Hence it is also used to indicate the fatigue resistance nature of the asphalt mixture (Wang, et al., 2019 & 2020). It is further observed that the D^R remains stable for different loading waveforms (Cheng et al., 2022). But this single parameter is insufficient to compare the fatigue performance of the different asphalt mixtures. The actual assessment of the fatigue performance of various mixtures is only possible by considering the effects of traffic, climate, and other pavements.

Sapp can evaluate the fatigue resistance of asphalt mixtures with varying parameters like binder quantities, grades, air void content, aggregate gradations, and age levels. After testing 105 different asphalt mixtures, it is clear that this S_{app} value is affected by the loading pattern and strain levels (Wang et al., 2020). The value of S_{app} decreases as the strain level increases. The S_{app} value varies with loading waveforms and strain levels (Cheng et al., 2022). S_{app} is ineffective at predicting the material's unique fatigue mechanism yet can still represent its fatigue life.

The VECD method is also used to predict the fatigue life of the asphalt mixtures. Four models exist to evaluate fatigue life using the VECD theory are given in **Eq. 3.31, 3.32, 3.33,** and **3.34,** respectively.

Model 1 (Lee & Kim 2000)

$$N_f = \frac{f\left(S_{1f}\right)^{P_1}}{P_1(0.125\,IC_{11}C_{12})^{\alpha_{1X}}}|E^*|^{-2\alpha 1}\varepsilon^{-2\alpha 1} \tag{3.31}$$

Model 2 (Kutay et al., 2009)

$$N_f = \sum_{S=1}^{S_f}\left[-\frac{\varepsilon_0^2}{2}|E^*|^2\frac{dC}{dS}|_S\right]^{-\alpha} f\Delta S_S \tag{3.32}$$

Model 3 (Underwood et al., 2010): Based on exponential law.

$$N_f = \frac{f_{red}2^{3\alpha}S_f^{\alpha-\alpha C_{12}+1}}{(\alpha-\alpha C_{12}+1)(C_{11}C_{12})^{\alpha}\left[(\beta+1)\varepsilon_{0,pp}|E^*|^{2\alpha}\right]k_1'} \tag{3.33}$$

Model 4 (Underwood et al., 2010): Based on the power law.

$$N_f = \frac{f_{red}2^{3\alpha}}{\left[(\beta+1)\varepsilon_{0,pp}|E^*|^{2\alpha}\right]k_1'}\int_0^{S_f}\left(abS^{b-1}e^{aS^b}\right)^{-a}dS \quad (3.34)$$

where β is the proportion of the cycle where the stress on the specimen is in tension, K_1 is the loading shape factor, and α is the constant related to the damage growth rate.

In this research work, to calculate and perform all mathematical parameters for assessing fatigue properties of different asphalt mixtures, FlexMAT Cracking is used. It incorporates Model 3 (Underwood et al., 2010). Model 1 (Lee & Kim 2000) is developed based on the fatigue data from the controlled-strain tension test, and S is calculated using **Eq. 3.21**. Model 2 (Kutay et al., 2009) is established for the tension-compression tests with a constant frequency, and S is calculated using **Eq. 3.23**. Model 3 and Model 4 (Underwood et al., 2010) are based on a piecewise approach, and damage parameter S is calculated using **Eq. 3.25.** The results obtained from the three models are different, where Models 1, 3, & 4 give higher fatigue life than Model 2 (Kutay & Lanotte 2018).

Four methods are mentioned in **Chapter 2** to conduct fatigue analysis in asphalt mixtures (i.e., fatigue life model, stiffness-modulus-based method, energy-based method and VECD method). The fatigue life model directly correlates the fatigue life of the asphalt mixtures and the test conditions (e.g., strain level, temperature). It is a simple yet powerful method to predict the fatigue life of asphalt pavements. However, the drawback of this model is that it cannot predict the damage propagation in asphalt mixtures (Cheng et al., 2022). The stiffness modulus-based testing method is advanced to predict the fatigue characteristics in asphalt mixtures using the stiffness attenuation trend, but it is again related to the testing conditions failing to give unique testing results. The problem with the different test conditions is the occurrence of identical analysis results, which restricts the derivation of the fundamental fatigue nature of the asphalt mixtures. On the contrary, energy-based and VECD methods can generate a unified fatigue law for asphalt mixtures independent of the loading conditions and reflect on the fatigue nature of the materials (Cheng et al., 2022). Hence, the VECD model is incorporated in this research work to assess the effect of RAP by fatigue and healing of the asphalt mixtures at different testing conditions. Detailed information on results and the calculations for VECD theory using FlexMAT are included in Appendix A of this report.

References

Chehab, G., Kim, Y.R. (2005). Viscoelastoplastic Continuum Damage Model Application to Thermal Cracking of Asphalt Concrete. *Journal of Materials in Civil Engineering 17(4)*.

Daniel J.S., Kim Y.R. (2002). Development of a Simplified Fatigue Test and Analysis Procedure Using a Viscoelastic Continuum Damage Model (with discussion). *Journal of Association of Asphalt Paving Technologists 71*, pp. 619–650.

Cheng, H., Sun, L., Wang, Y., Liu, L., Chen, X. (2022). Fatigue Test Setups and Analysis Methods for Asphalt Mixture: A State-of-the-Art Review. *Journal of Road Engineering 2(4),* pp. 279-308.

Kim, Y.R., Lee, H.J., Little, D.N. (1997). Fatigue Characterization of Asphalt Concrete using Viscoelasticity and Continuum Damage Theory. *Journal of the Association of Asphalt Paving Technologists 66,* pp. 520-569.

Kutay, M.E., Lanotte, M. (2018). Viscoelastic Continuum Damage (VECD) Models for Cracking Problems in Asphalt Mixtures. *International Journal of Pavement Engineering 19*, pp. 1-12.

Kutay, M.E., Gibson, N., Youtcheff, J., Dongré, R. (2009). Use of Small Samples to Predict Fatigue Lives of Field Cores: Newly Developed Formulation based on Viscoelastic Continuum Damage Theory. *Transportation Research Record 2127(1)*, pp. 90–97.

Lee, H.J., Kim, Y.R. (1998). Viscoelastic Continuum Damage Model of Asphalt Concrete with Healing. *Journal of Engineering Mechanics, 124(11)*.

Schapery, R. (1990). A Theory of Mechanical Behavior of Elastic Media with Growing Damage and other Changes in Structure. *Journal of the Mechanics and Physics of Solids 38(2)*, pp. 215-253.

Schapery, R.A. (1975). A Theory of Crack Initiation and Growth in Viscoelastic Media. *International Journal of Fracture 11*, pp. 141–159.

Schapery, R.A. (1984). Correspondence Principles and a Generalized J Integral for Large Deformation and Fracture Analysis of Viscoelastic Media. *International Journal of Fracture 25,* pp. 195–223.

Underwood, B.S., Kim, Y.R., Guddati, M.N. (2010). Improved Calculation Method of Damage Parameter in Viscoelastic Continuum Damage Model. *International Journal of Pavement Engineering 11(6)*, pp. 459-476.

Wang, Y., Kim, Y.R., (2019). Development of a pseudo strain energy-based fatigue failure criterion for asphalt mixtures. *International Journal of Pavement Engineering 20(10)*, pp. 1182–92.

Wang, Y.D., Underwood, B.S., Kim, Y.R. (2020). Development of a Fatigue Index Parameter, Sapp, for Asphalt Mixes using Viscoelastic Continuum Damage Theory. *International Journal of Pavement Engineering 23(2),* pp. 438–452.

Zeiada, W.A., Gudipudi, P.P., Underwood, B.S., Soulima, M.I. (2018). Effect of Loading Waveform Pattern and Rest Period on Fatigue Life of Asphalt Concrete using Viscoelastic Continuum Damage Model. *Transportation Research Record 2672*, pp. 451–461.

Zhang, Y., Luo, R., Lytton, R.L. (2013). Characterization of Viscoplastic Yielding of Asphalt Concrete. *Construction and Building Materials 47*, pp. 671–679.

Chapter 4

Materials and Test Methods

4.1 Introduction

To quantify the effect of reclaimed asphalt pavement (RAP) materials in the fatigue and healing performance of asphalt mixtures, frequency sweep stiffness and fatigue and fatigue-healing tests were performed in the laboratory. In Europe, there is no standardized description for the uniaxial test setup, and hence, AASHTO norms for the dynamic modulus and fatigue and fatigue-healing testing in this program were employed. First, the dynamic modulus tests are conducted in haversine load-controlled mode under compressive stress as per AASHTO T 342-11. Afterward, the fatigue and fatigue-healing tests were performed in an on-specimen mode in tension-compression loading mode as per AASHTO TP 107-18. The only significant difference between the fatigue and fatigue-healing tests is the application of loading with group rest periods to allow the restoration of mechanical properties (healing) under giving healing time at different temperatures. Before the cyclic tests (i.e., fatigue and fatigue-healing), fingerprint tests were conducted in the LVDT (linear variable differential transformer)-controlled tension-compression loading mode. Details of the materials and test methods employed are discussed in the next sub-sections.

4.2 Materials

For this study, three different mixtures were produced:

- Mixture 1, or M1 (100 % m/m virgin aggregates and 0 % m/m RAP),
- Mixture 2, or M2 (30 % m/m virgin aggregates and 70 % m/m RAP), and
- Mixture 3, or M3 (30 % m/m virgin aggregates and 70 % m/m RAP with a recycling agent).

The test program comprises producing three mixtures with varying compositions of RAP and recycling agents. Details of different types of mixtures produced for this research are given in **Table 4.1**. M2 and M3 were asphalt mixtures produced with 70% RAP and 30% of virgin aggregates (VAs), with the mixture named M1 to be used as a reference. The Anova 1817 recycling agent was used in M3, and its efficiency in balancing the rheological properties of the bituminous part of the RAP materials in M3 was assessed. Note that the target binder content in all mixtures was 4.3 % m/m, and the RAP materials contained 4.5 % m/m binder of 20 dmm pen grade.

Table 4.1. Description of the studied asphalt mixtures.

Mixture	Description	Composition
M1	AC22 Base 40/60	100%VA-0%RAP (reference)
M2	AC22 Base 35/50 +70%PR	30%VA-70%RAP
M3	AC22 Base 40/60 + 70%PR & agent *	30%VA-70%RAP + agent *

* Anova 1817 recycling agent (supplied by Cargill).

Three different pen-grade binders were used in the three different asphalt mixtures. The detailed physical properties of binders used in production and mixtures are mentioned in **Table 4.2.** Physical properties of binder and mixtures used in the test program.

M1, M2, and M3 were produced at Laboratorium Ontwikkeling Wegenbouw (Dura Vermeer), Eemnes, the Netherlands. All constituent materials to formulate the mixtures were procured directly from the asphalt plant production located next to the laboratory at Eemnes.

Table 4.2. Physical properties of binder and mixtures used in the test program.

Properties	Technical Specification	M1[*1]	M2[*2]	M3[*3]
Penetration [x 0.2-mm]	NEN-EN 1426:2015	30.0	19.0	39.0
Ring & Ball Temperature [°C]	NEN-EN 1427:2015	54.0	61.5	52.5
Binder Percentage [% m/m]	NEN-EN 13108-1:2006	4.5	4.5	3.9
Air Void Content [% V/V]	NEN-EN 13108-1:2006	4.5	3.8	3.7
Density [kg/m³]	NEN-EN 13108-1:2006	2507	2485	2483

production temperature [°C]: [*1] 165, [*2] 170, [*3] 165

Table 4.3. Percentages of materials used in the studied asphalt mixtures.

Building Code	Name of Material	Result matrix calculation [% m/m]		
		M1	M2	M3
4630 (v1.2)	Bestone 11/16 Norway	20.18	10.09	10.09
4620 (v1.2)	Bestone 8/11 Norway	11.84	4.12	4.12
4600 (v1.2)	Bestone 2/5 Norway	7.53	1.78	1.78
4610 (v1.3)	Bestone 4/8 Norway	13.46	3.45	3.45
5030 (v1.2)	Scottish granite 0/2 Scotland	9.07	-	-
5120 (v1.2)	Coarse sand 0/2 Netherlands	27.22	9.20	9.20
6110 (v1.0)	Wigro 50K 0/0.1 Winterswijk	4.90	0.01	0.01
6190 (v1.0)	Own dust 0/0.1 AMI	1.50	0.20	0.20
7273TT (v1.0)	Anova 1817 ANOVA 1817	-	-	0.20
7010 (v1.0)	Penetration bitumen 40/60	4.30	-	-
7030 (v1.0)	Penetration bitumen 70/100	-	-	0.95
7040 (v1.0)	Penetration bitumen 160/220	-	1.15	-
8023TT2207 (v1.2)	Recycled Asphalt Pavement 0/16 APE	-	70	70

Table 4 is also tabulated using information about aggregate gradation (CROW 0/22 base layer mixture). Based on the information tabulated, **Figure 4.1** is plotted, representing that the gradation curves plotted are in the maximum and minimum permissible ranges. The curve indicates dense-graded mixtures with a small proportion of small aggregates.

Table 4.4. Aggregate gradation of the studied asphalt mixture.

Sieve size [mm]	min. [% m/m]	max. [% m/m]	Percentage passing [% m/m]		
			M1	M2	M3
22.4	98.0	100.0	100	100	100
16.0	88.4	100.0	97	90	95
11.2	72.0	90.0	85	70	81
8.0	-	-	69	54	68
5.6	-	-	60	44	58
2.0	36.0	50.0	44	33	43
0.5	-	-	27	24	29
0.18			13	12	12
0.125	4.1	14.1	10	10	9
0.063	4.0	10.0	6	8	7.2
Binder content [% m/m]	3.7	4.9	4.5	4.5	3.9

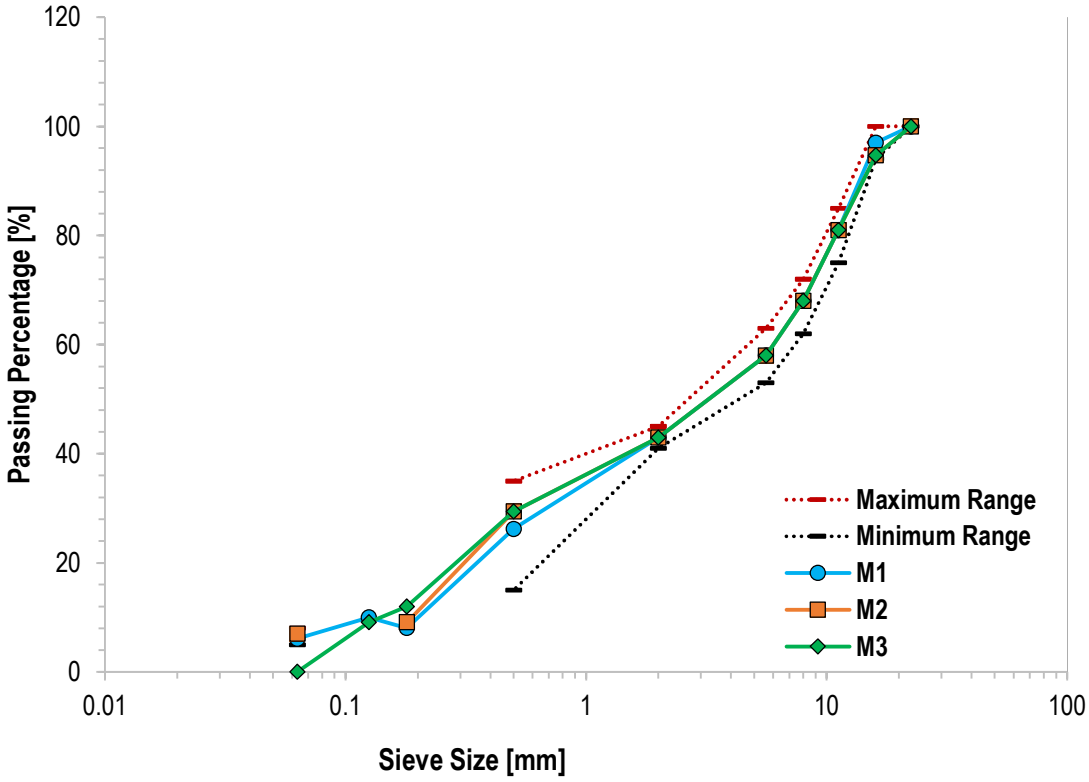

Figure 4.1. Aggregate gradation curves of the studied asphalt mixtures.

Superpave gyrator compacted specimens of 160 mm height and 120 mm diameter were kept in the temperature-controlled storage room at 12°C for a week, and then they were cored to obtain specimens of the desired dimensions of 100 mm diameter with polished ends. A thickness of 5 mm from both ends was polished with a polishing machine available at TU Delft, and specimens ready to test with 150 mm height and 100 mm diameter were obtained. Note that it was ensured that no specimens were loaded on top of one another during storage. According to AASHTO TP 107-18, the height of the specimen should be 130 mm, but in this study, a specimen with a height of 150 mm was used to maintain a minimum height-to-diameter ratio of 1:1.5 (process of specimen preparation before testing is given in **Figure 4.2**).

(a) (b) (c) (d) (e) (f)

Figure 4.2. Specimen: (a) as received from Dura Vermeer (b) mounted in core cutter at TU Delft lab (c) after cored out (d) mounted in polishing machine (e) after coring and polishing (f) mounted in the hydraulic testing machine ready for stiffness testing.

4.3 Dynamic Modulus Test

Dynamic modulus values were measured over a range of temperatures and frequencies of loading with prepared master curves for characterizing asphalt mixtures for pavement thickness design and performance analysis (AASHTO T 342-11). The dynamic modulus tests in this study were performed in accordance with AASHTO T 342-11. These tests were performed on Instron 8800 Fasttrack controller and IST Labtronic 8400 controllers without any confinements.

The applied axial haversine compressive load on the specimen and resulting axial strains were recorded as a function of time and used to calculate the dynamic modulus and the phase angle. The dynamic modulus tests were performed for -5, 5, 10, 20, 30, 40 and 50°C for frequencies and number of cycles at each frequency as in **Table 4.6**.

Figure 4.3 shows the haversine compressive load at 25 Hz at 10°C. The load varied with the temperature changes as per AASHTO T 342-11, and the range of dynamic stress to be applied to the specimen is provided in **Table 4.5**. However, the input to the mechanical testing system at TU Delft takes load as an input parameter. Hence, the stress was converted to load using the specimen's geometry and was linearly interpolated to the temperature at which the tests were performed.

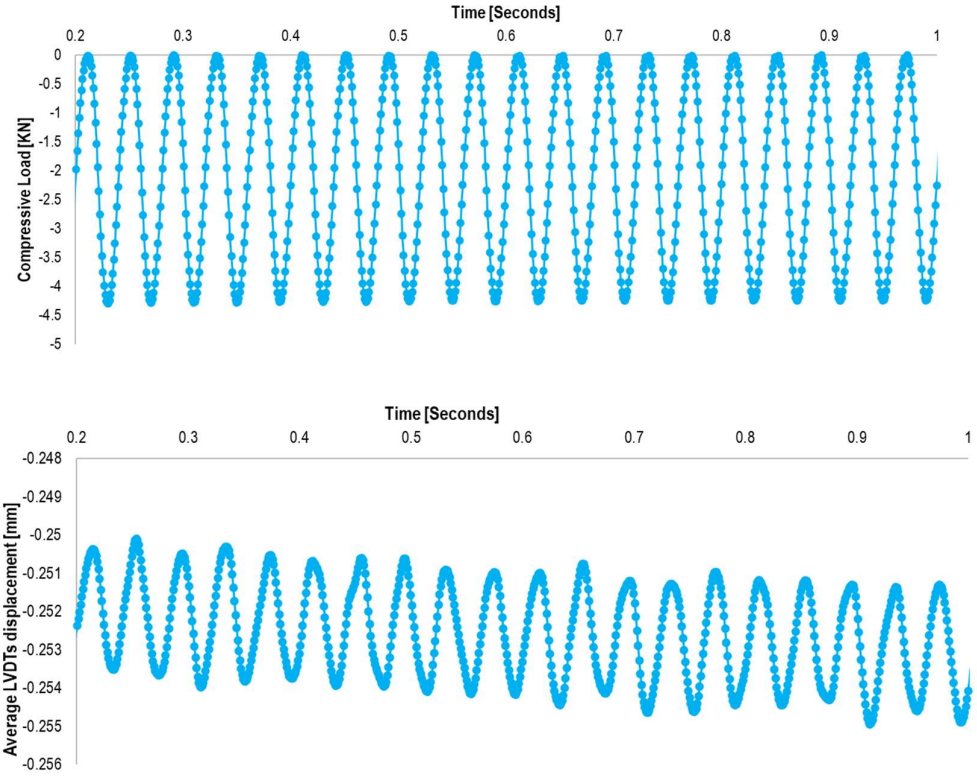

Figure 4.3. A characteristic plot of (a) compressive load vs. time during the dynamic modulus test (b) average LVDTs displacement vs. time during the dynamic modulus test per AASHTO T 342-11 (M1 at 25 Hz and 10°C).

Table 4.5. Stress ranges applied on specimens during dynamic modulus tests (AASHTO T 342-11).

Temperature [°C]	-10	4	21	37	54
Stress range [kPa]	1400 to 2800	700 to 1400	350 to 700	140 to 250	35 to 70

According to AASHTO TP 342-11, performing the dynamic modulus test starting from a lower temperature and higher frequency is recommended to minimize damage to the specimen. The specimen was mounted between two loading platens diameter of 104±1 mm. The number of cycles at each frequency for which the dynamic modulus test was performed is given in **Table 4.6.** The stiffness is expected to increase, and the phase angle decreases with the frequency increase. The stiffness also decreased with an increase in the testing temperature compared to the same frequency range. The results obtained in this study are given in **Chapter 5**.

Table 4.6. The number of cycles for different frequencies.

Frequency [Hz]	25	10	5	1	0.5	0.1
Number of cycles	200	200	100	20	15	15

Three LVDTs were mounted at 120° to measure the displacement for a gauge length of 80 mm in the middle of the sample (**Figure 4.4**). In-house MP3 software records filtered loads, range of load in cycles, displacements, average displacements, and phase angle. The data was then processed using empirical relations to calculate the dynamic modulus of elasticity for different asphalt mixtures. The gauge length of 80 mm was kept constant for all tests. As per AASHTO T 342-11, the ends of all stiffness-tested specimens shall be smooth and perpendicular to the axis of the specimen. No gluing of specimens in the test setup is required as the test is performed in compressive loading mode. Friction-reducing end treatments were placed between the specimen ends and the loading platens. Instead of 0.5 mm thick latex membranes, a Teflon sheet with a plastic membrane was used, stuck with 1 gram of white grease (see **Figure 4.4**). In this way, the extra tensile stresses produced on the ends of the specimen were reduced due to the elongation of the latex membrane under compressive loadings. A ball and plate arrangement was introduced in the specimen setup to maintain constant contact between the loading platens and ends of the specimen under compressive load when it was not glued.

Figure 4.4. (a) White Vaseline and plastic sheet for end treatments (b) Ball and plate arrangement for uniform load distribution in stiffness testing.

The loads on specimens to be produced to conduct the stiffness test at different temperatures were calculated and given in **Table 4.7.**

Table 4.7. Load applied in dynamic stiffness test at different temperatures.

Temperature [°C]	-5	5	10	20	30	40	50
Load as per norm [kN]	-7.00	-5.00	-4.20	-2.50	-1.82	-0.95	-0.35

It is to be noted that the temperatures used in the test were different from the AASHTO recommendation, for which the loads were interpolated. The dynamic modulus test data post-processing was done using FlexMAT. The dynamic modulus and phase angle calculated, along with the temperature and frequencies for three mixtures, were taken and processed in FlexMAT (**Appendix A**). Test results are discussed in **Chapter 5**.

4.4 Fatigue Test

4.4.1 End treatment

In the uniaxial cyclic fatigue test, end treatment is required to adhere the specimen to the loading platens. First, both the loading platens (104±1 mm diameter) were thoroughly cleaned by brushing the end plates with sandpaper. The end plates were sandblasted to increase the adhesion bond in the specimen and platen before being used in the test using the facility available at DEMO TU Delft. After cleaning the plates, the surfaces were wiped and cleaned with acetone. A powdered glue, "Pedi-kit 860 A" mixed with X60 hardener, was prepared to adhere the end plates and specimens to each other. A safety mask was put on before the preparation of glue. Firstly, the bottom end of the specimen was glued manually. 20 grams of glue powder was weighed in a paper cup and mixed with 10-12 ml of hardener. Consistency in glue preparation was one of the most important and challenging tasks performed in the laboratory. The prepared glue paste was poured and spread uniformly over the loading platens. The bottom end of the specimen was then placed over this glue and was confined with two PVC rings at the bottom. These PVC rings enhanced the gradual distribution of stresses at the end, providing better confinement around the specimen and helping in centering the specimen. Later, it was left to cure for 20-25 minutes (see **Figure 4.5**).

Figure 4.5. (a) Sandblasted loading plates and (b) different equipment required for end treatment (Powdered glue, 3M mask, specimen, hardener, rubber gloves, PVC rings, Mixing cup & Acetone).

After gluing the lower end, the specimen was mounted in the mechanical testing system. Then, a new glue mix was prepared and poured onto the lower platen mounted in the setup. The lower plate was compressed with the controller in the load-controlled mode,

mechanically gluing the specimen's top part (**Figure 4.6**). Note that the mixing and placing of glue should be completed in 20-25 s. It is again cured for 20-25 minutes, and then the tests can be conducted.

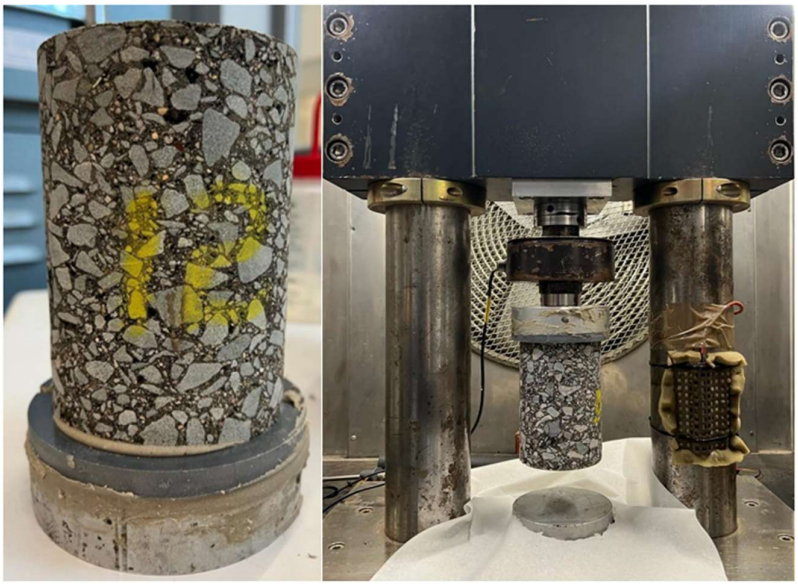

Figure 4.6. Gluing (a) the lower end of the specimen and (b) the upper end under compression loading.

4.4.2 Fingerprint test

It is important to conduct the fingerprint test at the beginning of the fatigue test to determine the material's initial complex modulus of elasticity. A low strain magnitude (50-75 μ-strain) |E*| test to be conducted at fatigue test temperature and the same frequency confirms the findings from the dynamic modulus tests (Zeiada et al., 2013). The value of the complex modulus may vary among specimens with different mixtures. As per AASHTO TP 107-18, the fingerprint test should be performed in tension-compression loading mode. The test was conducted at 10 Hz, with a target strain range of 50 to 75 μ-strain, and at the designated test temperature in a strain-controlled manner. The test should last 50 cycles, with 100 data points recorded per cycle using the appropriate software. In-house MP3 software records the readings, including load, LVDT deformations, frequency, and the number of cycles. The fingerprint value obtained from the test was an important factor in determining the target strain levels to be applied on the specimen, as per AASHTO TP 107. Hereafter, a specimen was left to rest for 20 to 45 min before starting the fatigue and fatigue-healing tests.

4.4.3 Uniaxial tension-compression fatigue test

After the end treatment and the fingerprint test, the specimen mounted is put under repeated cyclic loading to conduct a fatigue test. This test was performed strain-controlled. Detail on the selection of testing mode is given in **Appendix B**. The applied load and on-specimen axial strain response were measured and used to calculate the necessary quantities.

The cyclic fatigue testing in this study was performed at 10, 20 and 30°C for 10 Hz on all three mixtures. The cyclic fatigue test was conducted on two replicas for every mixture for every three mixtures. A total of 18 specimens were tested for continuous cyclic fatigue tests comprising 2 replicas of 3 mixtures tested at 3 temperatures. The on-specimen strain rate of 200 μ-strain peak to peak in sinusoidal tension-compression loading mode is applied. This

strain rate was optimized after conducting cyclic fatigue tests on several specimens to have enough cycles for all temperature values before the failure. Details on a selection of 200 μ-strain are in **Appendix B**. The data acquisition was made with the help of MP3 software in two separate files:

i. First few full cycles with data acquisition at 0.001 s for 100 points per cycle.
ii. Parallel running file with 1 point per cycle at 0.1 s acquisition time.

FlexMAT software was used to perform the post-processing of the fatigue data. The data recorded was thus formatted in the required format fed in FlexMAT to conduct the mathematical calculations based on Viscoelastic Continuum Damage (VECD) theory. Details on formatting the file are in **Appendix A**. The outputs of FlexMAT mathematical equations involved in Simplified Viscoelastic Continuum Damage (S-VECD) theory were used to predict the characteristic damage curve. These damage characteristics represent the fundamental relationship between the damage and the material integrity of asphalt mixtures. It has already been mentioned that these properties are independent of temperature, frequency, and loading mode. Involving the LVE properties of asphalt mixtures, the characteristic damage curve can be used to analyze the fatigue of asphalt mixtures (AASHTO TP 107-18).

4.5 Uniaxial Tension-Compression Fatigue-Healing Test

As mentioned above, the fatigue-healing test methodology is like continuous cyclic fatigue testing. The only difference is the application of rest periods to different stages of damage in specimens (i.e., 0.9C, 0.8C, 0.7C, etc.). The healing tests were performed on a total of 54 specimens of three different mixtures at three different temperatures (10, 20 and 30°C) for three rest periods (40, 80, and 160 s). The use of adhesive for end treatments and the procedures used in testing were unchanged.

4.5.1 Duration and mode of application of rest periods

To assess the effect of different factors on the healing properties of asphalt mixtures, different mixtures, temperatures, and rest periods were incorporated in this study. A manually implemented group rest period in cyclic fatigue was conducted at a frequency of 10 Hz for three different rest periods at three different temperatures for three different mixtures summing up to 27 different testing conditions. The rest periods were chosen based on the study performed by NASEM 2010. This study assumes a pavement design life of 40 years and a total of 20 million Equivalent Single Axle Load (ESAL). If an average rest period is drawn from this data in time, it comes out to be 63 s. It indicates that at an average of 63 s (i.e., 40 years divided by 20 million ESALs), the pavement is under a traffic load of one axle. The decision to take one value of rest period below average (as for reference, 0 s rest period is already performed as continuous fatigue testing) and two other values higher than average. A healing study with different rest periods was done with the smallest rest period is about 2 minutes. The results showed that even with 10 s of the rest period, initial healing due to the crack wetting might happen fast during the rest period. It is suggested to keep the healing period much smaller than 2 minutes used (Si et al., 2002).

Though this average rest period is theoretical, it will be too time-consuming to model it mechanistically in the laboratory. Therefore, a decision to have accelerated testing for healing with group rest healing was adopted over pulse rest healing. The group rest period

test is much faster than the pulse-rest test, such that a group rest test with 60 s rest period take a testing time of 3 h, including the temperature conditioning, but a pulse-rest test with the same rest period may last for several days (Ashouri 2014). With three rest periods at three temperatures, an effort to plot a healing master curve was also incorporated into this study (Chapter 5).

4.5.2 Application of rest periods

At the beginning of fatigue testing, the strain rate was decided so that the testing sequence results in a reasonable number of cycles to the failure of the specimen. This enables the implications of rest periods to assess healing and avoid the long testing time. Group rest periods were introduced at different damage levels in each specimen to account for the effect of the amount of damage prior to the application of the rest period on the healing potential of the material as well. The pseudo-stiffness parameter was calculated based on the fingerprint test calculated on the specimen and the stiffness calculated during the rest period.

The strain-controlled tension-compression cyclic test was interrupted by different rest periods at different percentage reductions in the specimen's initial stiffness (damage stages) (e.g., 0.9C, 0.8C, 0.7C and 0.6C). Where 0.9C corresponds to 10% of damage in the specimen, the specimen at the beginning of the test can bear a higher load with time decreases. The peak-to-peak load values were the load values at which the specimen applied the rest period. An event can be created on the controller such that load cycles are interrupted and a rest period is provided with an external stopwatch. The machine is to be started manually after a rest period and with a further 10% of the damage; the rest period was provided again.

Performing the test in this way, healing potential change concerning the damage level before applying the rest periods and the damage growth rate can also be monitored. The test was also performed on three mixtures and temperatures for different rest periods. The effect of the healing potential on the material due to substantial factors can also be obtained.

Overall, this part of the report summarized the major parameters and details about the materials and test methods employed for assessing the fatigue damage propensity and the healing potential of asphalt mixtures containing recycling materials. In the next chapter, the results of the test program are presented.

References

American Association of State Highway and Transportation Officials. *Determining the Dynamic Modulus and Flow Number for Asphalt Mixtures Using the Asphalt Mixture Performance Tester (AMPT)*. AASHTO T 378, Washington, D.C., 2017.

American Association of State Highway and Transportation Officials. *Determining the Damage Characteristic Curve of Asphalt Concrete from Direct Tension Cyclic Fatigue Tests*. AASHTO TP 107, Washington, D.C., 2014.

American Association of State Highway Transportation Officials. *Determining Dynamic Modulus of Hot-Mix Asphalt Concrete Mixes*. AASHTO T 342-11, Washington, D.C., 2011.

Ashouri, M. (2014). *Modeling Microdamage Healing in Asphalt Pavements using Continuum Damage Theory*. Ph.D. Thesis, North Carolina State University.

National Academies of Sciences, Engineering, and Medicine. (2010). *Validating the Fatigue Endurance Limit for Hot Mix Asphalt*. Washington, D.C.: The National Academies Press.

Si, Z., Little, D.N., Lytton, R.L. (2002). Characterization of Microdamage and Healing of Asphalt Concrete Mixtures. *Journal of Materials in Civil Engineering 14*(6), pp. 461-470.

Zeiada, W.A., Kaloush, K.E., Underwood, B.S., Mamlouk, M.S. (2013). Effect of Air Voids and Asphalt Content on Fatigue Damage using the Viscoelastic Continuum Damage Analysis. In *Airfield and Highway Pavement: Sustainable and Efficient Pavements,* pp. 1122-1133.

Chapter 5

Fatigue and Healing Laboratory Results and Discussion

5.1 Introduction

In this chapter, the results and the outcomes of the experimental program performed during this study are described. The outcomes of dynamic modulus testing, cyclic fatigue and fatigue-healing testing are mentioned. The comparison of the effect of RAP materials and the recycling agent on the fatigue and healing of asphalt mixture is also discussed.

5.2 Dynamic Modulus Test Results

Dynamic modulus test was performed as per AASHTO T 342-11. Details on the test method are discussed in **Chapter 4.**

5.2.1 |E*| values for load variations with temperature as per AASHTO T 342-11

The stiffness, |E*|, of the asphalt mixture, which is a measure of its resistance to deformation under the applied load, is a material property, so varying the load with respect to temperature and frequency should not bring any difference in the testing. Asphalt is a viscoelastic material, so its mechanical behavior is influenced by its elastic and viscous properties. The |E*| of asphalt is primarily governed by its elastic response, while the viscous response is related to its ability to dissipate energy through relaxation. The number of cycles at which the test was performed for each frequency is given in **Table 4.5**. The |E*| test was performed per set of loads with the temperature provided in **Table 4.6**.

Figure 5.1 shows the |E*| values for different frequencies for all mixtures. For a fixed temperature, the value of |E*| decreased with a decrease in the frequency. With lower frequency, the viscous effect exceeds the elastic response, giving a lag in the load signal and displacement signal, increasing the phase angle and lowering |E*|. With the increase in temperature, the |E*| value decreased, but the phase angle increased as the material tended to behave more soft. Phase angle in asphalt mixtures increased with an increase in the temperature due to a reduction in the viscosity of the binder, softening of the material and enhanced relaxation behavior at higher temperatures. Enhanced relaxation behavior means a less stiff behavior where the time available for relaxation between the load cycles increases, leading to more energy dissipation and a less stiff response of the material, which is vice-versa in the case of higher frequency.

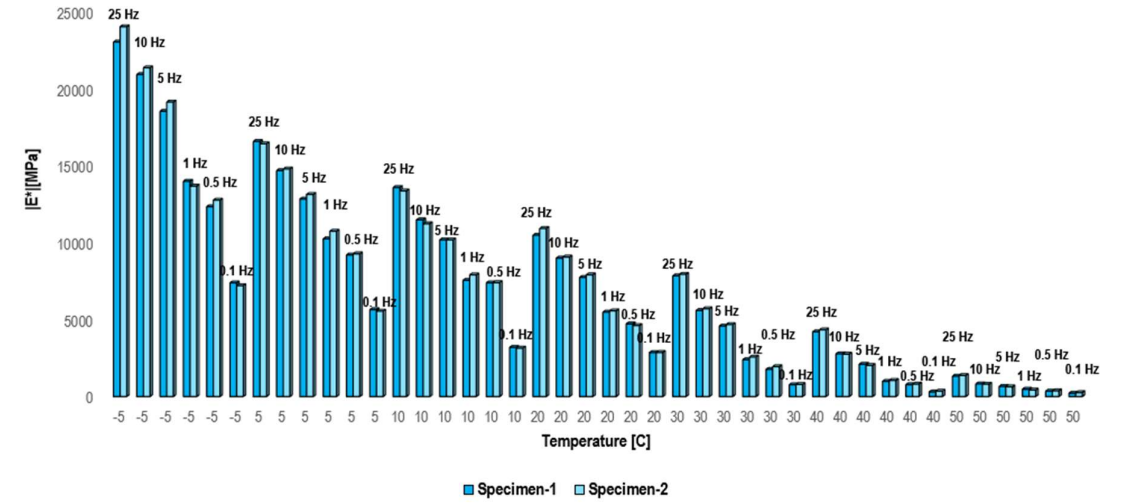

(a)

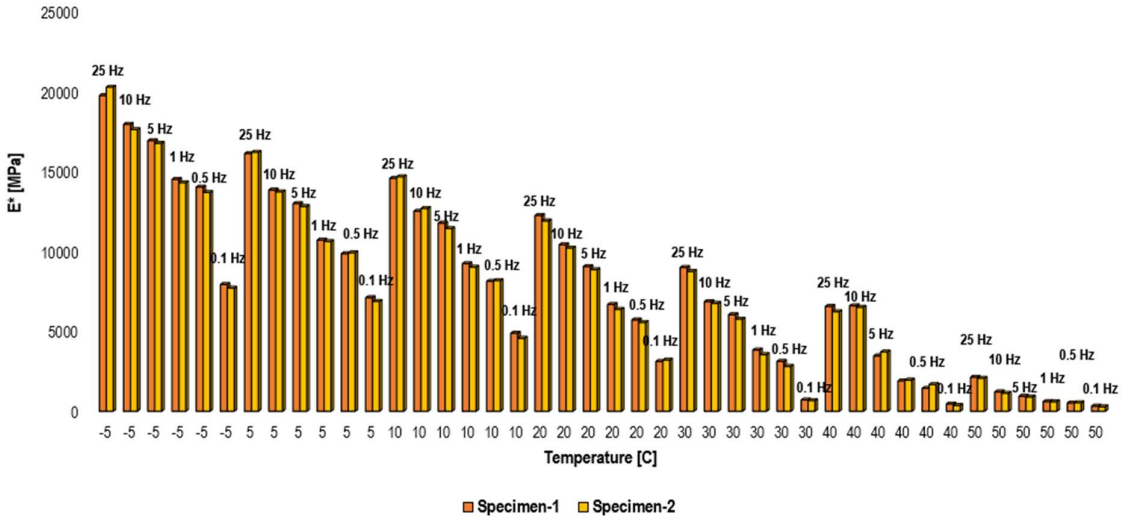

(b)

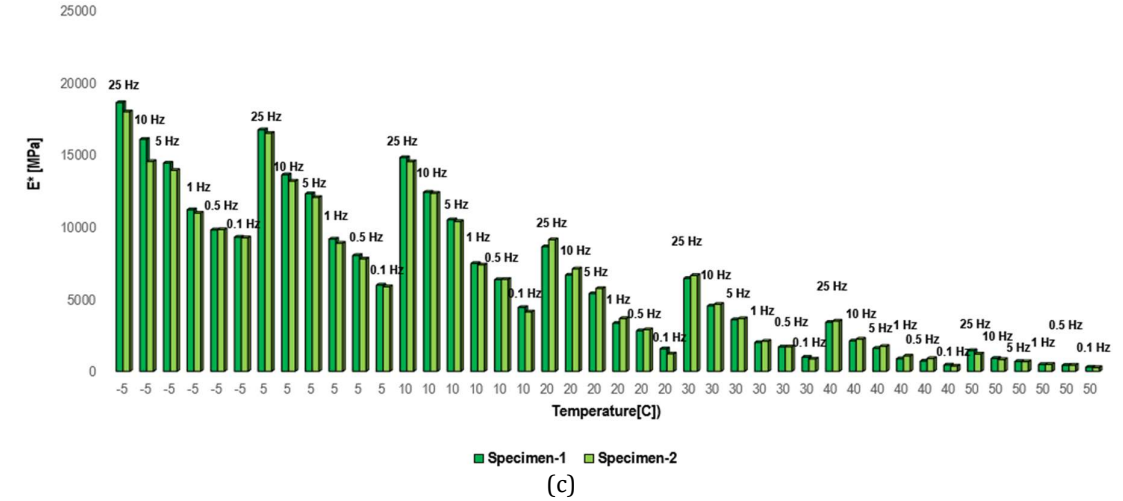

(c)

Figure 5.1. Variation in values of dynamic modulus among two specimens of three different mixtures.

5.2.2 Stiffness and phase angle master curves

The post-processing of |E*| results was done using FlexMAT™ cracking software. Details on the procedure of this post-processing are given in **Appendix A**. With the |E*| and phase angles calculated at different frequencies and temperatures for the two replicas of the three mixtures, a master curve is plotted using TTSP. This allows the estimation of phase angles and |E*| of mixtures at different temperatures, which are important in understanding and predicting the performance under various conditions. The reference temperature used by FlexMAT is 21.1°C.

Figure 5.2 shows that M2 (i.e., the mixture with 70% RAP) was the stiffest for all the frequencies and temperatures due to the presence of an aged binder. M3 was the softest material even though it also has the same amount of RAP as M2, as a recycling agent implicates the softness in the mixture. All three combinations differed in stiffness; one was stiffer than the reference mixture, and the other was softer. Also, these phase angles were plotted with the reduced frequency in **Figure 5.3.** With an increase in the frequency, the phase angle decreases. As with an increase in the frequency, the |E*| of the material increased, and the phase angle between the load and displacement decreased.

For the cyclic fatigue analysis using the S-VECD theory, the LVE properties for analysis are tabulated below, which are the output of FlexMAT. With the LVE properties mentioned in **Table 5.2** (using values of *a1*, *a2*, and *a3*), the shift factor for different temperatures was calculated using **Eq. 5.1**. The shift factor calculated for all mixtures is further plotted in log scale with the temperatures in **Figure 5.4**. These shift factor values were used for healing predictions in the upcoming section.

Relaxation modulus describes the stress relaxation of a material with time. With time, the stress in asphalt mixtures gradually dissipates. The mixture with higher relaxation modulus is resistant to permanent deformation and less prone to rutting. The maximum slope of the relaxation modulus vs. time plot is drawn in the log-log scale in **Figure 5.** It is termed the damage evolution rate denoted by *m* – note $\alpha = (1/m) + 1$ for the strain-controlled test. The values calculated for the damage evolution rate are mentioned in **Table 5.3.** The higher the *m* value, the lower the alpha value; hence higher the damage development rate. These factors were calculated automatically in FlexMAT. After calculating the LVE properties using the dynamic modulus test data, the next step is to assess the fatigue and healing characteristics of the mixtures covered in the following section.

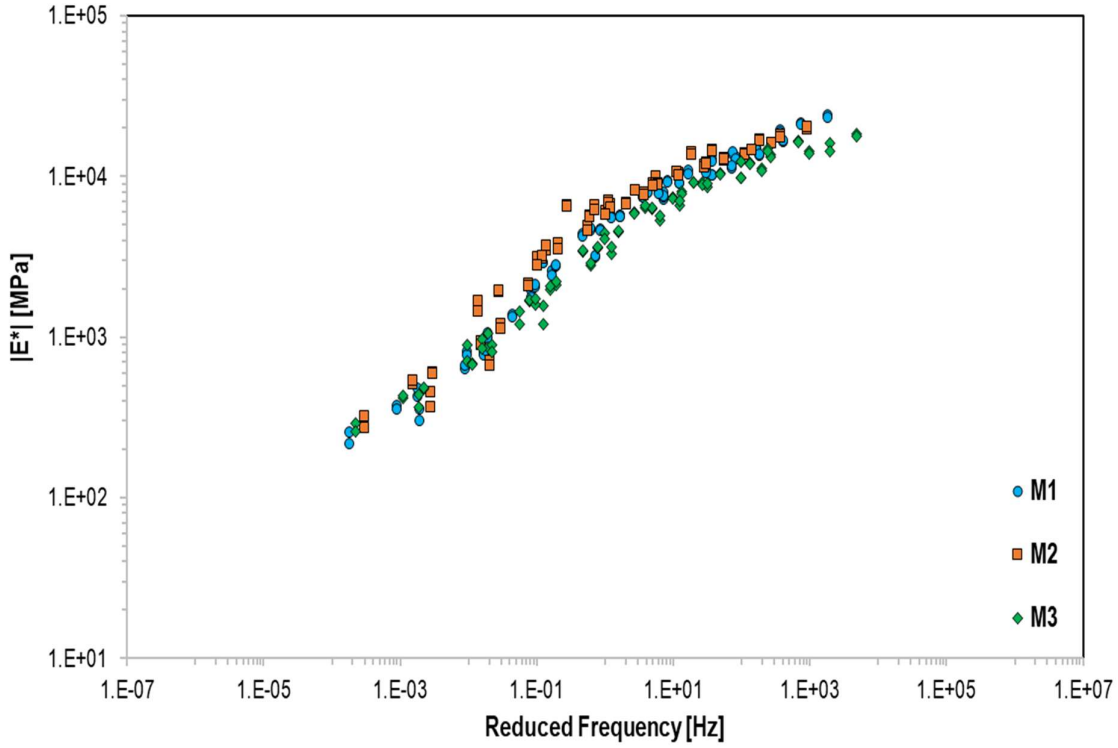

Figure 5.2. Dynamic modulus master curve.

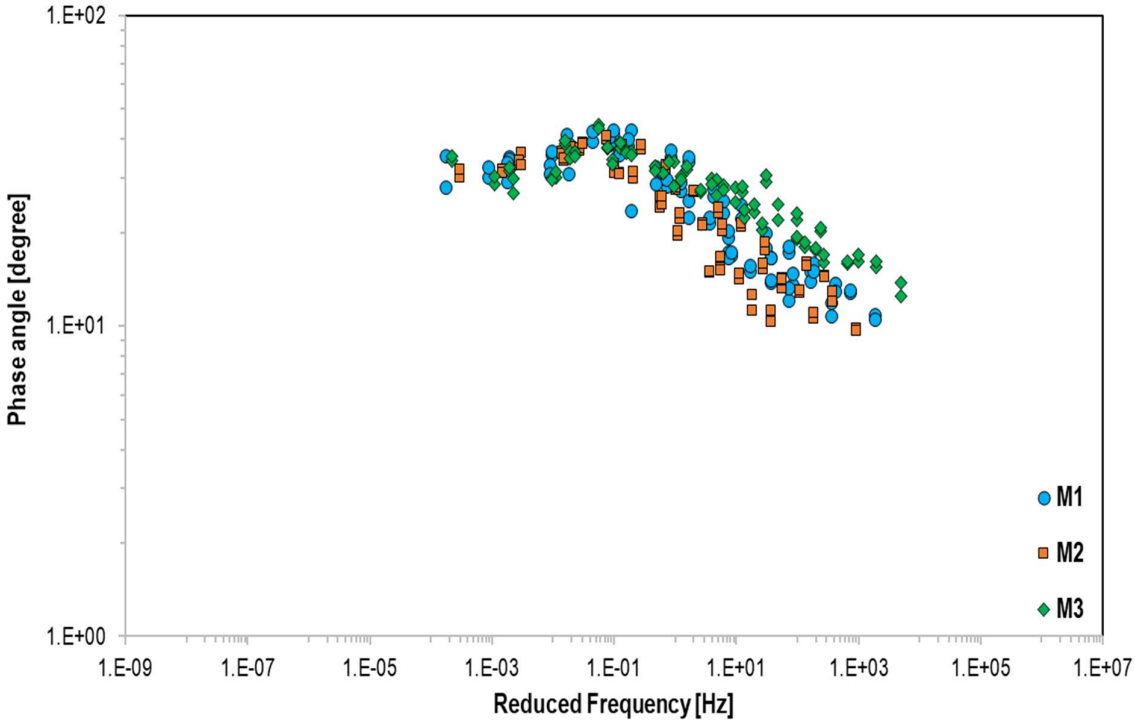

Figure 5.3. Phase angle master curve.

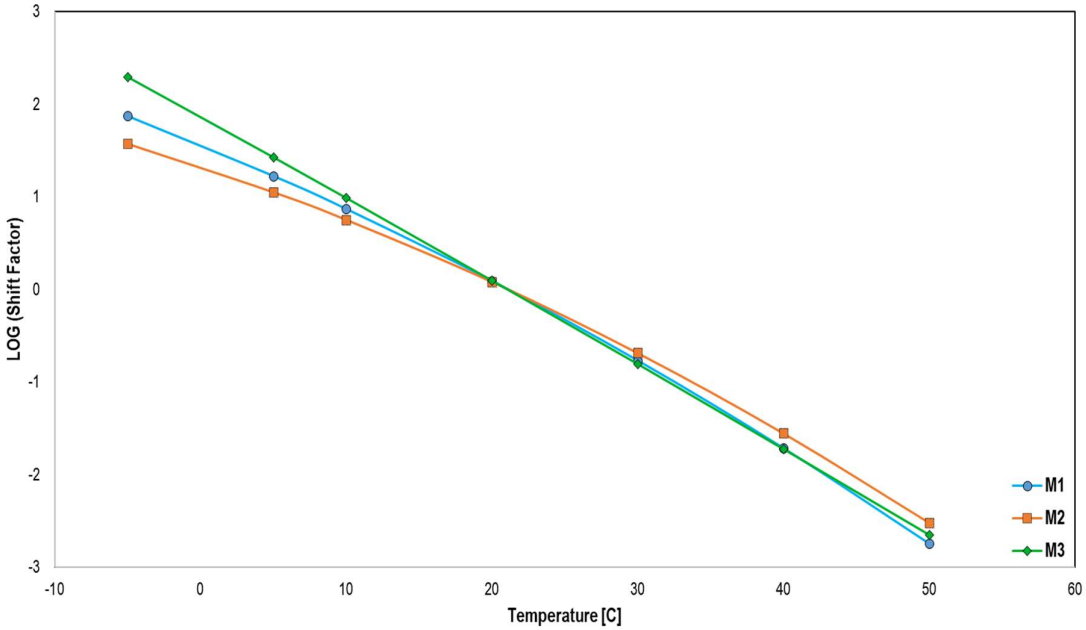

Figure 5.4. Shift factors calculated for different mixtures at different temperatures.

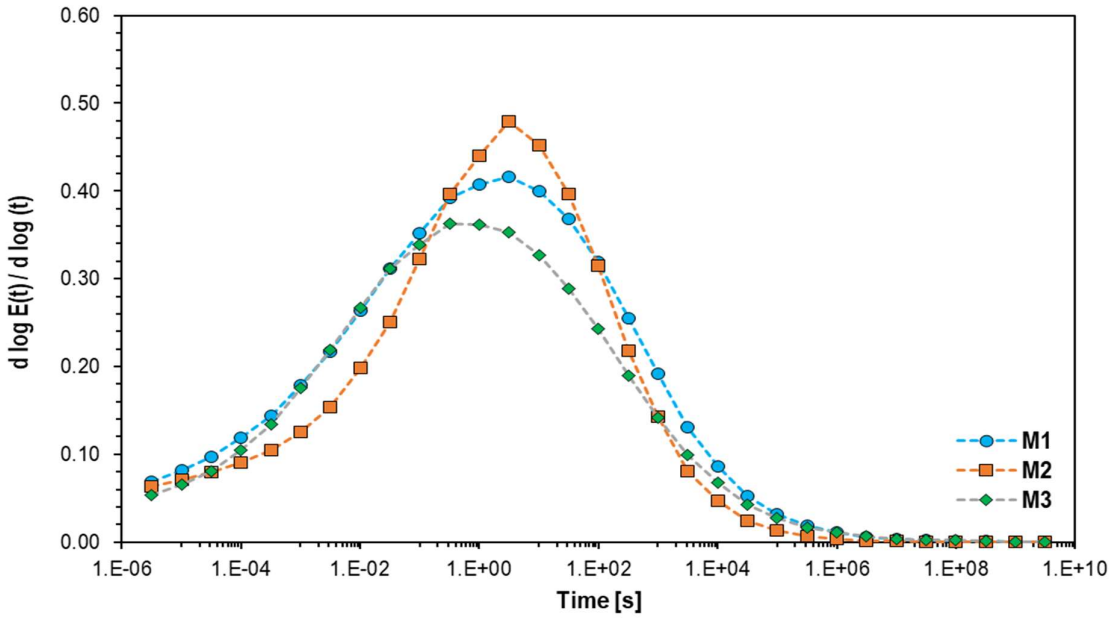

Figure 5.5. The slope of the relaxation curve (E(t)) vs. time (t) in the log-log scale.

Table 5.1. LVE Properties calculated by FlexMAT.

LVE properties	M1	M2	M3
E_{inf}	89766.31	136524.61	133731.46
Poisson's Ratio	0.3	0.30	0.30
T_{REF} (°C)	21.1	21.1	21.1
Shift Factor *a1*	-0.00043	-0.000491606	-6.97422E-05
Shift Factor *a2*	-0.06475	-0.052224789	-0.086749187
Shift Factor *a3*	1.556068	1.320810782	1.861457778

Table 5.2. Shift factors for different temperatures.

Temperature	a_T (M1)	a_T (M2)	a_T (M3)
-5	73.99228	37.12312989	196.5441666
5	16.65868	11.15312829	26.66663935
10	7.343496	5.615679742	9.70491388
20	1.231681	1.201358866	1.254807631
30	0.169768	0.204937795	0.157113743
40	0.01923	0.02787727	0.019050341
50	0.00179	0.003023829	0.002236881

Table 5.3. Damage evolution rates for different mixtures.

Mixture	m	α (alpha)
M1	0.4158	3.39
M2	0.4789	3.06
M3	0.3622	3.71

5.3 Uniaxial Tension-Compression Fatigue Test Results

Strain-controlled fatigue testing was performed in tension-compression mode. The constant strain rate of 200 μstrain was used for all temperatures and mixtures. The failure criterion for the mixture's fatigue failure was when the specimen's stiffness was reduced to 50% of its initial value. Due to the higher stiffness of the materials used, sometimes at lower temperatures like 10°C, this 50% reduction in stiffness is difficult to achieve due to the sudden failure of the material; hence the number of cycles giving this brittle failure is the fatigue life of mixtures. The tests were performed on two replicas for each set of testing.

Considering the variations within the specimen of the same mixtures, AASHTO TP 107-18 suggests conducting the fingerprint test to calculate this initial value. The variation in fingerprint values of specimens at different temperatures is shown in

Figure 5.6. With the increase in the temperature, the material's stiffness decreased. The fingerprint tests validated the results obtained from the earlier dynamic modulus tests. M3 was the softest mixture for all the temperatures, whereas M2 was the stiffest material. The stiffness of M1 lies between the stiffness of the other two mixtures.

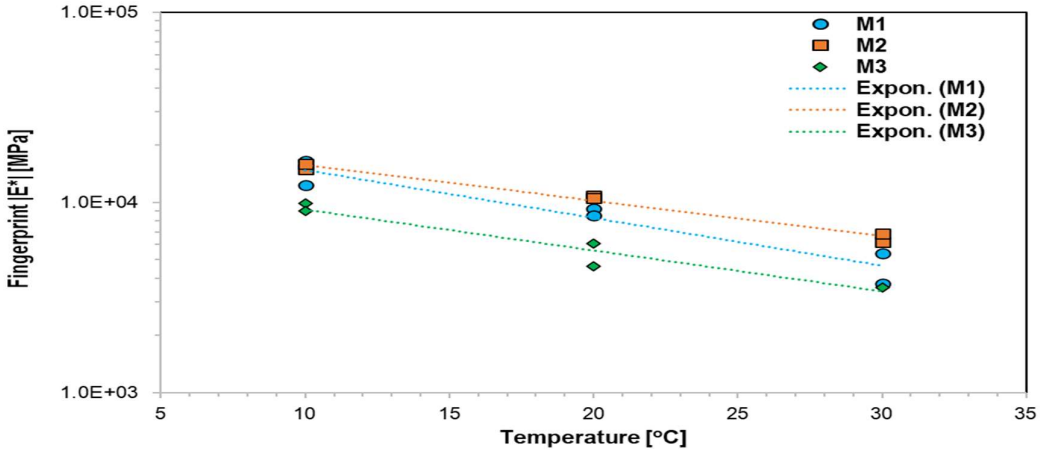

Figure 5.6. Variation of fingerprint values of different mixtures with temperatures.

In cyclic fatigue testing, the damage accumulated in the specimen with increased cycles, decreasing the material's stiffness. One such example from fatigue testing is shown in **Figure 5.6**. The material's stiffness decreased with the increase of damage cycles, leading to an increase in the phase angle (**Figure 5.7**).

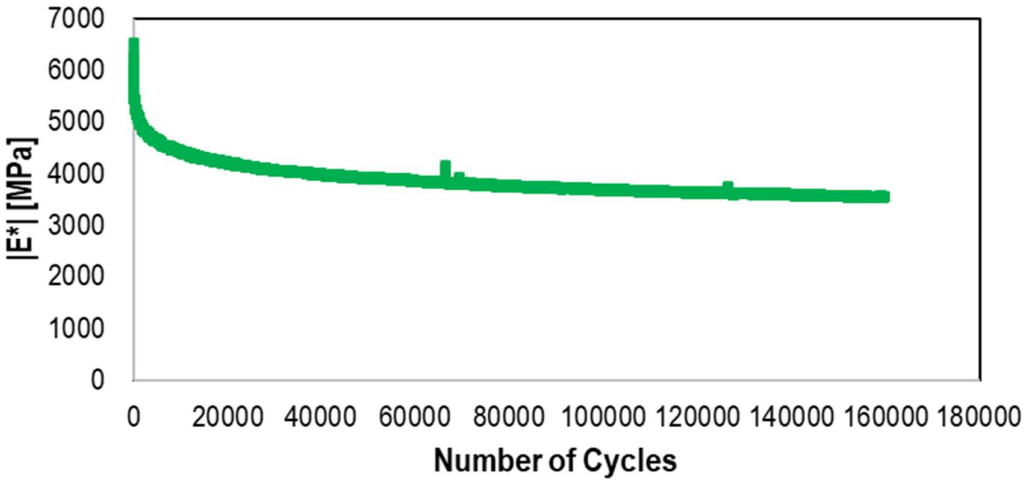

(a)

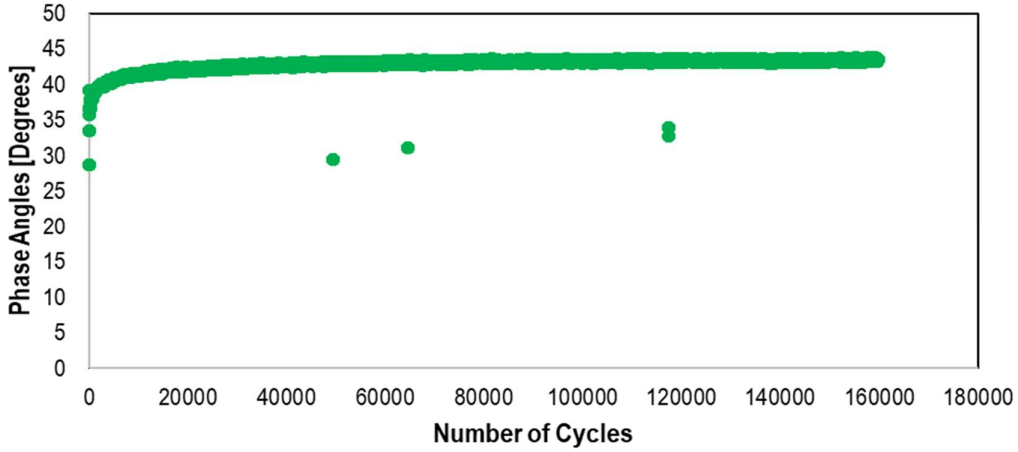

(b)

Figure 5.7. Representative plots for (a) stiffness and phase angle variation with the number of cycles in fatigue test for M3 at 20°C.

Table 5.4. summarizes the results of the cyclic fatigue tests. All three mixtures could not have the 50% reduction in stiffness as they failed in a brittle manner at 10°C. For other temperatures involved in fatigue testing, most specimens reached the 50% reduction in stiffness and satisfied the failure criterion.

Table 5.4. Summary of uniaxial cyclic fatigue testing for all mixtures (200 μstrain peak-to-peak).

Temperature [°C]	Mixture Type	Fingerprint |E*| [MPa]	Minimum Damage in C	Number of Cycles (To failure C= 0.5)
10	M1	16511.71	0.80	1.71E+04
10	M1	12338.07	0.87	1.47E+04
20	M1	9280.35	0.57	3.27E+04
20	M1	8527.53	0.53	7.58E+04
30	M1	3719.50	0.51	1.20E+05
30	M1	5403.67	0.53	1.37E+05
10	M2	14920.27	0.86	9.10E+03
10	M2	15873.13	0.82	9.65E+03
20	M2	10797.86	0.65	3.33E+04
20	M2	10550.55	0.66	2.48E+04
30	M2	6184.29	0.5	1.23E+05
30	M2	6818.88	0.44	7.91E+04
10	M3	9857.55	0.87	2.77E+04
10	M3	8978.94	0.85	2.09E+04
20	M3	4629.65	0.44	4.57E+05
20	M3	6089.33	0.5	1.60E+05
30	M3	3584.25	0.6	2.90E+05
30	M3	3097.83	0.6	2.147E+05

The number of cycles to failure for all the mixtures at different testing temperatures is plotted in **Figure 5.8.** It is observed that M3, with a recycling agent, had the highest fatigue life at all temperatures. Although the rate of stiffness reduction in M3 was the highest in the initial cycles, the failure was prolonged. It is due to the softness induced by the effect of the recycling agent in the mixture. M2, the stiffest mixture, failed quicker than the other two at all temperatures. At higher temperatures, M2 did not fail in a brittle manner at lower damage but rather had gradual damage and prolonged failure. Similar was the trend followed by M3.

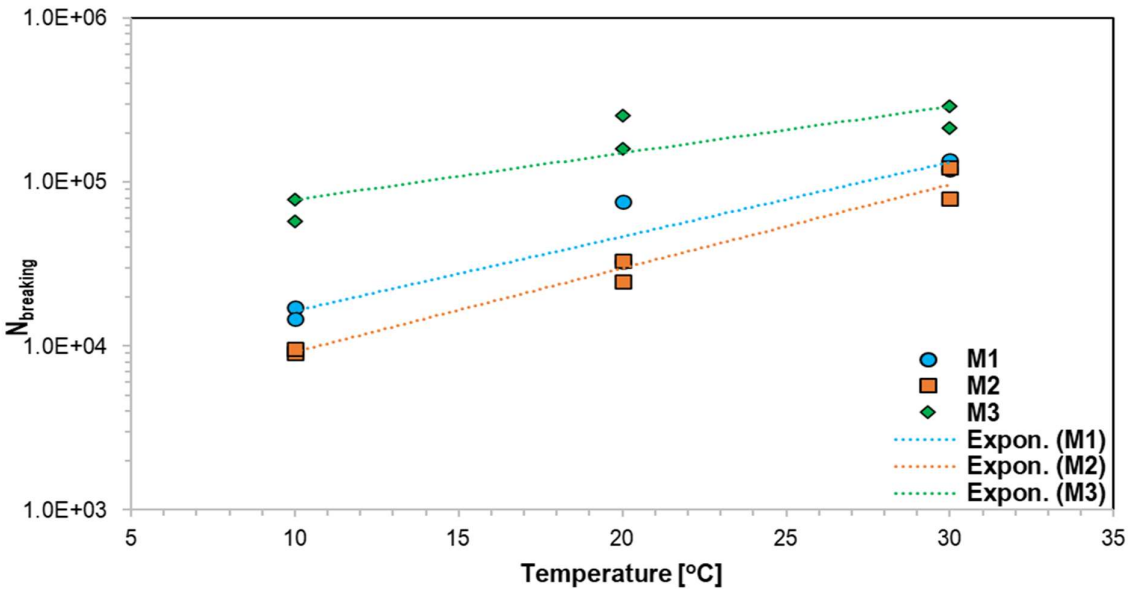

Figure 5.8. Number of cycles to failure for all mixtures vs. the temperature.

Furthermore, raw fatigue data was formatted in the required format of FlexMAT to perform the VECD calculations (**Appendix A**). The *C*-*S* curves for the mixtures at different temperatures were the output of FlexMAT and plotted in **Figure 5.9**, **Figure 5.10,** and **Figure 5.11.**

At 30°C, all mixtures showed a higher amount of accumulated damage expressed by the variable showing the damage (i.e., *S*). The value of pseudo-stiffness *C* achieved by all mixtures was higher at higher temperatures. It is due to the gradual accumulation of the damage in the mixture and not a brittle failure which was the case at 10°C. For a particular damage level, *C* supposedly *C*=0.7, the specimen undergoing the lowest damage is M3, whereas the highest damage was in M2. This trend justified the number of cycles to failure of the materials plotted in **Figure 5.9.** i.e., M3 was the mixture with the highest life while M2 with the lowest. At failure, i.e., *C* = 0.5, the damage accumulated and experienced by the mixtures followed the M1>M2>M3 trend. The positive effect of recycling agents and the higher percentage of recycled asphalt materials to reduce the damage in the mixture were assessed.

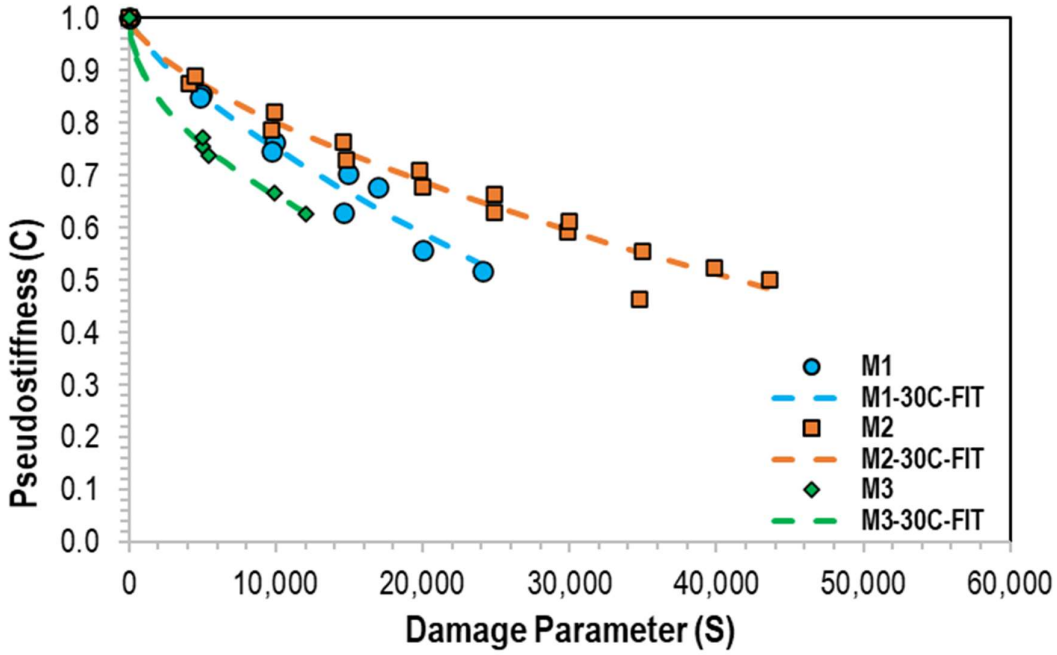

Figure 5.9. Damage characteristics curve for all mixtures at 30°C.

At 20°C, the results and trend mentioned above were obtained. It is generally suggested to perform fatigue testing in asphalt mixtures involving the VECD formulations around this temperature. The characteristic damage curve for M1 exceeds the M2 curve due to its sudden failure. With accumulating lower damage, the specimen failed, making it unable to predict the *C*-*S* curve for lower values of pseudo-stiffness. Another reason for this sudden failure was the inclusion of RAP material in the mixture, which made the mixture stiff.

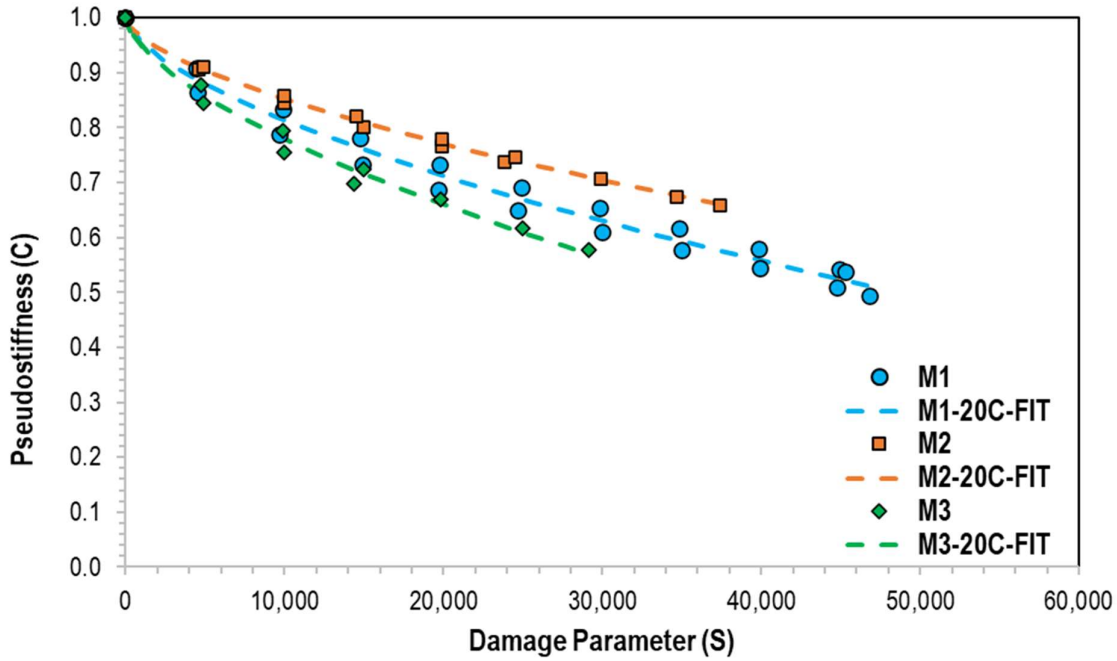

Figure 5.10. Damage characteristics curve for all mixtures at 20°C.

It was difficult for the mixtures to predict their damage characteristics curve at 10°C for the same strain rate due to the early brittle failure of specimens. But still, the trend of results was like that observed in the damage characteristics results for higher temperatures. No mixture could reach the *C* value below 0.8. The maximum damage accumulated was more in M2 than in both the mixtures at the observed value of *C*. The damage characteristics plot for all the mixtures at 10°C is plotted in **Figure 5.11.**

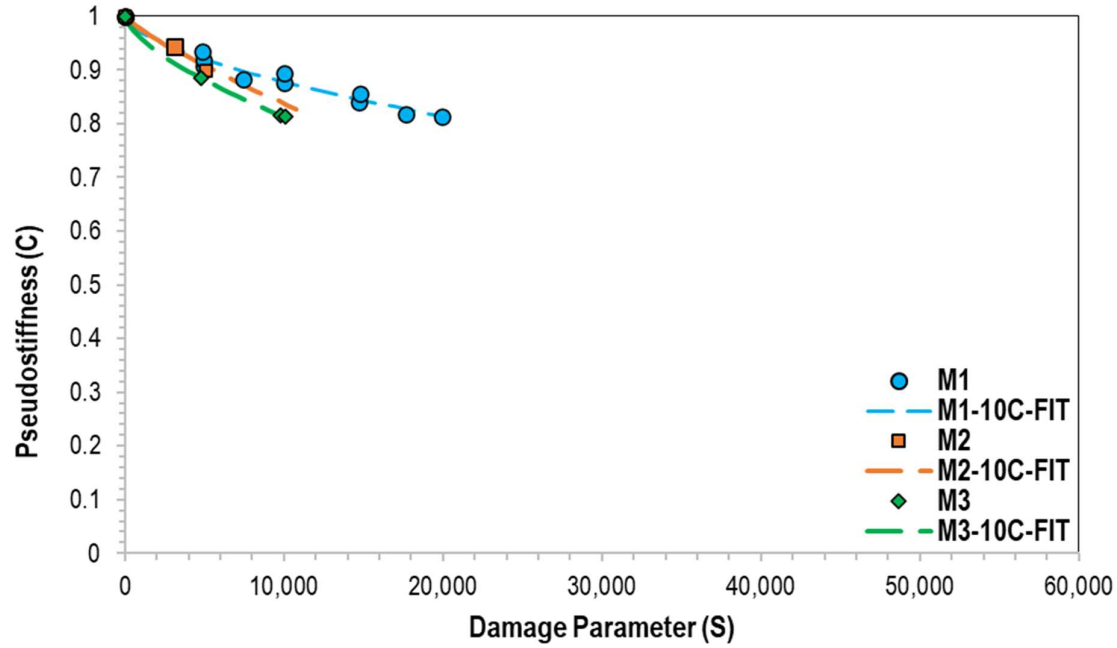

Figure 5.11. Damage characteristics curve for all mixtures at 10°C.

Further, all the damage characteristics curves for all the mixtures at all the temperatures are plotted in one curve in **Figure 5.12.** This curve helped understand the behavior of the damage characteristics curve for all the mixtures at different temperatures. Although the theory says that this curve is independent of testing temperature, the curves plotted were not identical, which were identical in the case of different strain rates. This phenomenon is because the VECD theory only considers damage accumulation in the material caused by the tensile part in the loading wave and ignores the potential healing of the material that takes place during the compression portion of the loading due to the healing of micro-cracks (Cheng, 2022b). "The VECD formulations will not produce a single *C-S* curve that can be used to predict the response of a truly random loading that includes tension, compression as well as rest periods" – (Kutay & Lanotte, 2018). The distinction in considering the damage and healing effects in a loading wave in the VECD method is still a future research area.

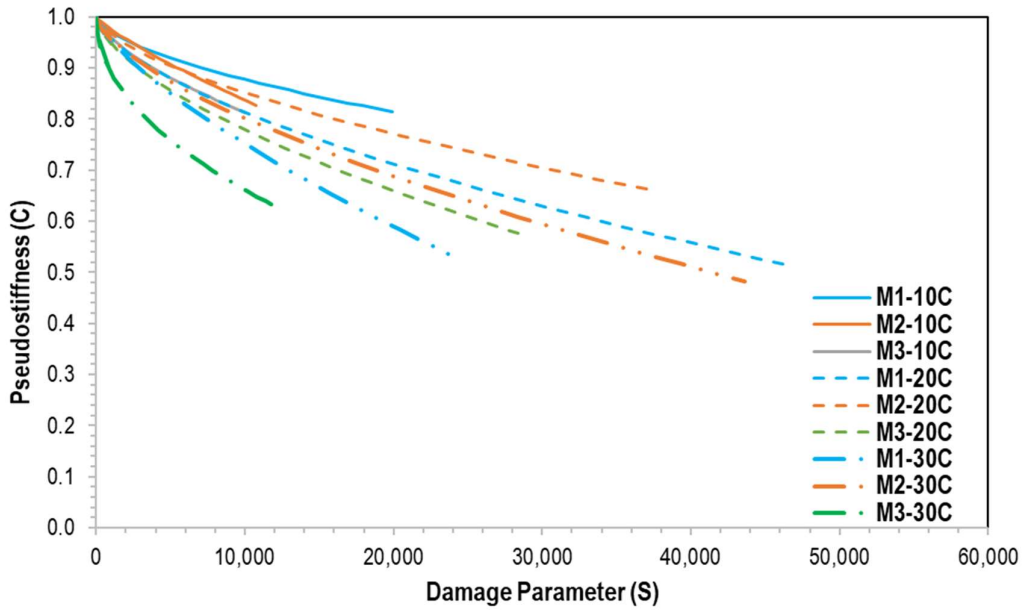

Figure 5.12. Damage Characteristics curves for all the mixtures at all test temperatures.

The theory discusses how the damage characteristics curve based on the VECD formulations is independent of the loading rate, frequency of loading, temperature of testing, and so on. A test was also carried out on M2 at 20°C for 300 μ-strain. It is observed that the two C-S curves obtained followed a similar trend and almost the same amount of damage accumulated. There was some variation in the output curves, making a curve with 300 μstrain move upward, mainly because the specimen at a higher strain rate could not reach the same level of pseudo-stiffness before failure, with almost similar damage accumulated. The damage characteristics curve for both strain levels is plotted in **Figure 5.13.**

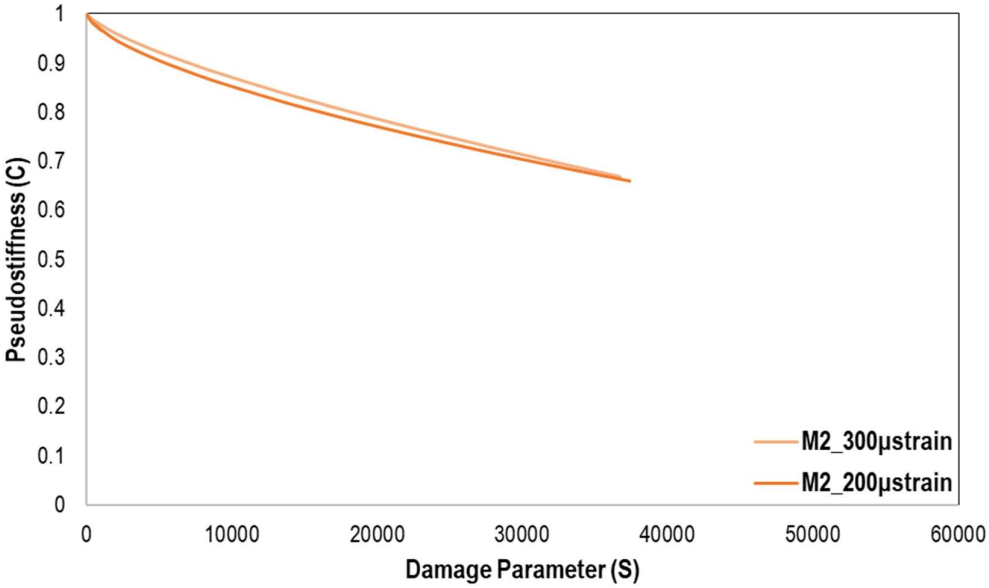

Figure 5.13. Damage characteristics curve at two different strain rates.

5.4 Uniaxial Tension-Compression Healing Test Results

The uniaxial tension-compression fatigue-healing tests were performed to assess the self-healing capacities of the mixtures. The fatigue-healing tests were done on three mixtures (M1, M2 and M3) at three different temperatures (10, 20 and 30°C) and three different rest periods (40, 80 and 160s). Two replicas were used in testing for all combinations of testing. These rest periods were applied at different stages of damage levels in the specimen. With the rest periods implication, the healing phenomenon is expected to help mixtures recover lost stiffness by healing micro-cracks - this phenomenon of increase in stiffness modulus is given in **Figure 5.14.** The stiffness modulus curves plotted for all the cases are in **Appendix C**. The recovery of stiffness modulus due to micro-cracks healing was higher for longer rest periods.

It is also observed that the recovery of stiffness modulus was different for different temperatures with the same rest periods. The higher the temperature, the higher the recovery. As the temperature increased, the binder in the mixture became more flowable and healed the micro-cracks, resulting in a higher recovery. The implication of rest periods also increased the time and number of cycles to failure given in **Figure 5.15.**

Among the three mixtures incorporated for healing assessment, the highest potential recovery in all temperatures and rest periods was most in M3. For all the mixtures, even for the shortest duration of rest period adopted in this research work, there is an increase in the stiffness values of all the mixtures, as shown in Figure 5.16. After transforming the data in the required format, as explained in Appendix A, data was fed into FlexMAT to perform the S-VECD calculations. The damage characteristics plots for different temperatures for all mixtures are given in **Figure 5.17 to Figure 5.19.** It is observed that after each rest period, there was an increase in the stiffness modulus of the specimen. The damage growth in the material was faster after each rest period, indicating that the material regained its strength partially during each healing period. After the rest period, weak bonds were reopened during the reloading part, which resulted in rapid damage growth.

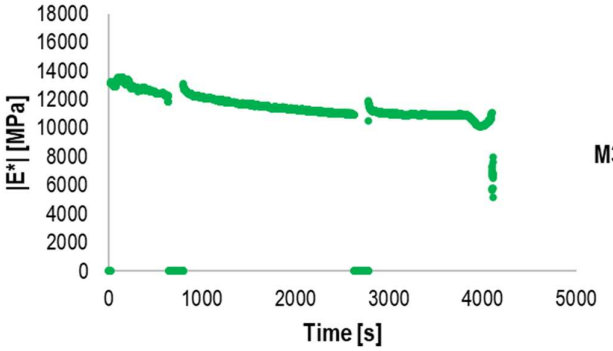

(a)

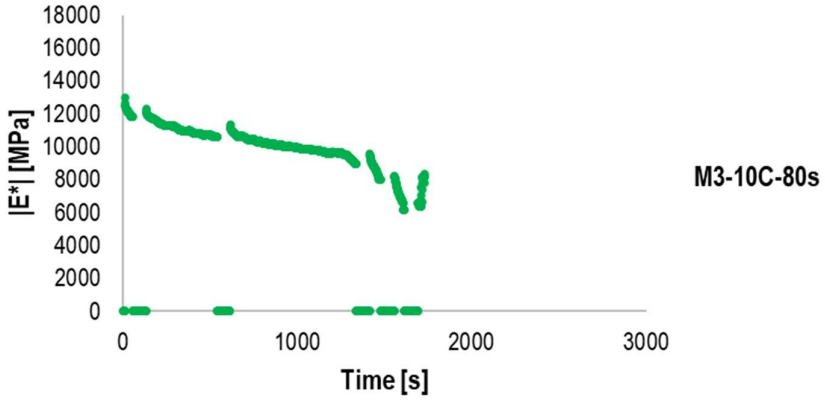

(b)

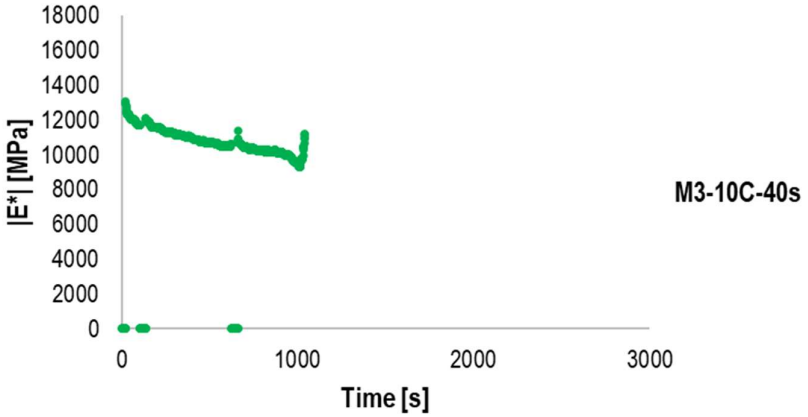

(c)

Figure 5.14. Comparison of the stiffness modulus variation during fatigue-healing tests: (a) 160 (b) 80 (c) 40 s rest periods.

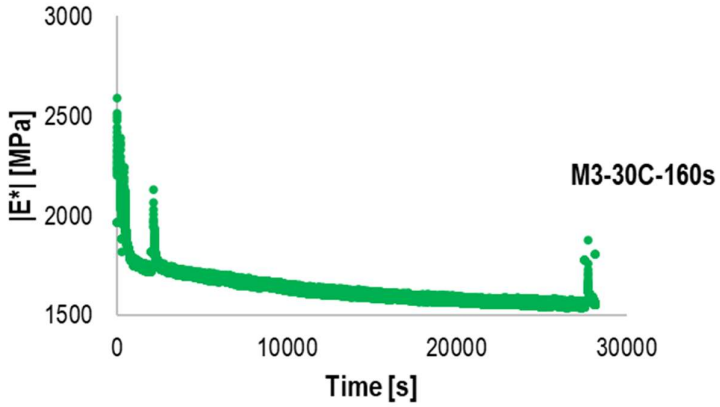

(a)

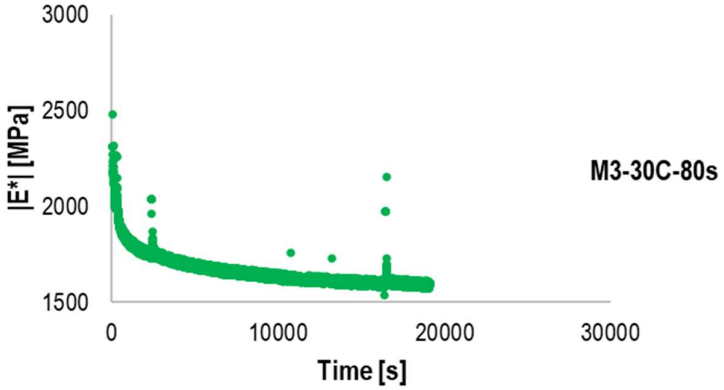

(b)

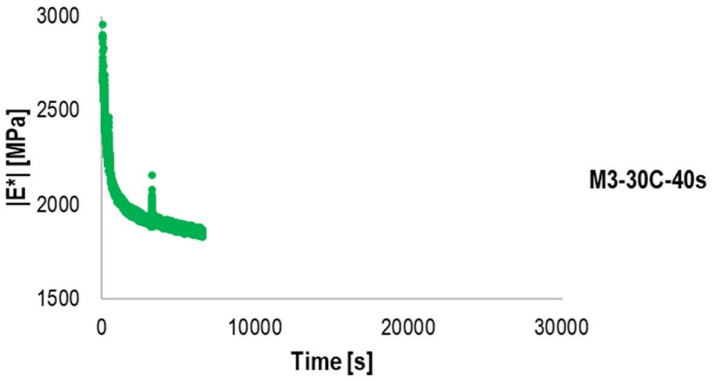

(c)

Figure 5.15. Visual comparison of the increase in time to failure with an increase in rest periods: (a)160 s, (b) 80 s, (c) 40 s.

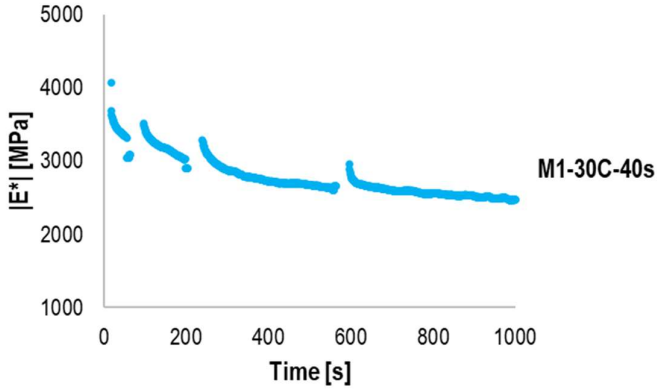

(a)

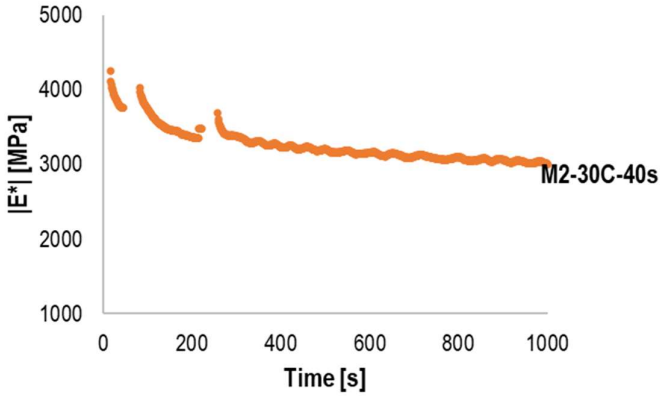

(b)

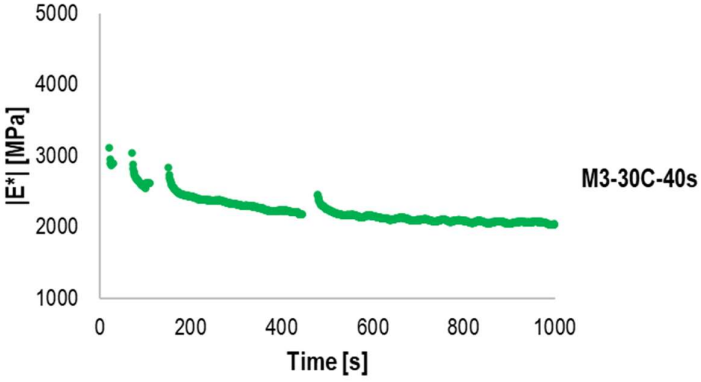

(c)

Figure 5.16. Comparison of recovery of stiffness in three mixtures (a) M1, (b) M2, (c) M3.

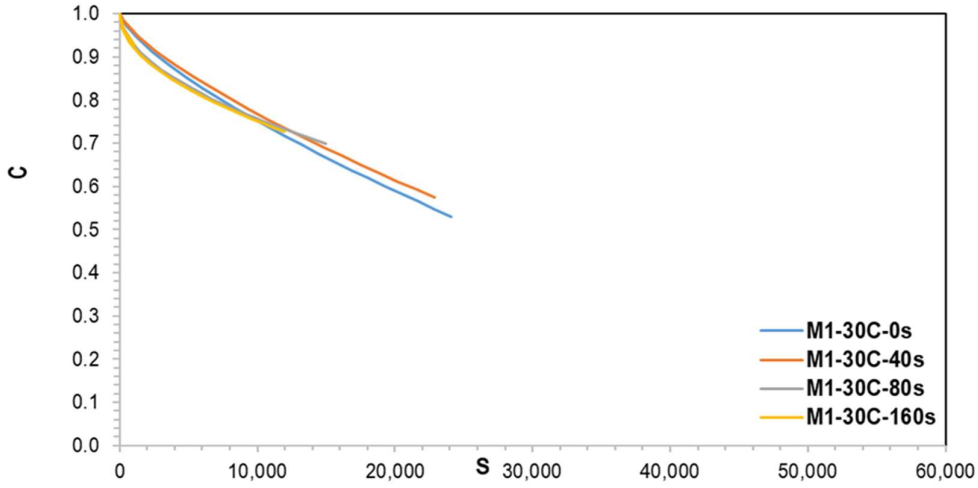

(a)

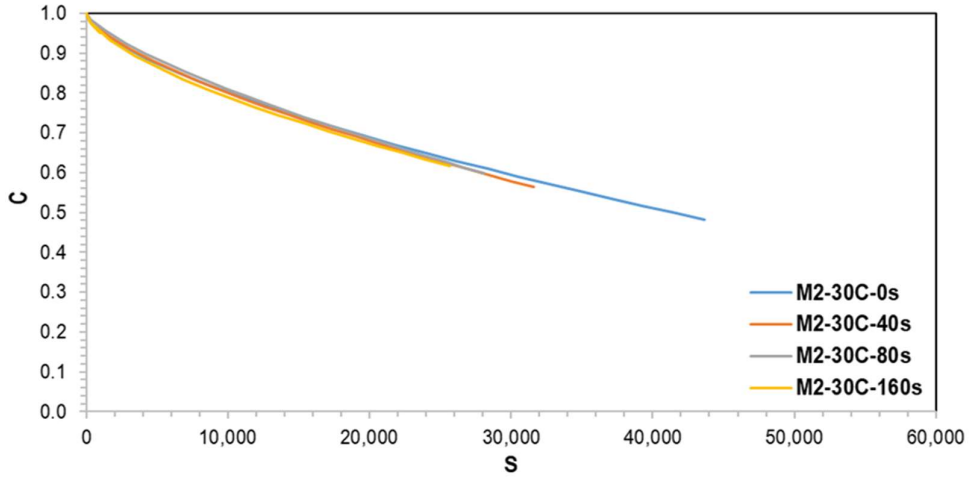

(b)

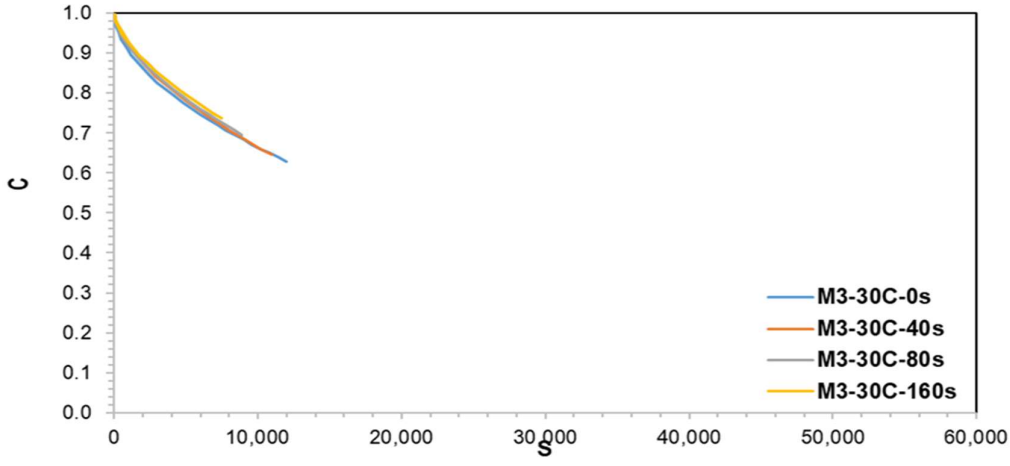

(c)

Figure 5.17. C-S curves for three mixtures at 30°C (a) M1, (b) M2, (c) M3.

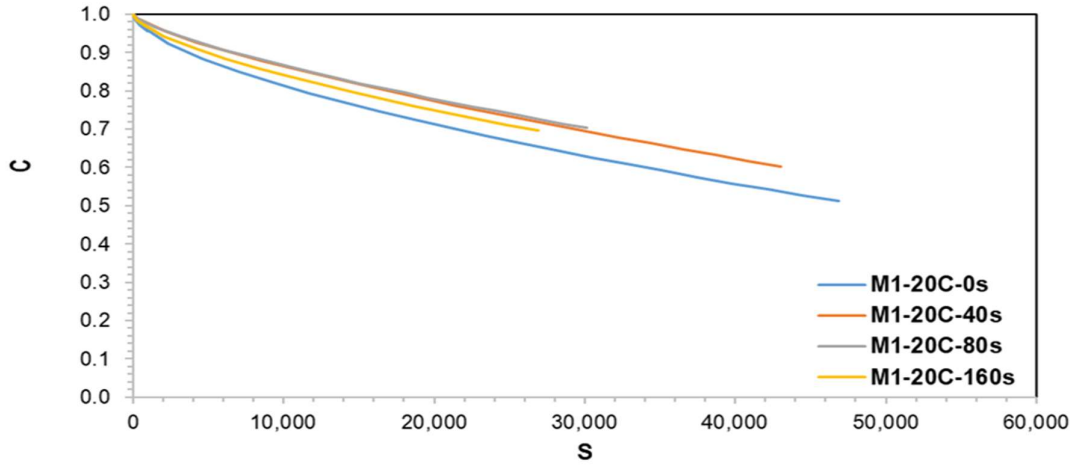

(a)

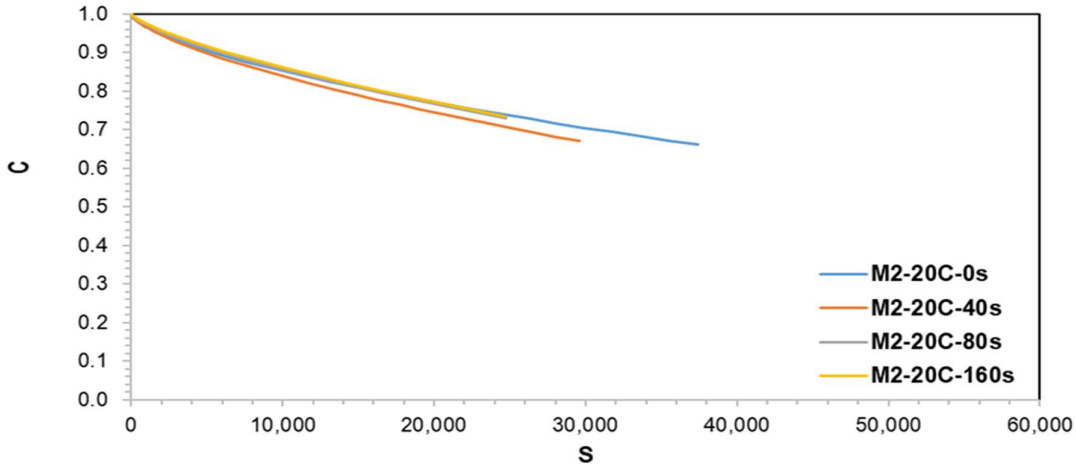

(b)

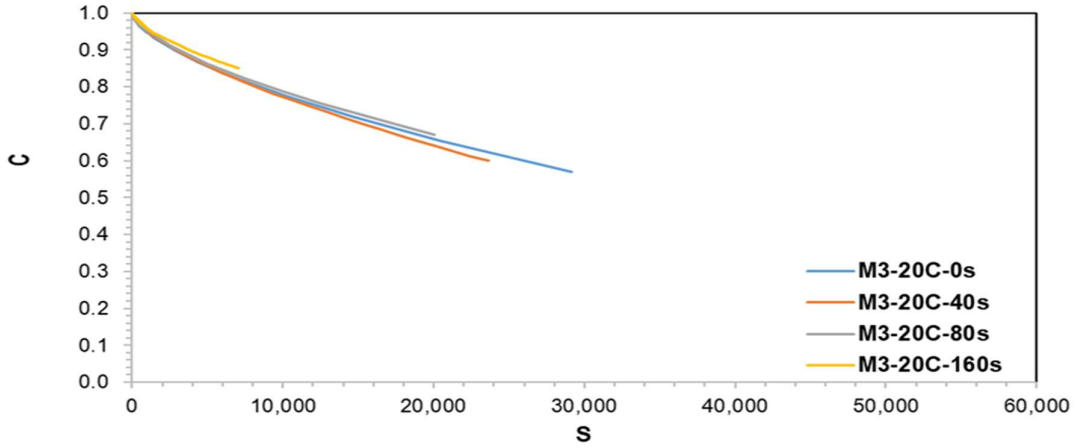

(c)

Figure 5.18. C-S curves for three mixtures at 20°C (a) M1, (b) M2, (c) M3.

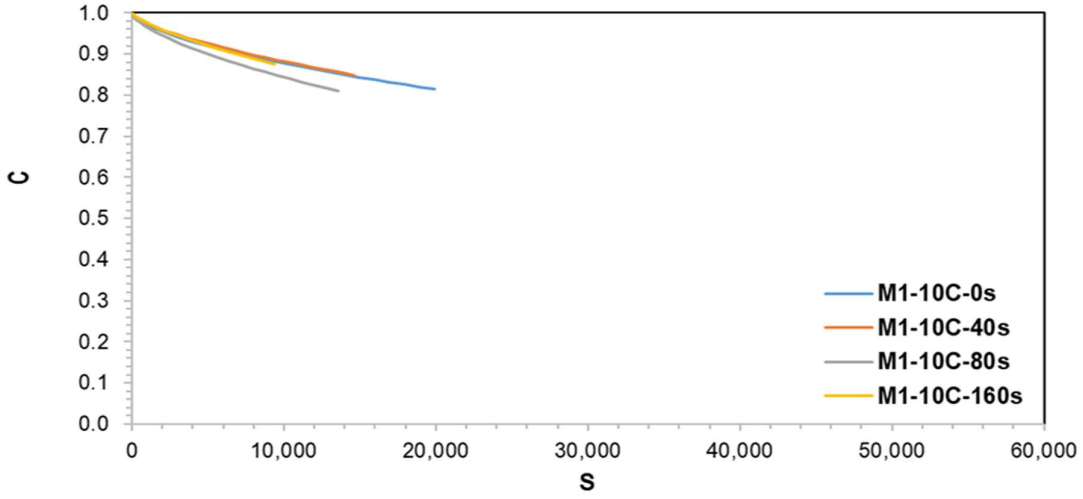

(a)

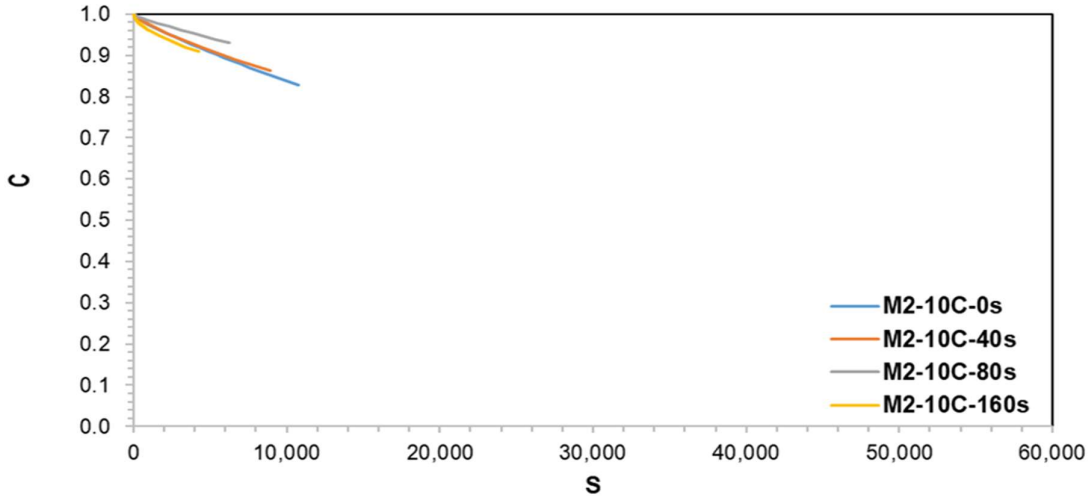

(b)

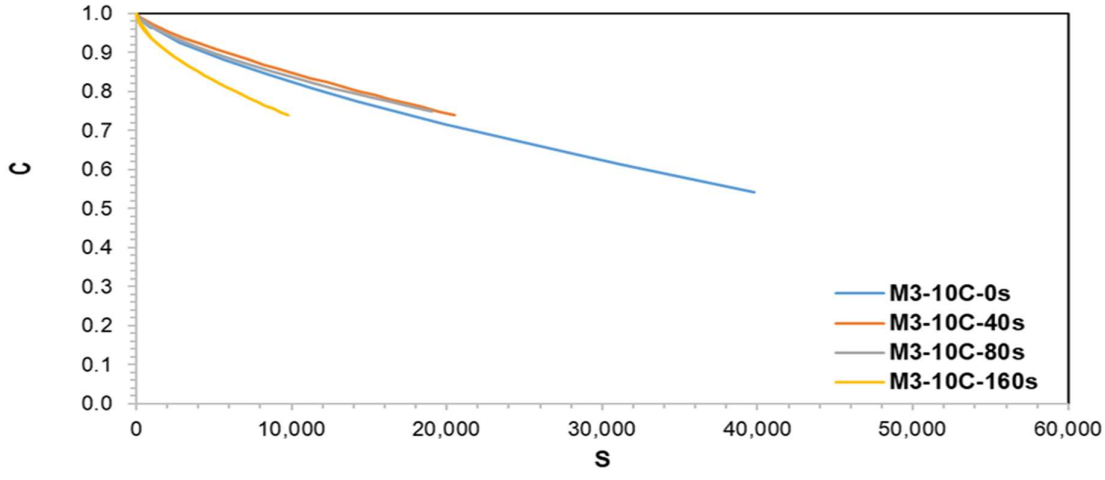

(c)

Figure 5.19. C-S curves for three mixtures at 10°C (a) M1, (b) M2, (c) M3.

The damage characteristics *C-S* curve are plotted for all the rest periods for all the mixtures at all temperatures with the damage characteristics obtained from continuous fatigue testing**.** It is observed that the *C-S* curves length shortened as the rest period duration increased. This shortening of length signifies that with an increase in the rest period, the amount of damage accumulated in the specimen is less, ultimately enhancing the mixture's fatigue life. This trend is followed in all the mixtures for all the temperature cases. It is observed that with an increase in temperature, the healing effect became more effective and hence gave consistent damage characteristic curves, which was not the case at 10°C. The higher the temperature, the higher the healing effect in the mixtures, and the more consistent the curves become. This is reported by Zeiada et al. (2018) that these differences are due to the healing effect of the rest periods on the asphalt material during the unloading stage. The VECD model does not account for the healing mechanisms during the rest period; hence, producing the *C-S* curve becomes difficult. It is also observed that a higher amount of damage is accumulated for all the mixtures at higher temperatures before the failure.

5.4.1 Prediction of healing percentages

Healing was calculated with three different methods. These methods were based on the recovery of damage level in the specimen, based on the internal state variable that accounts for damage accumulation (i.e., *S*), and based on the number of cycles. After predicting the *C-S* curve for the group rest healing tests, the healing model was applied for the mixtures in the functional form, including the effect of temperature, damage level before applying the rest period, and the rest period duration. The important factor required to calculate the healing percentages in the mixture is the initial stiffness of the mixture. Hence, the fingerprint test was conducted for all the specimens used for the testing.

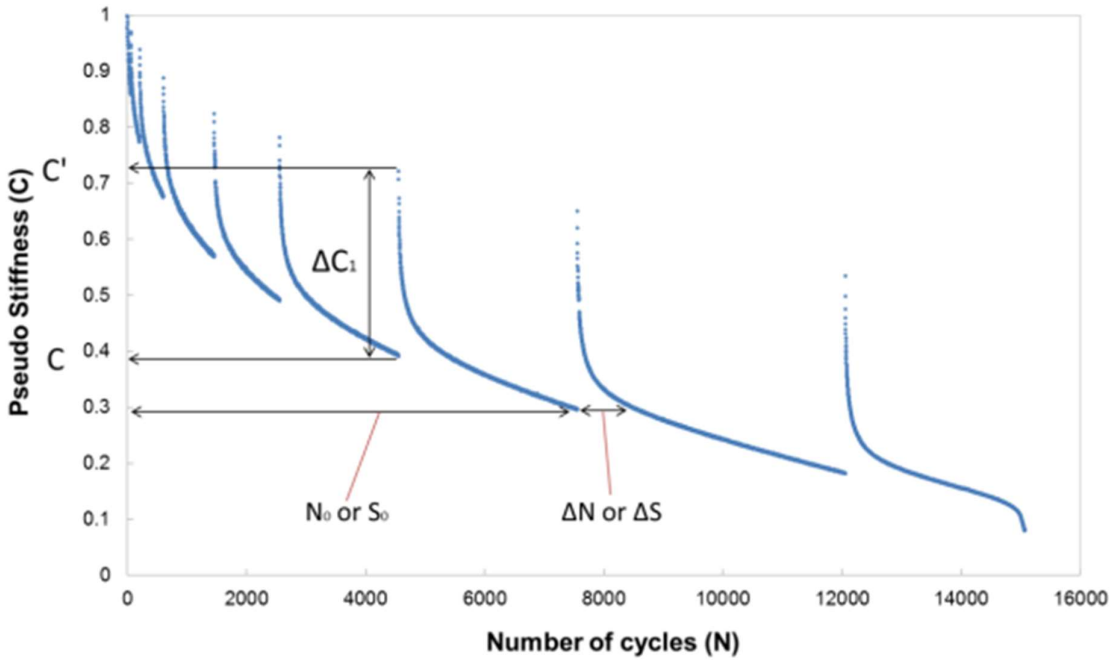

Figure 5.20. Parameters to calculate the damage level and the healing percentages (Ashouri 2014).

Method 1: Based on the damage level.

In Method 1, the group rest period is applied based on the different stages of the damage level decided. The pseudo-stiffness prior to the application of the rest period is termed C, and the starting value of the stiffness of the material after the application of the rest period or at the beginning of reloading is termed C'. This is often termed the recovered pseudo-stiffness of the specimen at the end of the rest period. The healing percentage is calculated using **Eq. 5.1.**

$$\%H_c = \frac{C' - C}{1 - C} * 100 = \frac{\Delta C}{1 - C} \tag{5.1}$$

where C is the pseudo stiffness before the application of the rest period, and C' is the pseudo-stiffness of the material after the recovery in stiffness during the rest period. C' is always expected to be greater than C. Hence, ΔC is to be positive, and the $\%H_s$ is the calculated percentage healing due to an applied rest period. This healing percentage is expected to increase with the temperature increase and the rest period's duration. All mixtures at all temperatures follow this trend. One example of such a trend is shown in **Figure 5.21**. Rest all the curves for all mixtures for all sets of temperature and rest periods are given in Appendices. It is observed that the highest healing potential at 20°C is in M3. The highest healing in all the mixtures for all temperatures was at a 10% damage level of the material (i.e., 0.9C), and it decreased with a further increase in the damage level. It is due to the transition of micro-cracks into macro-cracks that are impossible to heal during the rest period. The mixtures used also comprised 70% recycled material, making the mixture stiffer. Thus, reaching subsequent lower values of damage level (e.g., 0.6C in M1-20C in **Figure 5.21 (a)**) at lower temperatures is sometimes difficult.

In the case of M2-20C**,** it is also observed that with the increase in the duration of the rest period, the capacity of a material to achieve a higher damage level increased. This may be due to the rest periods allowing the material to release the energy stored in the system, which was ultimately the reason for failure restricting the failure in materials due to phenomena such as strain hardening.

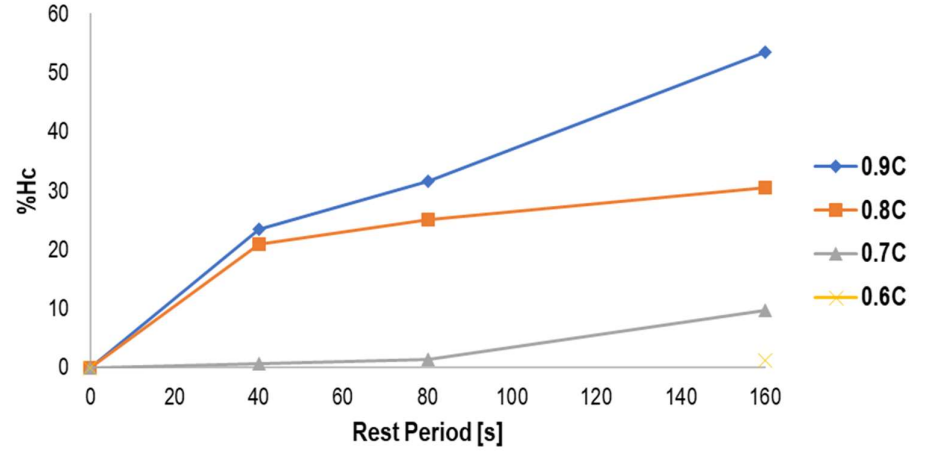

(a)

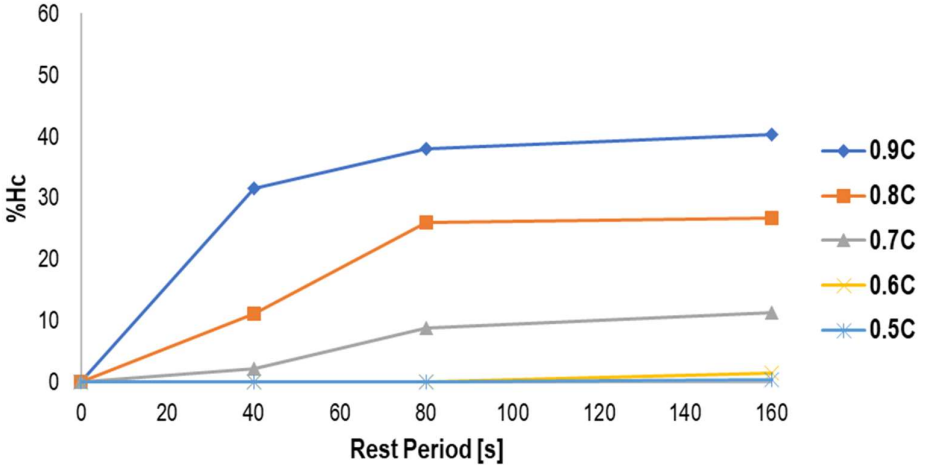

(b)

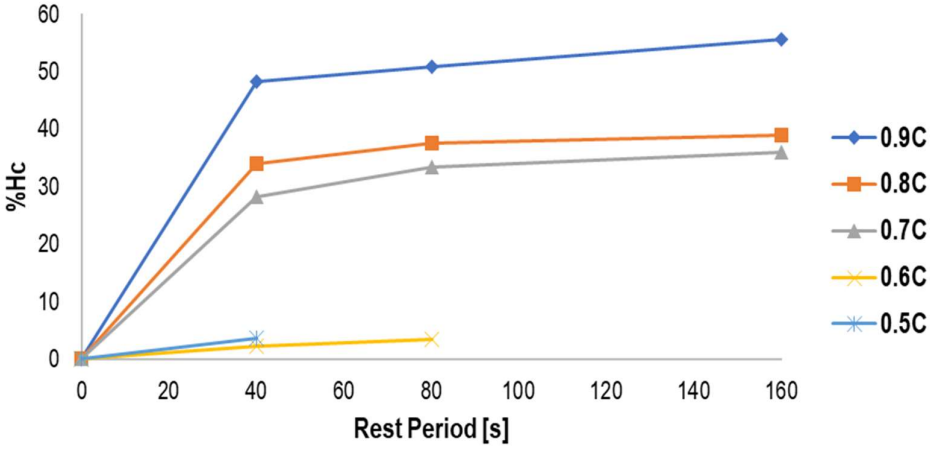

(c)

Figure 5.21. Percentage healing calculation as a function of damage level based on Method 1 at 20°C for (a) M1, (b) M2, and (c) M3.

Method 2: Based on the number of cycles.

In Method 2, the healing percentages were calculated based on this increase in the number of cycles given in **Eq. 5.2.** Once the specimen reaches the stage of damage level, the rest period is applied to the specimen. It is based on the horizontal shift of the *C-N* curve due to the healing caused by applying the rest period. For pseudo stiffness values before the application of the rest period, the load cycles to reach that damage level are noted. After healing, there will be an increase in the pseudo stiffness due to healing, and it takes extended load cycles to reach the same pseudo stiffness level. This difference in the load cycles or the shift in *C-N* leads to calculating the healing percentage.

$$\%H_n = \frac{\Delta N}{N_0} * 100 \tag{5.2}$$

where N_0 is the number of load cycles applied to the specimen before the rest period start, ΔN is the horizontal shift of the *C-N* curve due to the healing caused by the application of the rest period, and $\%H_N$ is the percentage healing of the material due to an applied rest period.

One example of the healing percentage calculation using this method is shown in **Figure 5.2.** Other results for the different sets are given in **Appendix D**. It is observed that with increased temperature, the material induces a softness and reduction in stiffness and hence can undergo a greater number of damage cycles before failure during the healing test. Although with an increase in the temperature, the damage rate increases. Based on the number of cycles, the healing percentage calculated is highest at 30°C. It means that the number of cycles required by the specimen to reach the same damage level prior to the rest period application is highest at this temperature and hence has the highest healing potential. It is also observed that the number of cycles to reach the prior damage level after 0.7C is lower, which signifies a higher damage growth rate with an increase in the damage level of specimens. For lower damage levels, e.g., 0.9C and 0.8C, the healing capability in the material is the highest at this level, as there is the origination of micro-cracks which can be healed with the application of the rest periods. But with a further increase in the damage level in the specimen, the width of these micro-cracks increases and turns into macro-cracks that cannot be healed with short rest periods.

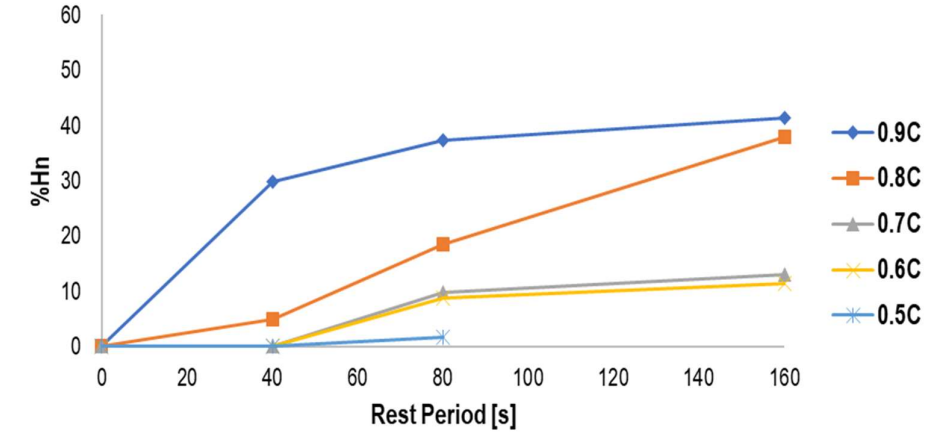

(a)

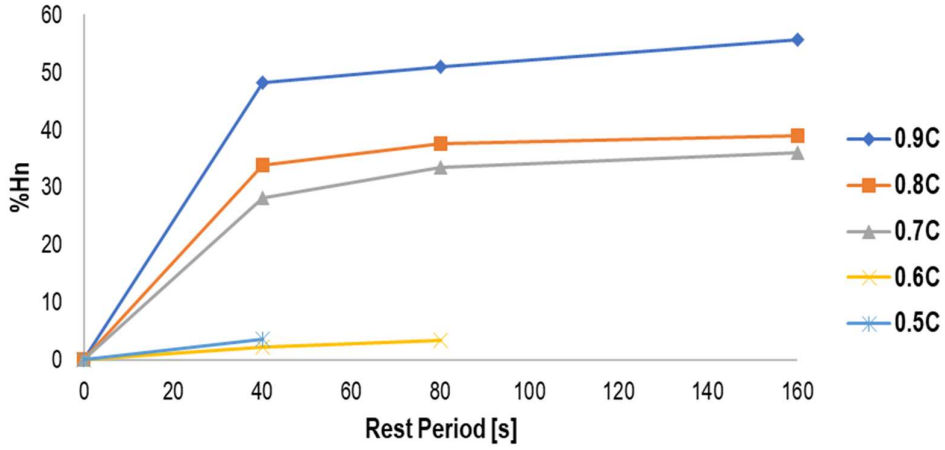

(b)

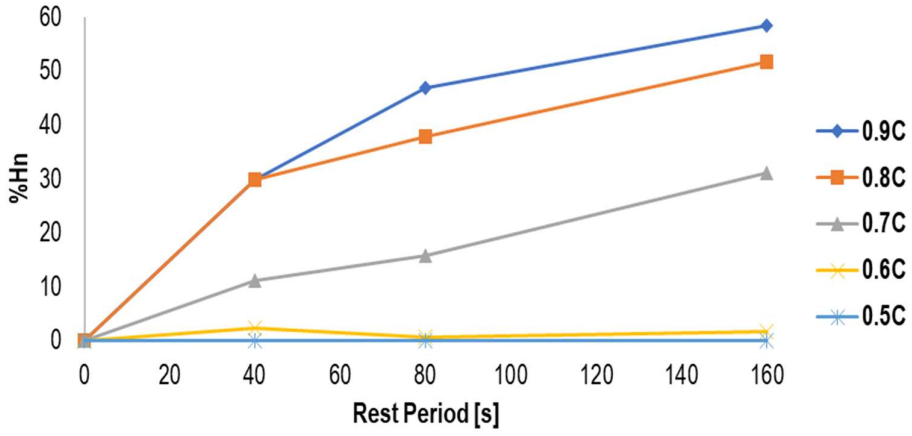

(c)

Figure 5.22. Percentage healing calculation as a function of the shift in load cycle based on Method 2 for M3 at (a) 10, (b) 20, and (c) 30°C.

Method 3: Based on the damage parameter variable.

In Method 3, the specimen's healing percentage was calculated based on the horizontal shift of the *C-S* curve due to the healing caused by applying the rest period. A similar concept as the assessment of healing based on the number of cycles is used in this method as well. The *C* value at which the rest period was applied gave a corresponding value for the variable to define damage parameter *S*. After applying the rest period, the *C* value increased due to healing. In reloading, a shifted *C-S* curve was obtained (**Figure 5.20**). The difference in the *S* value for the same damage level in the specimen before and after the rest period is calculated and used in **Eq. 5.3.** to calculate the healing percentage.

$$\%H_s = \frac{\Delta S}{S_0} * 100 \tag{5.3}$$

where S_0 is the damage parameter value before the rest period application, ΔS is the horizontal shift of the *C-S* curve due to the healing caused by the application of the rest period, and $\%H_s$ is the healing percentage calculated.

This method is incorporated for the healing model predictions. The calculated healing percentage from this method for all the mixtures is given in **Figure 5.23**, **Figure 5.24**, and **Figure 5.25.**

This general trend of increase in the healing potential with an increase in rest period and the temperature is the same for all three methods mentioned above. The amount of healing or the quantification of healing by three methods differs with each method. It is evident from the plots above that the longer rest periods, when applied at the lower level of damage, have more potential to heal. It is due to the formation of small micro-cracks that can be healed quickly. A greater amount of healing was achieved in the case of higher temperatures and longer rest periods for M3. The measured percentage of healing for different rest periods at different temperatures by Method 3 is the basis for the prediction of the healing model in the following part of this thesis.

In some cases, it is difficult to assess the healing percentages for damage levels below 0.8 at 10°C for M2, for example. This was the case for most mixtures above the damage level of 0.5 at all temperatures due to specimen failure for *C* values greater than 0.5. It is because of the comparatively higher stiffness of the mixtures employed.

The percentage of healing changes with respect to the change in rest period duration at any temperature and damage level, which follows the power form behavior (Ashouri, 2014). This will be the basis for predicting the healing master curves for all three mixtures incorporating the analogy of T-TSP. The following sections of this thesis will cover the prediction of healing percentage master curves and the healing model for all mixtures.

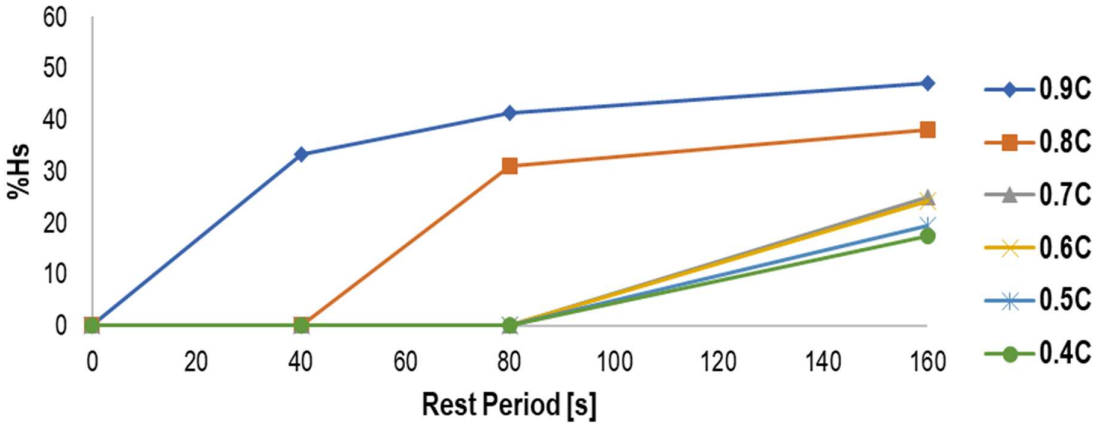

(a)

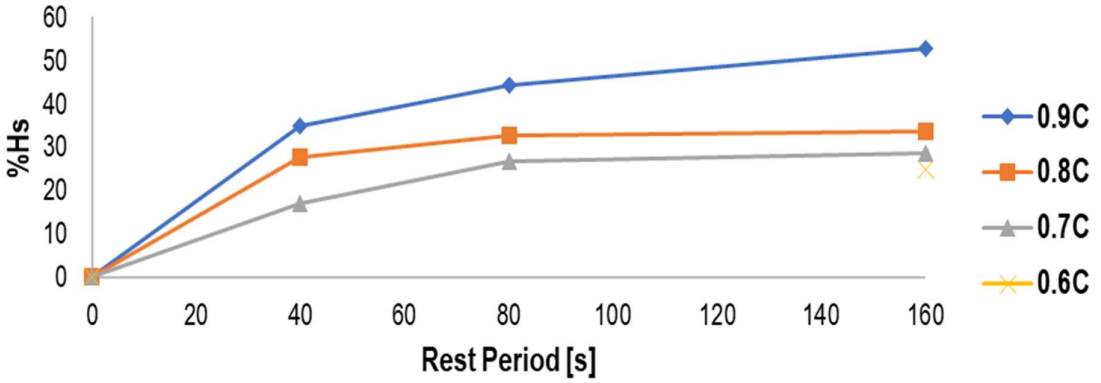

(b)

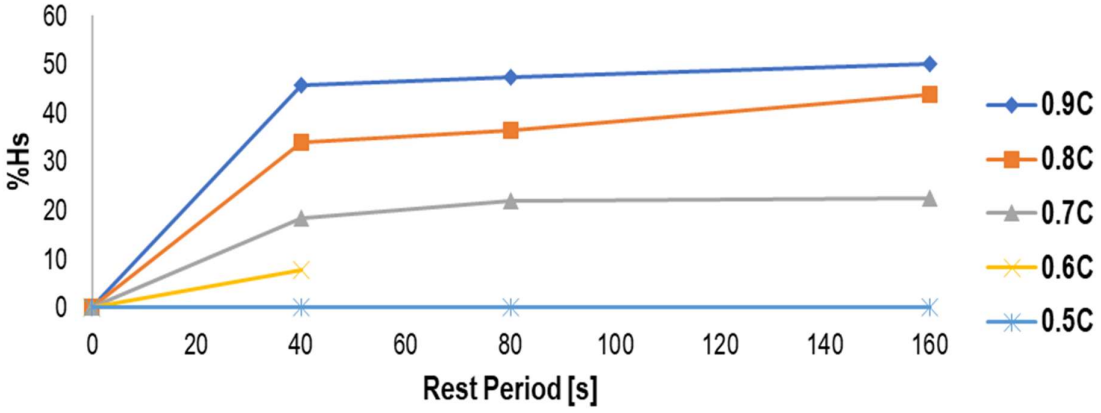

(c)

Figure 5.23. Percentage healing calculations for M1 based on Method 3 at (a) 10, (b) 20 and (c) 30°C.

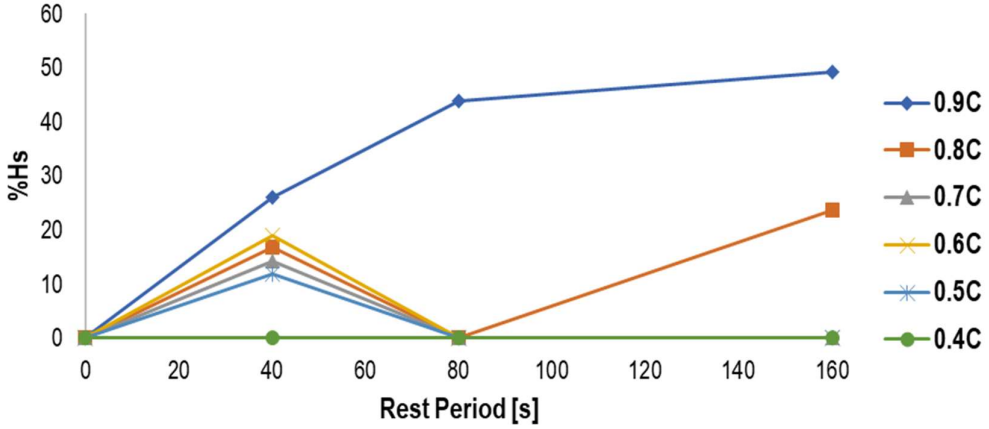

(a)

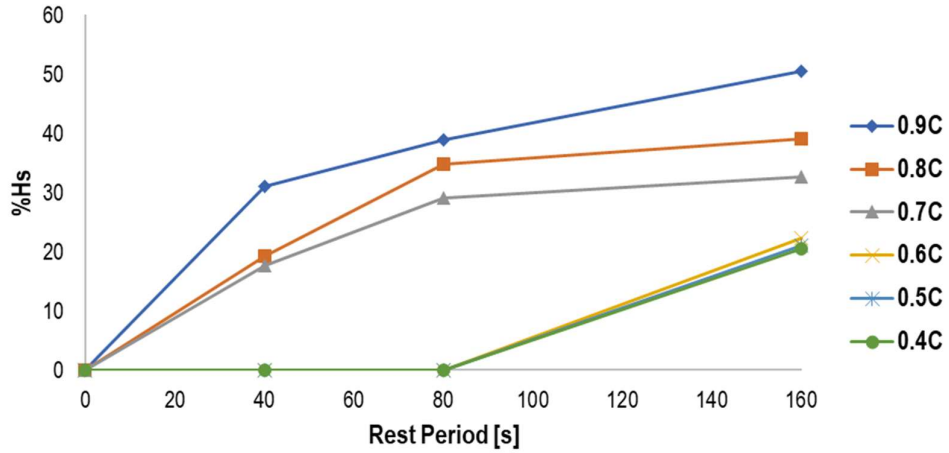

(b)

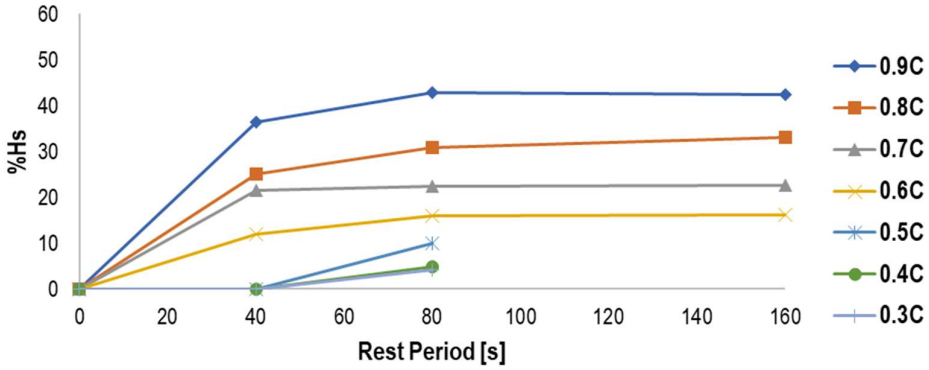

(c)

Figure 5.24. Percentage healing calculations for M2 based on Method 3 at (a) 10, (b) 20 and (c) 30°C.

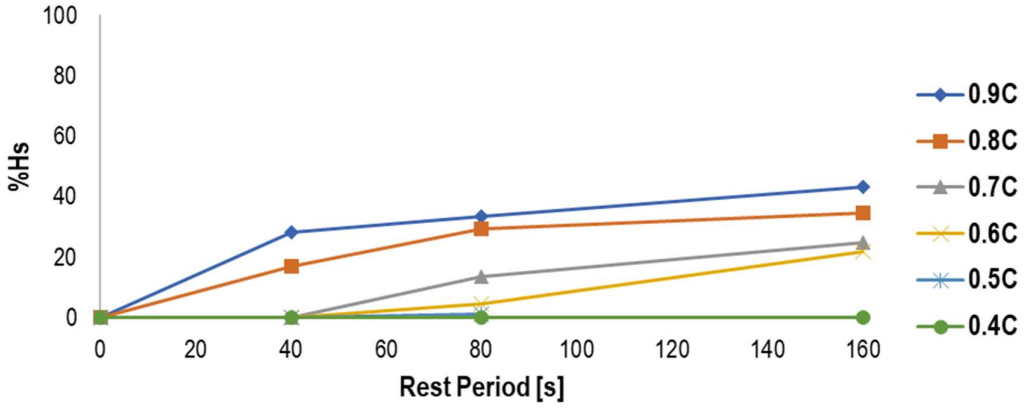

(a)

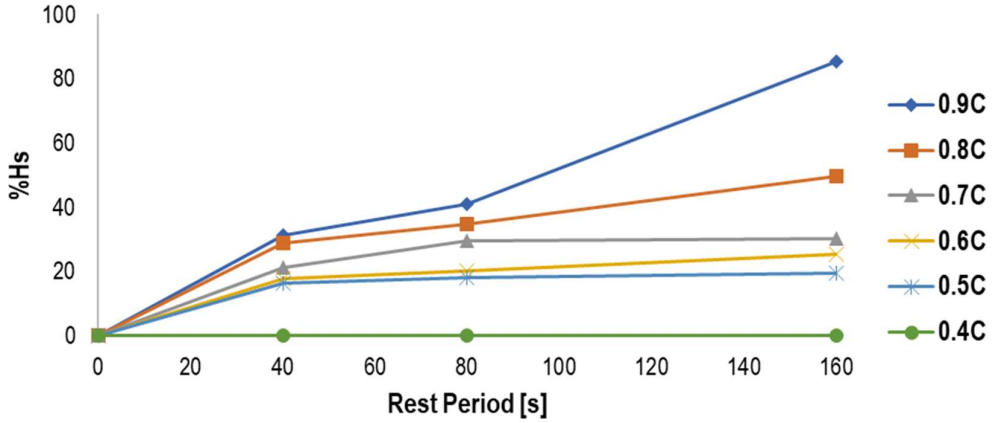

(b)

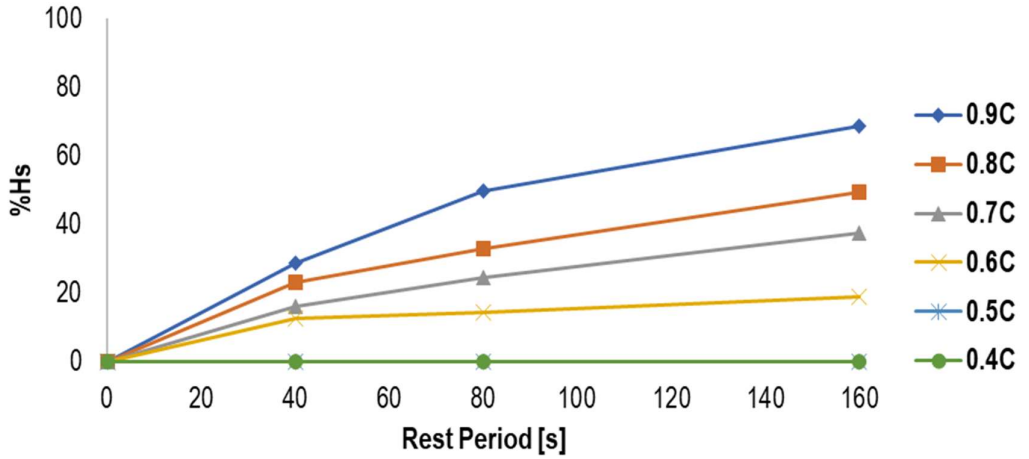

(c)

Figure 5.25. Percentage healing calculations for M3 based on Method 3 at (a) 10, (b) 20 and (c) 30°C.

5.4.2 Healing master curves

An effort is taken to combine the time-temperature effect for the mixtures used in this research work to predict the healing master curves based on the time-temperature shift factor (a_T) obtained from the dynamic modulus testing. The prediction of the healing master curves multi-step process is given in **Figure 5.26.** The shift factors for all the temperatures involved in the dynamic modulus testing are calculated using the output fitting parameters a_1, $a_{2,\&}$ a_3 of FlexMAT.

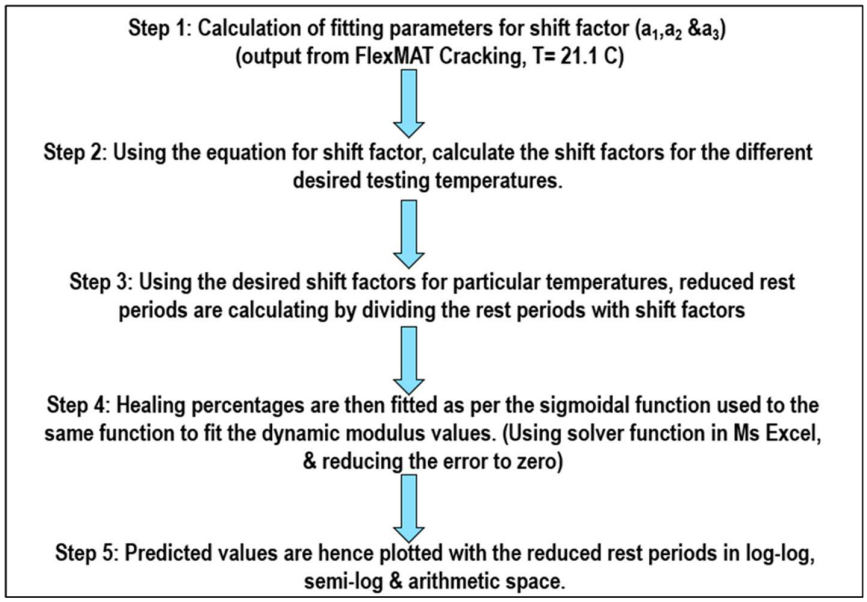

Figure 5.26. Steps involved in the prediction of the healing master curve.

Table 5.5. Fitting parameters from dynamic modulus test.

	M1	$M2_2$	M3
Fitting values a_1	-0.00043	-0.000491606	-6.97422E-05
Fitting values a_2	-0.06475	-0.052224789	-0.086749187
Fitting values a_3	1.556068	1.320810782	1.861457778

The relationship between the shift factors and the temperature is a second-order polynomial obtained from the dynamic modulus tests on the mixtures. Using **Eq. 3.3**, shift factors for the temperature at which the modulus testing was conducted, i.e., -5, 5, 10, 20, 30, 40 and 50°C.The healing master curve is to be predicted based on the tests performed for healing at 10, 20 and 30°C. The shift factors for temperatures used in the calculation are marked in bold in **Table 5.6.**

Table 5.6. Calculated shift factors for different temperatures.

Temperature	M1	M2	M3
-5	73.99228	37.12313	196.5442
5	16.65868	11.15313	26.66664
10	**7.343496**	**5.61568**	**9.704914**
20	**1.231681**	**1.201359**	**1.254808**
30	**0.169768**	**0.204938**	**0.157114**
40	0.01923	0.027877	0.01905
50	0.00179	0.003024	0.002237

Table 5.7. Calculated shift factors and reduced rest periods.

T [°C]	RP	M1		M2		M2	
		SF (aT)	Reduced RP	SF (aT)	Reduced RP	SF (aT)	Reduced RP
10	40	7.34	0.183	5.61	7.12	9.70	4.12
10	80	7.34	0.091	5.61	14.24	9.70	8.24
10	160	7.34	0.045	5.61	28.49	9.70	16.48
20	40	1.23	0.030	1.20	33.29	1.25	31.87
20	80	1.23	0.015	1.20	66.59	1.25	63.75
20	160	1.23	0.007	1.20	133.18	1.25	127.50
30	40	0.16	0.004	0.20	195.18	0.15	254.59
30	80	0.16	0.002	0.20	390.36	0.15	509.15
30	160	0.16	0.001	0.20	780.72	0.15	1018.37

To combine the effect of rest period time with the temperature of testing, a joint parameter called reduced rest period was calculated (Ashouri, 2014) using **Eq. 5.4.**

$$RP_{red} = \frac{RP}{a_T} \tag{5.4}$$

The healing percentages for all mixtures are plotted against the reduced rest periods. These healing percentages were tried to fit into a sigmoidal function form given in **Eq. 5.5.**

$$\log|\%Hs| = a + \frac{b}{1+\frac{1}{e^{d+g*log\,(RP_{red})}}} \tag{5.5}$$

The sigmoidal function involves four fitting parameters called sigmoidal coefficients. To determine these coefficients, the solver function in MS Excel is used to minimize the error in **Eq. 5.5** and the log of the measured healing percentages. With these predicted healing percentages, healing master curves are plotted for all mixtures. With this, prediction of healing percentages for a damage level, temperature range and the rest period combination is possible. Three separate healing models for three mixtures are given in the next section.

5.4.3 Healing model prediction for M1, M2, M3

The predicted healing percentage with so-called reduced rest periods, including the effect of both the temperature and the rest periods, is plotted. These plots are plotted in arithmetic, semi-log and log-log space in **Figure 5.27** to **Figure 5.29** for all mixtures separately**.** The fitting parameters of percentage healing master curves, obtained to fit the sigmoidal function, are either constant or could be represented as a function of the damage level, i.e., C. These fitting parameters for all the three mixtures obtained using the solver function in excel, for all the three mixtures are given in **Table 5.8.** The constant values are used in the predicted healing equation directly. The fitted parameters, if follows increasing or decreasing order with respect to the damage levels in the materials, are fitted with straight lines. Else has been fitted with a polynomial function. For example, in the case of M2, the value of fitting parameter a is constant for all the damage levels with the value 0.000137; hence it is directly replaced in the equation. For the same mixture, the d value is 0; hence the equation reduces to **Eq. 5.9.** It is also noted that the master curves are not predicted for damage levels less than 0.6C. Below that damage level, due to stiffer mixtures used in this research, it was difficult to assess the damage below 0.6C in the mixtures. M3 showed the maximum healing potential. It is also observed that the healing master curves for the mixtures

form almost a constant curve after a certain value which defines that the recovery in stiffness of the mixtures is constant after a fixed value of rest period. For example, in M1 at 0.9C, the healing potential after a 250 s rest period is almost constant for any value of the rest periods.

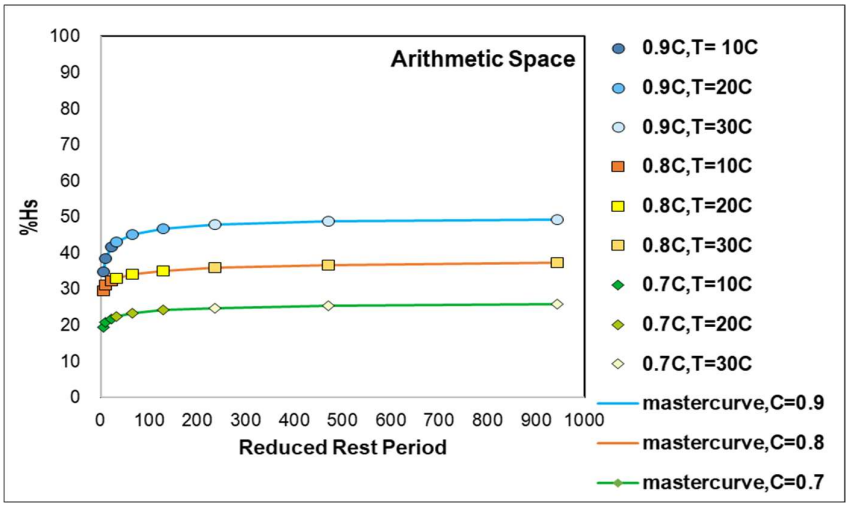

(a)

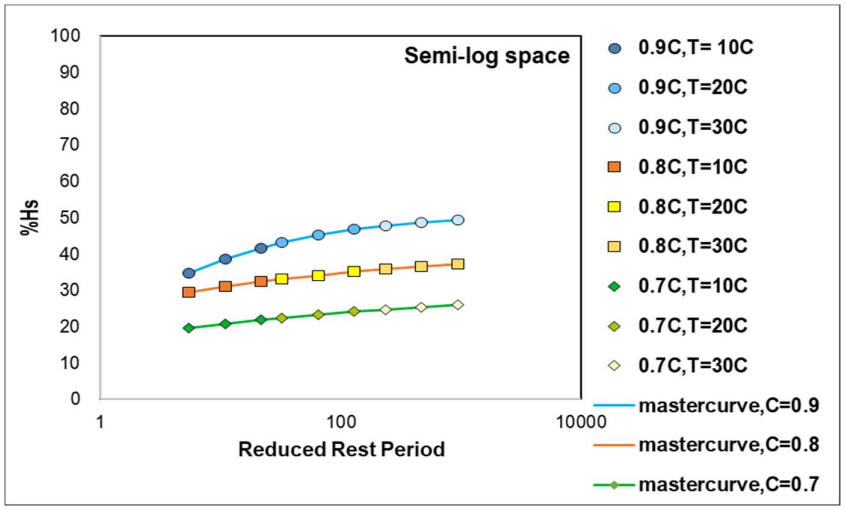

(b)

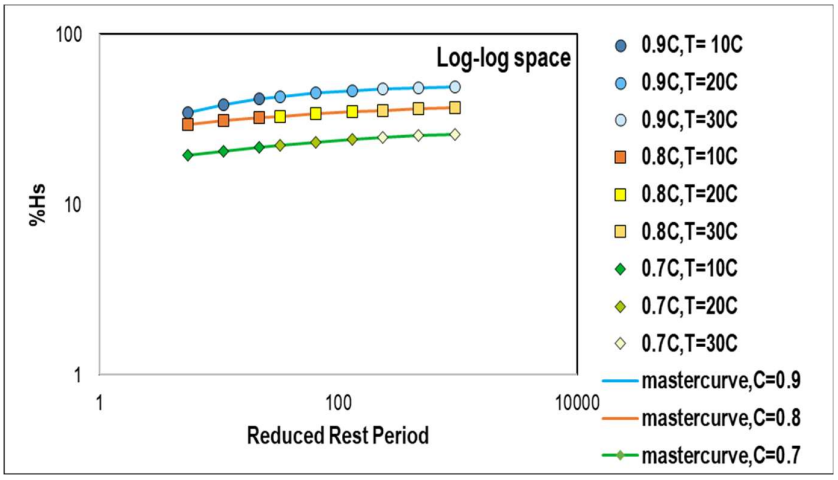

(c)

Figure 5.27. Percent healing master curves at various damage levels in (a)arithmetic space, (b)semi-log space, & (c) log-log space for M1.

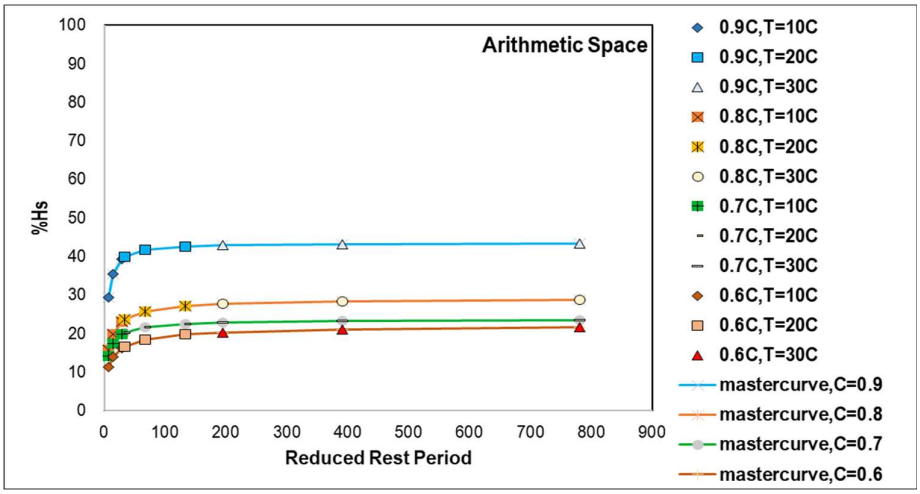

(a)

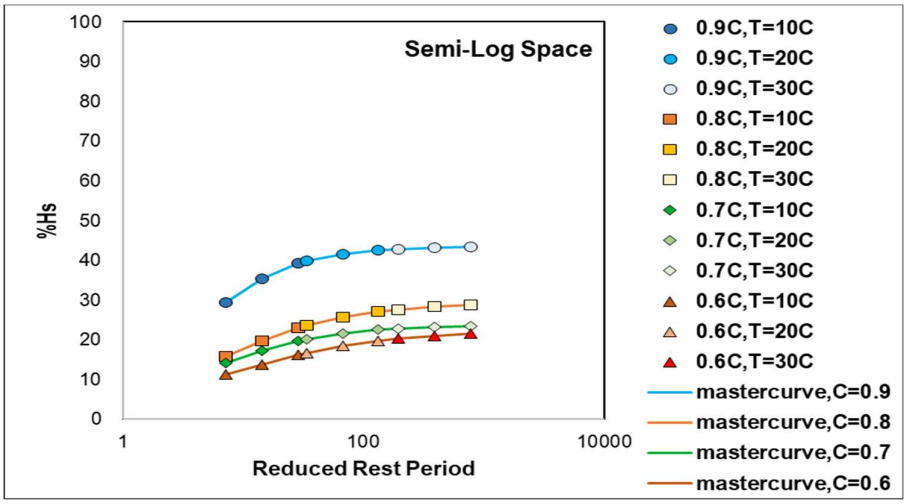

(b)

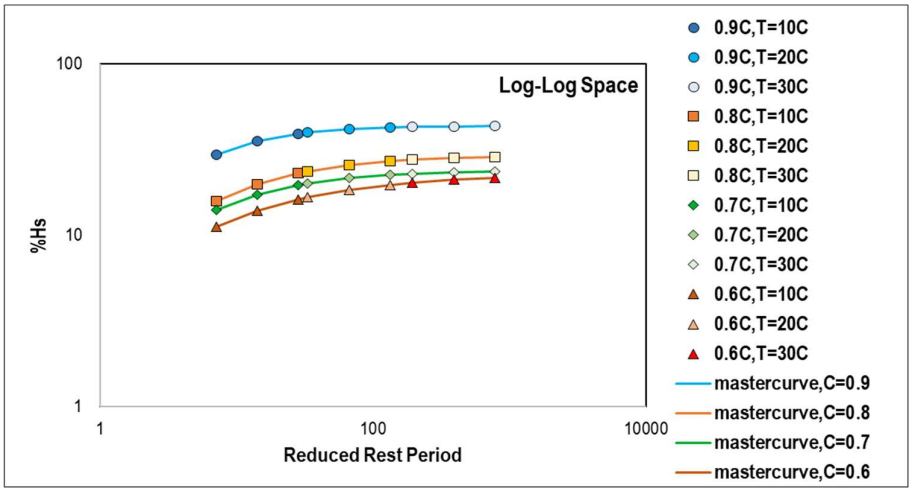

(c)

Figure 5.28. Percent healing master curves at various damage levels in (a)arithmetic space, (b)semi-log space, & (c) log-log space for M2.

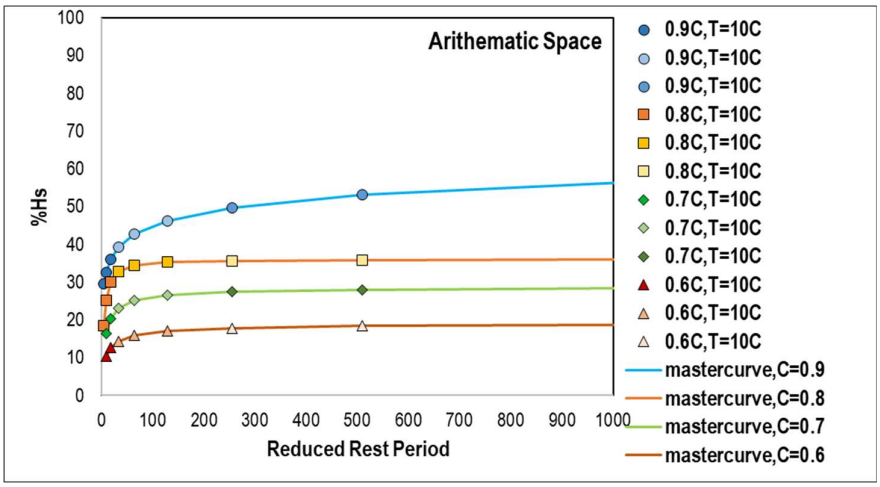

(a)

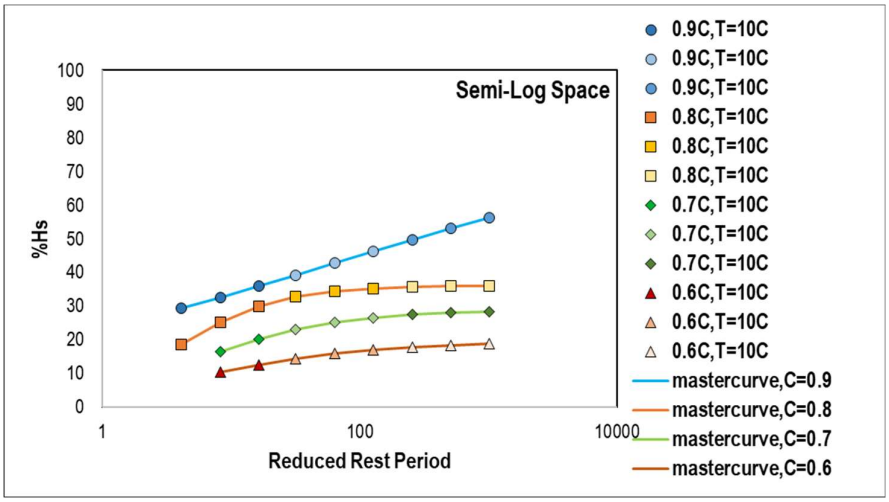

(b)

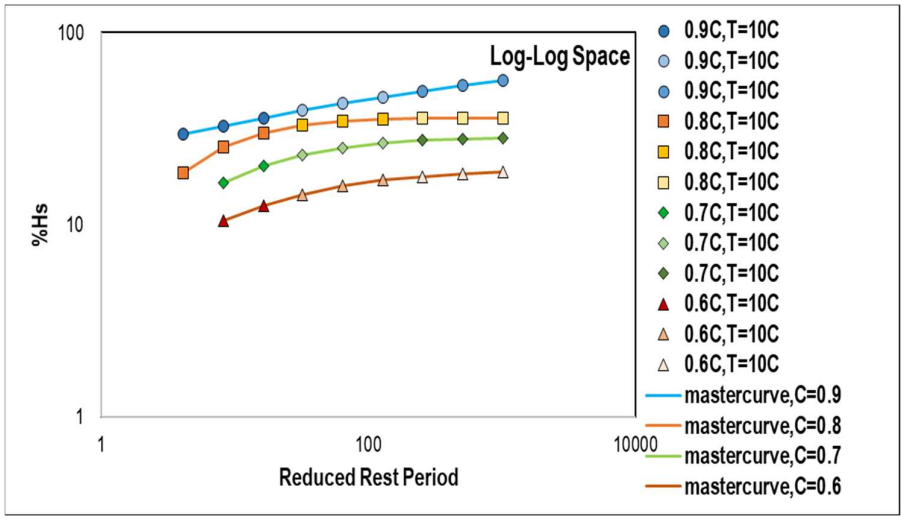

(c)

Figure 5.29. Percent healing master curves at various damage levels in (a)arithmetic space, (b)semi-log space, & (c) log-log space for M3.

Prediction of the healing percentages for all three mixtures at 25°C for a 300s rest period. Shift factor values calculated for M1, M2, & M3 are 0.470, 0.5115, & 0.4455 respectively. It was obtained that the maximum healing potential using the healing equations predicted above was observed in the case of M3, i.e., 46.38%. For M2, it was 24.46%, and 42.29% for M1. The effect of the recycling agent can be seen as visible in the healing potential of the mixture. The softness induced by the recycling agent lets the mixture behave ductile; hence, at higher temperatures, the binder becomes less viscous and can easily flow in the small microcracks responsible for the recovery of strength during the rest period. M2 is the stiffest material with the aged binder; this brittle binder behavior restricts its healing capacity.

5.5 Summary

The primary objective of this research was to examine fatigue and healing in asphalt mixtures composed of recycled pavement materials and a recycling agent, and the key findings are listed below.

- Dynamic modulus tests were conducted according to AASHTO T 342-11 to evaluate the linear viscoelastic properties of the asphalt mixtures. FlexMAT was utilized to process the data, and based on the results, M2 exhibited the highest stiffness while M3 had the lowest. The reference temperature for the tests was 21.1°C. Shift factors were calculated for all temperatures in the fatigue and healing tests using the dynamic modulus analysis output. It should be noted that these tests were conducted within a temperature range of -5 to 50°C, frequencies ranging from 0.1 to 25 Hz, and under haversine compressive cyclic loading in accordance with the standard. No special measures were taken for the specimen ends during the test.

- Uniaxial cyclic fatigue tests were conducted using tension-compression loading mode at temperatures of 10, 20, and 30°C, with a constant peak-to-peak strain of 200 μstrain at a frequency of 10 Hz. The rationale for choosing tension-compression loading mode is explained in Appendix B. Prior to the fatigue tests, a fingerprint test was performed in tension-compression loading mode, applying a range of 50-100 μstrain at 10 Hz, to determine the initial stiffness and pseudo-stiffness of the asphalt mixtures. It is important to note that end treatment was necessary for the fingerprint and fatigue tests, as the testing was in tension-compression mode.

- Among the tested mixtures, M3 exhibited the highest resistance to failure under cyclic loading, withstanding a greater number of load cycles before reaching failure. On the other hand, M2, being the stiffest mixture, demonstrated a brittle or sudden failure at lower temperatures. The failure pattern of the mixtures was significantly influenced by temperature. At 10°C, all mixtures displayed brittle failure, but M3 showed the ability to sustain the highest number of load cycles. However, at higher temperatures, such as 30°C, all mixtures exhibited an extended capacity to endure more failure load cycles. This can be attributed to the less viscous behavior of asphalt mixtures at higher temperatures. Despite having a higher damage growth rate, the mixtures displayed a softer response, effectively restricting brittle or instantaneous failure.

- Following the necessary transformation of the fatigue test dataset for FlexMAT analysis, damage calculations were performed based on the viscoelastic continuum damage (*C-S*) theory for all three asphalt mixtures used. The results showed that M2 accumulated the highest amount of damage, while M3 exhibited the least damage at all temperatures, despite having the highest damage growth rate among the mixtures. Interestingly, the expectation of obtaining identical *C-S* curves for different temperatures was not observed in this study. According to existing literature, this is due to the current inefficiency of the viscoelastic continuum damage (VECD) model to account for healing. Previous studies have indicated that the current VECD model can only consider the damaging effects of tension loading and does not consider the healing capacity of the material at different temperatures. It is now widely acknowledged that the amount of healing experienced by the material varies at different temperatures. Therefore, achieving identical *C-S* curves became a challenge in this research, as the current VECD model does not adequately capture the healing process.

- According to the VECD theory, the damage accumulated in a specimen is considered independent of the loading rate. Fatigue tests were conducted in this research work using two different strain rates: 200 and 300 μstrain. As expected based on VECD, the resulting curves were identical, confirming the independence of damage accumulation from the loading rate. This observation aligns with the theory and supports that the loading rate does not significantly affect the damage accumulation in the tested specimens.

- Group-rest period healing tests were conducted to evaluate the self-healing or recovery capacity of the asphalt mixtures at different temperatures and rest periods. Rest periods of 40, 80, and 160 s were applied at various stages of damage in the asphalt mixtures for different temperatures. Three different methods were employed to quantify the recovery to determine the healing percentages at different damage levels. The results indicated a consistent trend of increased healing percentages with longer rest periods at higher temperatures across the mixtures. However, at 10°C, the mixtures exhibited limitations in surpassing a damage level of 0.8C or undergoing more than 20% damage. Consequently, obtaining a clear trend of healing percentage was challenging at this temperature. M3 demonstrated the highest healing recovery among the mixtures at all temperatures and rest periods. At higher temperatures, there was a significant increase in the percentage of stiffness recovery observed in M3. It was also observed that the healing percentage tended to rise with an increase in temperature. Additionally, a longer rest period resulted in greater recovery in stiffness. An interesting phenomenon was also observed during the experiments: the specimens subjected to shorter rest periods failed earlier than those with longer rest periods, even at 10°C. In other words, specimens with shorter rest periods exhibited reduced resistance to failure, highlighting the importance of rest periods in the damage characteristics of asphalt mixtures.

- The damage characteristics curves for all the healing tests were generated using the FlexMAT software. An interesting observation was made regarding these curves and the different rest periods employed. At higher temperatures, such as 20 and 30°C, the curves followed a similar trend for different rest periods. This is expected because the rest period or loading mode does not impact the shape of the curve. However, for all mixtures, an increase in the duration of rest periods resulted in shorter *C-S* curves, indicating that

longer rest periods led to less damage in the mixtures. At 10°C, shorter curves were obtained for all three mixtures, but it is important to note that this does not signify less damage in the mixtures. The short length of the curves is attributed to the quick failure of the mixtures at lower temperatures due to their higher stiffness. Therefore, it should be interpreted that even with the minimum amount of damage, the specimens failed at 10°C.

- In addition to the experimental data, the time-temperature superposition principle (TTSP) was applied to predict healing percentages. A sigmoidal function, similar to the one used to predict the dynamic modulus master curve, was employed to estimate healing percentages. Considering the damage parameters, healing master curves were generated for each of the three mixtures at different damage levels. Using these predicted healing equations, healing percentages for various rest periods and temperatures could be calculated. The details of these models can be found in Appendix F of the report. For example, the healing percentage was calculated for a 300 s rest period at 25°C for a 10% damage state. In M3, the highest healing percentage of 46.3% was obtained among all three mixtures, indicating its superior healing capability. On the other hand, M1 exhibited a healing percentage of approximately 25%, suggesting a relatively lower healing capacity than M3.

- The healing master curves reveal an important finding: after a certain rest period, the healing percentage reaches a stagnant or constant value, indicating a limit to the healing capacity of the material, beyond which it becomes inefficient in repairing micro-cracks. It is important to note that the healing process does not lead to 100% recovery for the mixture, even if the specimen is left for extended rest periods. There are inherent limitations to the healing potential of the material, and achieving complete restoration is not feasible.

In summary, the testing and analysis results indicate that M2 exhibited the highest stiffness among the mixtures, followed by M1 and M3. This higher stiffness in M2, attributed to the use of reclaimed pavement material, made it more prone to failure compared to the other mixtures. M1 and M3 demonstrated relatively lower stiffness. Interestingly, despite having the same amount of reclaimed asphalt material, M3 showed the highest damage growth rate during testing for shorter durations, gradually leading to failure. However, the presence of a recycling agent in M3 contributed to its resistance to failure, allowing it to withstand a shorter number of cycles. This behavior can be attributed to the softness or ductile behavior induced by the recycling agent. Among all the mixtures, M3 exhibited the maximum tendency for healing or recovery. It displayed a higher healing capacity compared to M1 and M2. It is worth noting that characterizing the mixtures for a damage assessment at 10°C was challenging due to their higher stiffness. This limited the analysis and assessment of the mixtures' damage behavior at this temperature.

References

Ashouri, M. (2014). *Modeling Microdamage Healing in Asphalt Pavements Using Continuum Damage Theory*. Ph.D. Thesis, North Carolina State University.

Zeiada, W.A., Underwood, B.S., Pourshams, T., Stempihar, J., Kaloush, K.E. (2014). Comparison of Conventional, Polymer, and Rubber Asphalt Mixtures using Viscoelastic Continuum Damage Model. *Road Materials and Pavement Design 15(3)*, pp. 588-605.

Chapter 6

FlexPAVE Analysis

6.1 Introduction

The FlexPAVE performance prediction program was used to conduct reliable predictions about the asphalt pavement performance. This chapter will cover a detailed analysis based on the experimental outcome of the mixtures used in the study. Especially, FlexPAVE is a simulation program based on the S-VECD model that can incorporate moving loads (Fourier transform-based analysis) under realistic climate conditions. Two failure criteria are incorporated in this program: (i) the G^R failure criterion, which is independent of the temperature, loading mode, and amplitude, and (ii) the D^R failure criterion, which is introduced to account for the extrapolation issues in the G^R failure criterion, is arithmetic scale-based failure criteria where only the realization of one parameter (i.e., the slope of the linear relationship between the sum of (1-C) and N_f) is enough (see Eq.). The D^R failure criterion yields more realistic fatigue cracking performance prediction than the G^R failure criteria in the log-log scale (Wang 2018). The D_R criterion also considers that the average loss of integrity per cycle throughout an asphalt mixture's fatigue life, that is D^R is constant regardless of the temperature, mode of loading, and loading amplitude (see **Eq. 3.29**). The D^R failure criterion yields more realistic fatigue cracking performance prediction than the G^R failure criteria in the log-log scale (Wang 2018), and it was used as the failure criterion. Although rutting and cracking pavement distresses can be predicted using the FlexPAVE program, rutting was beyond the scope of this research. The research aims to assess and predict fatigue damage along a flexible pavement with M1, M2, and M3 mixtures as base layer materials.

6.2 Percentage Damage Definition in FlexPAVE

The damage level in FlexPAVE is defined using two triangles that overlap to a given reference cross-section area. One inverted triangle with a 170 cm base at the top surface and another triangle with a 120 cm base at the bottom layer define the reference cross-section area, as shown in **Figure 6.1** (Wang 2018).

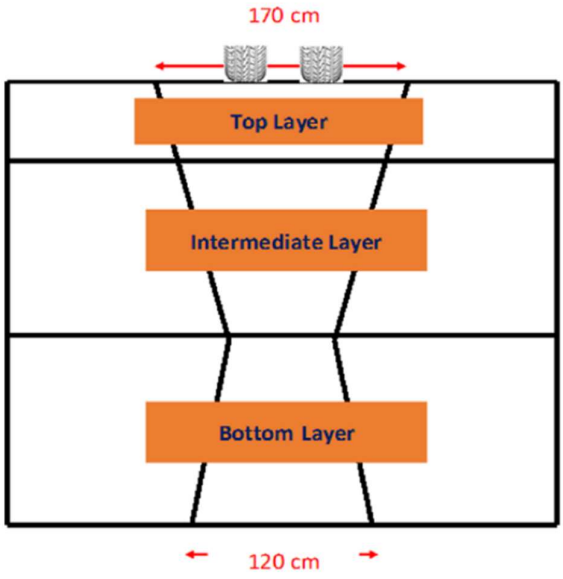

Figure 6.1. Reference area for"percentage damage" definition in FlexPAVE (Wang, 2018).

The percentage of damage is defined as the ratio of the sum of the damage factors within the reference area mentioned above to the reference cross-section area (**Eq. 6.1**).

$$Percentage\ Damage = \frac{\sum_{i=1}^{M} Damage\ Factor * A_i}{\sum_{i=1}^{M} A_i} \quad (6.1)$$

where *I* is the nodal point number in the finite element mesh, *M* is the total number of nodal points in the finite element mesh, A_i is the area of by nodal point, i is the node number, $\sum A_i$ is the reference area. Note that the damage is represented with the damage contours to show the location as well as the damage level of damage.

Damage factors in FlexPAVE are calculated differently for different damage criteria. In the case of the G^R criterion, the damage factor is calculated based on Minor's law given in **Eq. 6.2.** The D^R criterion damage factor is given in **Eq. 6.3**.

$$Damage\ Factor = \frac{N}{N_f} \quad (6.2)$$

$$Damage\ Factor = \frac{1 - C_{avg}}{D^R} \quad (6.3)$$

where C_{avg} is the average reduction in the pseudo-stiffness per cycle up to the current number of the load cycles, 1-C_{avg} represents the average reduction in the pseudo-stiffness per cycle up to the current number of the load cycle, D^R is the average reduction in the pseudo-stiffness up to failure.

6.3 Percentage Cracking on the Field from Percentage Damage in FlexPAVE

As per *Distress Identification Manual* developed for the long-term pavement performance program, 'fatigue cracking' is defined as the inter-connected cracks that occur due to the repeated loadings on the wheel path (Miller and Bellinger 2003). In FlexPAVE, the percentage cracking, which is calculated, is reported as the ratio of the sum of the fatigue cracking area to the total lane area. When checked for various pavements, the relation between the percentage damage on the field and the percentage cracking appears to be an exponential or power-type function (Wang 2019). The damage percentage in FlexPAVE is based on the damage occurring in pavement cross-section, i.e., the x-z plane of the pavement structures, where z is the depth. However, in the field, the fatigue performance is measured in the x-y plane, where y is the travel direction. To overcome this prediction, a transfer function, an empirical calibration function, is implemented in the final step of the distress prediction process. This is similar to the one in the Mechanistic-Emperical Pavement Design Guide (MEPDG) software. An S-shape curve or sigmoidal function is used to predict this transfer function, and the function is consistent with MEPDG (NCHRP 2004). The functions are given in **Eq.6.4**.

$$\%Cracking = \frac{50}{1 + C_{f1} e^{[C_{f2}(logC_{f3} - log\%damage)]}} \quad (6.4)$$

where Cf1, Cf2, and Cf3 are the calibration factors with values 0.342, 13.97, and 16.38, respectively, and percentage damage is the output damage after design life in FlexPAVE. The percentage cracking mentioned above is mainly due to the bottom-up cracking under the action of vehicular loads. Using this function, the percentage of damage obtained in FlexPAVE can be converted to the percentage of cracking on the pavement. Note that the current FlexPAVE does

not account for the aging model. Neither it updates the stiffness values of the asphalt layers with the accumulation of damage in fatigue simulations.

6.4 Input Parameters for Pavement Performance Predictions

A typical Dutch multi-layer pavement structure is taken into consideration to perform the FlexPAVE performance predictions based on the output parameters from FlexMAT (see **Figure 6.2**). Due to the unavailability of VECD parameters and the fatigue damage properties, it was decided not to include the wearing course in the structure, which is considerably thinner than the binder course and base course, from the design structures. This section of the thesis will give the simulation results obtained by FlexPAVE with the different mixtures at different testing conditions. The FlexMAT cracking outputs (e.g., D^R and S_{app}) are saved in the required format and used as the input for FlexPAVE. An isothermal temperature of 20°C was adopted for the climate data, which was closer to what FlexMAT used for determining the VECD parameters (i.e., 21.1°C). The data from three AC 16 Bin/Base mixtures prepared for laboratory testing was considered for the pavement performance assessment. The Poisson's ratio for all the layers was 0.35 as the constant value.

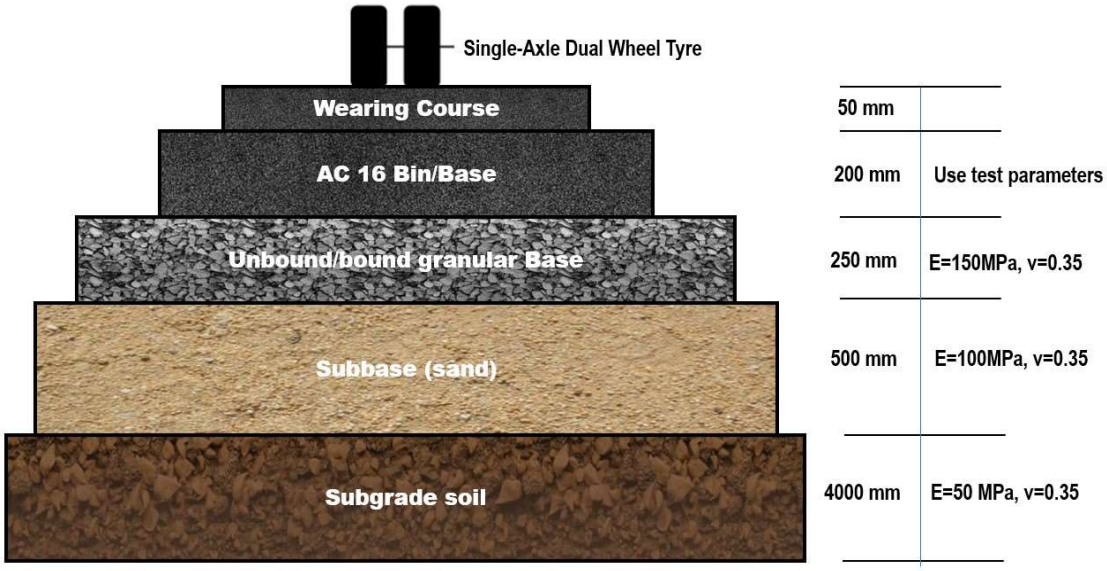

Figure 6.2 Reference pavement structure and properties used for FlexPAVE predictions.

2500 ESALs per day were considered to account for vehicular traffic. A single-axle load with dual-wheel tires is applied to the pavements. The axle load is 80KN, for which the single tire load is 20KN. The tire pressure was 827.37KPa. The contact area for tires and pavement was rectangular, with l/b as 1.5714, and the distance between the two wheels was 30.47 cm. The design velocity for the pavement was kept at 97 km/hr constant for all the simulations, and a 0.4% vehicular growth rate linearly with lane distribution factor as 1 was assumed.

6.5 Results and Discussions

6.5.1 Pavement performance with fatigue and healing

The output of all mixtures at 20°C both in fatigue and fatigue-healing and based on which the simulations for pavement structure were performed for 30 years of design life. Based on the

fatigue data, the percentage damage in all mixtures is depicted in **Figure 6.3.** The maximum damage occurred in M2 at the end of its design life, whereas M1 experienced the least damage. M3 has the highest damage growth rate in the initial years. The sudden decrease in the stiffness of M3 was also observed during the fatigue and healing tests performed in the laboratory. With the inclusion of recycled asphalt materials in M2, it was expected to have a higher damage percentage with time due to the presence of brittle components in the mixture. The mixture with the recycling agent (i.e., M3) behaved softer than the other mixtures, which might be the reason for a higher initial damage rate than the other two mixtures.

A comparison of the damage increase in the mixtures when healing was considered is shown in **Figure 6.5.** The most serious damage at the end of design life was observed in M2. Also, the healing ability of M3 was the highest. Especially, considering a rest period of 80 s into account, M3 was damaged 5.3% less without considering the healing effect (**Figure 6.5 (c)**). At the same time, it was almost 1% and 3.7% in the case of M1 and M2, respectively (see **Figure 6.5 (a) & (b)**). Here, the positive effect of the recycling agent on the damage propagation in the asphalt mixture is identified. With highly recycled pavement materials in M2 and M3, the material tends to hold higher stiffness which enhances the brittleness in the response and gives a higher percentage of damage when the vehicular load is applied. As time passes, the intensity of aging in the mixture with recycled material is higher than in the conventional asphalt mixture hence giving a higher percentage of damage.

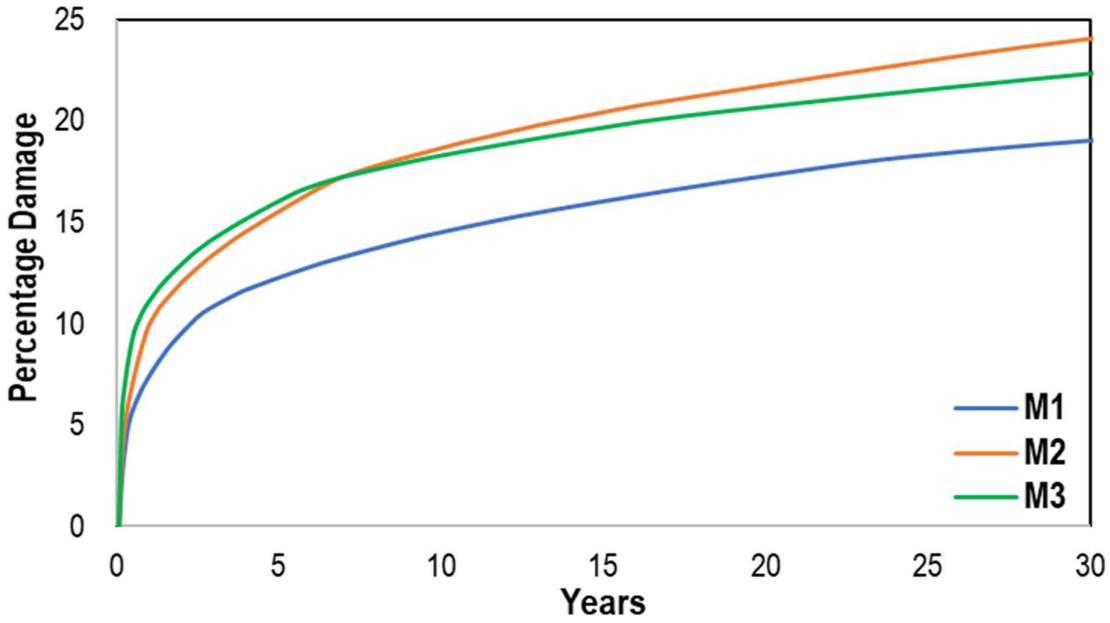

Figure 6.3 Damage for all mixtures in fatigue without considering the healing effect.

For both fatigue and healing tests output, separate simulations were run, keeping the other properties the same to assess the pavement performance accounting for fatigue and healing. The plots of percentage damage growth for 30 years considering fatigue and healing mechanism are given in **Figure 6.4**.

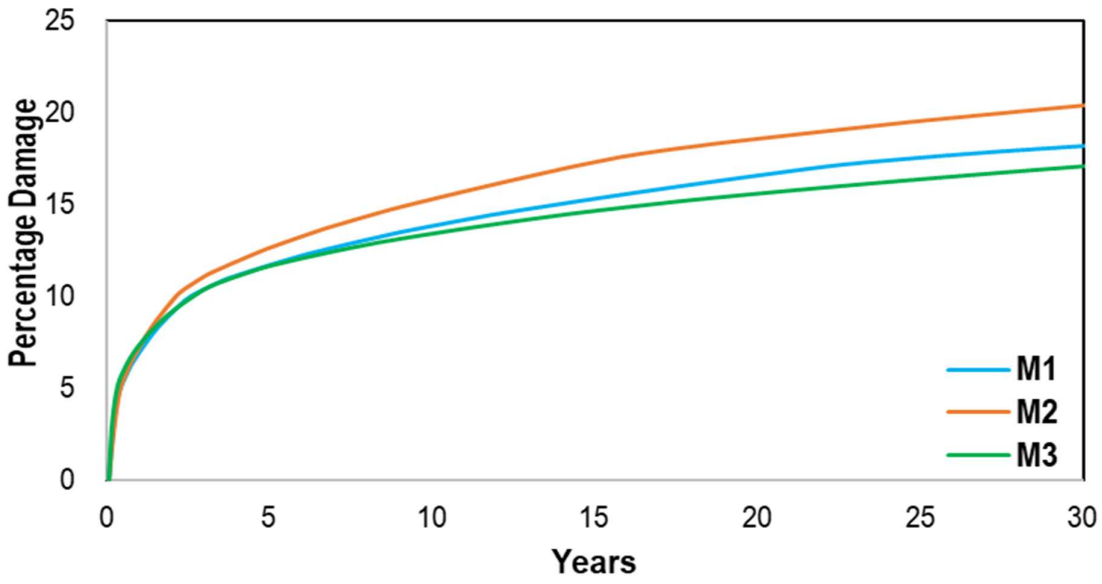

Figure 6.4 Damage growth for all mixtures in fatigue with considering the healing effect.

In **Table 6.1.,** for both the fatigue and healing percentage damages, using **Eq. 6.4.** the cracking percentage per lane area was calculated and tabulated. It can be seen that with the inclusion of a healing mechanism, there was a reduction in the percentage of damage across the cross-section of the pavement structure; subsequently, the percentage of cracking was also reduced. For M3, the maximum healing potential was recorded with the experimental data and the healing model prediction. It is seen that there was a maximum decrease in pavement surface cracking. The healing reduced the cracking percentages in the other two mixtures. The positive effect of including the healing mechanism in the pavement analysis can be seen here.

Table 6.1. Percentage damage and percentage cracking in the pavement structure in fatigue.

Mechanisms	**Fatigue Mechanism**			**Healing Mechanism**		
Mixtures	M1	M2	M3	M1	M2	M3
% Damage	19.02	24.06	22.35	18.19	20.4	17.08
%Cracking	43.93	48.39	47.53	42.33	45.85	39.51
% change in damage and cracking after the inclusion of healing mechanism			**Δ % Damage**	0.83	3.66	5.27
			Δ % Cracking	1.6	2.54	8.02

In the following section of the report, plots in **Figure 6.5** compare the effect of including the healing mechanism in the pavement performance analyzed for M1, M2, and M3. For M1, the damage percentage at the end of design life with and without the healing mechanism in consideration is around 1 %. M3 is more susceptible to healing identified from the experimental and is expected to have the highest reduction in the damage percentage upon application of vehicular loads. It is seen that there was almost a 5.3% reduction in the damage percentage of pavement structures, ultimately giving 8% less cracking on the pavement surface.

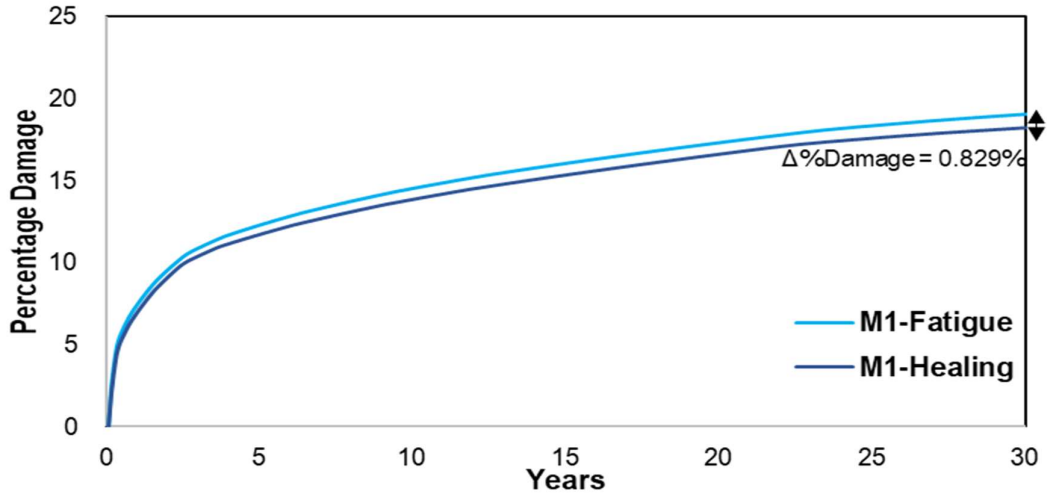

(a)

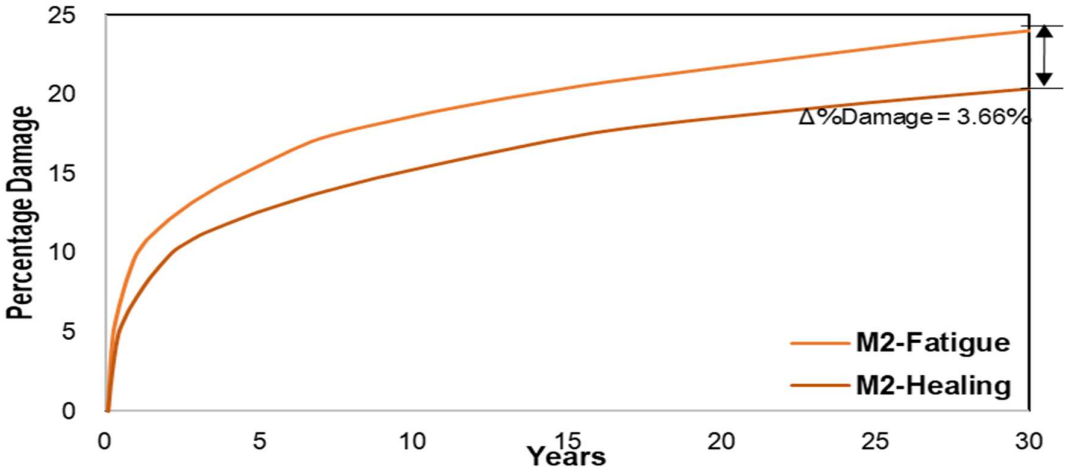

(b)

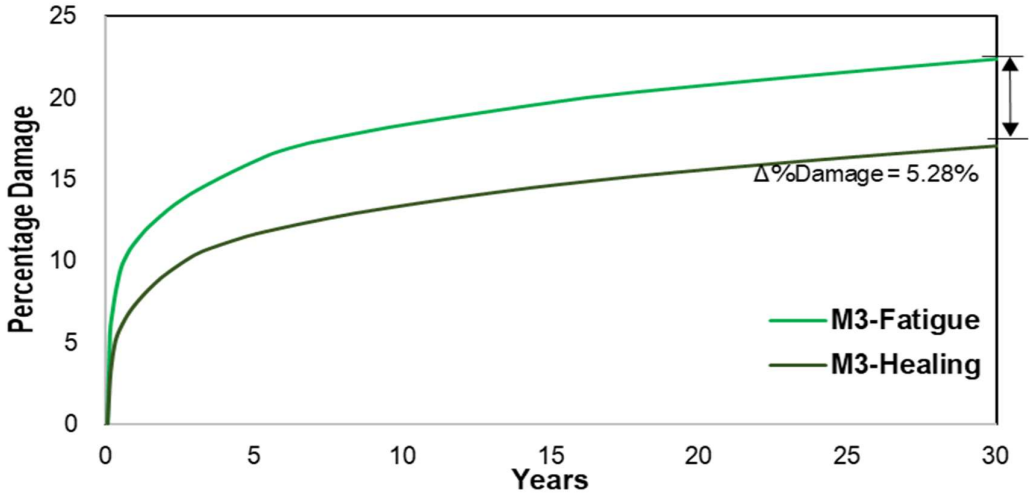

(c)

Figure 6.5. Damage growth of (a) M1, (b) M2, (c) M3 in fatigue and fatigue-healing.

The representative fatigue cracking finite element models of all 3 mixtures represent the damage propagation over 1 month, 6 months, 12 months, 5 years, 10 years, 20 years, 25 years, and 30 years (**Figure 6.6** and **Figure 6.7**) for both fatigue and fatigue-healing mechanism. In these damage contour plots, the scale shown on the right of each plot represents the damage factor**.** In these plots value of the damage factor as 0 is represented by blue color, and the value 1 is represented by red color. Blue color represents a completely intact element, whereas red implies a completely failed element.

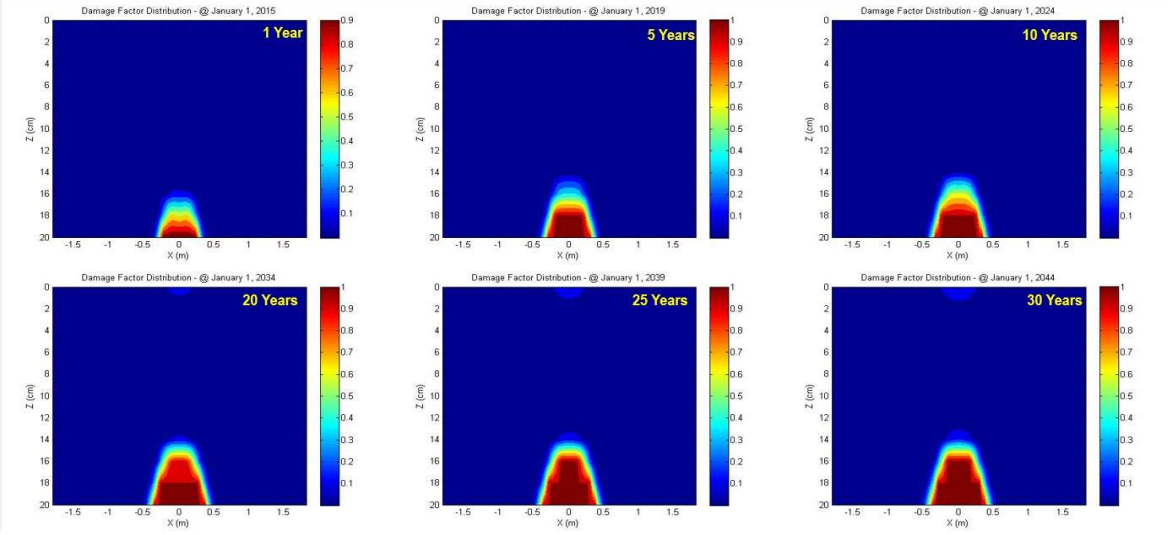

(a)

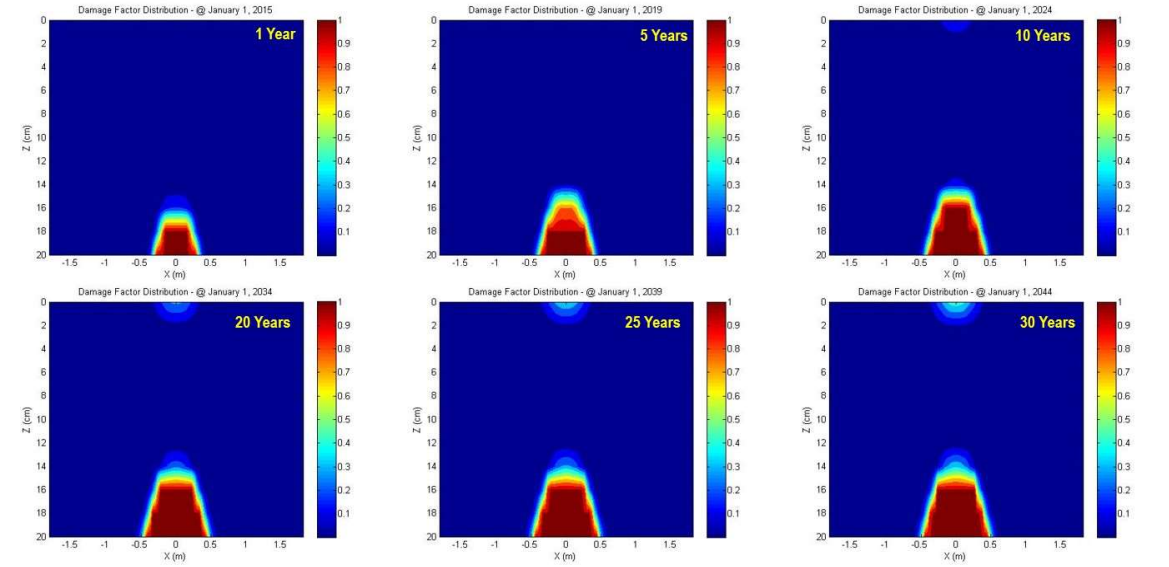

(b)

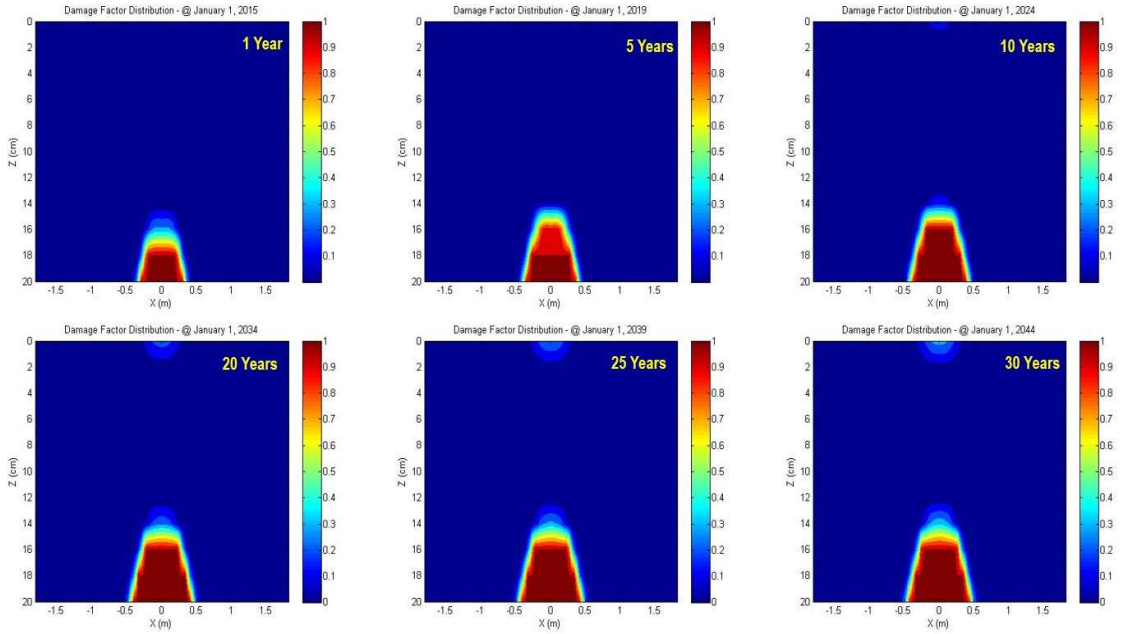

(c)

Figure 6.6 Damage propagation with fatigue mechanism over 30 years in (a) M1, (b) M2, (c) M3.

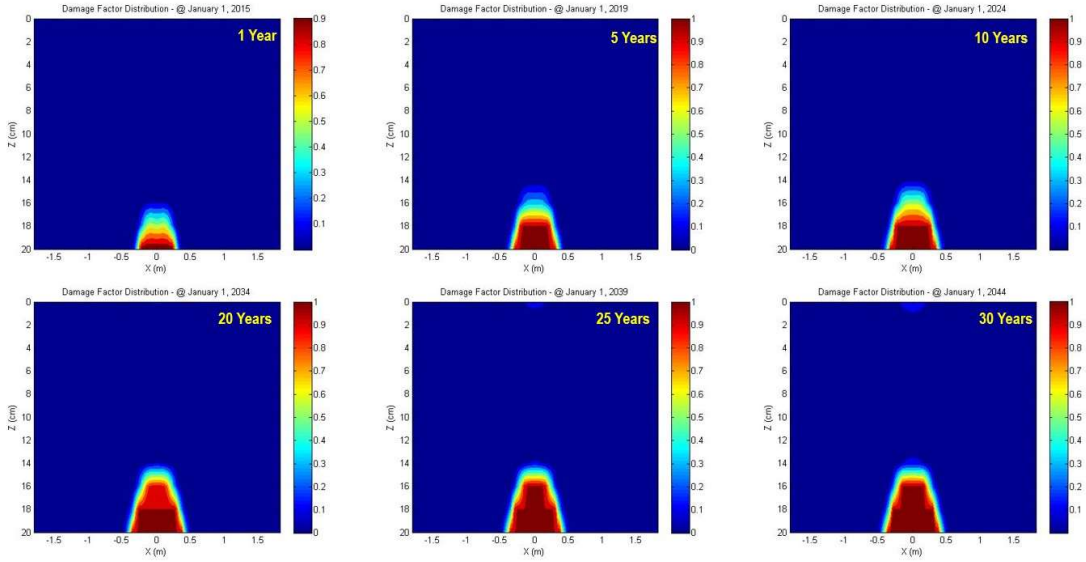

(a)

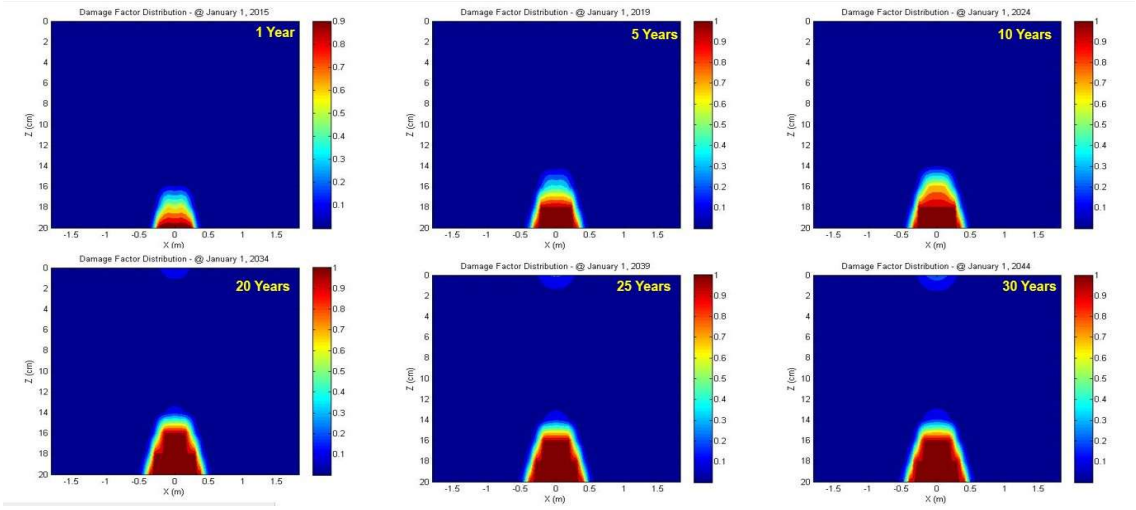

(b)

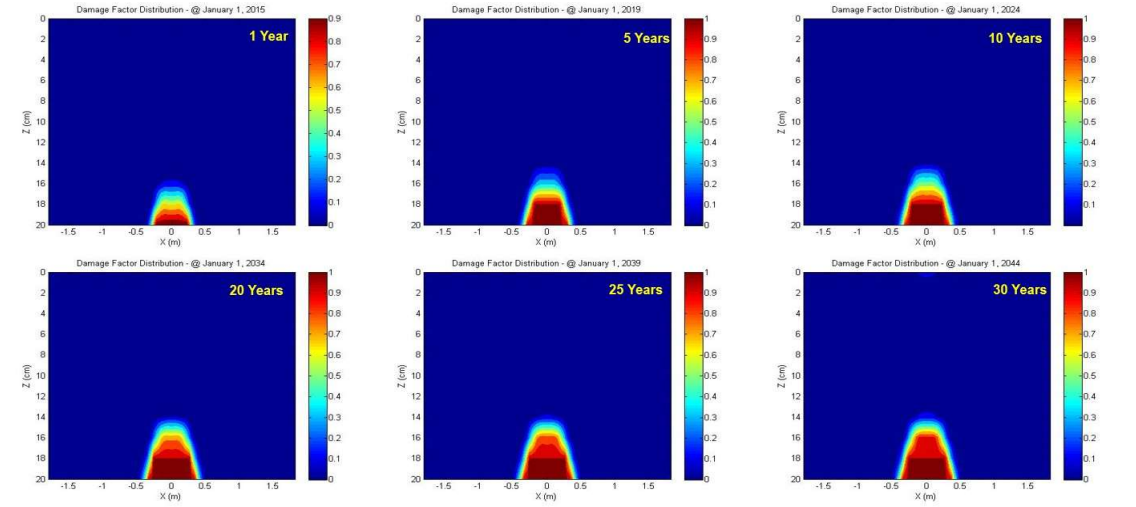

(c)

Figure 6.7 Damage propagation with fatigue-healing mechanism over 30 years in (a) M1, (b) M2, (c) M3

After the healing rest periods are considered, M3 turned out to be the material with the least percentage of damage after the end of the design life, whereas M2 remained the highest (**Figure 6.5**). The rest period would enhance the design life if considered. Even though the healing effect was considered, there was still higher damage in M3 in the initial months. It is also observed that most of the damage in all mixtures generally occurred in the initial 2 years of load application. Models for the other two mixtures are attached in **Appendix E** of the thesis.

6.5.2 Effect of temperature on pavement performance

For M3, the impact of changing the temperature while maintaining constant pavement structure and traffic conditions is also modeled. Both the fatigue data and the fatigue healing data simulations were run at 20 and 30°C. As the temperature rises, the damage percentage increases for both fatigue and fatigue-healing modes (**Figures 6.8 & 6.9**). At higher temperatures, pavement damage is always more pronounced - the tendency for the mixtures to heal increases with the temperature. When the healing mechanism was considered, the overall damage

percentage at 30°C after the design time of 20 years decreased by 7.3%. This difference for continuous fatigue testing was roughly 5%.

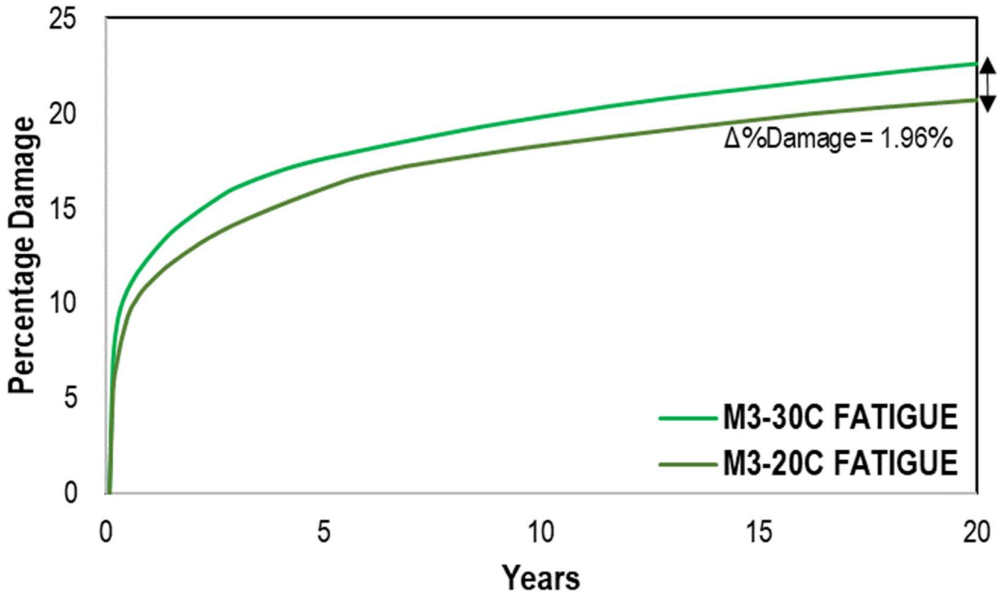

Figure 6.8 Comparison of damage growth in fatigue of M3 at 20 and 30°C.

The simulation was carried out similarly for the data output of M3 considering the healing rest durations at 20, 30, and 50°C. It has been noted that pavement structures suffer more damage at higher temperatures. It is crucial to note that the simulation, in this instance, used the results of the healing test at 20°C. Therefore, the output of the FlexPAVE only included the damage brought on by traffic and temperature variation when the input was left unchanged. The materials behavior was not examined at these temperatures in this study.

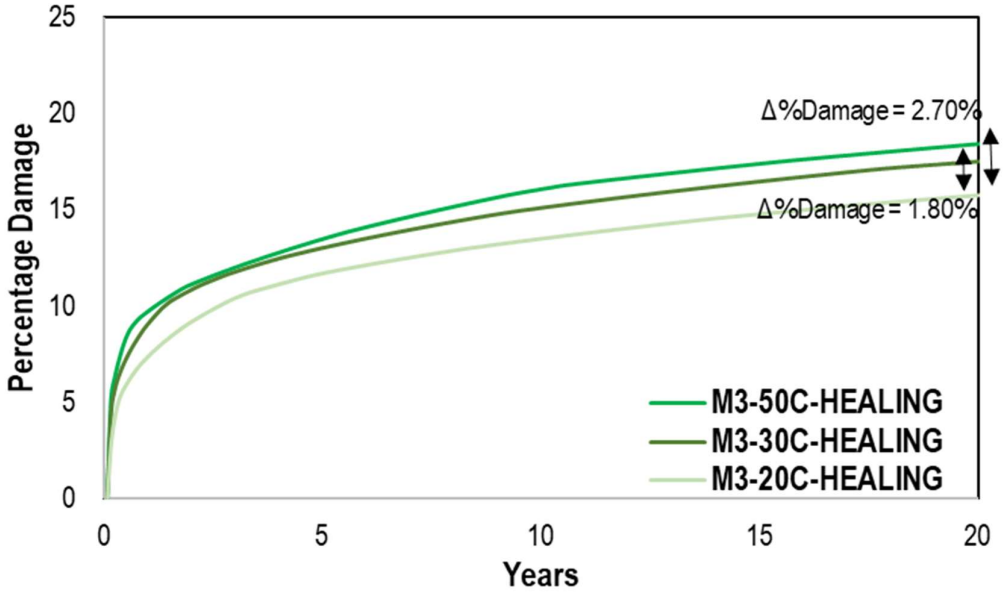

Figure 6.9 Comparison of damage growth in fatigue-healing of M3 at 20, 30 and 50°C.

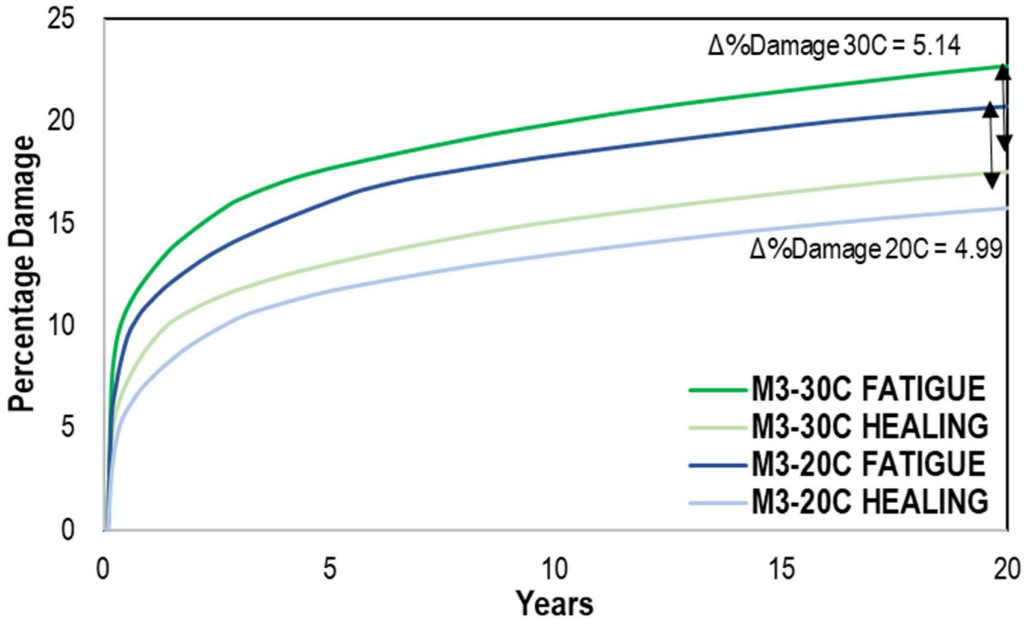

Figure 6.10 Comparison of damage growth in fatigue-healing of M3 at 20 and 30°C.

The recovery of stiffness was higher at higher temperatures due to more healing; hence, the difference in damage percentage due to the healing process was likewise higher at higher temperatures (see **Figure 6.10.**). This increase in the damage percentage was due to higher temperature due to the enhanced softness in the mixture, which made the mixture more susceptible to deformation. Higher temperatures also enhanced the oxidation rate and aging process in asphalt mixtures, making them brittle over time, reducing their ability to withstand cyclic loading, and increasing the fatigue cracking and damage percentage.

6.6 Conclusions

A comprehensive understanding of how the pavement will operate under a realistic load utilizing various combinations with both fatigue and healing mechanisms becomes clear after completing the pavement performance simulations in FlexPAVE. The major conclusions of this chapter are:

- In fatigue-only assessment, the highest damage percentage experienced was by M2, whereas the least was by M1. It was also observed that the highest damage percentage growth rate was incurred in M3 due to the softness induced by the recycling agent for an initial period.

- With healing analysis, the trend changed. M3 was the mixture with the least damage percentage after 30 years. At the same time, M2 was still the mixture with the highest damage percentage. The damage percentage growth was still the highest in M3 for an initial period. Moreover, a visible difference in the damage percentage at the end of 30 years was observed by considering the healing mechanism. In M1, M2, and M3, a difference of 0.82, 3.66 and 5.28 %, respectively, was observed with the healing mechanism.

- A transfer function was used to predict the percentage cracking on the surface of the pavements. For M3, by considering the healing mechanism in damage predictions, there was an 8.02 % reduction in the cracking percentage at the surface. This difference was 1.6 and 2.54 % for M1 and M2, respectively.

- In the case of M3, it can be observed that damage starts to accumulate on the top of the surface when only the fatigue mechanism was considered after ten years (see **Figure 6.8. (c)**). Incorporating the healing mechanism, this phenomenon was not observed anymore, which enhanced the pavement performance upon traffic loads. Although this phenomenon was the same for M1 and M2 for fatigue and healing, the intensity of these top-down cracks was smaller in the case of the healing mechanism.

- The effect of temperature variations on pavement performance was also assessed. The major effect of healing was visible in M3. With an increase in simulation temperature from 20 to 30°C, there was an increase of about 2 % in damage percentage. While considering healing, the simulations were run at 3 different temperatures. There was an increase of almost 3 and 2 % of damage in the pavements upon increasing temperature concerning 20°C.

- The recovery of stiffness as a result of healing was higher at higher temperatures; hence, the difference in damage percentage as a result of healing was likewise higher at higher temperatures**.** This difference was 4.99 % for 20°C, whereas for 30°C, it was almost 5.15 %.

References

National Cooperative Highway Research Program (NCHRP), 2004. *Guide for Mechanistic–Empirical Design of New and Rehabilitated Pavement Structures*. Transportation Research Board of the National Academies, Washington, D.C.

Miller, J.S., Bellinger, W.Y. 2014. *Distress Identification Manual for the Long-Term Pavement Performance Program (Fifth Revised Edition)*. Washington D.C.: Federal Highway Administration (FHWA), FHWA-HRT-13-092.

Wang, Y. (2019). *Development of the Framework of Performance Engineered Mixture Design for Asphalt Concrete*. Ph.D. Thesis, North Carolina State University.

Chapter 7

Conclusion & Recommendations

7.1 Conclusions

In this research work, an answer was sought to the following question:

"How to assess the effect of reclaimed pavement materials and recycling agents on the fatigue and healing characterization of the asphalt mixtures?"

This part of the section describes the conclusions drawn during the research work.

The primary objective of this research study is to analyze and describe three distinct mixtures in terms of their fatigue and healing properties. The researchers conducted a series of experiments to enhance their understanding of these mixtures. Rather than solely comparing the results among the three mixtures, the focus was on characterizing each mixture individually and highlighting their key differences. The comprehensive assessment of the mixtures' fatigue and healing properties involved several steps. Initially, extensive experimental testing was conducted in a laboratory setting. Subsequently, mathematical predictions were made using VECD theory. Finally, the materials' parameters were inputted into finite element modeling software to gain a clear understanding of their performance under practical conditions.

- *How to perform laboratory testing and develop a method to quantify fatigue and healing characterization of the asphalt mixtures using VECD theory.*

The experimental assessment began with conducting dynamic modulus tests to obtain VECD parameters and linear viscoelastic properties of the mixtures. Subsequently, cyclic fatigue tests were performed in the on-specimen mode for tension-compression mode of loading at 200 μstrain for all three mixtures at three different temperatures to understand their fatigue behavior. The impact of healing was then evaluated by incorporating group rest periods during continuous cyclic fatigue tests at various temperatures. A dedicated group-rest healing test was conducted to assess the effect of rest periods and temperature on all three mixtures. Three different rest periods were accounted for in the testing as well. A group rest period was applied to the specimen after it reached different damage levels, and during those rest periods, the material tended to heal due to the closure of micro-cracks. A manual method was developed to apply rest periods during the healing test process. After completing the testing phase, the focus shifted towards conducting mathematical calculations and post-processing results using FlexMAT Cracking software based on VECD theory. This software facilitated the generation of damage characteristic curves for both fatigue and healing tests. A thorough comparison was then conducted, utilizing these damage characteristic curves to elaborate on the damage propagation and behavior of the mixtures during the tests. This analysis provided insights into how the mixtures responded to fatigue loading, as well as the effectiveness of the healing process in mitigating damage.

- *Which would be the reliable healing model for asphalt mixtures containing recycled asphalt materials and recycling agents involving temperature, damage state, and rest periods?*

Further, a reliable healing model for each asphalt mixture with reclaimed pavement material and recycling agent was derived using a sigmoidal function using the predicted healing percentages, including the effect of temperature, damage levels, and the duration of rest periods. Healing master curves for three different mixtures for different damage levels and reduced rest period are presented. The healing percentages for mixtures at a particular damage state can be calculated for any temperature and duration of rest periods. These models verify that the time-temperature superposition principle (T-TSP) concept does hold for asphalt materials during the rest periods in which the material heals. FlexMAT Cracking, a software developed based on the VECD theory, was used to perform and predict fatigue damage parameters. Three different quantification models were utilized to determine the healing percentage based on the number of damage cycles, *S,* the parameter that accounts for accumulated damage in the mixture, and damage level. As the rest period is increased, the healing percentages tend to increase. Similarly, with an increase in temperature, the healing percentages also tend to increase. Indeed, as the damage level of the mixtures increases, the healing percentage tends to decrease. This is because higher levels of damage often result in wider cracks and more severe structural degradation. Because of this, the damage rate also increased as the damage level in the mixture escalated, even with the application of rest periods. Consequently, the recovery and healing of such extensive damage become increasingly challenging, reducing the healing percentage. The results indicated a consistent trend in healing percentage concerning the level of damage, rest period, and temperature across all three methods. Healing percentages were directly influenced by temperature and rest period, with higher values observed as these factors increased. However, reaching the original undamaged state became increasingly challenging as the material's damage level became more severe. The maximum tendency to heal was concluded in M3, although with 70% of reclaimed asphalt material, but used with the doze of recycling agent.

- *How to examine the flexible pavement performance using the mixtures tested in the laboratory, which combines the time-scale differences and layered viscoelastic analysis?*

In addition, the author utilized FlexPAVE software to analyze the performance of a multi-layered typical Dutch pavement structure incorporating the mixtures studied, considering realistic vehicle loads and environmental conditions. Detailed results with simulations were provided, highlighting the positive impact of implementing healing as a damage mechanism. Simulation results regarding the effect of temperature variations on pavement performance were presented. At higher temperatures, the mixtures exhibited greater healing capacity, resulting in a lower percentage of damage in pavement cross-section across all mixtures. To quantify the extent of damage on the pavement surface, a transfer function from the previous study was employed, which transformed the damage percentage across the asphalt layer's cross-section into a percentage of cracking on the surface per area. By incorporating the healing mechanism in performance predictions, the simulations indicated a reduction of approximately 5% in the percentage of damage across the cross-section and an 8% reduction in surface cracking percentage for M3 (i.e., 70% reclaimed asphalt material + recycling agent). While these

differences were most pronounced for Mixture 3, positive effects were also observed for the other asphalt mixtures in the study.

7.2 Recommendations & Future Work

The present study has shed light on various aspects of fatigue and healing characterization of asphalt materials and has provided valuable insights into it. However, as with any research endeavor, there are still avenues for further exploration and opportunities for improvement. In this section, we outline the future work and recommendations that can build upon the findings of this study, aiming to expand knowledge, address limitations, and contribute to the field of assessment of asphalt materials. These suggestions encompass both theoretical advancements and practical applications, offering a roadmap for future researchers and stakeholders to enhance our understanding and implementation of study incorporated in this research.

- An attempt to assess these materials for healing under pulse rest healing work can be performed, and the difference in the mode of application of rest periods can be assessed, which is closer to the resting phenomenon occurring in the pavements in use.

- The work performed in this research involves uniaxial cyclic fatigue testing, whereas contractors use 4 point bending test to assess the fatigue characteristics of the asphalt mixtures. A similar study on 4 point bending test can be performed, and the correlation between both methods can be studied. This way, the asphalt damage can be assessed based on both phenomenological and mechanistic approaches.

- This research involves strain-controlled testing, whereas the material response under stress-controlled testing differs. A comparative study between both modes can be studied.

- Furthermore, in this research work, the author could not validate the identical damage characteristics C-S curves for same mixtures at different temperatures. More detailed research can be performed on this topic, leading to modifications in the current VECD formulations.

- Micromechanical studies on the failure pattern of different mixtures involving the healing mechanism can be an interest for future studies. There is a difference in the failure line in M1, M2 and M3 at different temperatures.

- A comparative study for asphalt materials characterization with uniaxial testing (VECD Theory) and 4-point bending beam test. A correlation factor between the fatigue life from both the methods can be calculated as in **Figure 7.1.**

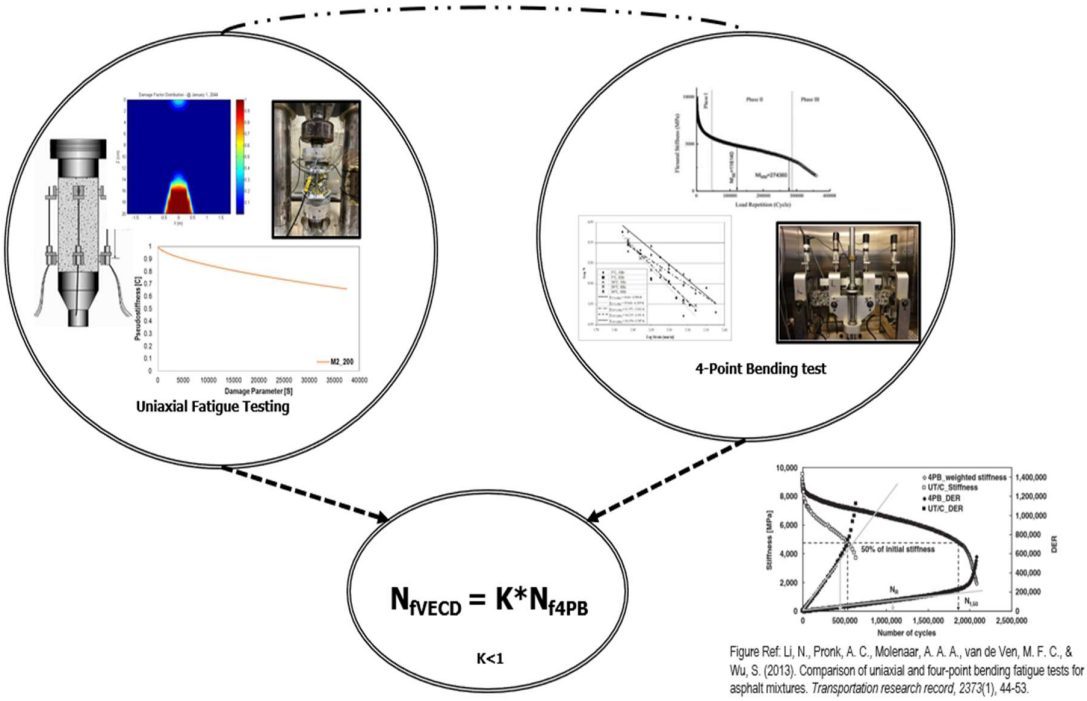

Figure 7.1. Possible correlation in fatigue life of 4-point bending and uniaxial fatigue testing.

A

FlexMAT™ Cracking

A.1. Data Processing using FlexMAT

FlexMAT is used in this study to speed up the mixture analysis approach, assisting in predicting critical parameters that serve as primary inputs for mechanistic-empirical simulations in the FlexPAVE software. However, it has been found that new users may face difficulties when using this software. As a result, this section of the study aims to provide a thorough understanding of how to use FlexMAT efficiently. FlexMAT is a spreadsheet-like software that runs alongside Microsoft Excel. FlexMAT performs most of the operations and calculations in the background using VBA code inaccessible to users.

Two different FlexMAT programs are available, as mentioned in **Figure A.1** (i.e., FlexMAT Cracking and FlexMAT Rutting). FlexMAT Cracking v2.1.3-2022-12 is the tool used for analysis in this study. It examines the models of dynamic modulus, fatigue cracking, and aging. This software can also calculate apparent damage capacity (S_{app}). FlexMAT Rutting is another program that aids in analyzing the permanent deformation index and the rutting strain index (RSI). The determination of these parameters is outside the scope of this study.

Figure A.1 shows a list of results from the FlexMAT Cracking software that are basic and important parameters for mix analysis. Each module will cover the procedure involved in the analysis utilizing FlexMAT Cracking.

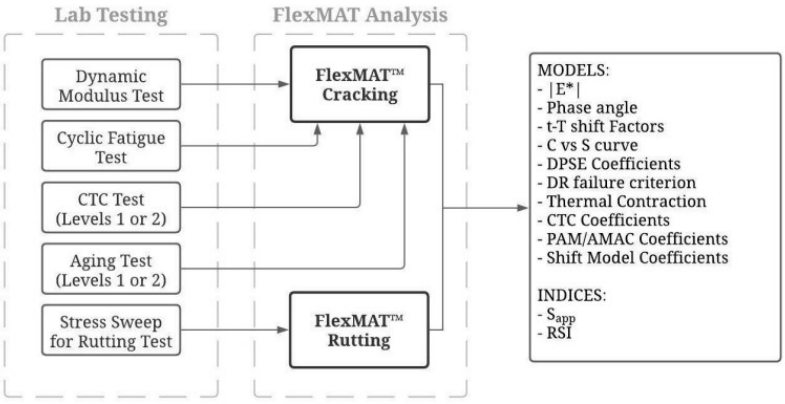

Figure A.1. FlexMAT™ flow overview.

The testing phase of this research is carried out in the pavement engineering laboratory, and the output data is recorded using in-house MP3 software. The output is a comma-separated value file (see **Figure A.2**).

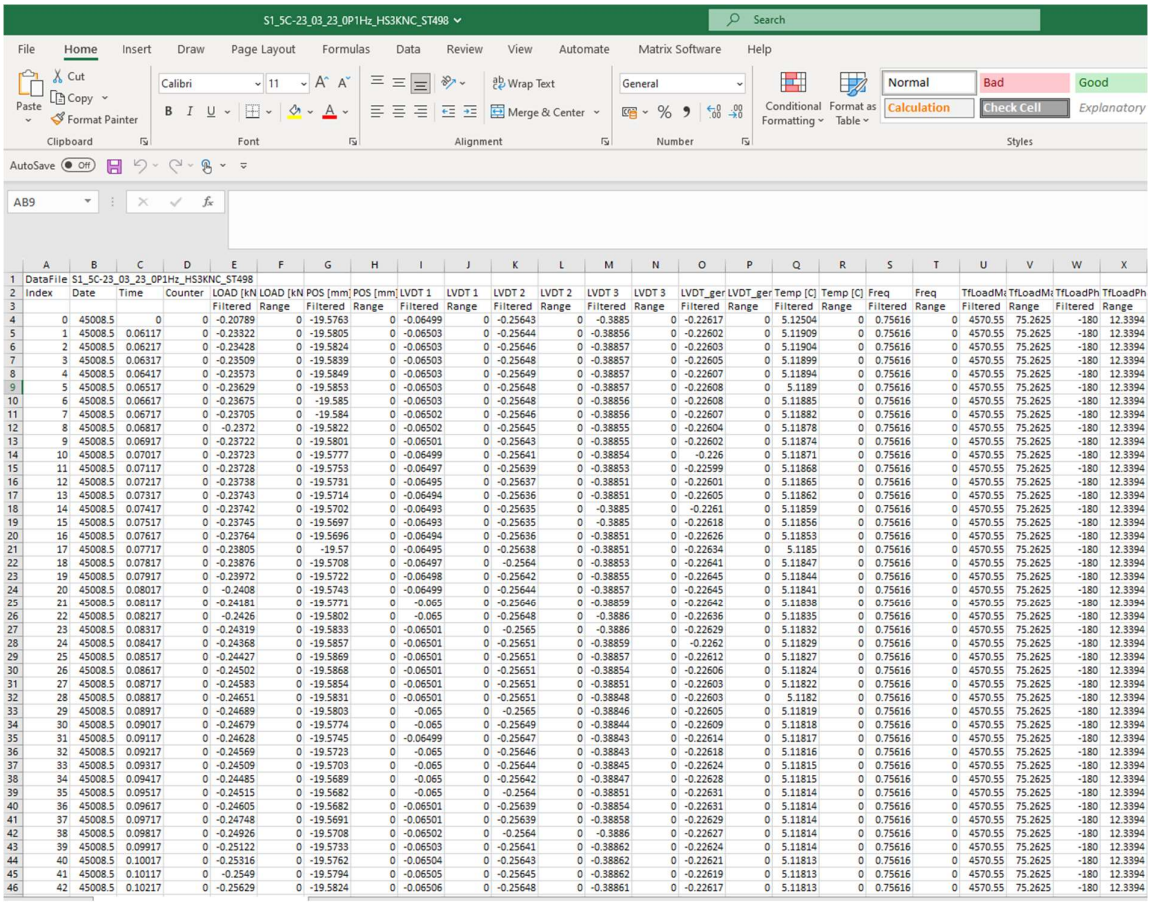

	A	B	C	D	E	F	G	H	I	J	K	L	M	N	O	P	Q	R	S	T	U	V	W	X
1	DataFile	S1_5C-23_03_23_0P1Hz_HS3KNC_ST498																						
2	Index	Date	Time	Counter	LOAD [kN	LOAD [kN	POS [mm	POS [mm	LVDT 1	LVDT 1	LVDT 2	LVDT 2	LVDT 3	LVDT 3	LVDT_ger	LVDT_ger	Temp [C]	Temp [C]	Freq	Freq	TfLoadMa	TfLoadMa	TfLoadPh	TfLoadPh
3					Filtered	Range	Filtered	Range	Filtered	Range	Filtered	Range	Filtered	Range	Filtered	Range	Filtered	Range	Filtered	Range	Filtered	Range	Filtered	Range
4	0	45008.5	0	0	-0.20789	0	-19.5763	0	-0.06499	0	-0.25643	0	-0.3885	0	-0.22617	0	5.12504	0	0.75616	0	4570.55	75.2625	-180	12.3394
5	1	45008.5	0.06117	0	-0.23322	0	-19.5805	0	-0.06503	0	-0.25644	0	-0.38856	0	-0.22602	0	5.11909	0	0.75616	0	4570.55	75.2625	-180	12.3394
6	2	45008.5	0.06217	0	-0.23428	0	-19.5824	0	-0.06503	0	-0.25646	0	-0.38857	0	-0.22603	0	5.11904	0	0.75616	0	4570.55	75.2625	-180	12.3394
7	3	45008.5	0.06317	0	-0.23509	0	-19.5839	0	-0.06503	0	-0.25648	0	-0.38857	0	-0.22605	0	5.11899	0	0.75616	0	4570.55	75.2625	-180	12.3394
8	4	45008.5	0.06417	0	-0.23573	0	-19.5849	0	-0.06503	0	-0.25649	0	-0.38857	0	-0.22607	0	5.11894	0	0.75616	0	4570.55	75.2625	-180	12.3394
9	5	45008.5	0.06517	0	-0.23629	0	-19.5853	0	-0.06503	0	-0.25648	0	-0.38857	0	-0.22608	0	5.1189	0	0.75616	0	4570.55	75.2625	-180	12.3394
10	6	45008.5	0.06617	0	-0.23675	0	-19.585	0	-0.06503	0	-0.25648	0	-0.38856	0	-0.22608	0	5.11885	0	0.75616	0	4570.55	75.2625	-180	12.3394
11	7	45008.5	0.06717	0	-0.23705	0	-19.584	0	-0.06502	0	-0.25646	0	-0.38856	0	-0.22607	0	5.11882	0	0.75616	0	4570.55	75.2625	-180	12.3394
12	8	45008.5	0.06817	0	-0.2372	0	-19.5822	0	-0.06502	0	-0.25645	0	-0.38855	0	-0.22604	0	5.11878	0	0.75616	0	4570.55	75.2625	-180	12.3394
13	9	45008.5	0.06917	0	-0.23722	0	-19.5801	0	-0.06501	0	-0.25643	0	-0.38855	0	-0.22602	0	5.11874	0	0.75616	0	4570.55	75.2625	-180	12.3394
14	10	45008.5	0.07017	0	-0.23723	0	-19.5777	0	-0.06499	0	-0.25641	0	-0.38854	0	-0.226	0	5.11871	0	0.75616	0	4570.55	75.2625	-180	12.3394
15	11	45008.5	0.07117	0	-0.23728	0	-19.5753	0	-0.06497	0	-0.25639	0	-0.38853	0	-0.22599	0	5.11868	0	0.75616	0	4570.55	75.2625	-180	12.3394
16	12	45008.5	0.07217	0	-0.23738	0	-19.5731	0	-0.06495	0	-0.25637	0	-0.38851	0	-0.22601	0	5.11865	0	0.75616	0	4570.55	75.2625	-180	12.3394
17	13	45008.5	0.07317	0	-0.23743	0	-19.5714	0	-0.06494	0	-0.25636	0	-0.38851	0	-0.22605	0	5.11862	0	0.75616	0	4570.55	75.2625	-180	12.3394
18	14	45008.5	0.07417	0	-0.23742	0	-19.5702	0	-0.06493	0	-0.25635	0	-0.3885	0	-0.2261	0	5.11859	0	0.75616	0	4570.55	75.2625	-180	12.3394
19	15	45008.5	0.07517	0	-0.23745	0	-19.5697	0	-0.06493	0	-0.25635	0	-0.3885	0	-0.22618	0	5.11856	0	0.75616	0	4570.55	75.2625	-180	12.3394
20	16	45008.5	0.07617	0	-0.23764	0	-19.5696	0	-0.06494	0	-0.25636	0	-0.38851	0	-0.22626	0	5.11853	0	0.75616	0	4570.55	75.2625	-180	12.3394
21	17	45008.5	0.07717	0	-0.23805	0	-19.57	0	-0.06495	0	-0.25638	0	-0.38851	0	-0.22634	0	5.1185	0	0.75616	0	4570.55	75.2625	-180	12.3394
22	18	45008.5	0.07817	0	-0.23876	0	-19.5708	0	-0.06497	0	-0.2564	0	-0.38853	0	-0.22641	0	5.11847	0	0.75616	0	4570.55	75.2625	-180	12.3394
23	19	45008.5	0.07917	0	-0.23972	0	-19.5722	0	-0.06498	0	-0.25642	0	-0.38855	0	-0.22645	0	5.11844	0	0.75616	0	4570.55	75.2625	-180	12.3394
24	20	45008.5	0.08017	0	-0.2408	0	-19.5743	0	-0.06499	0	-0.25644	0	-0.38857	0	-0.22645	0	5.11841	0	0.75616	0	4570.55	75.2625	-180	12.3394
25	21	45008.5	0.08117	0	-0.24181	0	-19.5771	0	-0.065	0	-0.25646	0	-0.38859	0	-0.22642	0	5.11838	0	0.75616	0	4570.55	75.2625	-180	12.3394
26	22	45008.5	0.08217	0	-0.2426	0	-19.5802	0	-0.065	0	-0.25648	0	-0.3886	0	-0.22636	0	5.11835	0	0.75616	0	4570.55	75.2625	-180	12.3394
27	23	45008.5	0.08317	0	-0.24319	0	-19.5833	0	-0.06501	0	-0.2565	0	-0.3886	0	-0.22629	0	5.11832	0	0.75616	0	4570.55	75.2625	-180	12.3394
28	24	45008.5	0.08417	0	-0.24368	0	-19.5857	0	-0.06501	0	-0.25651	0	-0.38859	0	-0.2262	0	5.11829	0	0.75616	0	4570.55	75.2625	-180	12.3394
29	25	45008.5	0.08517	0	-0.24427	0	-19.5869	0	-0.06501	0	-0.25651	0	-0.38857	0	-0.22612	0	5.11827	0	0.75616	0	4570.55	75.2625	-180	12.3394
30	26	45008.5	0.08617	0	-0.24502	0	-19.5868	0	-0.06501	0	-0.25651	0	-0.38854	0	-0.22606	0	5.11824	0	0.75616	0	4570.55	75.2625	-180	12.3394
31	27	45008.5	0.08717	0	-0.24583	0	-19.5854	0	-0.06501	0	-0.25651	0	-0.38851	0	-0.22603	0	5.11822	0	0.75616	0	4570.55	75.2625	-180	12.3394
32	28	45008.5	0.08817	0	-0.24651	0	-19.5831	0	-0.06501	0	-0.25651	0	-0.38848	0	-0.22603	0	5.1182	0	0.75616	0	4570.55	75.2625	-180	12.3394
33	29	45008.5	0.08917	0	-0.24689	0	-19.5803	0	-0.065	0	-0.2565	0	-0.38846	0	-0.22605	0	5.11819	0	0.75616	0	4570.55	75.2625	-180	12.3394
34	30	45008.5	0.09017	0	-0.24679	0	-19.5774	0	-0.065	0	-0.25649	0	-0.38844	0	-0.22609	0	5.11818	0	0.75616	0	4570.55	75.2625	-180	12.3394
35	31	45008.5	0.09117	0	-0.24628	0	-19.5745	0	-0.06499	0	-0.25647	0	-0.38843	0	-0.22614	0	5.11817	0	0.75616	0	4570.55	75.2625	-180	12.3394
36	32	45008.5	0.09217	0	-0.24569	0	-19.5723	0	-0.065	0	-0.25646	0	-0.38843	0	-0.22618	0	5.11816	0	0.75616	0	4570.55	75.2625	-180	12.3394
37	33	45008.5	0.09317	0	-0.24509	0	-19.5703	0	-0.065	0	-0.25644	0	-0.38845	0	-0.22624	0	5.11815	0	0.75616	0	4570.55	75.2625	-180	12.3394
38	34	45008.5	0.09417	0	-0.24485	0	-19.5689	0	-0.065	0	-0.25642	0	-0.38847	0	-0.22628	0	5.11815	0	0.75616	0	4570.55	75.2625	-180	12.3394
39	35	45008.5	0.09517	0	-0.24515	0	-19.5682	0	-0.065	0	-0.2564	0	-0.38851	0	-0.22631	0	5.11814	0	0.75616	0	4570.55	75.2625	-180	12.3394
40	36	45008.5	0.09617	0	-0.24605	0	-19.5682	0	-0.06501	0	-0.25639	0	-0.38854	0	-0.22631	0	5.11814	0	0.75616	0	4570.55	75.2625	-180	12.3394
41	37	45008.5	0.09717	0	-0.24748	0	-19.5691	0	-0.06501	0	-0.25639	0	-0.38858	0	-0.22629	0	5.11814	0	0.75616	0	4570.55	75.2625	-180	12.3394
42	38	45008.5	0.09817	0	-0.24926	0	-19.5708	0	-0.06502	0	-0.2564	0	-0.3886	0	-0.22627	0	5.11814	0	0.75616	0	4570.55	75.2625	-180	12.3394
43	39	45008.5	0.09917	0	-0.25122	0	-19.5733	0	-0.06503	0	-0.25641	0	-0.38862	0	-0.22624	0	5.11814	0	0.75616	0	4570.55	75.2625	-180	12.3394
44	40	45008.5	0.10017	0	-0.25316	0	-19.5762	0	-0.06504	0	-0.25643	0	-0.38862	0	-0.22621	0	5.11813	0	0.75616	0	4570.55	75.2625	-180	12.3394
45	41	45008.5	0.10117	0	-0.2549	0	-19.5794	0	-0.06505	0	-0.25645	0	-0.38862	0	-0.22619	0	5.11813	0	0.75616	0	4570.55	75.2625	-180	12.3394
46	42	45008.5	0.10217	0	-0.25629	0	-19.5824	0	-0.06506	0	-0.25648	0	-0.38861	0	-0.22617	0	5.11813	0	0.75616	0	4570.55	75.2625	-180	12.3394

Figure A.2. Raw data as collected from the laboratory.

Whereas the FlexMAT Cracking v2.1.3-2022-12 data file must be in ASCII format. The laboratory's .csv file is initially turned into an Excel spreadsheet. At first, the dynamic modulus is computed for all temperatures and frequencies. Then, a comma-separated file in accordance with the AMPT-Dynamic Modulus Data Standard draft v2.0 guideline is formed (see **Figure A.3**). The data for all the frequencies and temperatures is tabulated in a separate Excel file. This data is copied in the newly formatted .csv file formed. Further, this .csv file is opened in text format (see **Figure A.4**) and make sure to put version 2.0 manually entered.

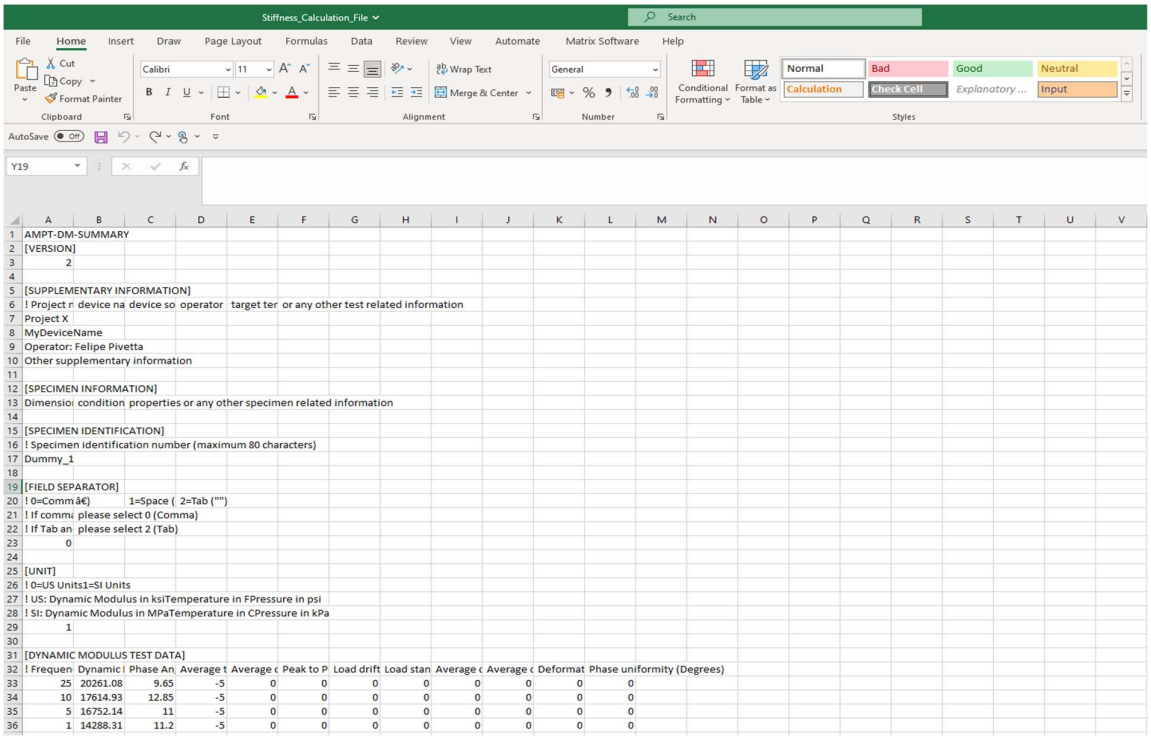

	A	B	C	D	E	F	G	H	I	J	K	L	M	N	O	P	Q	R	S	T	U	V
1	AMPT-DM-SUMMARY																					
2	[VERSION]																					
3	2																					
4																						
5	[SUPPLEMENTARY INFORMATION]																					
6	! Project n	device na	device so	operator	target ter	or any other test related information																
7	Project X																					
8	MyDeviceName																					
9	Operator: Felipe Pivetta																					
10	Other supplementary information																					
11																						
12	[SPECIMEN INFORMATION]																					
13	Dimensio	condition	properties or any other specimen related information																			
14																						
15	[SPECIMEN IDENTIFICATION]																					
16	! Specimen identification number (maximum 80 characters)																					
17	Dummy_1																					
18																						
19	[FIELD SEPARATOR]																					
20	! 0=Comm â€)		1=Space (	2=Tab ("")																		
21	! If comma	please select 0 (Comma)																				
22	! If Tab an	please select 2 (Tab)																				
23	0																					
24																						
25	[UNIT]																					
26	! 0=US Units1=SI Units																					
27	! US: Dynamic Modulus in ksiTemperature in FPressure in psi																					
28	! SI: Dynamic Modulus in MPaTemperature in CPressure in kPa																					
29	1																					
30																						
31	[DYNAMIC MODULUS TEST DATA]																					
32	! Frequen	Dynamic	Phase An	Average t	Average c	Peak to P	Load drift	Load stan	Average c	Average c	Deformat	Phase uniformity (Degrees)										
33	25	20261.08	9.65	-5	0	0	0	0	0	0	0	0										
34	10	17614.93	12.85	-5	0	0	0	0	0	0	0	0										
35	5	16752.14	11	-5	0	0	0	0	0	0	0	0										
36	1	14288.31	11.2	-5	0	0	0	0	0	0	0	0										

Figure A.3. Formatted .csv file as per Flex MAT guidelines.

```
Stiffness_Specimen1_Mix1 - Notepad
File  Edit  Format  View  Help
AMPT-DM-SUMMARY
[VERSION]
2.0

[SUPPLEMENTARY INFORMATION]
! Project name, device name, device software version, operator, target temperature, or any other test related information,,,,,,
Project X
MyDeviceName
Operator: Felipe Pivetta
Other supplementary information

[SPECIMEN INFORMATION]
Dimensions, conditioning time, properties or any other specimen related information,,,,,,,,

[SPECIMEN IDENTIFICATION]
! Specimen identification number (maximum 80 characters)
Dummy_1

[FIELD SEPARATOR]
! 0=Comma (“,”), 1=Space (“ “)," 2=Tab ("" "")",,,,,,,,
! If comma and space are used together, please select 0 (Comma),,,,,,,,,,
! If Tab and space are used together, please select 2 (Tab),,,,,,,,,,
0

[UNIT]
! 0=US Units1=SI Units
! US: Dynamic Modulus in ksiTemperature in FPressure in psi
! SI: Dynamic Modulus in MPaTemperature in CPressure in kPa
1

[DYNAMIC MODULUS TEST DATA]
! Frequency (Hz), Dynamic Modulus (MPa or ksi), Phase Angle (Degrees), Average temperature (C or F), Average confining pressure (kPa or psi), Peak to Peak Average Strain (micro-strain), Load drift (%), Load standard error (%), Average de
25,24062.07454,10.84,-5,0,0,0,0,0,0,0,0
10,21393.75961,12.83,-5,0,0,0,0,0,0,0,0
5,19163.64017,10.78,-5,0,0,0,0,0,0,0,0
1,13694.01042,12.06,-5,0,0,0,0,0,0,0,0
0.5,12779.08442,13.81,-5,0,0,0,0,0,0,0,0
0.1,7213,17.31,-5,0,0,0,0,0,0,0,0
25,16449.43294,13.7,5,0,0,0,0,0,0,0,0
10,14811.09703,14.92,5,0,0,0,0,0,0,0,0
5,13151.32017,13.56,5,0,0,0,0,0,0,0,0
1,10758.01333,15.01,5,0,0,0,0,0,0,0,0
0.5,9287.348394,16.807,5,0,0,0,0,0,0,0,0
0.1,5561.15,22.36,5,0,0,0,0,0,0,0,0
25,13380.43211,15.93,10,0,0,0,0,0,0,0,0
10,11245.05459,17.21,10,0,0,0,0,0,0,0,0
5,10191.96861,16.61,10,0,0,0,0,0,0,0,0
1,7917.414387,19.22,10,0,0,0,0,0,0,0,0
0.5,7412.817357,21.37,10,0,0,0,0,0,0,0,0
0.1,3151.55,28.04,10,0,0,0,0,0,0,0,0
25,10936.8353,17.83,20,0,0,0,0,0,0,0,0
10,9077.13704,22.1,20,0,0,0,0,0,0,0,0
5,7921.313759,23,20,0,0,0,0,0,0,0,0
```

Figure A.4. .txt file of the final output format file.

Then, all the commas in this file are removed and saved to a separate folder. Two specimen replicas are evaluated for each mixture. As a result, two separate .txt files are saved in separate folders for each specimen. It should be mentioned that the FlexMAT Cracking v2.1.3-2022-12 can

use several replica data sets for computations, and it takes the data from a specific folder containing .txt files with data in the correct format. These files can now be imported into the FlexMAT program for analysis. FlexMAT cracking is useful for most of the models related to materials characterization. Cyclic fatigue testing and aging analysis depend on the dynamic modulus characterization, the initial model to be analyzed in the FlexMAT cracking software. The dynamic modulus model used in the FlexMAT cracking v2.1.3-2022-12 is the 2S2P1D (2 spring, 2 parabolic creeps & 1 dashpot model) model (**Figure A.5**). This model is simple with the formulation, as a combination of springs, dashpot, and parabolic elements. The calibration of this model is easy as well, and it gives very good modeling of the bitumen with a large range of frequencies and temperatures (Yusoff, 2010).

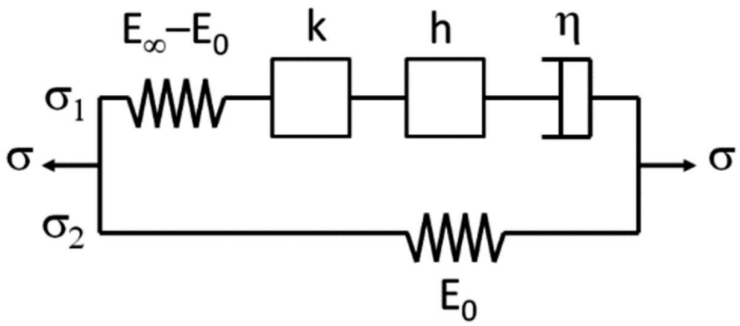

Figure A.5. Representation of the 2S2P1D model (Gayte, 2016).

The above-mentioned 2S2P1D model for dynamic modulus characterization is based on work performed in the past (Olard a& Benedetto, 2003). Based on the data provided, the dynamic modulus master curve is defined. The following equations compute the time-temperature shift factor, with 21.1°C as the reference temperature.

$$a_T = 10^{(a_1 T^2 + a_2 T + a_3)} \quad \text{(A.1)}$$

$$a_1 = c_1 \quad \text{(A.2)}$$

$$a_2 = c_2 - 2c_1 T_{ref} \quad \text{(A.3)}$$

$$a_3 = c_1 T_{ref}^2 - c_2 T_{ref} \quad \text{(A.4)}$$

where a_T is the time-temperature superposition's shift factor, T_{ref} is the reference temperature, C_1 and C_2 are the fitting coefficients, T is the temperature in °C and a_1 , a_2 & a_3 are the shift factors coefficients.

To calculate the damage evolution rate parameter (α), the following equation is used:

$$\alpha = \left(\frac{1}{m}\right) + 1 \quad \text{(A.5)}$$

where m is the maximum slope of the relaxation modulus in the log-log scale, and α is the damage evolution rate parameter.

The first analysis is dynamic modulus characterization, and the inputs in FlexMAT are the folders containing the results from AMPT's dynamic modulus test. However, in this study, the testing is done in UTM, and the output data is collected by TU DELFT's in-house software, which differs from AMPT's output format. As a result, data preparation is required to carry out the analysis in FlexMAT. First, ensure this version of FlexMAT is unblocked before downloading it. The version

that is currently accessible is generally encrypted and guarded. Start the software by pressing Alt+S; the first window will display (**Figure A.6**).

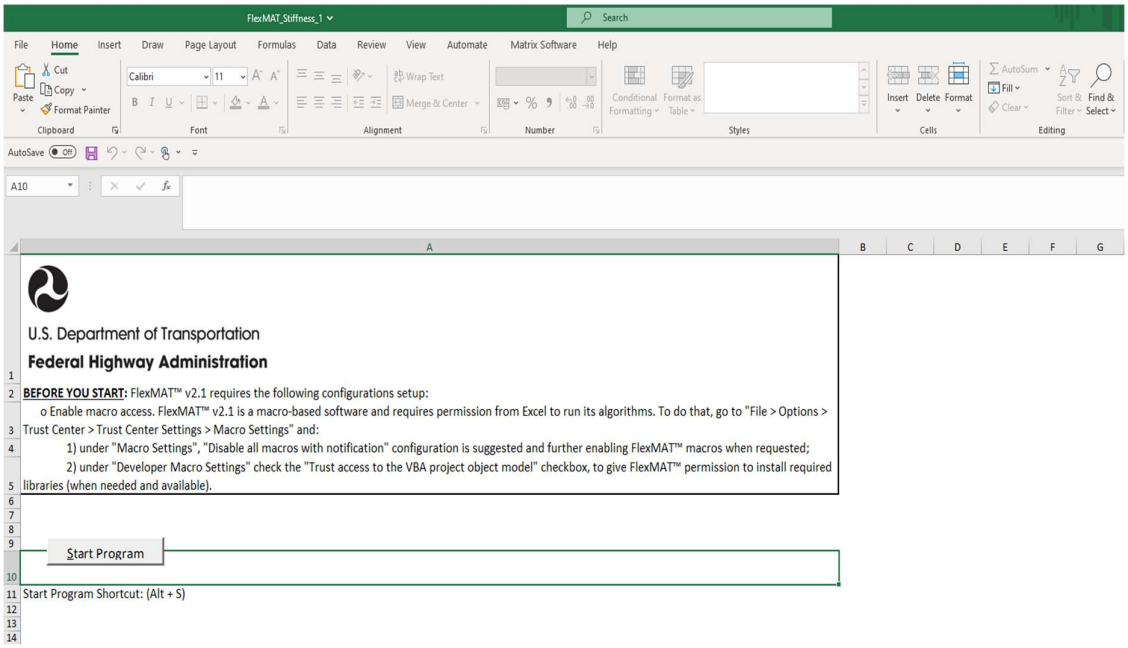

Figure A.6. Start window in FlexMAT.

To start the analysis, the first step is formatting the data as mentioned above. Later, save the .txt files in separate folders for each mixture type with several replicates.

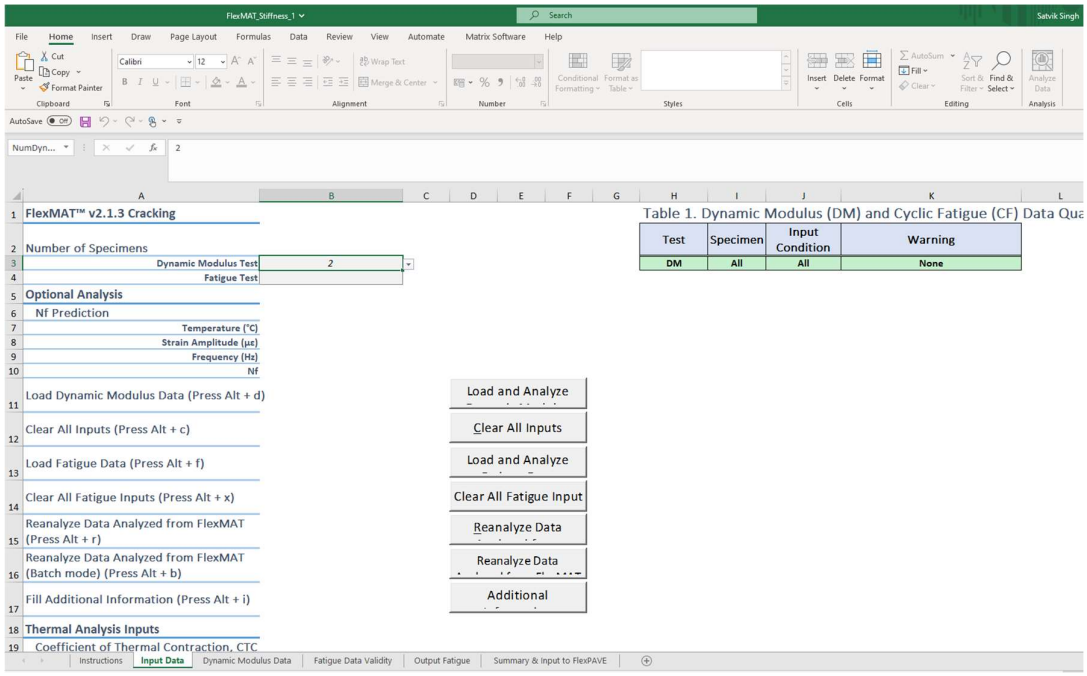

Figure A.7. FlexMAT dynamic modulus input screen.

In this research, two replicates for each mixture type at each temperature are tested. To start the dynamic modulus analysis, in the 'Input Data' screen from the drop-down menu 'B3', choose the

number of specimens involved in the testing (see **Figure A.7).** Then click on 'Load and Analyze Dynamic Modulus Data', where choose the .txt files for each specimen from the folders specified. Once all the specimens have been selected, the analysis will begin automatically.

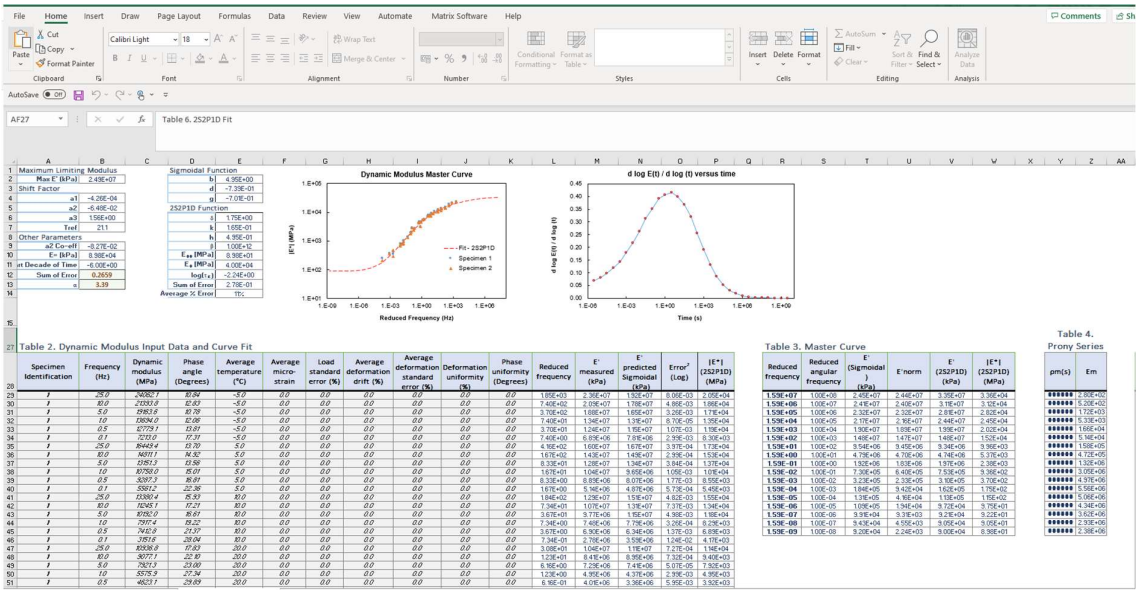

Figure A.8. Output window in FlexMAT.

Similarly, the fatigue and fatigue-healing test output file obtained from MP3 software differ from the AMPT output file. To be used in the FlexMAT, the output file must be prepared according to the AMPT-Fatigue Data Standard draft v2.0.

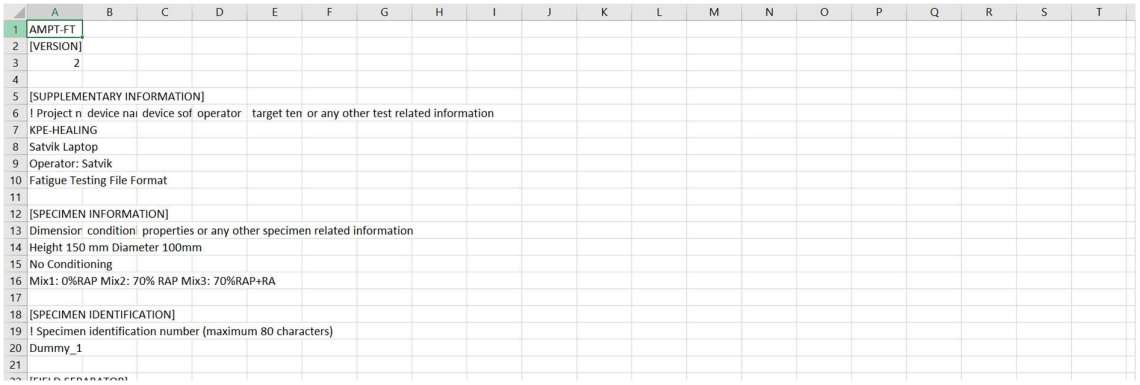

Figure A.9. Format .csv file as per FlexMAT fatigue requirements.

First, an Excel macro sheet that has processed columns and rows as required by the FlexMAT based on the laboratory output files is created. MP3 loads and displacements are transformed into stresses and strains, among other things. Following the calculation of the data in the required format, a comma-separated file is created in accordance with the standard draft. Later, open this file in .txt format and manually enter version 2.0. After that, this must be saved in the specimen's designated folder. To be analyzed, each specimen needs its folder.

```
AMPT-FT
[VERSION]
2.0

[SUPPLEMENTARY INFORMATION]
!Project name, device name, device software version, operator, target temperature, or any other test related information
Project KPE HEALING GRADUATION THESIS PROJECT
Operator: Satvik Pratap Singh

[SPECIMEN INFORMATION]
!Dimensions, conditioning time, properties or any other specimen related information

[SPECIMEN IDENTIFICATION]
Dummy_1_C2

[FIELD SEPARATOR]
! 0=Comma (","), 1=Space (" "), "" 2=Tab ("""   """)"""
! If comma and space are used together, please select 0 (Comma)
! If Tab and space are used together, please select 2 (Tab)
0

[UNIT]
1

[TEST PARAMETERS]
!Frequency, Target temperature, Axial gauge length, Dynamic Modulus Fingerprint Test Parameters, Target on-specimen peak-to-peak micro-strain, or


[TEST DATA]
!Supplemental test data such as complete Dynamic Modulus Fingerprint Test including parameters like modulus, cycle Count, phase angle, stress, mi

[PID TUNING QUALITY PARAMETERS]
! Machine Compliance Factor, Target on-specimen peak to peak strain
1.883,420

[FINGERPRINT TEST DATA]
! Time (sec), Axial stress (kPa or psi), Peak to Peak Actuator Strain (micro-strain), LVDT Axial Strain #1 (micro-strain), LVDT Axial Strain #2 (
5,32.29,8.323,9.046,6.989,9.864,18.05,0.036621,0.000916,0.000633,0.000489,0.00069
5.001,17.76,4.161,7.302,5.463,9.21,18.05,0.020142,0.000458,0.000511,0.000382,0.000645
5.002,4.305,8.323,5.777,5.245,4.632,18.05,0.004883,0.000916,0.000404,0.000367,0.000324


[FINAL FINGERPRINT DYNAMIC MODULUS]
7153

[FATIGUE INITIAL CYCLES TEST DATA]
! Time (sec), Axial stress (kPa or psi), Peak to Peak Actuator Strain (micro-strain), LVDT Axial Strain #1 (micro-strain), LVDT Axial Strain #2 (
0,1.615,-3.381,-0.531,-1.308,0.136,18.05,0.001831,-0.000372,-0.000037,-0.000092,0.00001
0.001,1.615,-3.381,-0.531,-1.526,1.008,18.05,0.001831,-0.000372,-0.000037,-0.000107,0.000071
0.002,1.615,-3.381,-0.313,-0.654,-0.082,18.04,0.001831,-0.000372,-0.000022,-0.000046,-0.000006
0.003,2.691,0.78,-0.313,0,-2.044,18.04,0.003052,0.000086,-0.000022,0,-0.000143
0.004,2.691,0.78,-0.095,0.436,-1.39,18.04,0.003052,0.000086,-0.000007,0.000031,-0.000097


[FATIGUE TEST DATA]
! Cycle, Dynamic Modulus (MPa or ksi), Phase Angle (Degrees), Peak to Peak Stress (kPa or psi), Maximum Stress (kPa or psi), Minimum Stress (kPa
ils), Minimum Actuator Displacement (mm or mils), LVDT Maximum Displacement #1 (mm or mils), LVDT Minimum Displacement #1 (mm or mils), LDVT Maxi
10,5946,27.36865,2639.662,1026.298,-1591.92,766.709,443.942,461.398,411.875,458.552,-11.704,-789.902,-165.762,-629.193,-152.37,-567.845,-165.095,
20,5772.6,28.0028,2595.393,1116.712,-1461.143,763.58,449.604,467.292,416.437,465.083,-7.543,-789.902,-181.893,-651.646,-169.591,-589.643,-181.661
30,5668.9,28.407,2573.941,1152.231,-1405.173,763.696,454.048,471.888,420.271,469.984,-7.543,-777.418,-187.125,-661.455,-176.13,-599.234,-189.073,
```

Figure A.10. .txt files as per format required by FlexMAT.

To characterize the fatigue cracking properties using FlexMAT, cyclic data from AMPT and dynamic modulus properties are required. After completing the dynamic modulus calculations, cyclic fatigue testing analysis is performed. The number of specimen replicas for a certain testing set is performed, and the data in the prescribed format is saved in separate folders. In the 'Input Data' screen, with cell 'B4', the number of specimens on which the test has been performed is chosen.

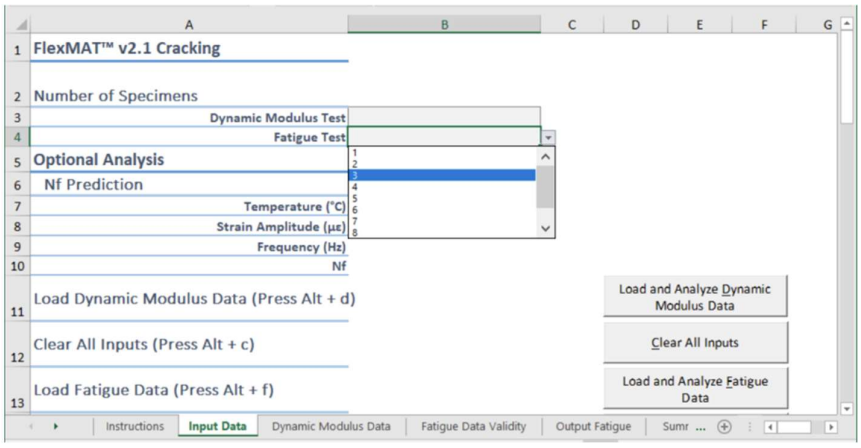

Figure A.11. FlexMAT cyclic fatigue input screen.

After that, 'Load and Analyze Fatigue Data' is clicked, opening the folder where the dedicated files are saved for each specimen. When files are opened in this window, the analysis automatically starts giving out the results in the fatigue output window.

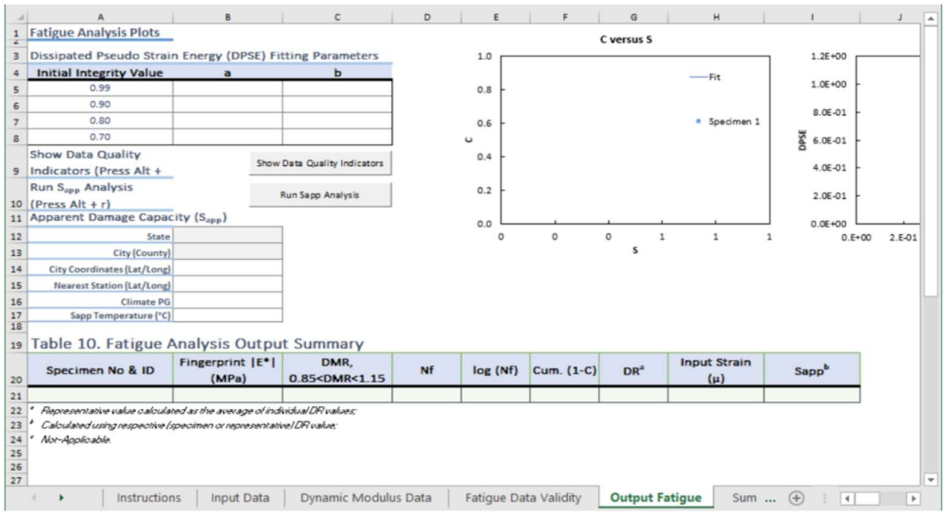

Figure A.12. FlexMAT cyclic fatigue model overview screen.

In FlexMAT cracking, the S-VECD model is incorporated for the damage characterization. The theoretical background of this model is given in **Chapter 3**. The important outputs from this analysis with respect to this research work are (1) damage characteristics curve (*C*-*S* curve); (2) failure criterion (D^R); (3) dissipated pseudo strain energy characterization (DPSE) (4) apparent damage capacity (S_{app}).

The background process involved in the cyclic fatigue characterization is a multi-step process. Initially, an individual *C*-*S* calculation is performed. Every input data is analyzed independently, and a *C*-*S* curve is calculated for each specimen following the procedure as per AASHTO TP 107-18. After this, a fitting equation, as mentioned below, is applied to this curve to have a representative *C*-*S* curve.

$$C(S) = 1 - C_{11}\, S^{C_{12}}$$

where C is the material's pseudo stiffness or integrity, S is the damage parameter quantifying damage accumulated in the mixture, and C_{11} and C_{12} are the fitting coefficients. In between the specimens, to avoid the biasing in the representative curves based on the greater number of points for any specimen, a filtering process is applied, accounting for the nearest lower calculated C value every 5000 incremental steps in the S parameter.

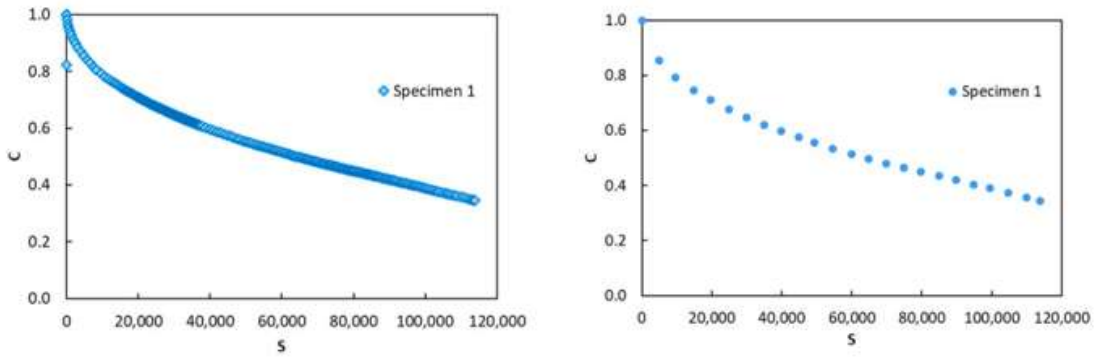

Figure A.13. *C*-*S* curve (a) before and (b) after representative fitting filtering.

Then the analysis moves in the direction of calculating the failure criterion. FlexMAT™ is software implemented with this failure criterion (Wang, 2017). It uses the concept of the point at which the product of several cycles (N_f) and applied peak-to-peak stress reaches its local maximum.

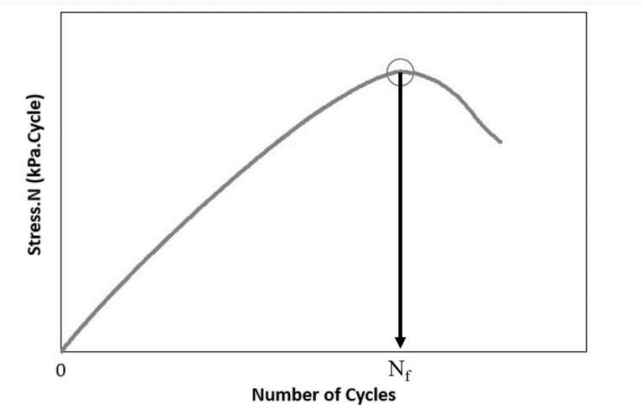

Figure A.14. Failure cycle determination (Felipe, 2021).

In addition, DPSE-reduced strain rate characterization is performed in the analysis to determine DPSE as a function of decreased strain rate for given material integrity. To get the relaxation modulus of the mixture, a monotonic tensile test is simulated within the software utilizing the damage characteristics curve coefficients and a Prony series representation of the dynamic modulus (Felipe, 2021). The rest of the information in this analysis is outside the scope of this study work but may be found in the mentioned work.

After all the calculations have been performed, a set of data quality indicators (DQI) have been developed in the software to assist the users in identifying the problems in the data. To get this DQI for individual specimens, click on 'Show Data Quality Indicators', which enables the 'Data Quality Indicators' screen as shown in **Figure A.15.** This window enables the visible verification of the PID tuning quality by comparing the measured strain and the command strain as a function of time in the 'PID Tuning Quality' graph.

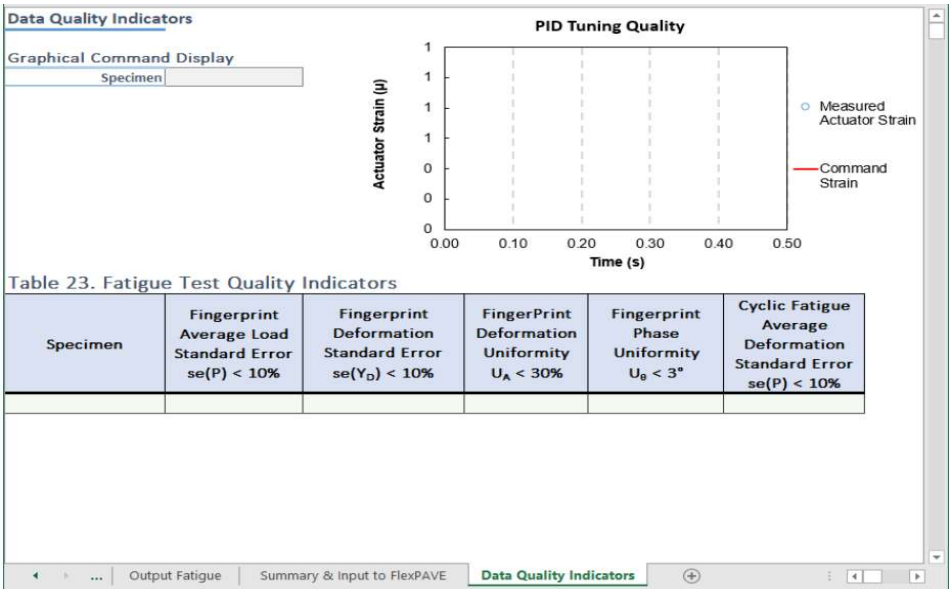

Figure A.15. Data quality indicator screen.

References

Do Canto Pivetta, F. (2021). Development of Software Programs for Performance Related Specifications of Asphalt Concrete Pavements.

Etheridge, R. A., Wang, Y. D., Kim, S. S., & Kim, Y. R. (2019). Evaluation of fatigue cracking resistance of asphalt mixtures using apparent damage capacity. *Journal of Materials in Civil Engineering*, *31*(11), 04019257.

Gayte, P., Di Benedetto, H., Sauzéat, C., Nguyen, Q.T. (2016). Influence of Transient Effects for Analysis of Complex Modulus Tests on Bituminous Mixtures. *Road Materials and Pavement Design 17(2)*, pp. 271-289.

Olard, F., & Di Benedetto, H. (2003). General "2S2P1D" model and relation between the linear viscoelastic behaviours of bituminous binders and mixes. *Road materials and pavement design*, *4*(2), 185-224.

Yusoff, N. I. M., Airey, G. D., & Hainin, M. R. (2010). Predictability of complex modulus using rheological models. *Asian Journal of Scientific Research*, *3*(1), 18-30.

B

Laboratory Testing and Development

B.1 Dynamic Modulus Test Results

In **Figure B.1. (a), (b), & (c),** a plot of dynamic modulus with 6 different frequencies at 6 different temperatures. It is evident from the plot that the increase in the temperature decreases the value of stiffness. The stiffness increases with the increase in frequency at the same temperature.

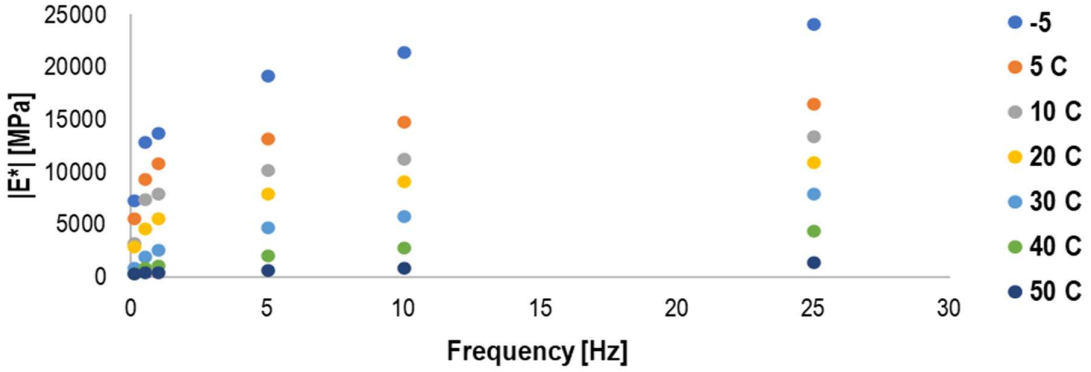

(a)

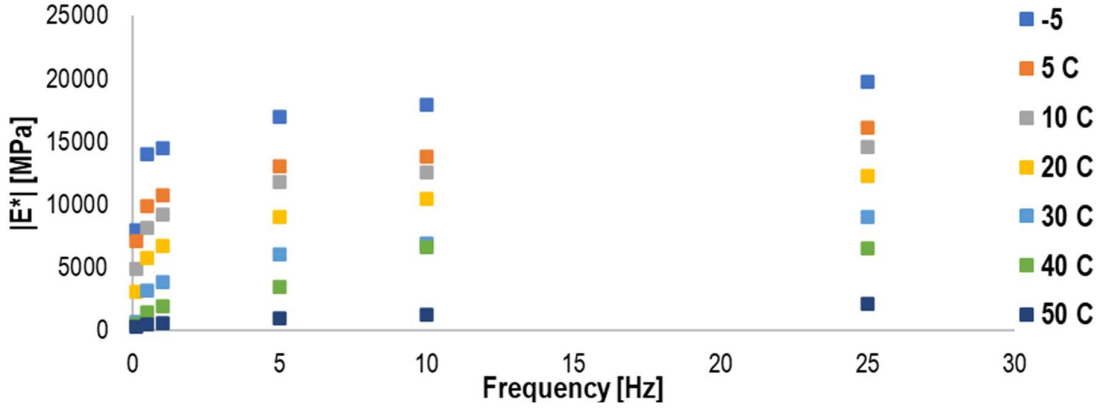

(b)

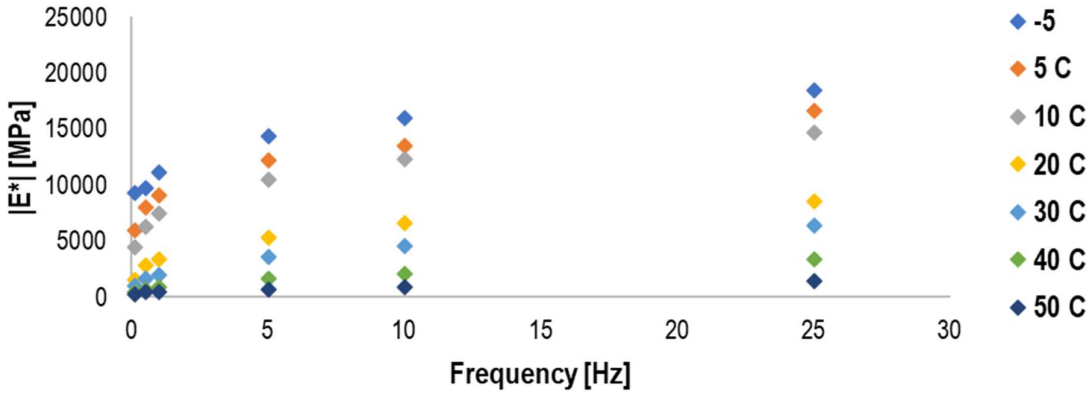

(c)

Figure B.1. |E*| vs Frequency for M1, M2, M3 (Loads as per AASHTO T 342-11).

B.2. Glue Line Failure

As previously stated, the samples are glued on both sides with plastic rings. Sometimes, if the glue is not properly dispersed around the sample due to practical inefficiencies, reducing the strength of the glue line. The specimen subjected to cyclic loading with non-uniform gluing on the edges results in glue line failure. These fatigue and healing results are unacceptable for the assessments as, in such cases, the specimen remains intact, but the failure occurs at the glue line (mechanical properties of the sample are unassessed). In this research, work sample number 2276 (M3) faced this unfortunate incident (see **Figure B.2.**). This specimen results cannot be used for the assessment. This glue line failure can be seen in the **Figure B.2** below.

Figure B.2. (a) Glue line failure in specimen during fatigue testing and (b) intact specimen along with glue.

Powdered glue and a hardener are used in this study for the first time in the TU Delft laboratory. The specimen is hammered, and the rings are removed to test the glue's capability. It is also attempted to remove the hardened adhesive from the specimen to ensure its integrity. It is discovered that the adhesive is sufficiently intact with the specimen because asphalt material is also removed when an attempt is made to remove the glue. This demonstrates that the glue is strong enough to hold the material while fatigue and healing tests are performed.

Figure B.3. Failure in asphalt material while removing the glue.

To overcome this issue, a typical procedure uses two PVC rings at the bottom of the specimen, ensuring confinement and uniform stress distribution at the lower end. **Figure B.3** below shows the change in the specimen setup, which helped in conducting the test and ensuring failure in the material than the glue.

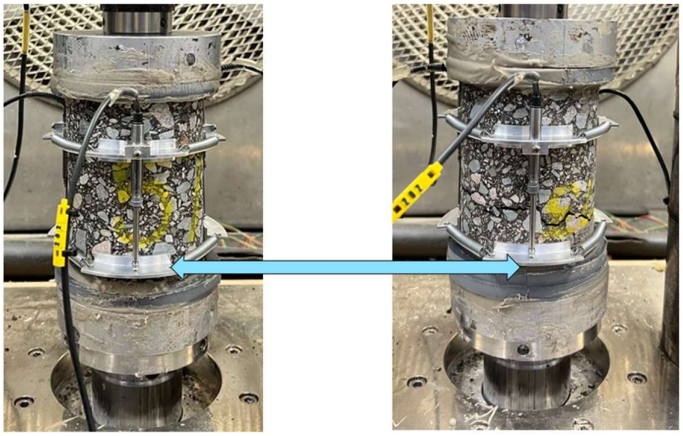

Figure B.4. Double PVC ring instead of one to give extra confinement.

B.3. Prediction of Phase Angles in MP3 Software

An attempt is made to predict the phase angle from the MP3 software. A separate script is written in Lua to predict the phase angle. An internal transfer function is introduced: the load ratio to the average of LVDTs in real-time. The software can predict the magnitude and argument of a complex number in real time using this transfer function. To check the results' reliability, an attempt, in the beginning, is made to predict it using a material of known phase angle. A Teflon cylinder of 150 mm height and 100 mm diameter is used to check the validity of the phase angle predicted by the MP3 software (see **Figure B.5**).

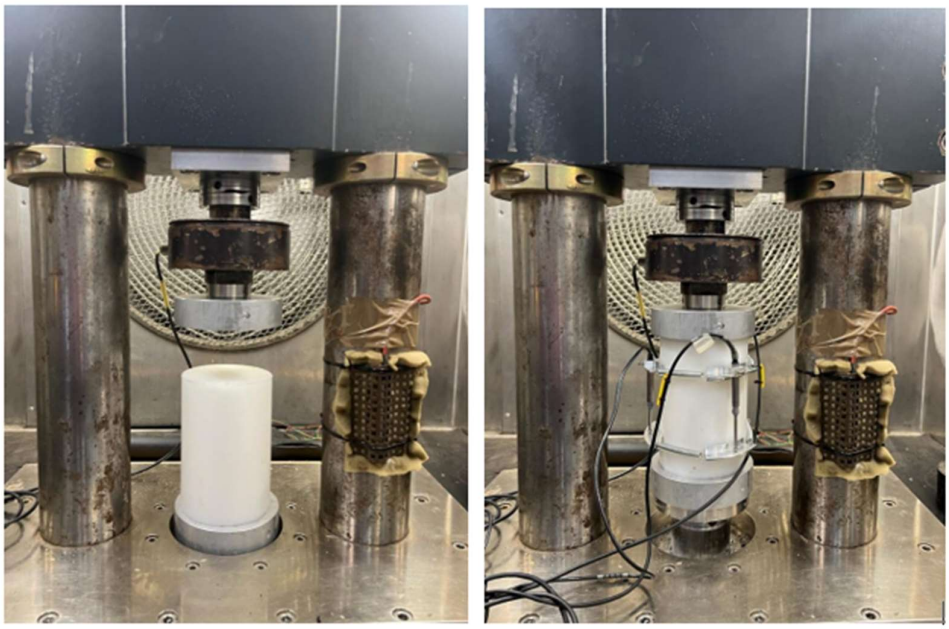

Figure B.5. (a) cylindrical Teflon (b) specimen mounted in MTS to check phase angles.

In general, from the experience of lab technicians, it is known that in Teflon, there is a minute lag in signals, which have a lower value of phase angles. For this, the test is run for 10 Hz frequency at 20°C. It is noted that the phase angle predicted by the software is closer to what is expected with an error of ± 2°. It is considered closer to what is expected, laying the groundwork for trust in the phase angle values recorded.

As per AASHTO TP 107-18, displacement-controlled repeated cyclic loading is applied to a cylindrical specimen till failure. A damage characteristic curve is constructed independent of temperature, frequency, and loading mode. In the initial phase of this research work, it is believed that the tension-only haversine loading at 10 Hz frequency for 20°C had an accelerated fatigue failure in the specimen and assessed fatigue-healing. Yet, it is repeatedly observed in the initial specimen that the failure line appears near the bottom ends of the specimen, which is generally not expected. The failure line is expected to occur between the mounted LVDT sensors.

Figure B.6. Failure pattern in pure tension mode of loading.

In the first few load cycles in the tension-only mode of loading, an impact tensile load is produced on the specimen, which is twice the amount of compressive load in the loading cycle.

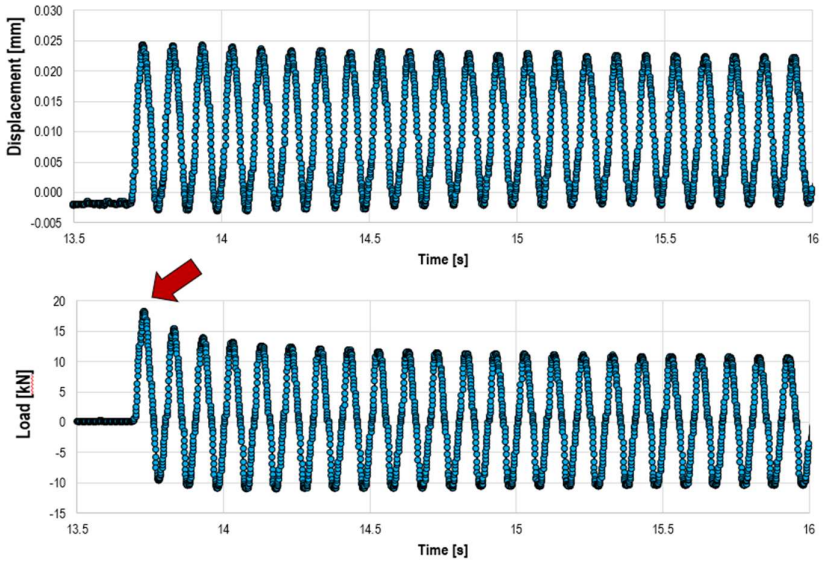

Figure B.7. Strain-controlled Haversine loading.

It is evident from **Figure B.7.** that this occurrence of higher impact load at the beginning of test cycles creates a weak zone in the specimen's bottom part, which is the reason for most of the unexpected failures.

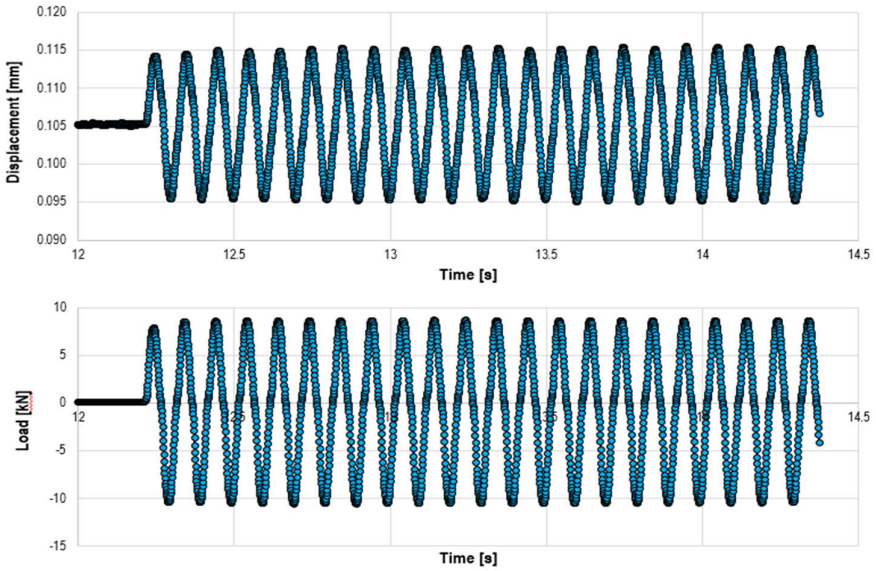

Figure B.8. Strain-controlled sine loading.

On the other hand (**Figure B.8.**), testing in the tension-compression loading mode brought a major difference in the initial testing cycles. In the load application with tension-compression mode, a stagnant steady state loading cycle with constant range is observed since the beginning without any fluctuation. The failure pattern observed with this mode of loading is what we expect, i.e., failure within the material (**Figure B.9.**). The failure line occurred in the middle of the mounted LVDT sensor. In other samples, a similar failure pattern is observed, which signifies the material failure in fatigue and fatigue-healing tests. It is visible that the loading cycles take a while to steady state.

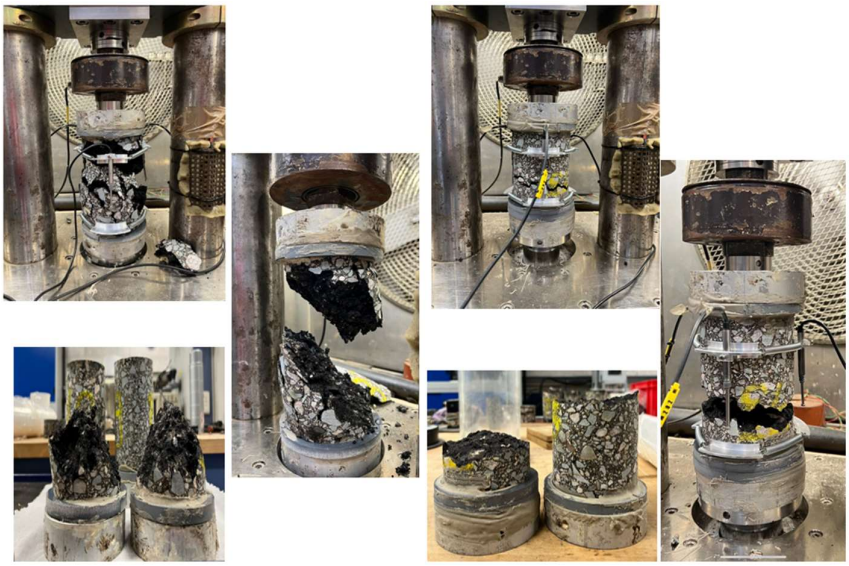

Figure B.9. Failure pattern in the tension-compression mode of loading.

B.4. Stress-Controlled vs. Strain-Controlled Fatigue Testing

1. Stress-controlled testing is preferred during the rest period to ensure no load is acting on the specimen, eliminating any doubt regarding the relaxation of stresses. This helps to maintain consistent and accurate results.
2. Norm suggests taking the input parameter as 300 μstrain peak-to-peak. However, predicting load based on strain rate may be difficult due to the variability of specimens. Therefore, using a fingerprint in a strain-controlled manner may be more practical for the normalization of load in your testing setup.
3. Following the approach used in the Netherlands, where the 4-point bending test is conducted in a strain-controlled manner, can make the results comparable to uniaxial testing. This consistency in testing methodology can help compare results obtained from different tests and setups.
4. Another advantage of strain-controlled testing is the increased safety of the testing machine. In stress-controlled testing, the strain keeps increasing even after specimen failure, which can cause oscillations and potentially damage the setup. Strain-controlled testing can help mitigate this risk and ensure safer testing conditions.

B.5. Some Pictures from Laboratory Work

Figure B.10. Cores and shell for gyratory compacted specimen.

Figure B.11. Demarcation of locations to mount LVDTs.

Figure B.12. Polishing machine and polished specimen.

Figure B.13. Sandblasting process and sandblasted loading platens.

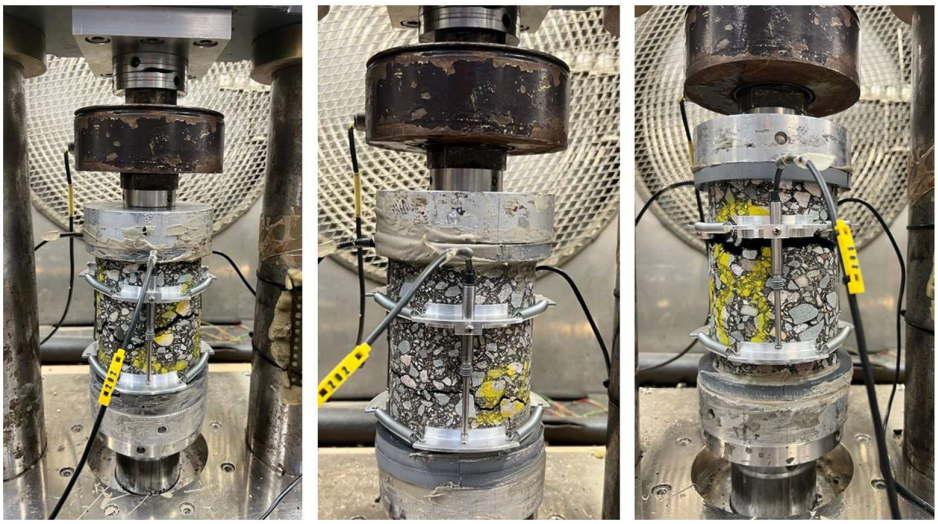

Figure B.14. Fatigue and fatigue-healing specimen failure in the material.

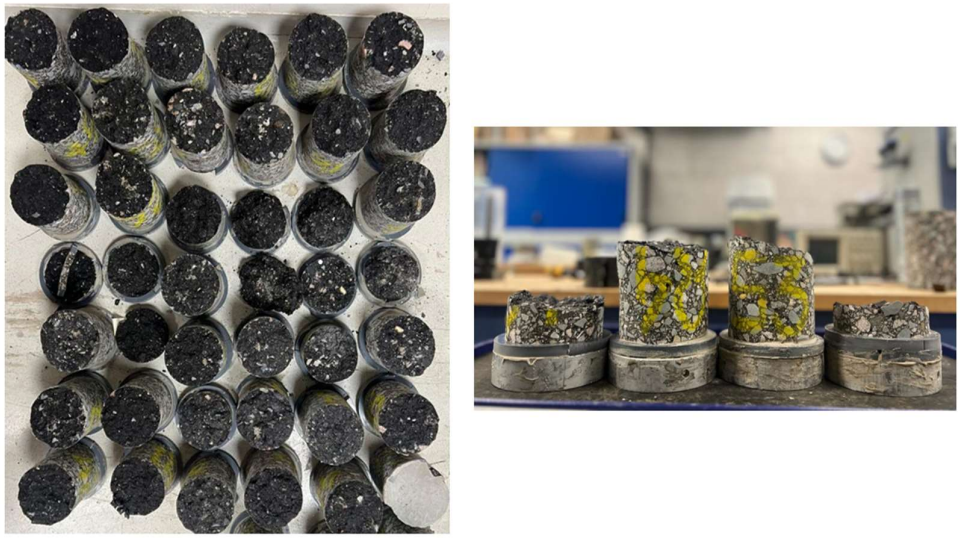

Figure B.15. Failed specimens after fatigue & healing testing.

C

Fatigue Test Results

C.1 Variation of Dynamic Modulus and Phase Angle with the number of cycles

Cyclic fatigue testing in uniaxial tension-compression mode is conducted for all mixtures at 10, 20, and 30°C. 200 μstrain peak-to-peak strain rate is applied to perform this test. With the increase of the load cycle on the specimen, the dynamic modulus value of the mixture decreases with an increase in the phase angle. The raw data was obtained from the laboratory for all the mixtures at all temperatures. The trend of decreasing stiffness and increasing phase angle is given from **Figure C.1** to **Figure C.9**. Two sets of curves for both specimen replicas are given in this section.

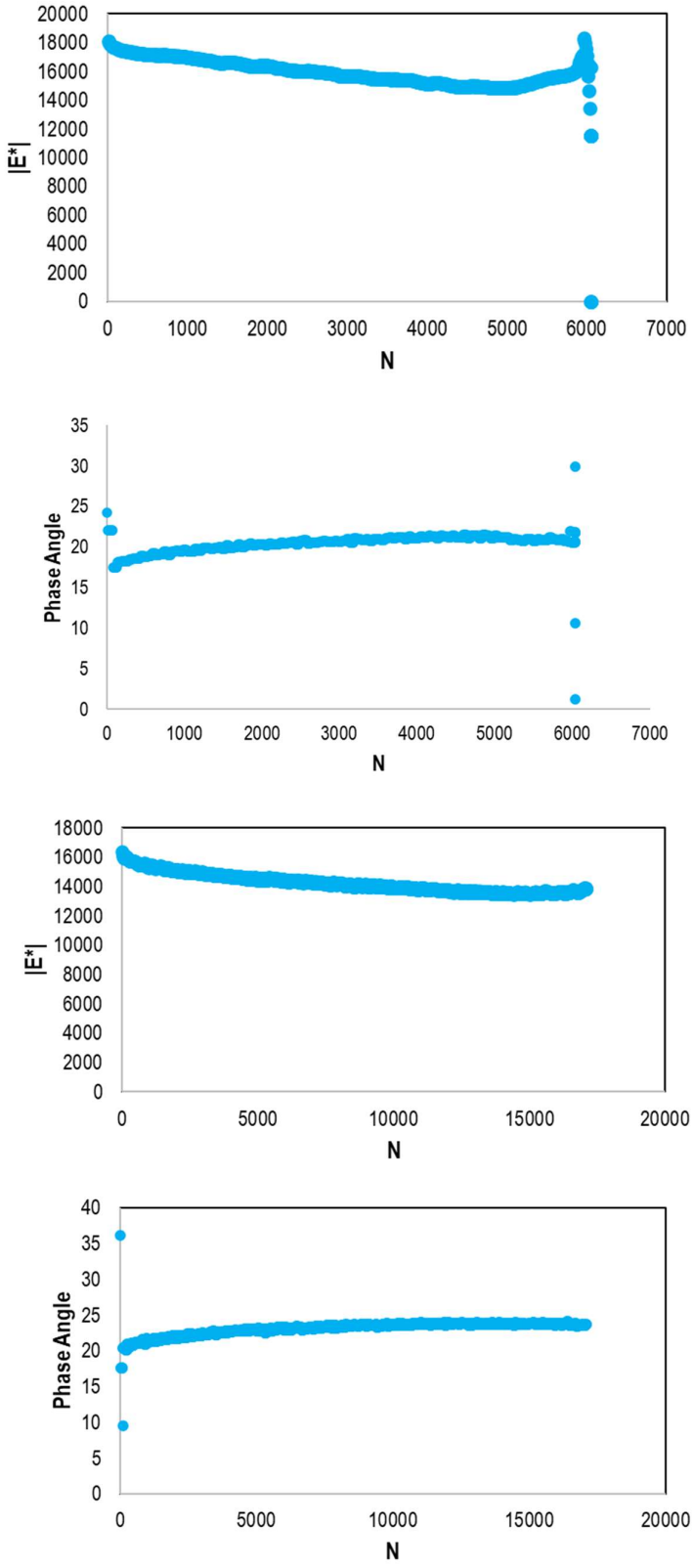

Figure C.1. M1 - Dynamic modulus and phase angle variation with N at 10°C.

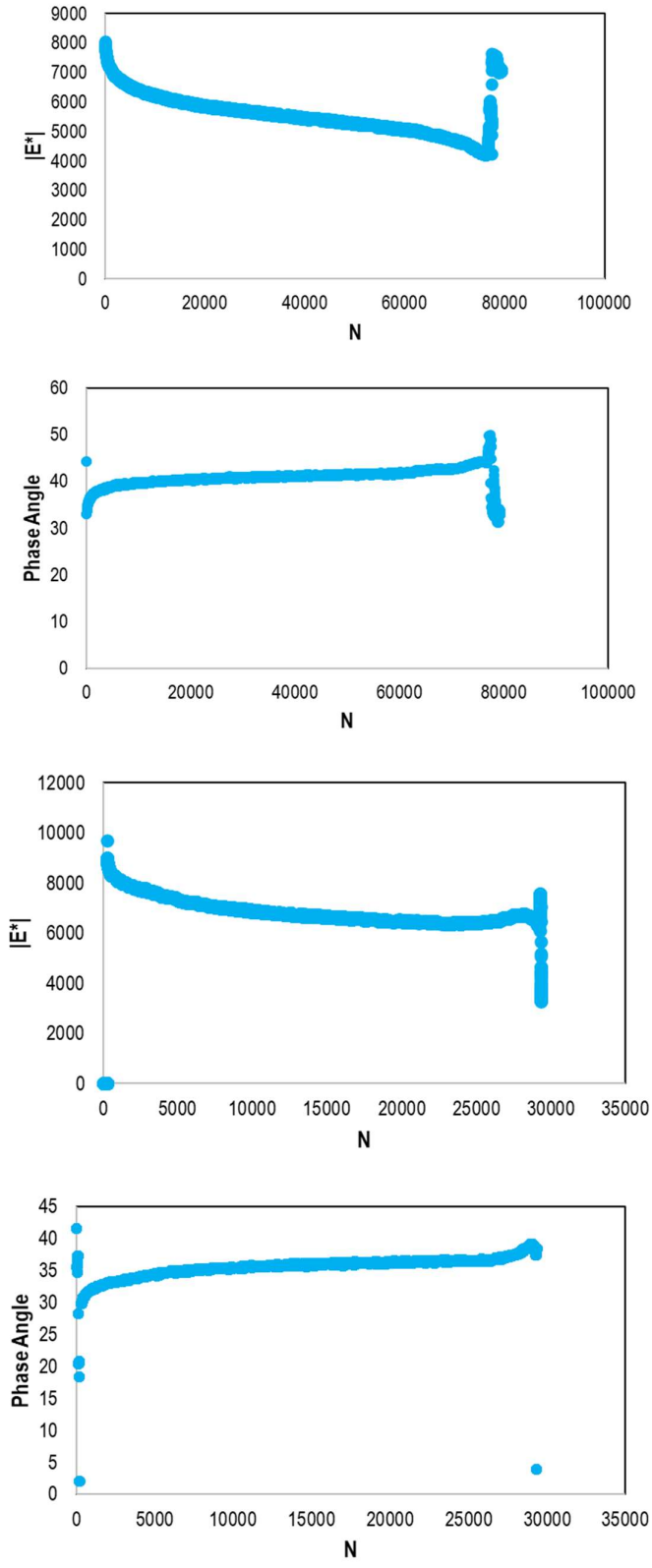

Figure C.2. M1 - Dynamic modulus and phase angle variation with N at 20°C.

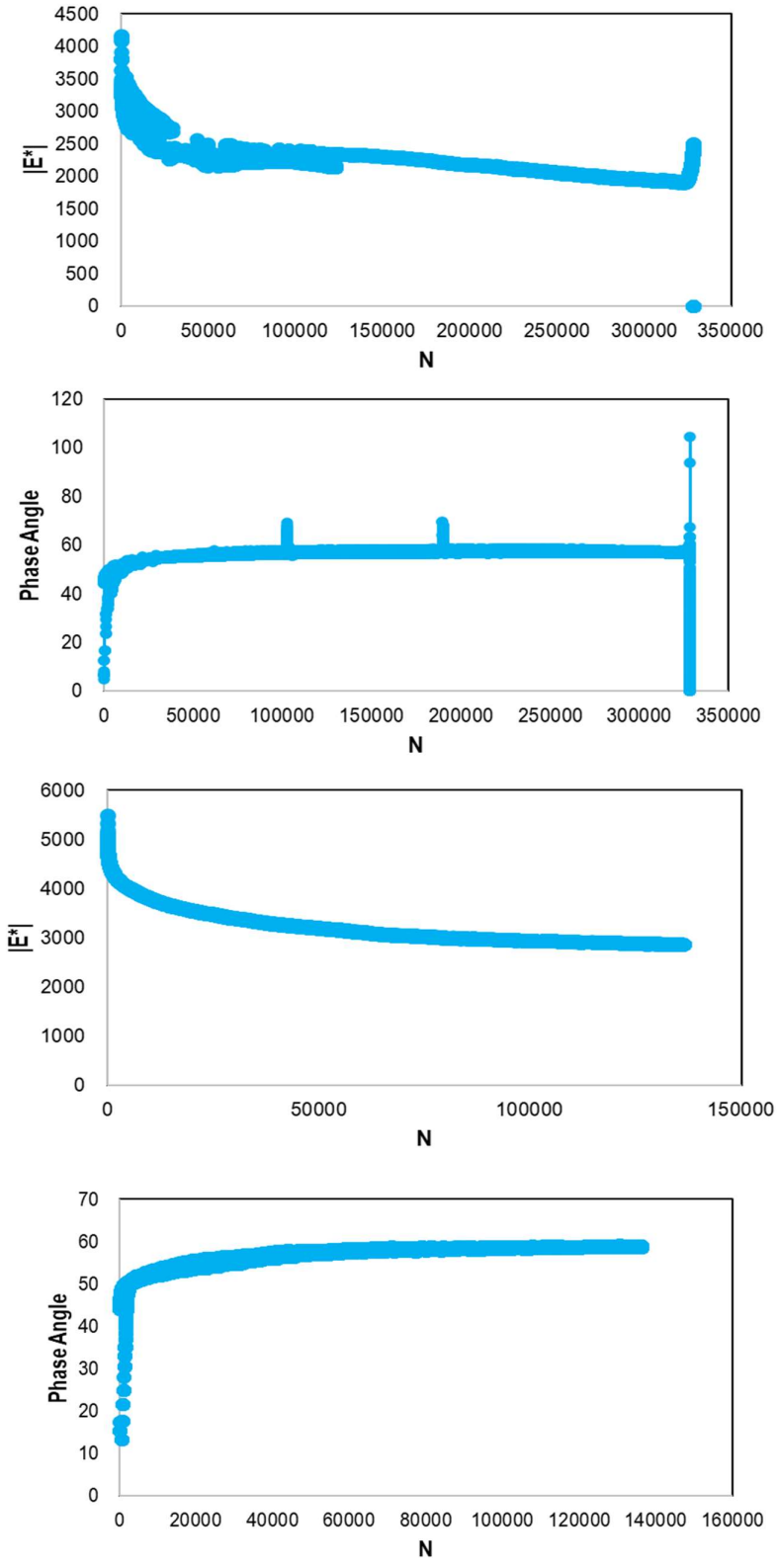

Figure C.3. M1 -Dynamic modulus and phase angle variation with N at 30°C

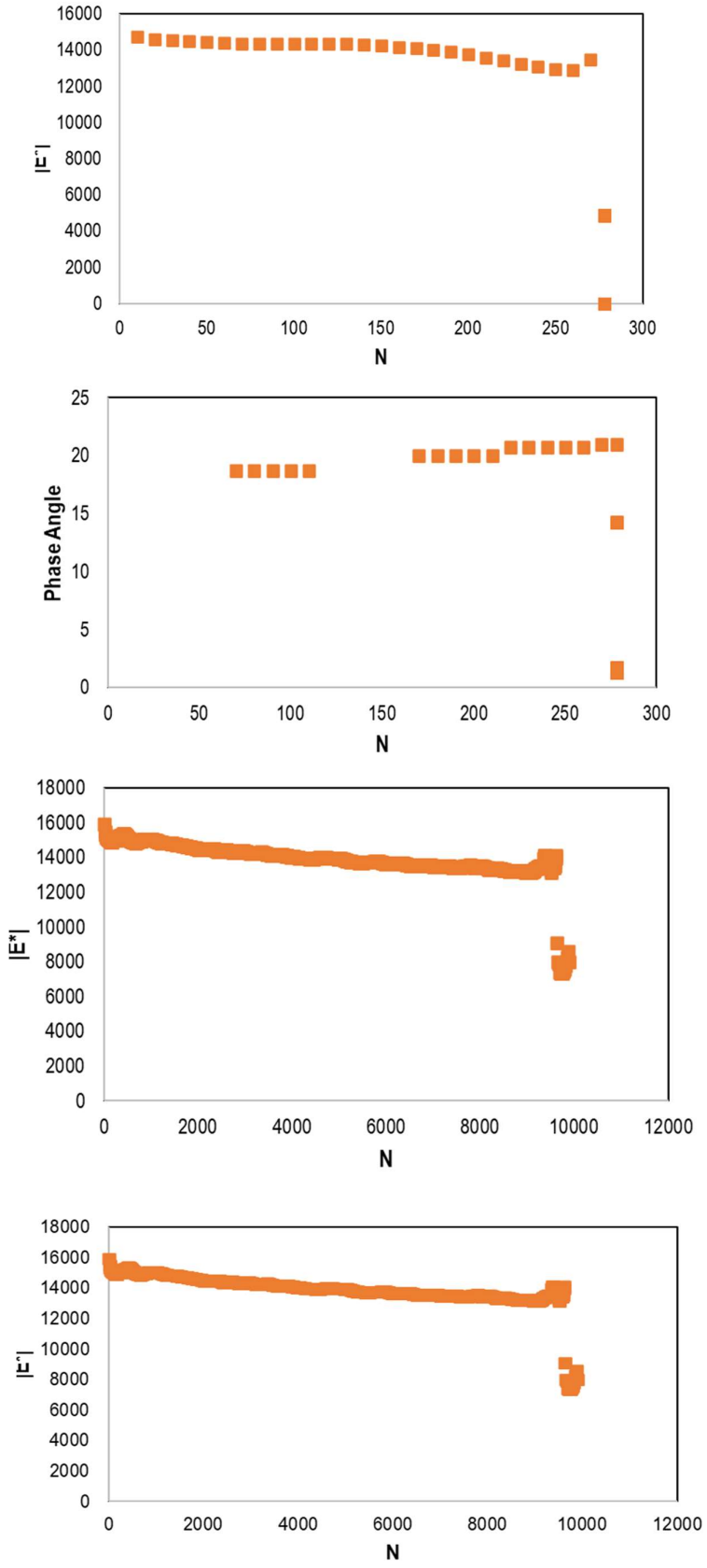

Figure C.4. M2 -Dynamic modulus and phase angle variation with N at 10°C

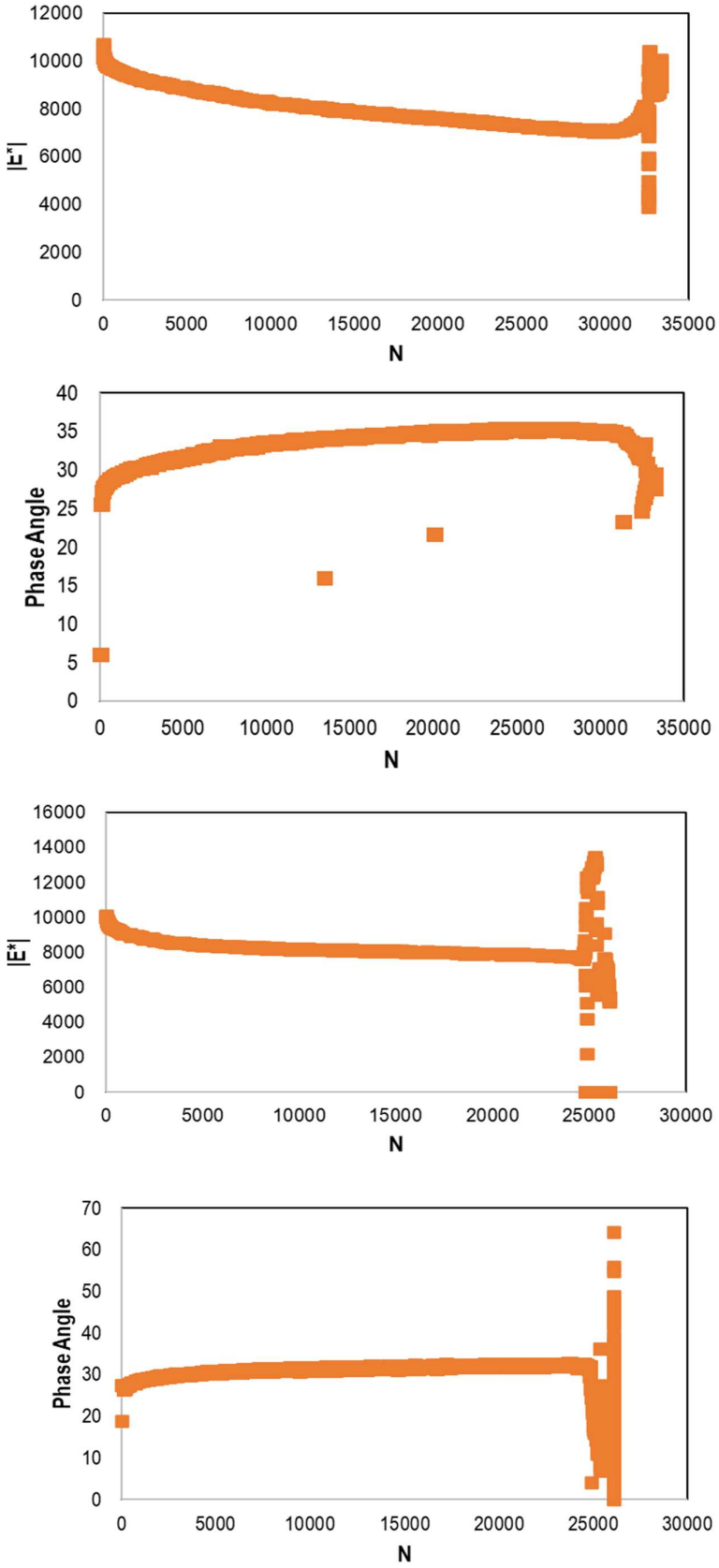

Figure C.5. M2 -Dynamic modulus and phase angle variation with N at 20°C

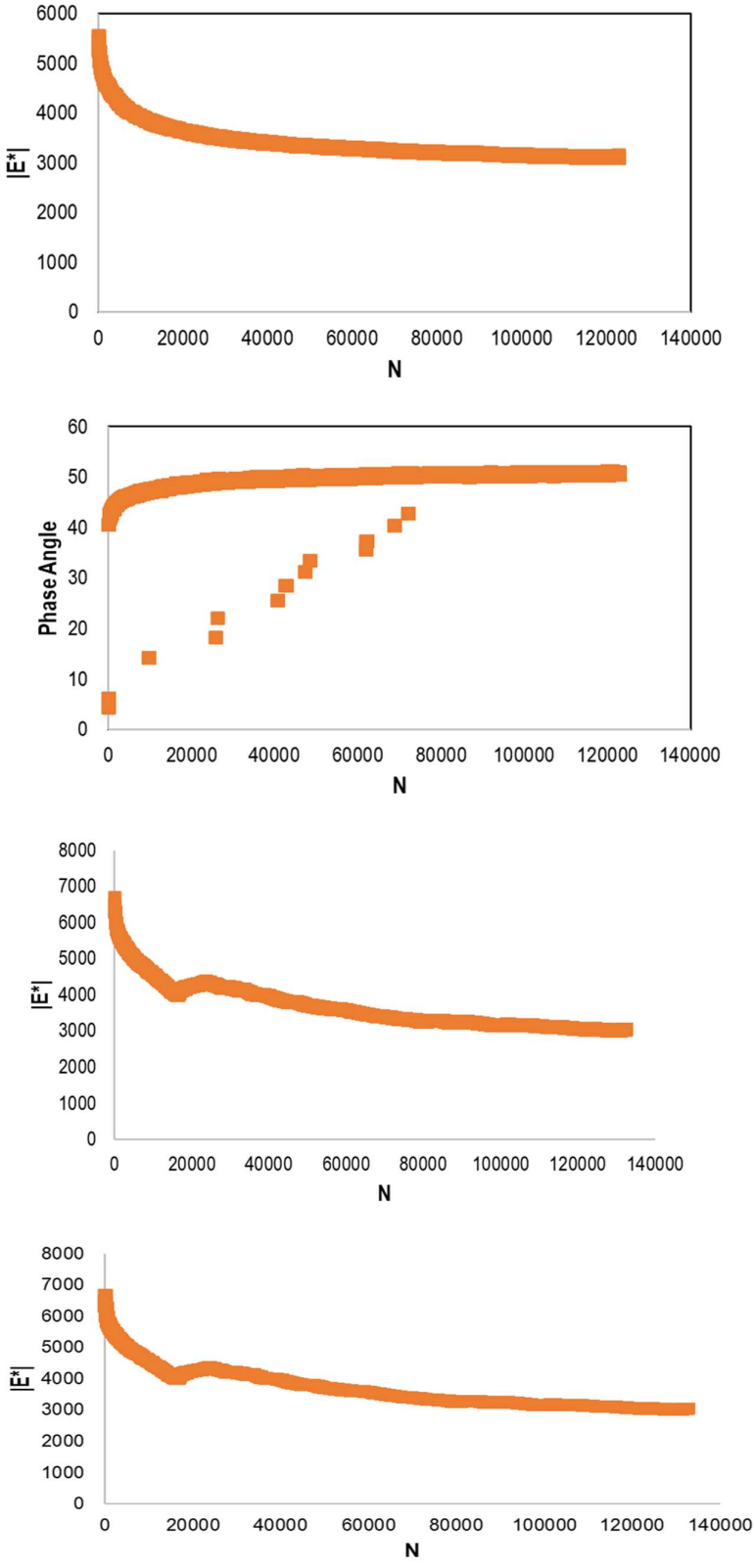

Figure C.6. M2 -Dynamic modulus and phase angle variation with N at 30°C.

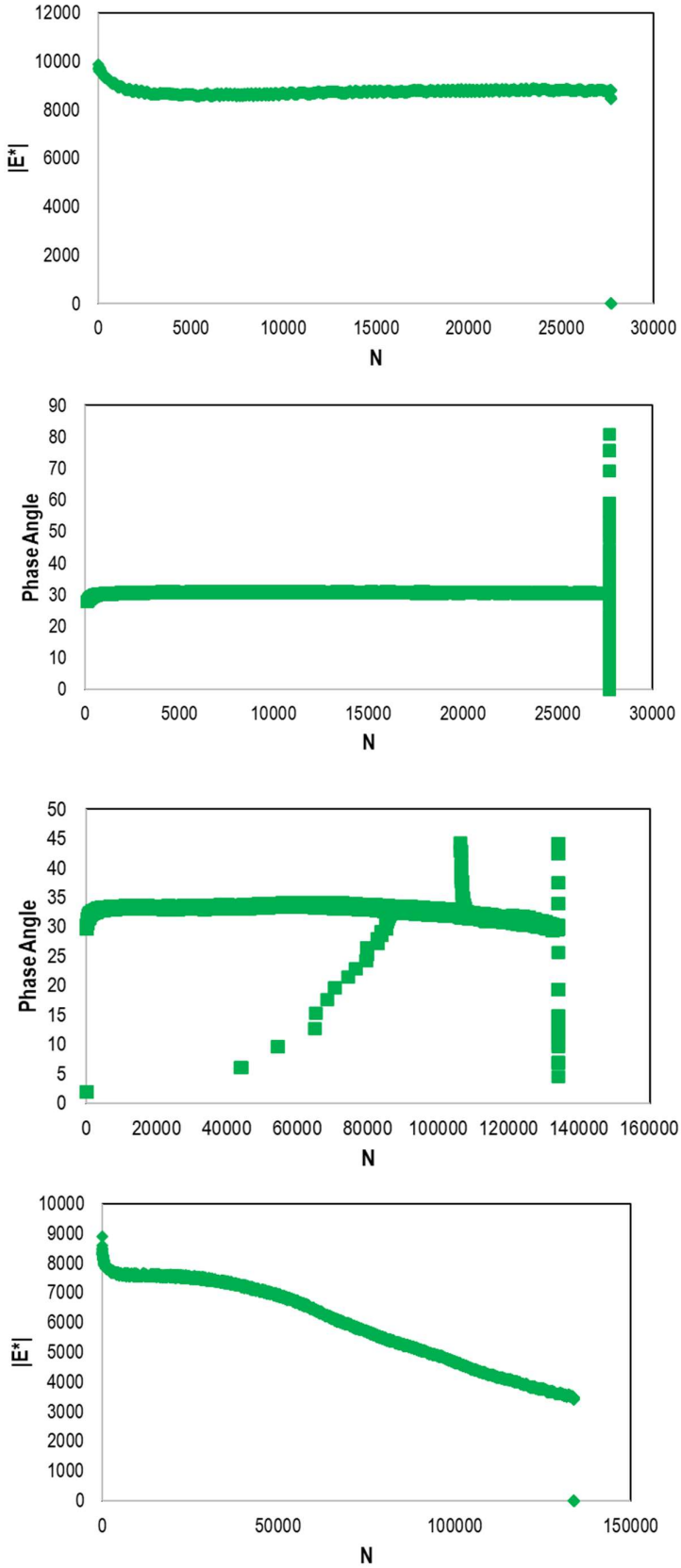

Figure C.7. M3 -Dynamic modulus and phase angle variation with N at 10°C.

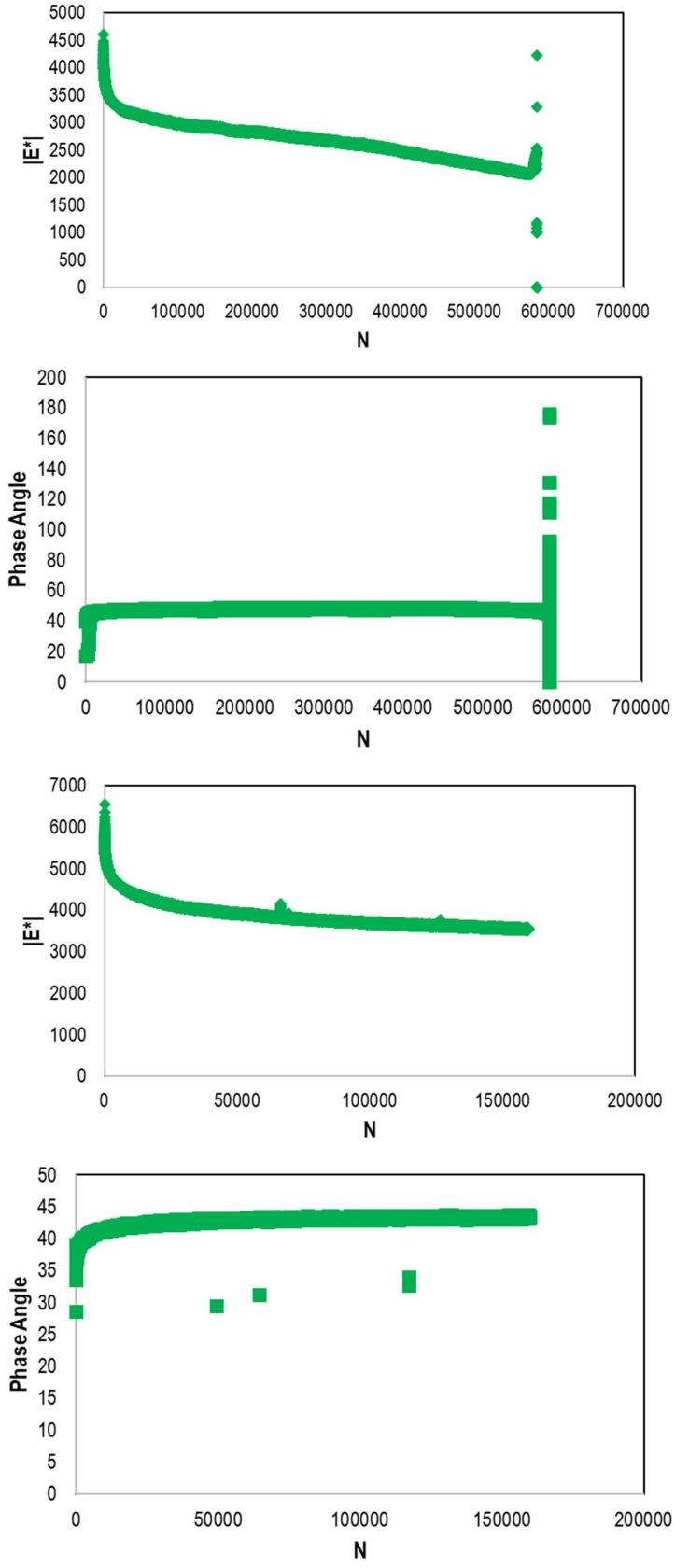

Figure C.8. M3 -Dynamic modulus and phase angle variation with N at 20°C

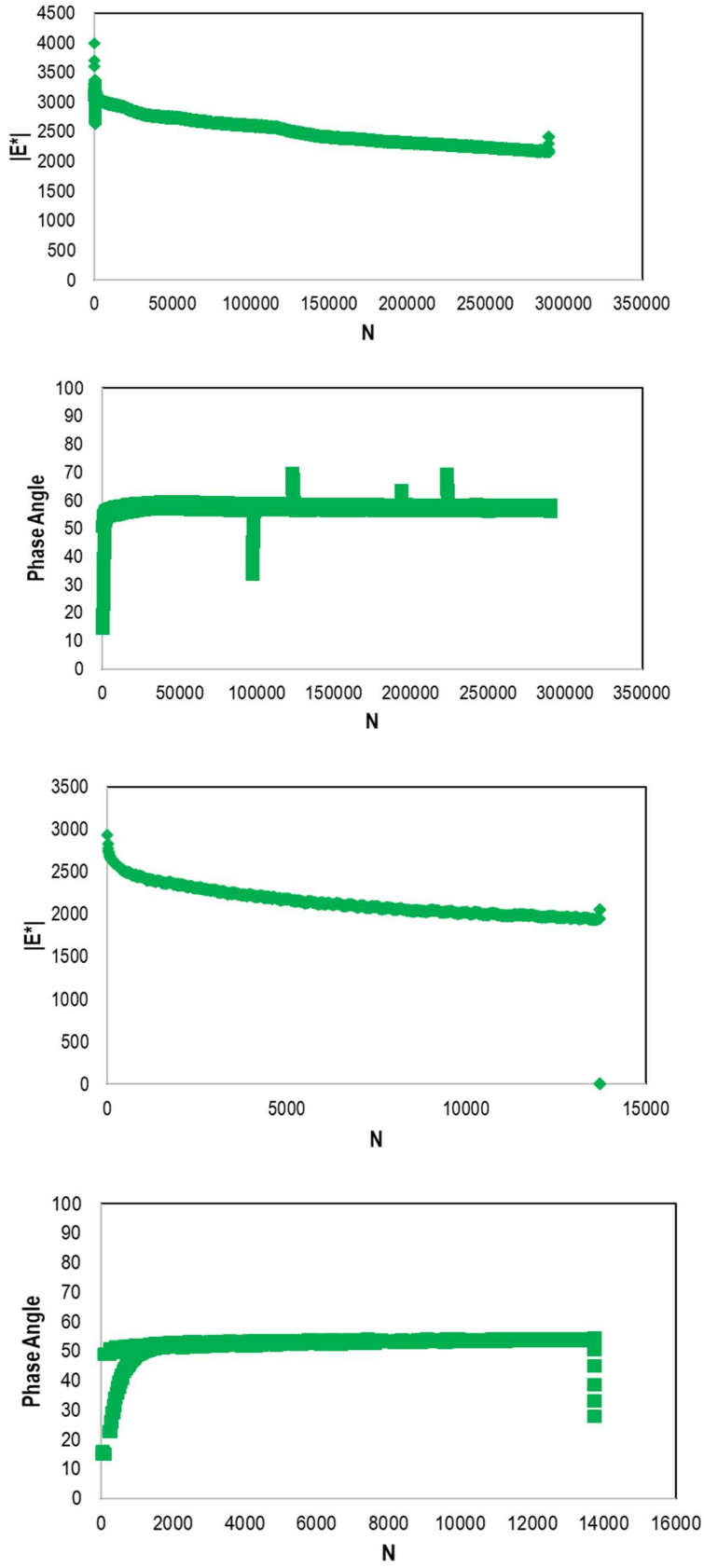

Figure C.9. M3 -Dynamic modulus and phase angle variation with N at 30°C

D

Fatigue Healing Test Results

D.1. Variation of Dynamic Modulus of Materials with Time

In cyclic fatigue and healing testing, it is expected that with the application of cyclic loadings, the dynamic modulus value of a mixture will decrease due to the formation of microcracks. Upon the introduction of the rest periods based on the damage levels in materials, these microcracks tend to heal. On reloading, there is again an increase in the dynamic modulus values of the mixtures due to possible recovery in the strength. This healing phenomenon is more prevalent at higher temperatures and longer rest periods. The higher the temperature, the higher the recovery of stiffness but the higher the damage growth rate. A longer rest period recovers the higher amount of stiffness in materials. The variation of all the mixtures at all the combinations of temperature and the rest periods are given in **Figure D.1** to **Figure D.8.**

The healing is quantified in the three methods in this research work. The formulation based on the variable representing the damage parameter is used to predict the healing model. The results of healing percentages calculated from the method based on the number of cycles are given in **Figure D.9** to **Figure D.17**. The percentages calculated for the healing follow a similar trend as calculated with other methods, i.e., with longer healing period and higher temperature, higher healing percentages are recorded. The most prominent mixture in the healing is M3. The formulation on which these results are based is given in **Eq. D.1.**

$$\%H_n = \frac{\Delta N}{N_0} * 100 \qquad \text{(D.1)}$$

where N_0 is the number of load cycles applied to the specimen before the rest period start, ΔN is the horizontal shift of the *C-N* curve due to the healing caused by the application of the rest period, & $\%H_N$ is the percentage healing of the material due to an applied rest period.

In simple words, the number of cycles before applying the rest period which led to a stage of damage level in the mixture based on C, is N_0. After that, with the application of a rest period, an increase in the C value is observed. The extra number of cycles required to reach the same damage level or the C value on reloading is N_1. The difference between these values of the number of cycles is given as ΔN. It means that with the application of rest period, the material can take more damage cycles to reach the same level of damage before the rest period.

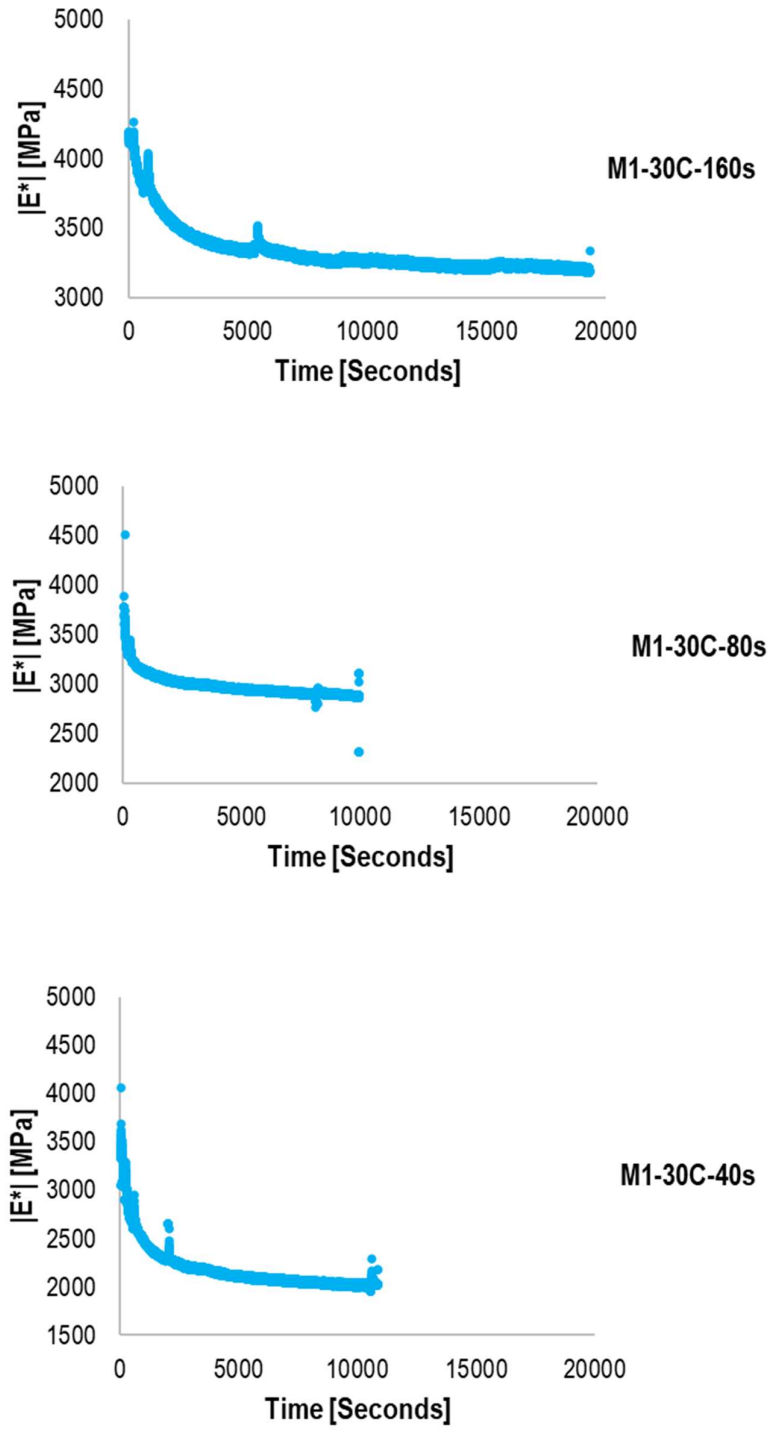

Figure D.1. Dynamic modulus values with time at 30°C for M1 at different rest periods.

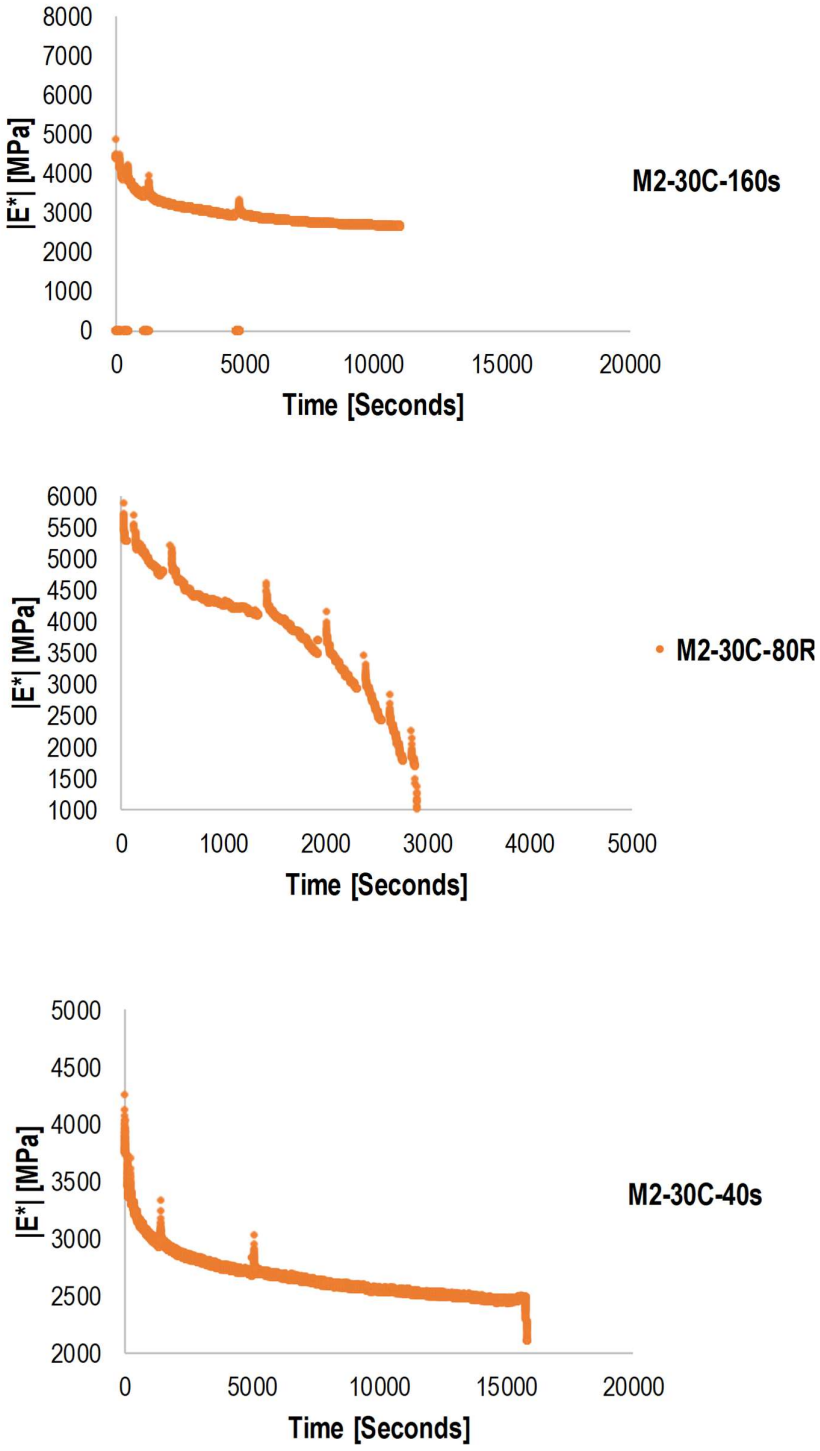

Figure D.2. Dynamic modulus values with time at 30°C for M2 at different rest periods.

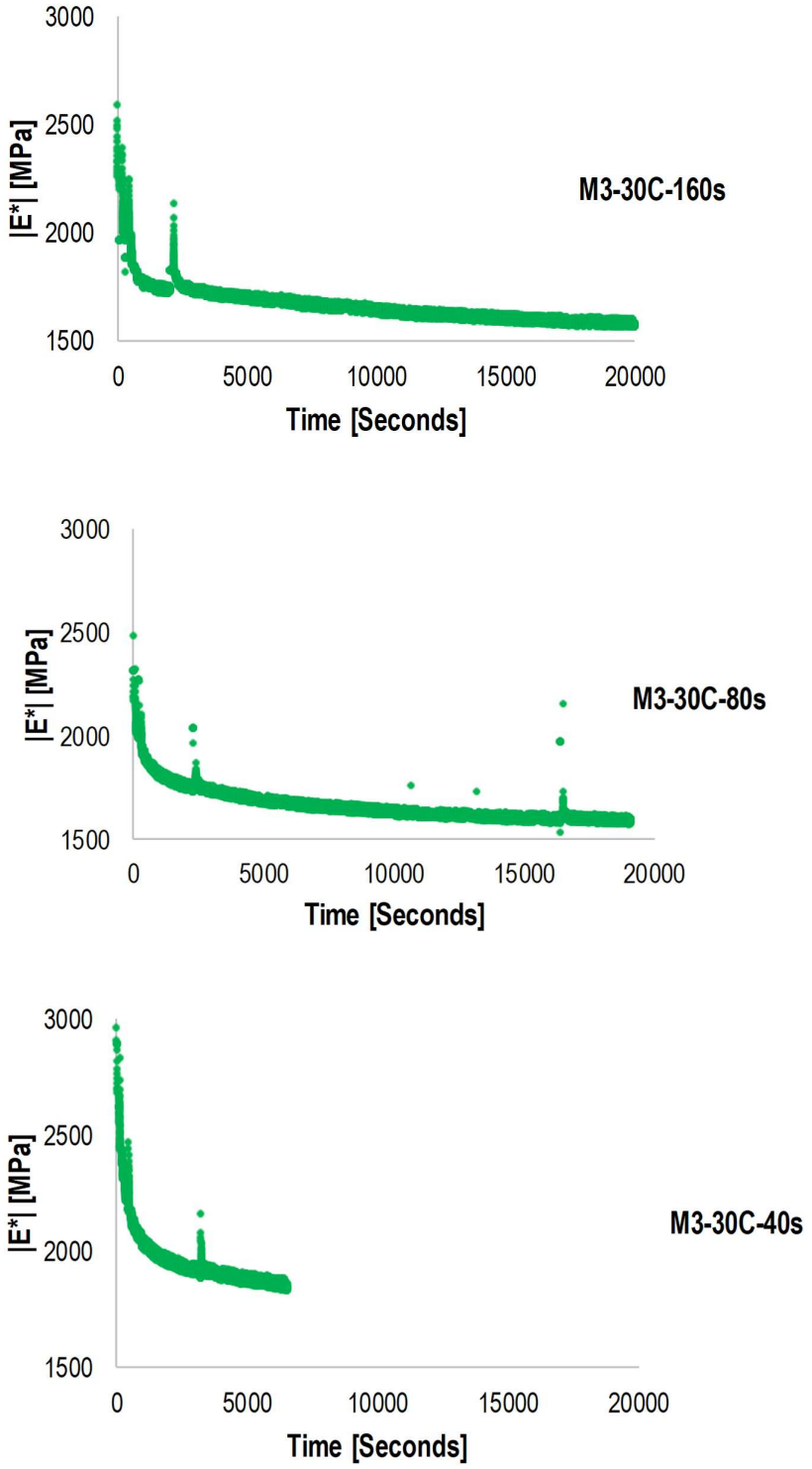

Figure D.3. Dynamic modulus values with time at 30°C for M3 at different rest periods.

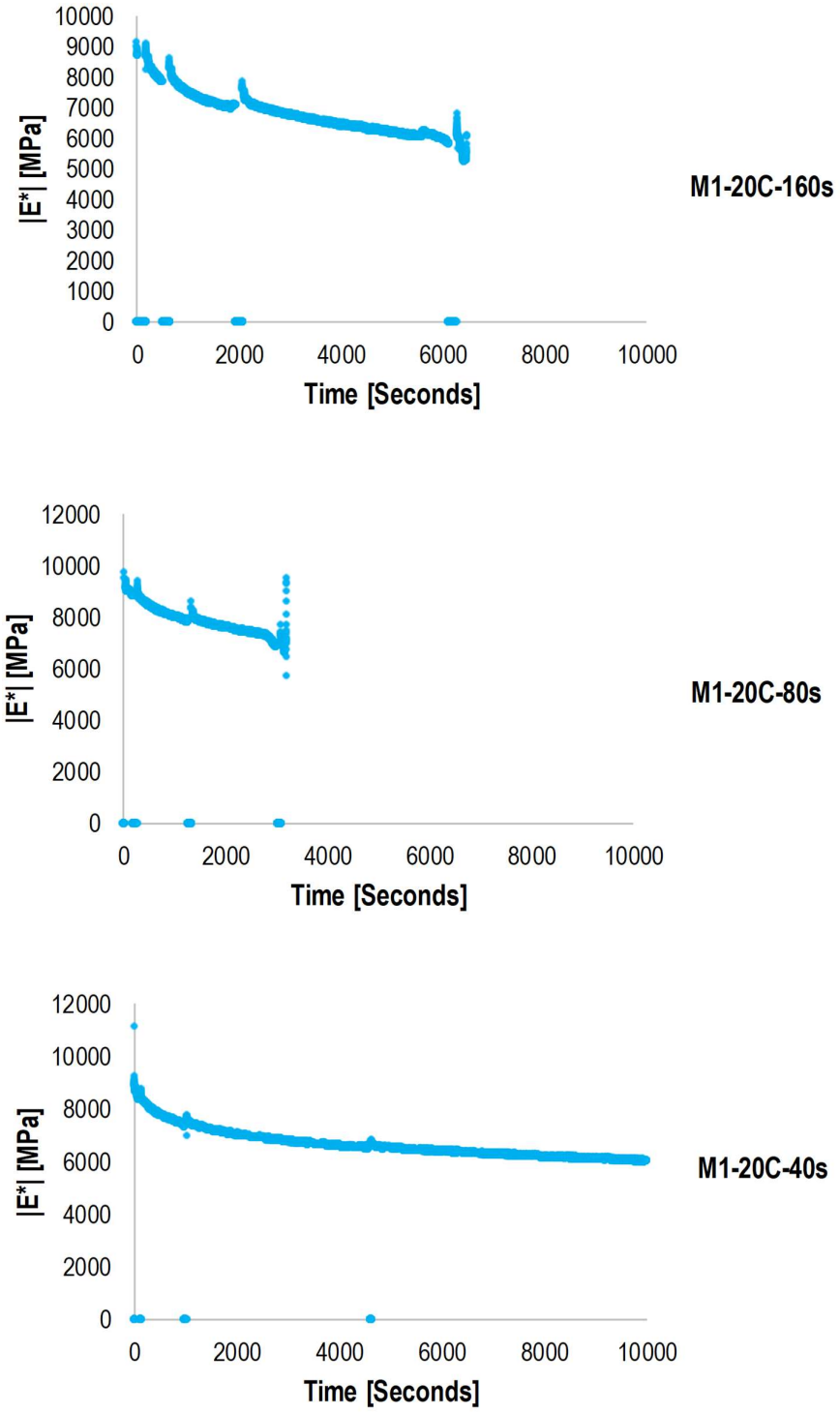

Figure D.4. Dynamic modulus values with time at 20°C for M1 at different rest periods.

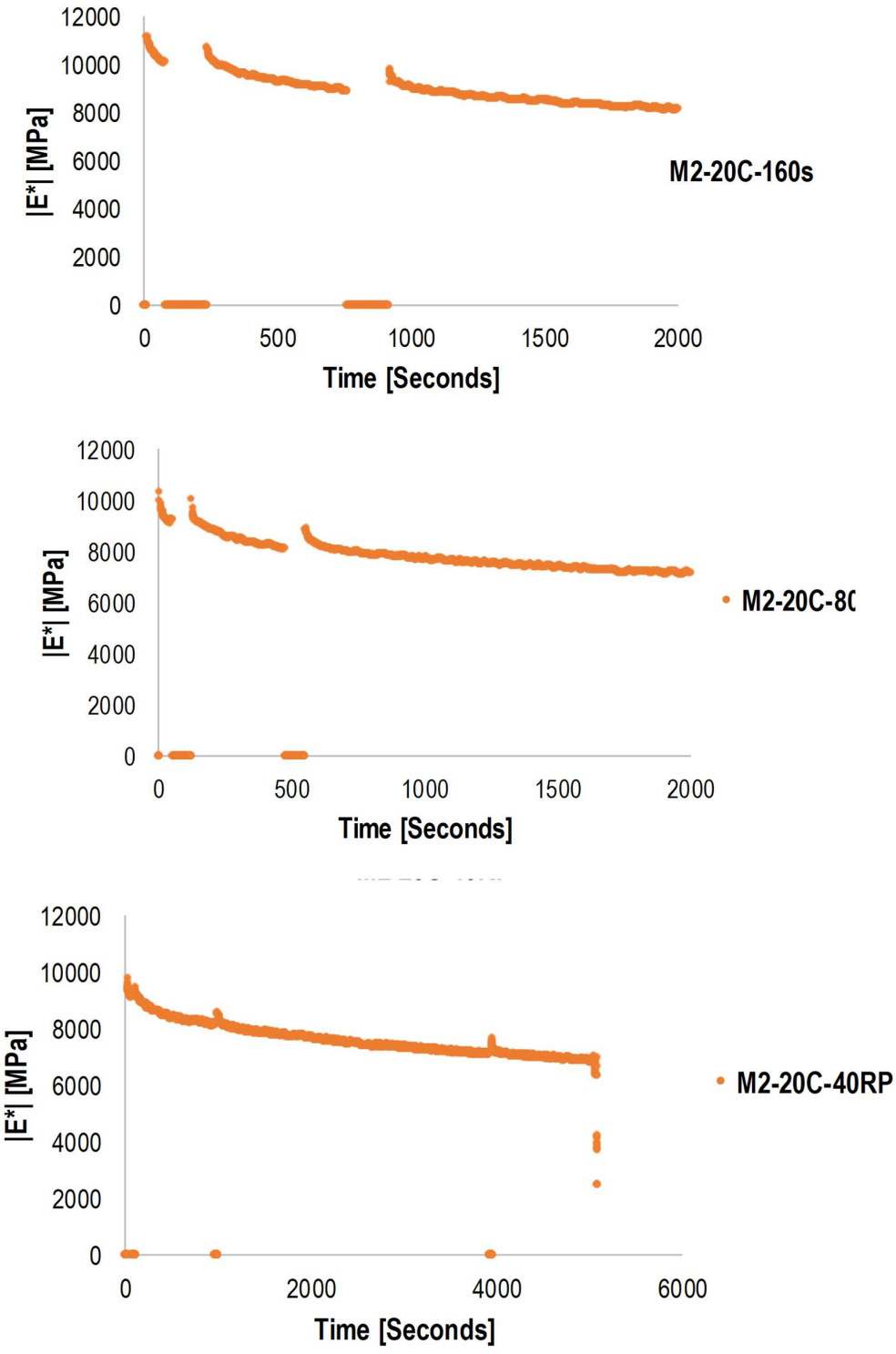

Figure D.5. Dynamic modulus values with time at 20°C for M2 at different rest periods.

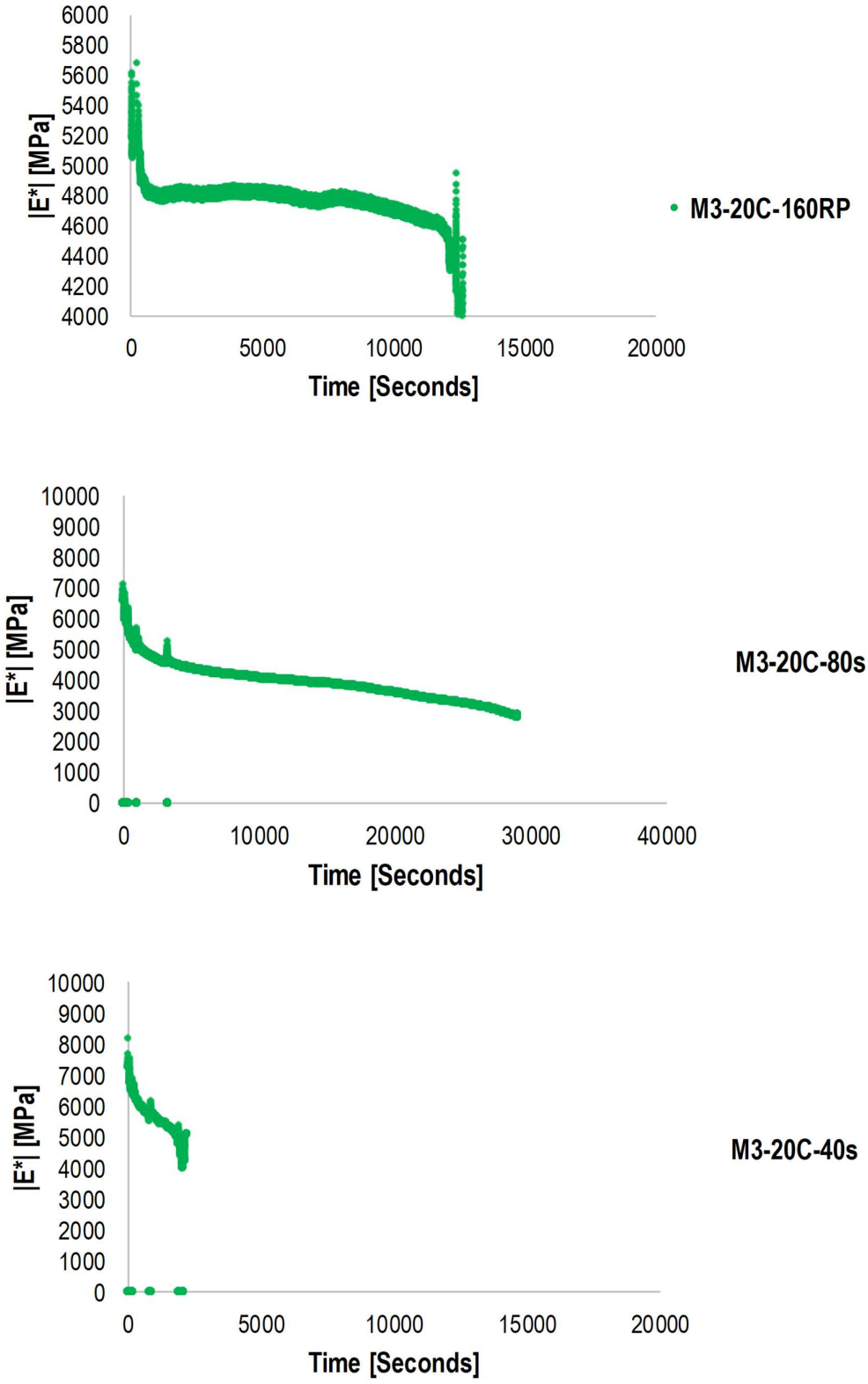

Figure D.6. Dynamic modulus values with time at 20°C for M1 at different rest periods.

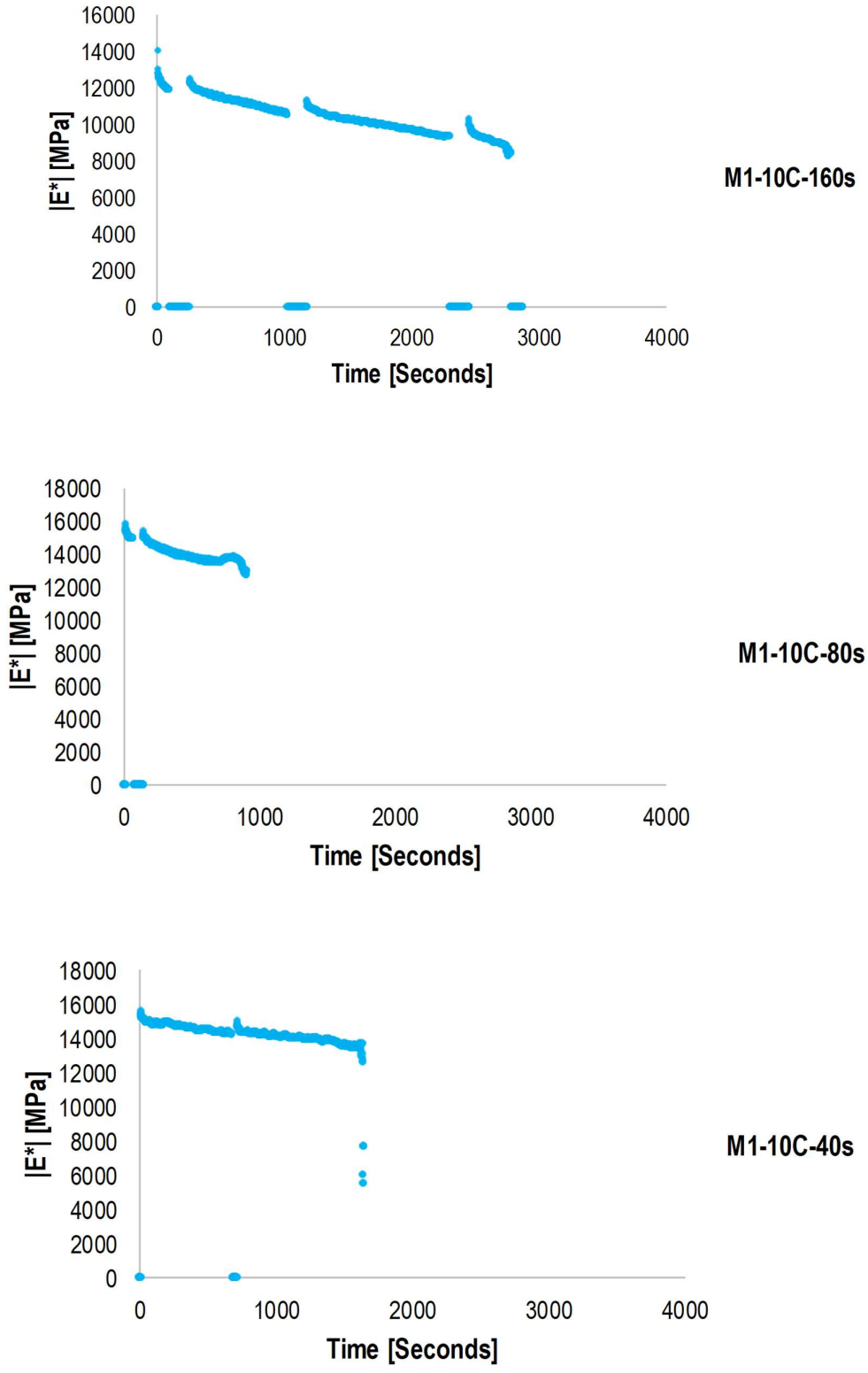

Figure D.7. Dynamic modulus values with time at 10°C for M1 at different rest periods.

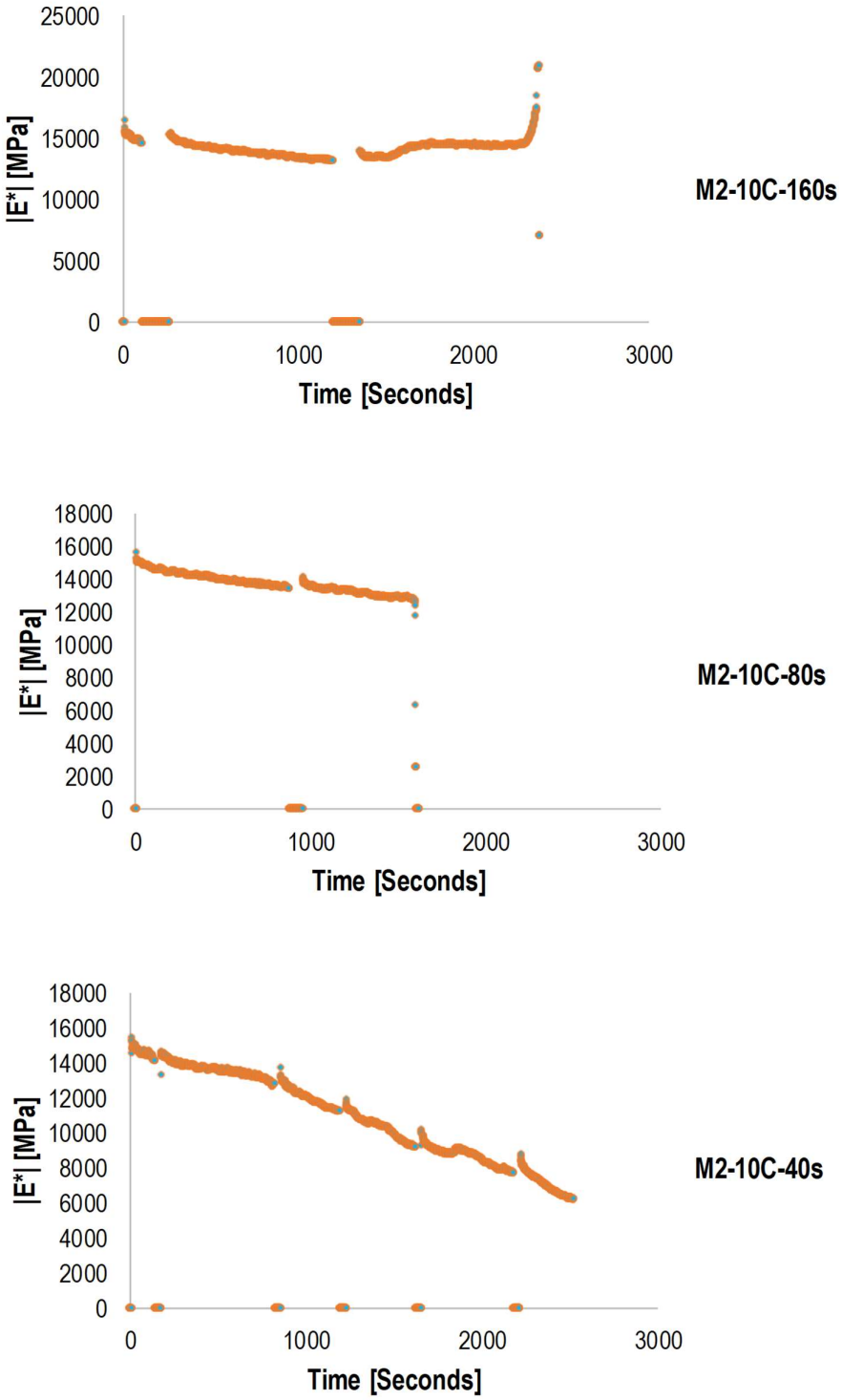

Figure D.8. Dynamic modulus values with time at 10°C for M2 at different rest periods.

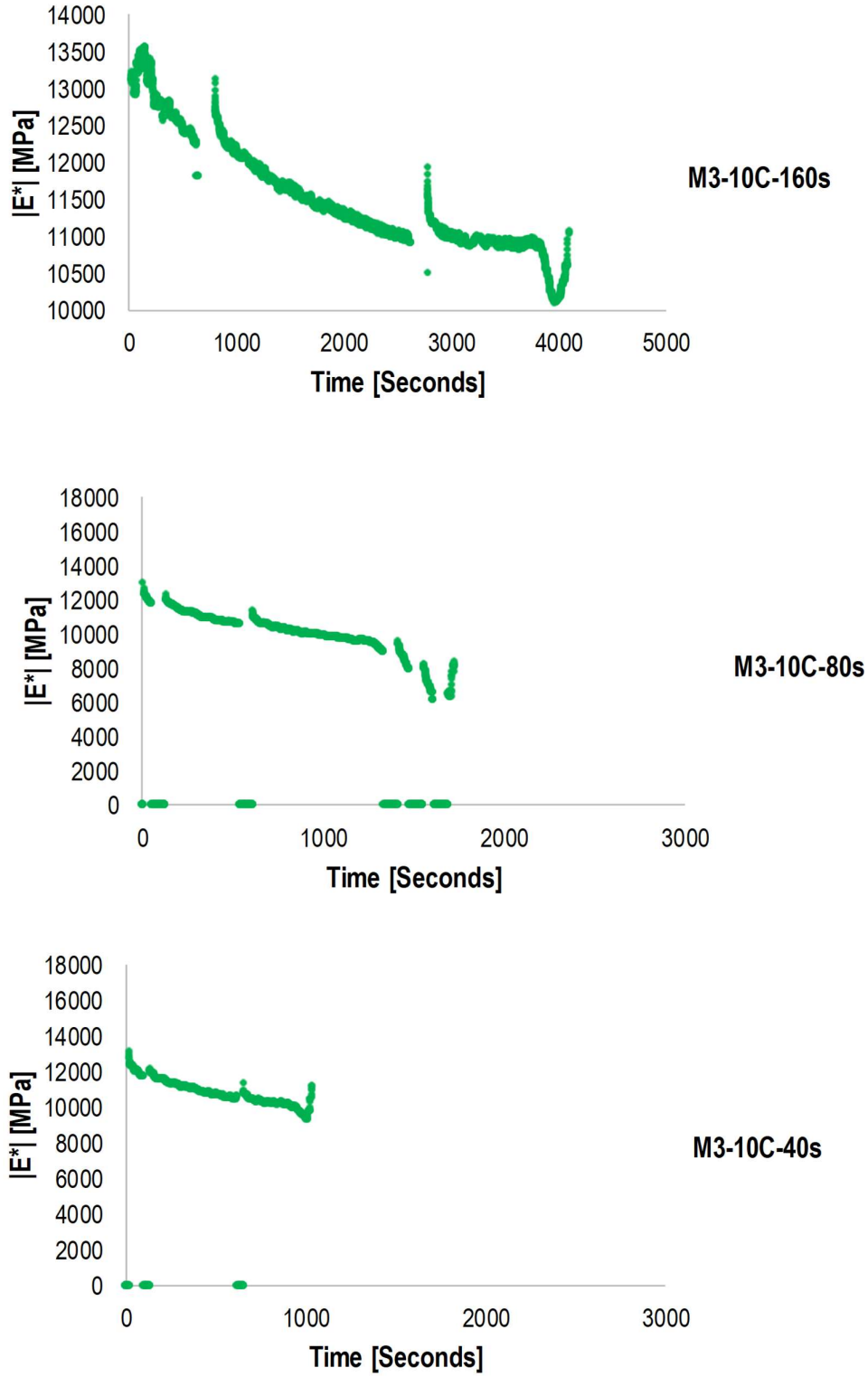

Figure D.9. Dynamic modulus values with time at 10°C for M3 at different rest periods.

D.2 Calculation of Healing Percentages Based on the Number of Cycles

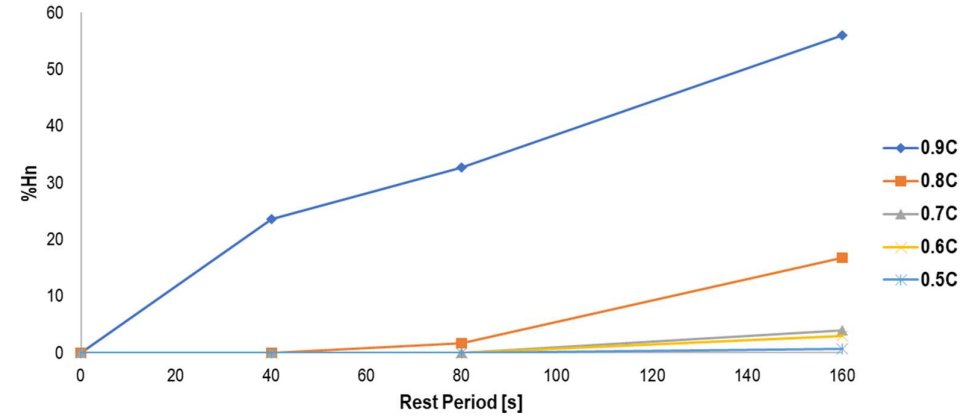

(a)

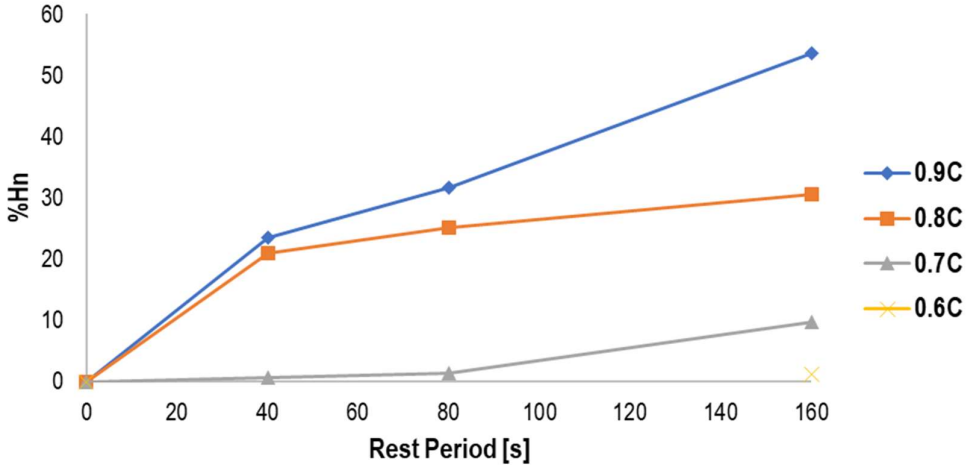

(b)

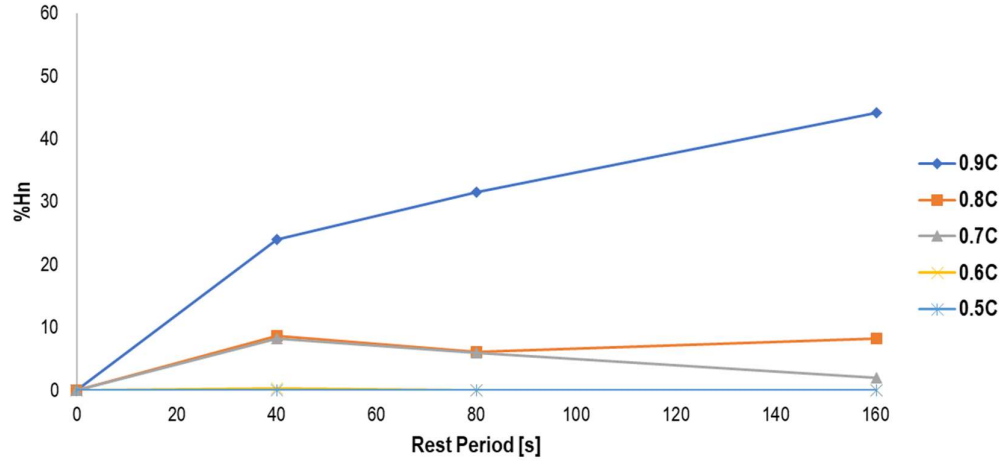

(c)

Figure D.10. Healing percentages for M1 at (a)10°C (b) 20°C (c) 30°C.

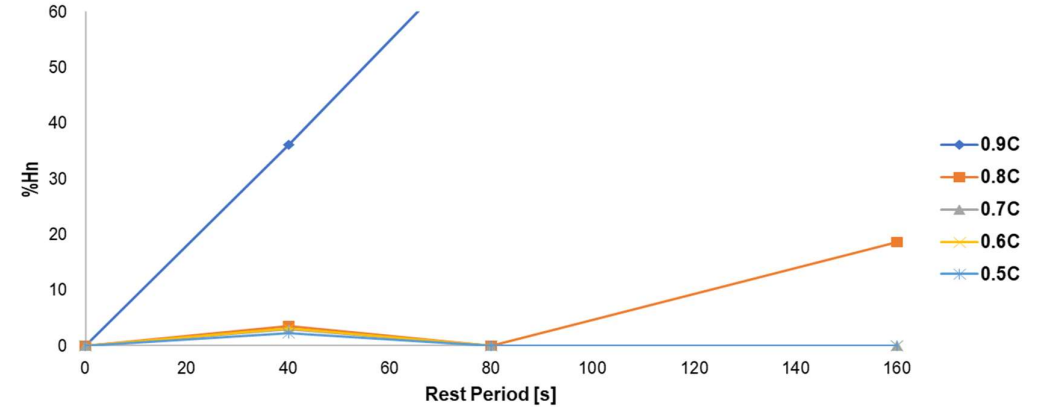

(a)

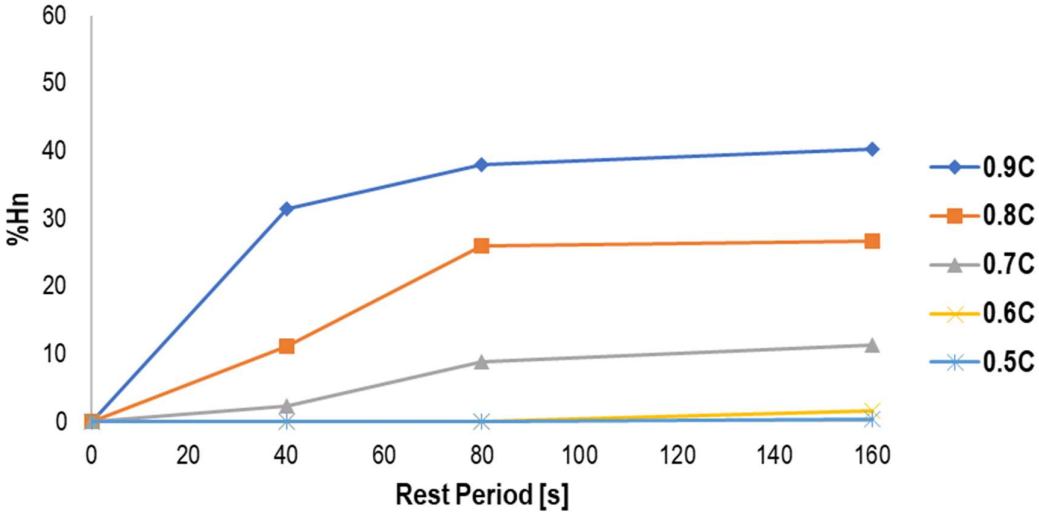

(b)

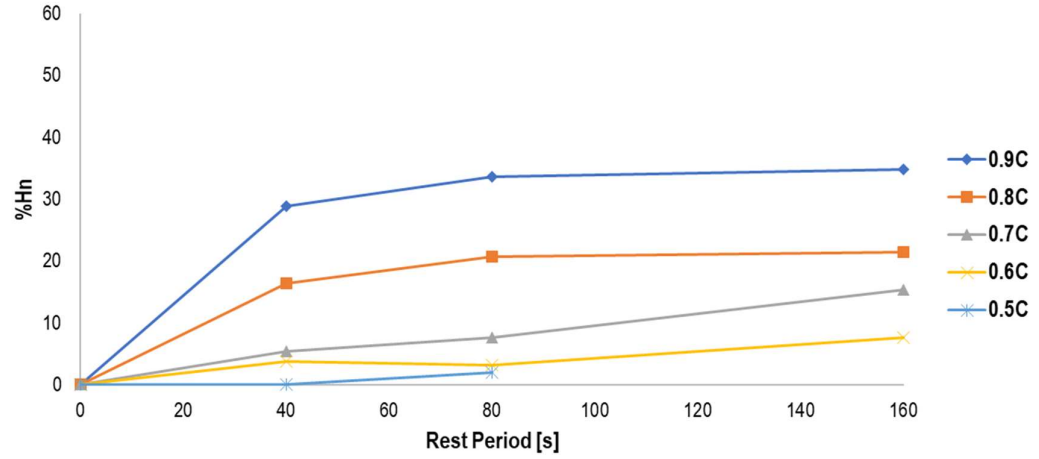

(c)

Figure D.11. Healing percentages for M2 at (a)10°C (b) 20°C (c) 30°C.

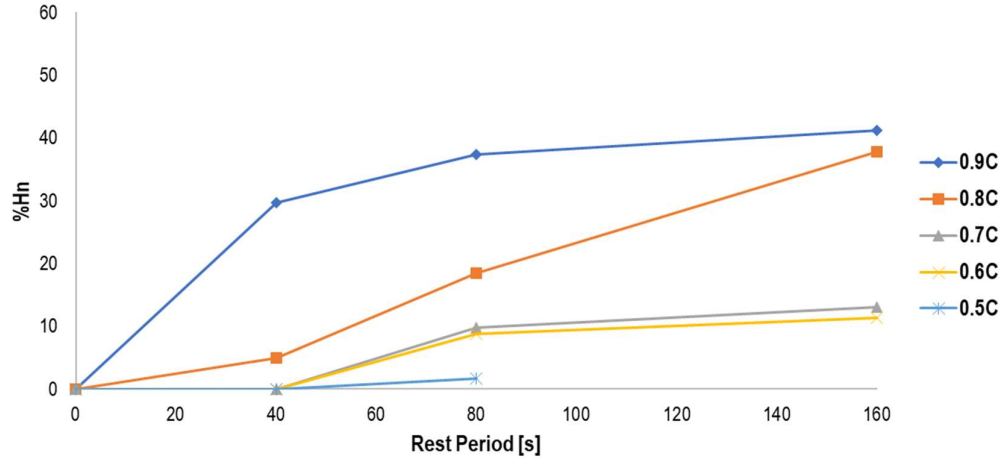

(a)

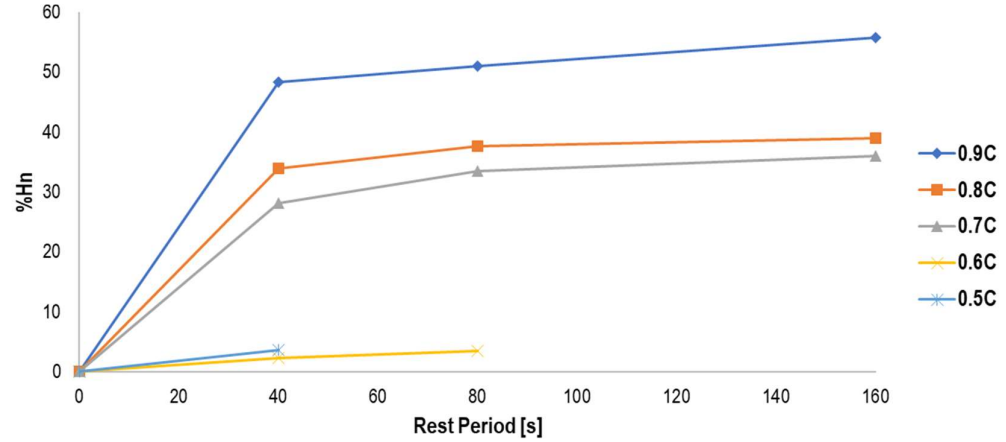

(b)

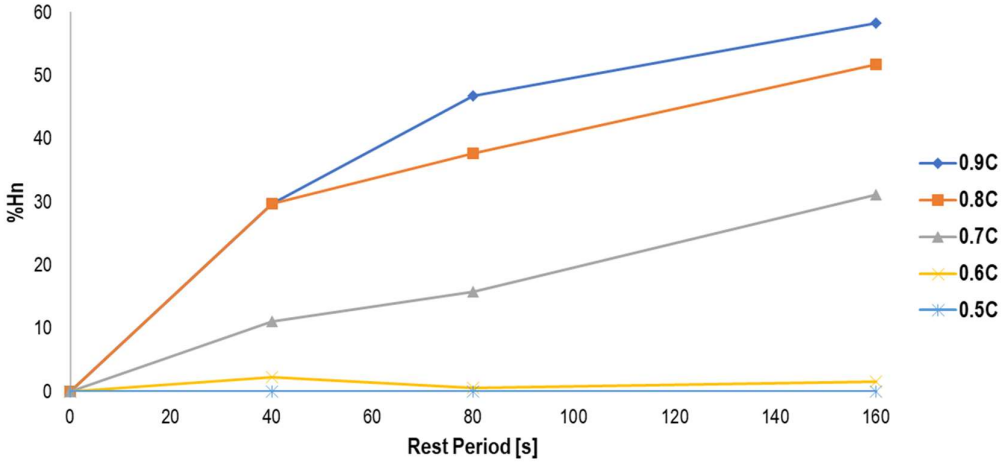

(c)

Figure D.12. Healing percentages for M3 at (a)10°C (b) 20°C (c) 30°C.

E

FlexPAVE Software

E.1 FlexPAVE simulations

The FlexPAVE Simulation performed at M3 healing and fatigue mechanism are discussed in **Chapter 6** of this report. The finite element models for the remaining two mixtures, i.e., M1 and M2, are given in this report section.

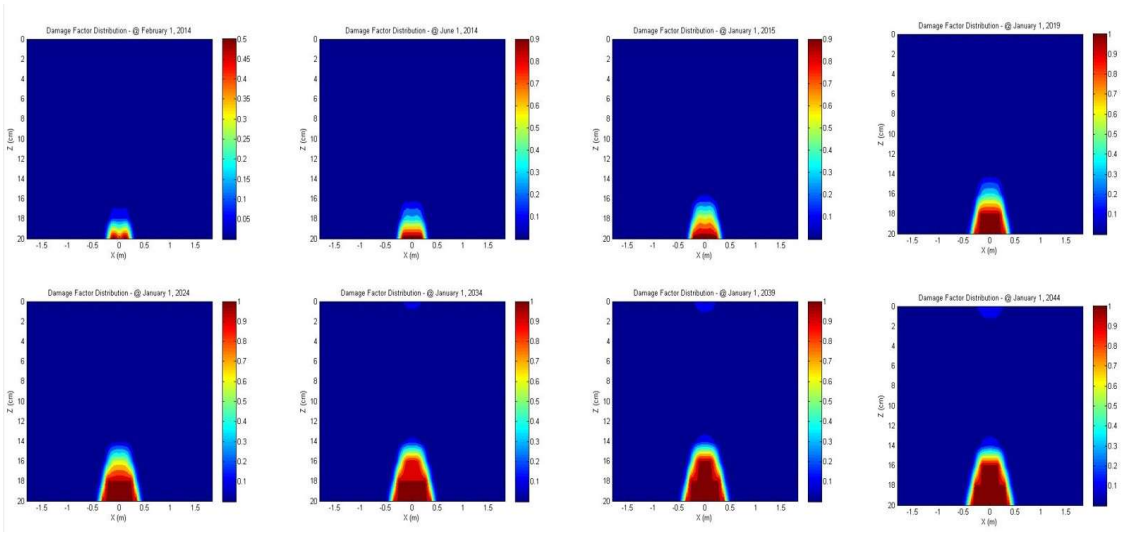

(a)

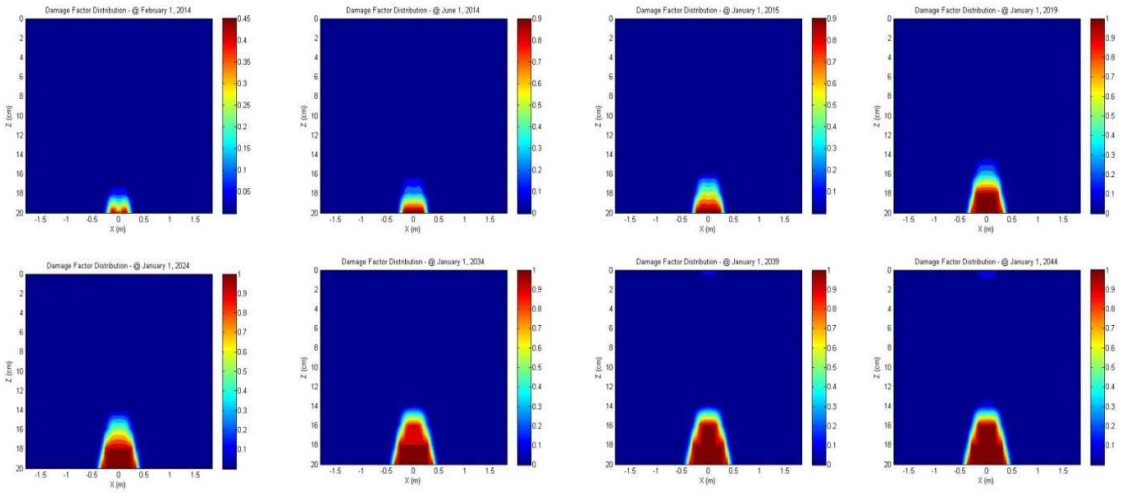

(b)

Figure E.1. Development of the cracks over 30 years in M1 with (a) fatigue (b) healing mechanism.

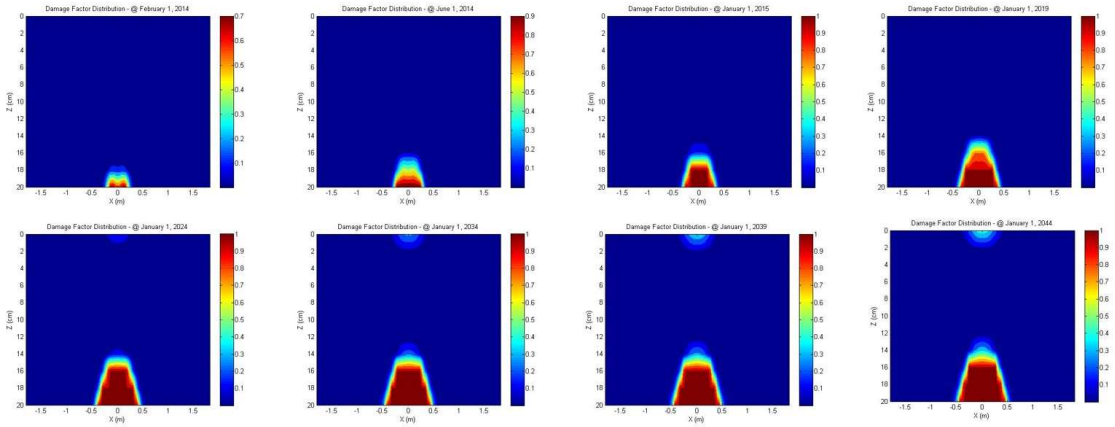

(a)

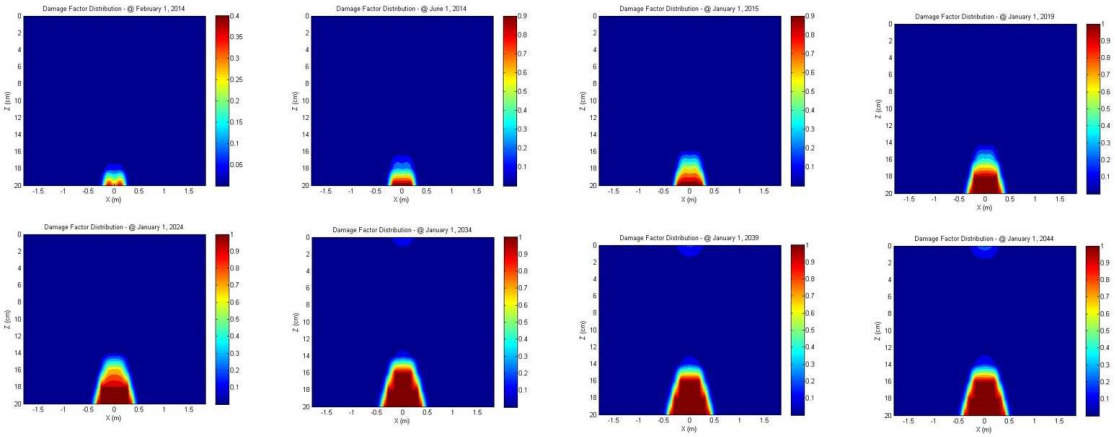

(b)

Figure E.2. Development of the cracks over 30 years in M2 with (a) fatigue and (b) healing mechanism.

The simulations performed on M1 with the stiffness variation in the sub-base layers of the pavement structure. The finite element models generated for these variations and the crack pattern over 30 years are given in the figures below.

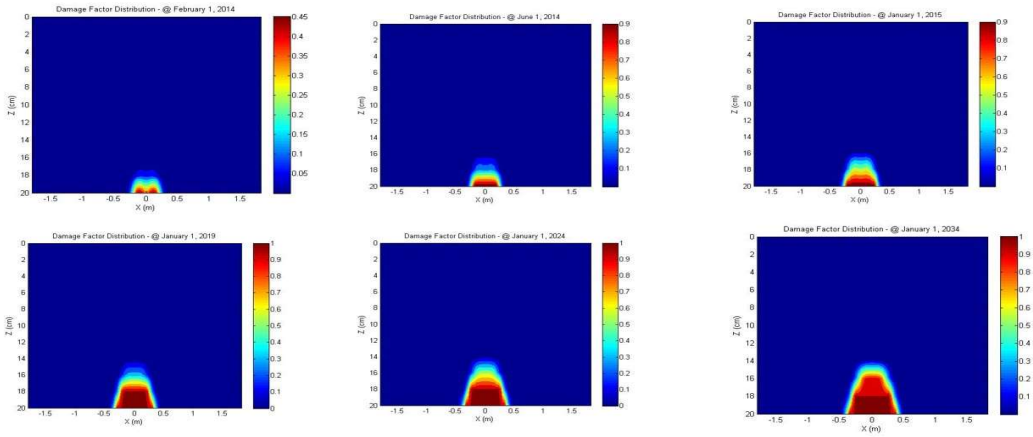

Figure E.3. Development of the cracks over 20 years in M1 for 150 MPa sub-base.

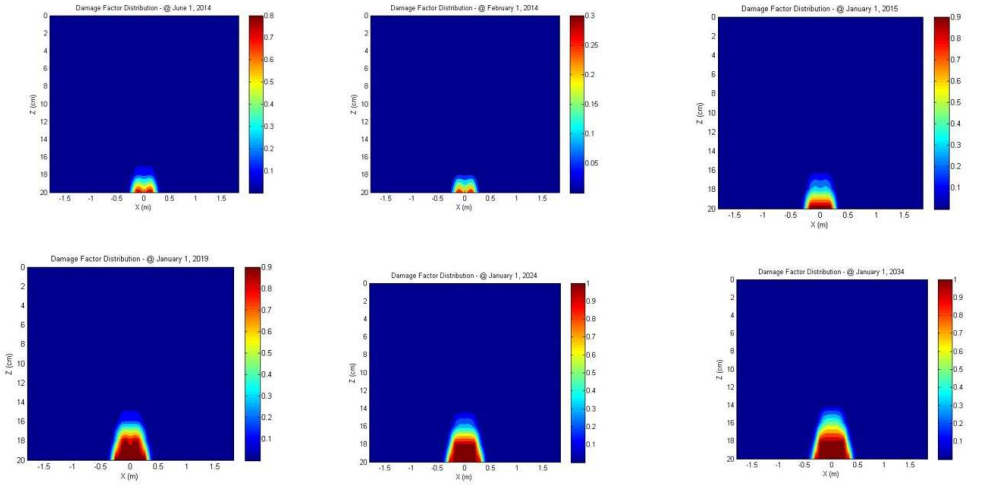

Figure E.4. Development of the cracks over 20 years in M1 for 300 MPa sub-base.

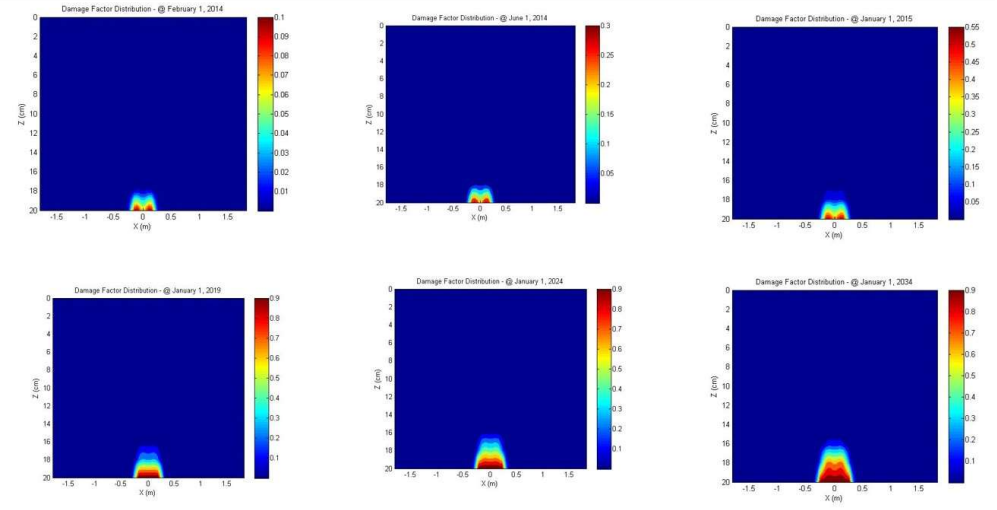

Figure E.5. Development of the cracks over 20 years in M1 for 700 MPa sub-base.

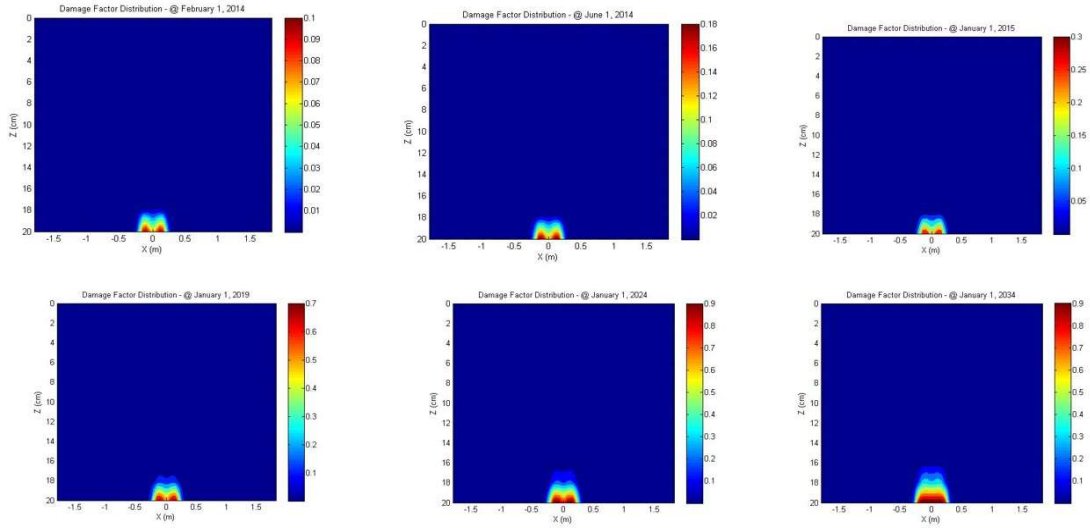

Figure E.6. Development of the cracks over 20 years in M1 for 1000 MPa sub-base.

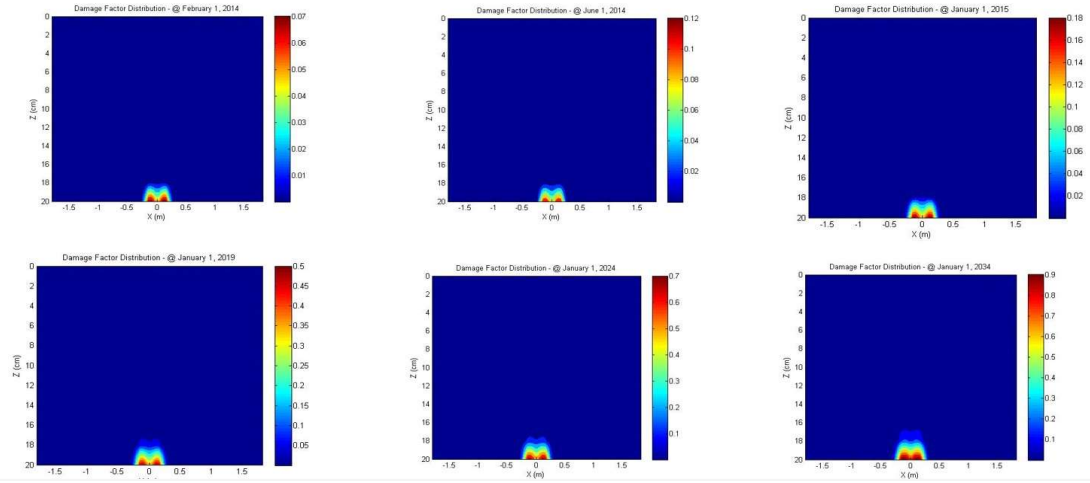

Figure E.7. Development of the cracks over 20 years in M1 for 1200 MPa sub-base.

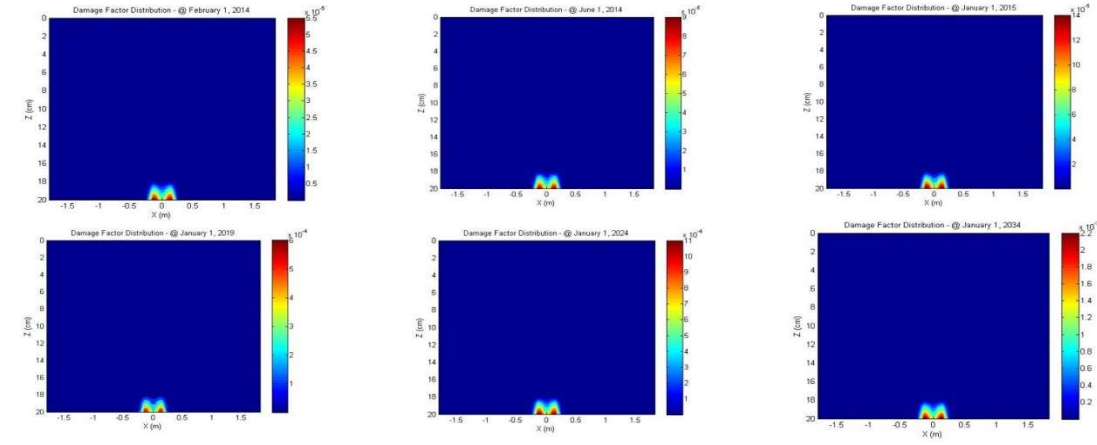

Figure E.8. Development of the cracks over 20 years in M1 for 4300 MPa sub-base.

F

Prediction of Healing Master Curves

F.1. Prediction of healing models for all the mixtures

In this section of the report, an effort to plot the healing master curve using the sigmoidal function mentioned in **Eq. F.1.** is performed. And the healing master curves are plotted in Chapter 5 of this report.

$$\log|\%Hs| = a + \frac{b}{1+\frac{1}{e^{d+g*log\,(RP_{red})}}} \quad \text{(F.1.)}$$

The three mixture's fitting parameters, when fitted to **Eq. F.1.** Using the solver function in Excel is given in **Table F.1.**

Table F.1. Fitting parameters for all mixtures.

	M1			M2				M3			
	0.9	0.8	0.7	0.9	0.8	0.7	0.6	0.9	0.8	0.7	0.6
a	1.24E-05	0.57	0.70	0.000137	0.000137	0.000137	0.000137	0.52	0	0	0
b	1.70	1.03	0.74	1.63	1.46	1.37	1.35	1.42	1.55	1.45	1.28
d	1.38	1.40	0.74	0	0	0	0	0.36	0	0	0
g	1.13	0.61	0.70	2.36	1.75	1.89	1.45	0.46	2.39	1.75	1.44

The fitting parameter's value is plotted with the damage level C (**Figure F.1** to **Figure F.3**) and fitted linearly and by means of polynomials.

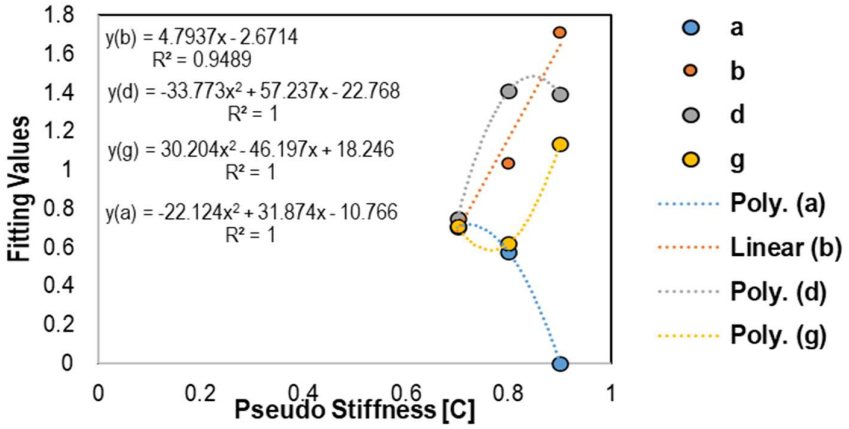

Figure F.1. Fitting parameters for percent healing master curves vs. damage level in M1.

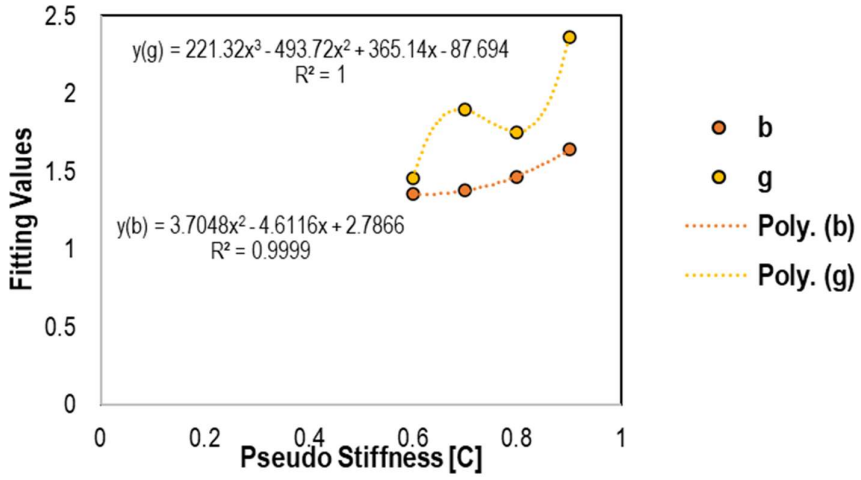

Figure F.2. Fitting parameters for percent healing master curves vs. damage level in M2.

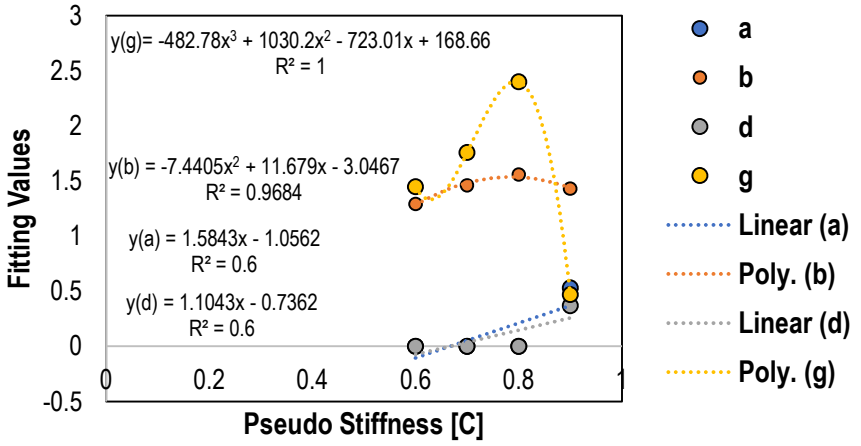

Figure F.3. Fitting parameters for percent healing master curves vs. damage level in for M3.

From above, it is obvious that there is a single healing master curve for each damage level. Hence after finding the master curves functional for all three asphalt mixtures and fitting it to percentage healing data, it would reflect the dependency of the healing to both rest periods and temperature through reduced rest periods parameter. Once the fitting for all the damage levels is done, it becomes easier to fit the parameters of the master curves in terms of the damage levels. Hence, the master curves are transformed into equations, showing the dependency of healing on reduced rest periods and the damage level. Using the sigmoidal function above in Eq. 5.5, the predicted healing percentage is calculated using this function and plotted to get the master curves for all three mixtures. The other parameters required to calculate the shift factors, i.e., a_1, a_2, & a_3 for all the mixtures, are obtained as an output from FlexMAT. The other parameters required to calculate the shift factors, i.e., a_1, a_2, & a_3 for all the mixtures, are obtained as an output from FlexMAT. The shift factors for all the mixtures at all the temperatures are already calculated, and the reduced rest periods will be calculated.

$$\log|\%Hs| = a + \frac{b}{1+\frac{1}{e^{d+g*log\,(RP_{red})}}} \quad \text{(F.2)}$$

where

$$RP_{red} = \frac{RP}{a_T}$$

$$log(a_T) = -4.26 * 10^{-4}T^2 - 0.0647T + 1.556$$

$$a = -22.124C^2 + 31.874C - 10.766$$

$$b = 4.7937C - 2.6714$$

$$d = -33.773C^2 + 57.237C - 22.768$$

$$g = 30.204C^2 - 46.197C + 18.246$$

The effect of the rest period and the temperature are combined in a reduced rest period, giving the healing function for **Mixture 2** in **Eq. F.2.**

$$\log|\%Hs| = 0.00137 + \frac{b}{1+\frac{1}{e^{g*log\,(RP_{red})}}} \quad \text{(F.3)}$$

where

$$RP_{red} = \frac{RP}{a_T}$$

$$log(a_T) = -4.91 * 10^{-4}T^2 - 0.0522T + 1.3208$$

$$a = 0.00137$$

$$b = 0.9456C + 0.7489$$

$$d = 0$$

$$g = 221.32C^3 - 493.72C^2 + 365.14C - 87.694$$

The effect of the rest period and the temperature are combined in a reduced rest period, giving the healing function for Mixture 3 in **Eq. F.3.**

$$\log|\%Hs| = a + \frac{b}{1+\frac{1}{e^{d+g*log\,(RP_{red})}}} \quad \text{(F.4)}$$

where

$$RP_{red} = \frac{RP}{a_T}$$

$$log(a_T) = -6.974 * 10^{-5}T^2 - 0.08674T + 1.861$$

$$a = 1.5843C - 1.0562$$

$$b = -7.4405C^2 + 11.679C - 3.0467$$

$$d = 1.1043C - 0.7362$$

$$g = -482.78C^3 + 1030.2C^2 - 723.01C + 168.66$$

These healing mentioned above prediction models (**Eq. F.2, F.3,& F.4**) can predict the healing percentages for any temperature and rest period for a given damage level in all three mixtures involved in the studies.